The Retinal Microvasculature in Secondary Progressive Multiple Sclerosis

This thesis is submitted to UCL for the Degree of Doctor of Philosophy

Sarah Houston

Primary Supervisor: Prof John Greenwood

Secondary Supervisor: Dr Adam Dubis

UCL Institute of Ophthalmology

11-43 Bath Street

London

EC1V 9EL

Declaration

I, Sarah Houston, confirm that the work presented in this thesis is my own. Where information has been derived from other sources, I confirm that this has been indicated in the thesis

Abstract

In light of new data regarding pathology of multiple sclerosis (MS), more research is needed into the vascular aspects of the disease. Demyelination caused by inflammation is historically thought of as the main cause of disability in the disease. Recent studies, however, have suggested that MS is in fact a spectrum of overlapping phenotypes consisting of inflammation, oxidative damage and hypoperfusion. The microvasculature plays an important role in all of these pathogenic processes and its dysfunction may therefore be of crucial importance to the development and progression of the disease. This thesis focuses on investigating the microvasculature of the retina as a surrogate for the brain by assessing the vascular structure, blood flow dynamics and oxygen transfer of the retinal blood vessels in secondary progressive multiple sclerosis (SPMS). Studying the retinal microvasculature using a multimodal imaging approach has allowed us to develop a more detailed understanding of blood flow in MS and to identify new imaging markers for trials into neuroprotective drugs in MS. The work done in this thesis demonstrated; i) a higher rate of retinal microvascular abnormalities in MS which progresses with disease severity, ii) evidence of retinal vascular remodelling in SPMS and iii) changes in blood velocity and flow in the retina in SPMS. These observations pave the way for future investigations into the mechanisms of vascular alterations and vascular dysfunction in MS, and provide a set of imaging markers to further explore other cerebrovascular diseases through the retina.

Impact Statement

By using the eye as a window to the brain, this thesis has expanded our knowledge of possible changes in microvascular function in multiple sclerosis and has provided a baseline for future investigation into the temporal vascular changes during disease progression. This thesis has demonstrated that high resolution imaging of retinal microvasculature is possible and fruitful in patients with multiple sclerosis, and could be used more widely in other neurological and systemic disorders to further understand subclinical impacts of disease. Indications of microvascular pathology in multiple sclerosis will increase traction for research into the microvascular impact of other brain diseases which also have devastating social and economic impact and where treatment options are also limited. The multimodal method development and baseline vascular parameters reported in this thesis will now be used for the analysis of images being captured as part of an ongoing clinical trial for the assessment of simvastatin treatment in SPMS. The semi-automated analysis tools for measuring retinal blood velocity developed in this thesis can also be applied to the study of numerous ophthalmic and systemic diseases where vascular function is thought to be affected. The use of multimodal imaging greatly enhanced the insights gained in this thesis and should be considered for diseases with subtle but significant microvascular effects in the retina. Following the findings in this thesis that the retinal microvasculature is impacted in MS, microvascular health should be recognised by neurologists and policy makers alike as a potentially significant element in the progression of MS worthy of further investigation and investment.

Acknowledgements

Firstly, I would like to thank all those from UCL who made this possible. I wish to thank my supervisors Prof John Greenwood and Dr Adam Dubis for their support over the past few years and the significant time and energy put into reviewing my work. I am grateful to the lab mates over the years who have made this journey possible, in particular thanks to Dr Joan Nuñez do Rio who has been a great source of support and advice during trying times. I have been so fortunate to make lasting friends in (soon-to-be Dr) Reena Chopra and Dr Iris Kleerekooper, who are inspirational in being both great scientists and even greater human beings. Special thanks I believe are also owed to Dr Axel Petzold whose enthusiasm for our work in MS has been a real inspiration to me. I would also like to express my gratitude to all the support staff at the IoO who have made the long journey smoother.

I am very grateful to those who volunteered their time for our studies, especially all the staff and students of UCL Institute of Ophthalmology. Thanks in particular are owed to the patients with MS who have taken part in our trials, as without their patience and enthusiasm this would not have been possible. Many thanks to the whole MSOpt team for their hard work and perseverance in making this trial possible. I am grateful also to the MS Society and NIHR Moorfields Biomedical Research Centre for funding my PhD and presenting me with numerous opportunities over the last few years.

Mo chairde agus mo chlann. Lasting friends make lasting impact, so thank you to Bepe and the lads. Thank you to my parents for all their support, especially to my Mum for emphasising the importance of independence while always being by my side. Thanks always to Aunty Lorraine for proving to me not even a third-degree sunburn can stop success. To Laura, sister and original teacher, thank you for your undying support; my achievements belong to you also. Finally, I am immensely grateful to Yogi whose daily reminder that I was “one day closer” really did make all the difference.

This thesis is dedicated to the memory of Harry Harrison who valued education, hard graft and a nice long walk.

Contents

List of Figures

List of Tables

Abbreviations

AD	Alzheimer's Disease
ANOVA	Analysis of Variance
AO	Adaptive Optics
AOSLO	Adaptive Optics Scanning Laser Ophthalmoscope
ART	Automatic Real Time
ASL	Arterial Spin Labelling
BBB	Blood Brain Barrier
BMC	Boston Micromachines Corporation
BOLD	Blood Oxygenation Level Dependant
BP	Blood Pressure
BRB	Blood Retinal Barrier
CD4	Cluster of Differentiation 4
CDI	Colour Doppler Imaging
CIS	Clinically Isolated Syndrome
CNS	Central Nervous System
COVID-19	Coronavirus Disease 19
D	Dioptre
DBP	Diastolic Blood Pressure
DR	Diabetic Retinopathy
EAE	Experimental Autoimmune Encephalitis
ECA	Erythrocyte Aggregate
ECR	Erythrocyte Ratio
EDSS	Enhanced Disability Status Scale
ET-1	Endothelin-1

ETDRS	Early Treatment in Diabetic Retinopathy Study
FOV	Field of View
GCIPL	Ganglion Cell – Inner Plexiform Layer
GCL	Ganglion Cell Layer
Gd	Gadolinium
HIF-1α	Hypoxia-inducible Factor 1 alpha
Hz	Hertz
ID	Inner Diameter
ILM	Inner Limiting Membrane
INL	Inner Nuclear Layer
IPL	Inner Plexiform Layer
IRT	Inner Retinal Thickness
IRC	Inner Retinal Cyst
IS	Inner Segment
L	Litres
LDF	Laser Doppler Flowgraphy
LSFG	Laser Speckle Flowgraphy
mm	Millimetre
MMO	Microcystic Macular Oedema
MRI	Magnetic Resonance Imaging
ms	Milliseconds
MS	Multiple Sclerosis
nm	Nanometres
NO	Nitric Oxide
NVU	Neurovascular Unit

OCT	Optical Coherence Tomography
OCTA	Optical Coherence Tomography Angiography
OD	Outer Diameter
ODR	Optical Density Ratio
OLM	Outer Limiting Membrane
ON -	Optic Neuritis Negative
ON	Optic Neuritis
ON +	Optic Neuritis Positive
ONH	Optic Nerve Head
ONL	Outer Nuclear Layer
OPL	Outer Plexiform Layer
OS	Outer Segment
PPMS	Primary Progressive Multiple Sclerosis
PR	Photoreceptors
px	Pixels
RBC	Red Blood Cell
RFI	Retinal Function Imager
RGC	Retinal Ganglion Cell
RI	Resistive Index
RNFL	Retinal Nerve Fibre Layer
RPE	Retinal Pigment Epithelium
RRMS	Relapsing-Remitting Multiple Sclerosis
SBP	Systolic Blood Pressure
SD	Standard Deviation
SD-OCT	Spectral Domain Optical Coherence Tomography

SLD	Super-Luminescent Diode
SLO	Scanning Laser Ophthalmoscopy
SPMS	Secondary Progressive Multiple Sclerosis
T1	T1 Weighted Image
TIF	Tagged Image File Format
UV	Ultraviolet
WBC	White Blood Cell
WCSA	Wall Cross Sectional Area
WLR	Wall to Lumen Ratio
WT	Wall Thickness
XT	X Time
µm	Micrometre

Introduction

1.1 Multiple Sclerosis

1.1.1 Overview

Multiple sclerosis (MS) is a chronic inflammatory demyelinating disease of the central nervous system (CNS). Typically, patients who develop MS present with clinically isolated syndrome (CIS), where patients experience only one episode of neurological symptoms which lasts 24 hours or more. In order for the patient to be diagnosed with MS, they must have at least one neurological relapse in addition to other clinical, laboratory and radiological findings (Thompson et al, 2017). Most patients with a single clinical episode constituting a CIS, usually involving the optic nerve, spinal cord or brainstem, that also have abnormal brain imaging will go on to experience further disease activity and develop clinically definite MS (Brex et al, 2002). Subsequently, most MS patients will experience "relapses" of neurological disability that are followed by complete or incomplete recovery, and are diagnosed with relapsing-remitting MS (RRMS). Relapses without complete recovery can cause significant disability accumulated over time. Over time, approximately 15-30% of RRMS patients will start to chronically accrue disability without clinical recovery, a disease type called secondary progressive MS (SPMS) (Thompson et al, 2018) (Figure 1.1), as it follows the initial relapsing phase. This is in contrast to a small minority of MS patients (approximately 15%) who present as primary progressive MS (PPMS), meaning they initially present with this progressive state of continuous clinical deterioration without recovery. Secondary progressive (SP)MS can be characterised into active, where there may be some evidence of relapses or new lesions on MRI, or inactive, where these indicators are absent (Lublin et al, 2014). Whilst most of the long-term disability experienced by MS patients is

accrued in the progressive states of the disease, there is still a sparsity of effective treatment options for these patients.

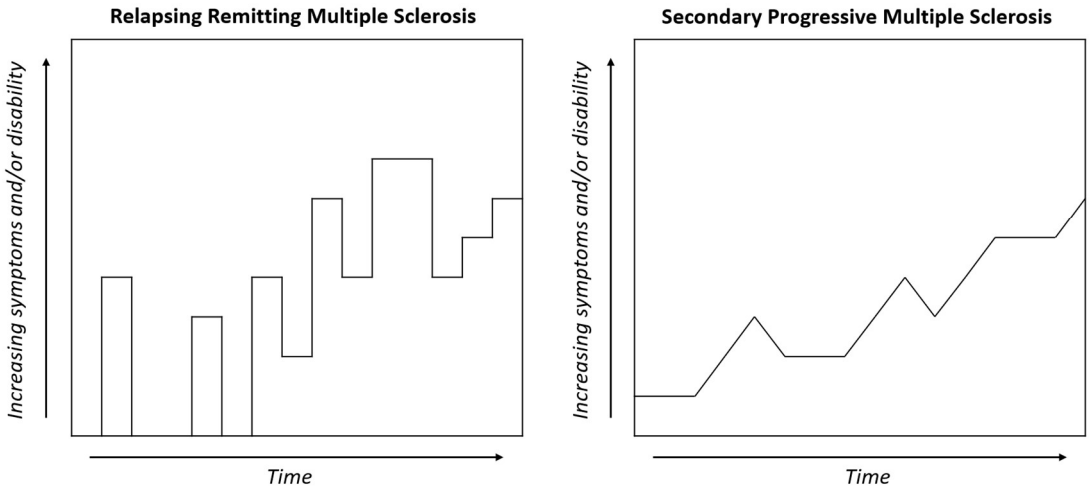

Figure 1.1: Description of disease course in relapsing remitting and secondary progressive multiple sclerosis. Adapted from Holland *et al* (2010).

1.1.2 Pathobiology of MS

The term "multiple sclerosis" derives from the original description of the disease as presenting with numerous sclerotic or scar-like lesions which develop in the white matter of the brain and spinal cord (Charcot, 1868; Pearce, 2005). These lesions are formed by acute focal inflammatory demyelination with limited remyelination, leading to axonal damage and functional loss. Demyelination refers to damage and loss of the myelin sheath, which is formed and maintained by oligodendrocytes and is essential for saltatory conduction in nerves. Neuropathological studies of MS patients show various typical aspects of MS associated CNS injury, consisting of neuronal and axonal loss, demyelination, oligodendrocytic damage and death and remyelination. The injury and loss of oligodendrocytes have been proposed to be important drivers of subsequent neuronal dysfunction and death.

1.1.3 Risk Factors and Triggers of MS

Although inflammation of the CNS is seen to be the primary initiating event in MS, the specific events that trigger this inflammation are still unknown. MS is thought to be triggered by a combination of lifestyle and environmental factors in an individual with a complex genetic risk profile for MS (Waubant et al, 2019).

One of the most prominent environmental factors in MS is geographic location. There is a latitudinal gradient of MS risk, where the prevalence increases with increasing distance from the equator. This effect has a number of possible explanations, most notably; genetic influence, vitamin D levels and UV radiation. MS has a significant familial recurrence rate, with first degree relatives having a higher risk of MS (2-5%) (Robertson et al, 1996; Sadovnick & Baird, 1988). Over 200 genetic risk variants have been identified for MS, each with only a small effect on the disease, yet it is the different combinations of these variants that likely contribute to an individual's susceptibility to MS (Baranzini & Oksenberg, 2017). This genetic component would contribute to the geographic variations in MS, but does not explain how risk among people of common ancestry changes when they migrate to areas of low or high risk (Hammond et al, 2000). This change of risk also only applies when an individual migrates before the age of 15, suggesting exposure to environmental factors early in life plays an important role in the disease's development (Ahlgren et al, 2012; Gale & Martyn, 1995). Increased vitamin D levels before the age of 20 are associated with a reduced risk of developing MS later in life (Munger et al, 2006). As vitamin D synthesis is dependent on UV radiation, the environmental risk factor of geographic location is possibly mediated by vitamin D exposure. Vitamin D is known to have broad-ranging effects on the immune system through suppression of B- and T- cell proliferation (Aranow, 2011), but UV radiation is also known to support the immune system, independent of its impact on

vitamin D by actions such as activation of B and T regulatory cells (Byrne & Halliday, 2005; Schwarz, 2008).

It has also been suggested that exposure to particular viruses could cause an autoimmune effect which initiates the MS process. Infection with Epstein-Barr Virus (EBV), a herpes virus widely present in the wider population (Balfour et al, 2013), has been associated with a higher risk of developing MS (Ascherio & Munger, 2007). The reasons for this association are unclear. EBV could have a specific effect on immune regulation, or its effect could be the result of "molecular mimicry" where a foreign antigen shares genetic or structural similarities with a self-antigen, and an immune response to the virus inadvertently cross-reacts with myelin to induce demyelination (Lang et al, 2002).

1.1.4 Immune Pathways of MS

There are multiple theories to describe MS pathogenesis. Firstly, damage occurs from the "outside-in", where CNS inflammation is the primary insult of the disease from which all other disease mechanisms follow. Secondly, damage occurs from the "inside-out", where neurodegeneration and microvascular damage causes blood-brain barrier (BBB) dysfunction, with inflammation as a secondary response. Thirdly, that both inflammation and neurodegeneration are independent processes which occur at different rates throughout the disease.

As many successful treatments for the relapsing remitting stage of MS target immune regulation or specific immune cell types it is clear that the immune system plays an essential role in the pathogenesis of MS. The "outside -in" hypothesis of MS describes how the disease could be triggered by the activation of peripheral autoreactive effector CD4 T cells that migrate into the CNS to initiate CNS damage (Malpass, 2012). Once trafficked into the CNS, autoreactive effector CD4 T cells become reactivated and recruit more T cells and

macrophages, causing further damage and establishing the inflammatory lesion. In RRMS, disease activity is primarily driven by formation of new acute focal MS lesions, where T lymphocytes entering the CNS elicit a local immune mediated response that incurs damage primarily to oligodendrocytes. However, inflammation is not only contained to the focal demyelinating lesions, as more subtle, diffuse forms are also seen, such as found in normal appearing white matter (Kutzelnigg et al, 2005). The presence of many different pathologic features in MS implies that the disease is not only inflammatory, but is creating an environment which is neurotoxic.

The "inside-out" model of MS (Stys et al, 2012) suggests that the initial trigger of MS is hypoxia, hypoperfusion and tissue energy failure followed by demyelination, inflammation and white matter loss. Tissue energy failure has been steadily gaining traction in MS research as an important causal factor in MS pathophysiology (Dutta et al, 2006; Dutta & Trapp, 2011; Lazzarino et al, 2017; Lu et al, 2000; Sadeghian et al, 2016). The hypothesis is that poor metabolic function, caused by poor perfusion and mitochondrial failure, creates a neurotoxic environment driving MS neurodegenerative processes. MS has been associated with ischaemic diseases of the brain, such as stroke (Hong et al, 2019) and venous thromboembolism (Christensen et al, 2012), suggesting a role for hypoxia in disease development. However, it is not clear whether decreased microvascular function causes an environment of energy failure which damages oligodendrocytes leading to BBB dysfunction, or is a result of reduced metabolic demand by atrophied tissue. Loss of myelination also causes increased energy demand from axons, especially if a more continuous mode of conduction is restored to the demyelinated axons. Additionally, local production of nitric oxide can result in mitochondrial inhibition, inducing a state of "virtual hypoxia" (Trapp & Stys, 2009). Axonal and neuronal degeneration are therefore key pathological features in the early phases and are potential causal factors of disease. Another potential explanation is that BBB dysfunction may precede immune cell infiltration

(Spencer et al, 2018). In both imaging and histological studies of MS, there is evidence to support this theory of initial BBB breakdown (Dawson, 1916; Filippi et al, 1998). Disruption of the BBB can been detected prior to the presentation of gadolinium (Gd) enhancing lesions, and other clinical and radiological signs of MS (Filippi et al, 1998). Seminal histological characterisation of MS lesions demonstrated that myelin breakdown invariably originated around parenchymal blood vessels (Dawson, 1916), which supports the theory that barrier breakdown is the initiating factor allowing for immune cell infiltration and neural lesion development.

The debate surrounding the exact genesis of MS, whether it is "outside-in" or "inside-out", is complicated by the variability of this disease. MS has a high degree of individual variation in its presentation, severity and progression (Thompson et al, 2018). It is possible that both models are accurate, and in fact take place at different stages of the disease process of MS patients, leading to variability and inconsistencies between patients.

1.1.5 Progression of MS

The exact events that lead to conversion from RRMS to SPMS are not yet known. Some argue that the brain exhausts its capacity to compensate for axonal loss (Trapp & Nave, 2008) as the remaining demyelinated axons have an increased energy requirement to maintain conduction velocity, which drains resources resulting in further cell damage and death (Herndon, 2002). Although focal demyelination is associated with clinical relapses, axonal loss is thought to be the primary cause of permanent disability in MS (Dutta & Trapp, 2011). The secondary progressive phase of MS has often been considered to be a stage where BBB dysfunction is no longer of relevance, and where heightened immune response is "compartmentalised" to the CNS.

The impact of inflammation on disease progression in progressive MS is also less clear. Lesions during the secondary progressive phase exhibit diminished inflammatory activity (Prineas et al, 2001) and circulating immune markers in SPMS patients are dampened (Soldan et al, 2004; Sorensen & Sellebjerg, 2001), yet neurodegeneration persists. While RRMS is related to focal, immune-mediated inflammatory processes that result in new plaque formation, progressive MS has been suggested to be related to more diffuse, global and continuous CNS damage. It is mediated by lower but steady concentrations of inflammatory cells and mediators, that produce a "slow-burning" inflammatory attack on the CNS. Progressive MS is also associated with generalised brain atrophy, caused by diffuse axonal injury and neuronal death, affecting the cortex and even "normal-appearing" white matter. As patients move into the secondary progressive phase, new focal regions of inflammation no longer appear and the remaining lesions grow slowly by radial expansion. Inflammation in this stage however is also not only contained to the focal demyelinating lesions, as diffuse forms are also seen, such as found in normal-appearing white matter (Kutzelnigg et al, 2005). These diffuse inflammatory changes have been shown to correlate with axonal loss leading to neurodegeneration and disability (Frischer et al, 2009). Inflammation is also argued to be compartmentalised in progressive MS as lymph follicle-like structures have been detected in the meninges and perivascular spaces of these patients (Prineas & Wright, 1978; Serafini et al, 2004) and their presence is associated with rapid disease progression and profound brain damage (Magliozzi et al, 2007). Ongoing subtle inflammation such as this may lead to vascular changes such as endotheliopathy (Plumb et al, 2002), causing hypoperfusion and neuronal damage.

1.1.6 Vascular Disease and MS

This low level, underlying inflammation may be associated with generalised vascular dysfunction within the CNS. There are reported associations between vascular disease and MS (Marrie et al, 2016; Roshanisefat et al, 2014; Tettey et al, 2014; Tseng et al, 2015). Vascular comorbidities, such as diabetes, heart disease, hypertension and peripheral vascular disease, are associated with more rapid disease progression in MS (Marrie et al, 2010). The work of Tseng *et al* (2015) suggested there is an increased risk of ischaemic stroke in MS, however a larger cohort study by Roshanisefat *et al* (2014) suggested this may be acute, with no significant risk of stroke one year following diagnosis. Population studies which attempt to correlate vascular events to MS are challenging in these cohorts due to variation of disease and lifestyle impact of disease burden.

Due to the success of immune modulating therapies in RRMS, MS research has been heavily focused on involvement of lymphocytes and other immune cells. However, erythrocytes may also play an important role in MS pathogenesis as a result of impaired antioxidant capacity and altered haemorheology, leading to peripheral oxidative stress and potential ischaemic tissue damage. Markers for oxidative stress in erythrocytes correlate with a higher Enhanced Disability Status Scale (EDSS) score, lesion load and increased disease duration in RRMS (Ljubisavljevic et al, 2014) however it is unclear as to whether this is a cause or effect of the disease. This concept of erythrocytic damage is supported by the high concentration of free serum haemoglobin in SPMS, and its correlation to brain atrophy (Lewin et al, 2016). It is hypothesised that low-grade chronic intravascular haemolysis releases free haemoglobin into the CNS across an already damaged blood-brain barrier along with the breakdown products haem and iron (Lewin et al, 2016). Interestingly, iron loading is a common feature in MS (Adams, 1988; Al-Radaideh et al, 2013; Craelius et al, 1982), and as it accumulates with age (Hallgren & Sourander, 1958) and disease (Bermel et al, 2005; Brass et al, 2006; Zhang et al, 2007) it can further increase oxidative tissue loss.

Iron is mainly stored in oligodendrocytes in the CNS, and with oligodendrocyte death free iron is released into the extracellular space (Hametner et al, 2013), contributing to the iron loading caused by intravascular haemolysis.

Whilst there is an association between multiple sclerosis and vascular pathology, it is difficult to determine the direction of causality. Hypoperfusion and tissue hypoxia could be the result of neurodegenerative processes or it could play a central role in the development of MS and its persistence through the secondary progressive phase.

1.1.7 Hypoxia and MS

There is increasing evidence suggesting that tissue hypoxia is an important factor in MS pathophysiology (Law et al, 2004; Marshall et al, 2016; Sosa & Smith, 2017; Yang & Dunn, 2015). Hypoxia can exacerbate inflammation and vice versa, due to common regulation signals involved in both inflammation and hypoxia responses (Cummins et al, 2006). Therefore, the link between hypoxia and inflammation in MS could be crucial to understanding the disease process. Increased infiltration of inflammatory cells and activation of microglia could also be another cause of reduced oxygen availability (Horstmann et al, 2013; Schroeter et al, 2009), which would lead to a mixed inflammatory and hypoxic phenotype as seen in MS.

MS lesions typically develop in watershed areas of the brain (Desai et al, 2016; Haider et al, 2016), which are most vulnerable to hypoxic damage due to the nature of their blood supply. Consistent with this, MS patients are found to have a reduced cerebral blood flow, even in areas of normal appearing white matter (Adhya et al, 2006; D'Haeseleer et al, 2013). Changes in cerebral perfusion in multiple sclerosis have been noted in multiple sclerosis of all subtypes, and progressive patients in particular show substantial areas of reduced perfusion (Adhya et al, 2006; Law et al, 2004; Rashid et al, 2004). Arterial spin

labelling (ASL), an MRI technique to measure rate and volume of cerebral perfusion, has been used to study this in MS. Bolus arrival time, a measure of haemodynamic function in the brain, as measured with ASL is delayed in RRMS (Paling et al, 2014), and is associated with disability. Cerebral hypoxia is, however, not a ubiquitous feature of MS, as a study on cortical microvascular oxygenation found that although on average there was an increased number of hypoxic regions in MS patients, there were some patients with little to no reduction in oxygenation (Yang & Dunn, 2015).

There is therefore no general consensus on the cause of hypoxia in multiple sclerosis, or whether this is due to a compromised vasculature, and if this is a cause or effect of MS. The temporality of this process is a subject for future work, but it is clear that microvascular damage in MS would be likely to further exacerbate the disease and its symptoms, and may serve as a useful target for MS therapies.

1.1.8 Treatment of MS

There are many challenges facing the development of an effective treatment for SPMS. Defining progression and understanding the disease mechanisms which lead to disability are major barriers to designing clinical trials and identifying therapeutic targets. Recent work has suggested that progressive forms of multiple sclerosis are part of a spectrum of overlapping phenotypes, therefore treatment may be required to target a various number of aspects to be effective.

Many of the drugs successfully used to treat the earlier relapsing remitting phase of MS have been investigated in progressive MS. Many immunomodulating therapies effective in RRMS (e.g. cyclophosphamide, β-interferon, fingolimod, natalizumab, glatiramer acetate) have been found to be ineffective in SPMS (Bornstein et al, 1991; Freedman et al, 2011;

Kapoor et al, 2010; Noseworthy, 1991; Rovaris et al, 2006; Smith & Cohen, 2016). Treatments aimed at neuroprotection (lamotrigine (Kapoor et al, 2010), tetrahydrocannabinol (Zajicek et al, 2013)) have also been ineffective. Ocrelizumab, a drug targeting CD20 markers on B lymphocytes, has however been approved for early progressive MS (Montalban et al, 2017). Mitoxantrone, a chemotherapy agent, has also been approved for use in SPMS with ongoing inflammation (Hartung et al, 2002) however with significant potential side effects, which have to be considered especially in younger patients.

One drug, simvastatin, has shown promise in slowing the progression of inactive disease. As part of a group of drugs widely used to treat hypercholesterolemia, simvastatin has an excellent safety profile ideal for long-term treatment. A phase II randomised controlled trial (MS-STAT) investigated high-dose simvastatin treatment in SPMS due to statin's reported impact on inflammation, yet found no effect of the drug on the immune markers tested (Chataway et al, 2014). Despite this, simvastatin treatment resulted in a ~40% reduction in the annualised rate of brain atrophy over two years of treatment (Chataway et al, 2014). This would suggest another mechanism is responsible for simvastatin's beneficial effect in these patients, which could be explained by statin's purported pleiotropic effects of improving vascular function and reducing oxidative damage (Wang et al, 2008). Although these results are promising, more research is necessary to elucidate the microvascular impact of MS and how treatment pathways could be directed towards microvascular protection and maintenance.

1.2 Eye and Brain Homology

The majority of research focussing on the impact of vasculature in MS has concentrated on cerebral vasculature. However, the cerebral vasculature is difficult to visualise and measure

in detail due to physical boundaries which obscure imaging (i.e. the skull). Non-invasive MRI based techniques to investigate cerebral blood flow, such as ASL, are available but are time intensive and their spatial resolution makes it difficult to pinpoint areas of vascular disturbance (Petcharunpaisan et al, 2010). Due to the anatomical and physiological similarities of retinal and cerebral microvasculature, the retina could be used as a non-invasive surrogate for studying cerebral blood vessels in MS. As the retina is an extension of the diencephalon during embryonic development, the brain and retina share a similar pattern of specialised vascularisation. The result is two separate vascular networks, but with very close anatomical correlations and similar regulatory mechanisms (Risau, 1997; Hughes et al, 2000).

Importantly, although the cerebral and retinal vasculature are virtually identical in structure and function, the retinal nerves are unmyelinated to allow for light to reach the photoreceptors unimpeded. This lack of myelination indicates that fundamental processes of MS pathogenesis would not take place in the retina as in the brain and therefore retinal pathology cannot directly reflect that of the brain. Demyelination outside of the retina, however, may still have downstream consequences to the retinal ganglion cells especially when damage is occurring within the visual pathway. Nevertheless, there are some examples of ongoing MS pathology in the retina in the absence of local myelin and seemingly unrelated to axonal damage, such as that found in the increased rate of retinal vasculitis in MS patients (Ortiz-Perez et al, 2013).

1.2.1 Autoregulation and the Neurovascular Unit

Circulation outside of the CNS is largely under autonomic control where blood flow is altered according to changes in arterial blood pressure. In contrast, blood flow in the brain is maintained at a constant level by altering vascular resistance, a process known as

autoregulation (Lassen, 1959). The retina is similarly autoregulated, ensuring that the dense vascular beds of the retina remain largely unchanged by increases in systemic blood pressure (Luo et al, 2015).

Cerebral and retinal vascular networks consist of tight barrier circulations in order to maintain the strict homeostasis of their vulnerable tissues. This barrier protects the neuronal tissue from exogenous toxins, allows blood composition to be buffered via the endothelium and restricts transport of material and cells across the endothelium. Vascular endothelial cells are a core component of both the blood-brain barrier and blood-retinal barrier. As they are unfenestrated and form tight junctions between cells, they limit transcellular and paracellular transport thus protecting the brain and retina, but they also form an interactive interface to allow for selective transport of essential nutrients into the brain and waste products into the blood.

The supporting cells of both the retinal and cerebral circulations, pericytes, provide structural support and help to establish the blood-retina and blood-brain barriers. Pericytes are the capillary analogue of vascular smooth muscle cells, and their contractile properties contribute to autoregulation in the brain and the retina (Herman & Damore, 1985). Unlike retinal pericytes, cerebral pericyte's phagocytic ability acts as a second line of defence (Rucker et al, 2000; Thomas, 1999). Pericytes mechanically regulate vessel wall integrity, therefore pericytic loss is known to lead to vessel permeability and tissue damage in both the brain and the eye (Trost et al, 2016). Retinal pericytes also cover more of the retinal network than their cerebral counterparts (Cogan & Kuwabara, 1984; Frank et al, 1990).

Endothelial cells and pericytes are also essential elements within the multicellular system known as the neurovascular unit (NVU) (Figure 1.2) (Stamatovic et al, 2008). Within the brain, the neurovascular unit consists of the blood vessels themselves in conjunction with neurons, astrocytes, pericytes and microglia (Hawkins & Davis, 2005; McConnell et al,

2017). The retina has a very similar structure consisting of the blood vessels in conjunction with retinal ganglion cells, microglia, astrocytes, Müller cells and pericytes (Metea & Newman, 2007). An important function of the NVU is in performing neurovascular coupling,, to protect the delicate cerebral tissue from changes in systemic blood pressure and to ensure adequate perfusion to neural tissue according to local neuronal demand (Muoio et al, 2014).

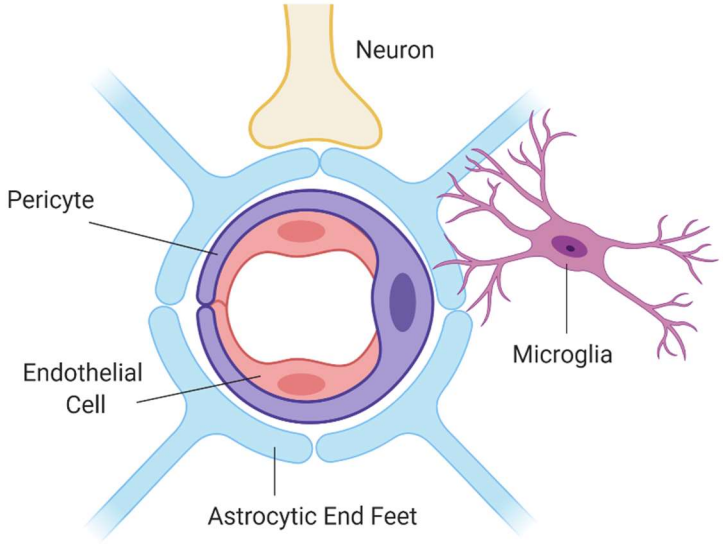

Figure 1.2: Schematic diagram of the neurovascular unit in the brain. Created with Biorender.com.

The cerebral vasculature is therefore composed of a number of different components which are common to both the brain and the eye, suggesting the retina could serve as a proxy for the brain in imaging. Techniques are available for imaging the cerebral vasculature, however they are limited in their resolution. Specialist MRI techniques such as blood oxygen level dependent (BOLD) imaging and ASL imaging have been developed for visualisation of perfusion and haemodynamic functions in the brain, however the spatial resolution of these techniques, based on acquisition time and spacing is low (up to 1mm), prohibits visualisation of small vessels or individual capillaries (Detre & Wang, 2002) . As

the majority of the retina is transparent to allow light to reach the photoreceptors, the vascular layers of the eye can be more readily visualised non-invasively, and multiple modalities have been developed in order to investigate both structure and function to micrometre resolution in the retina. Due to its accessibility and similarity to the brain, we could therefore use the retinal vasculature to explore how multiple sclerosis affects both tissues. In order to estimate the impact of microvascular changes in SPMS using the retina, we must first understand normal retinal microvascular structure and function.

1.3 Retinal Anatomy

The human eye is composed of three concentric layers; the external layer, made up of the sclera and cornea, the middle vascular layer consisting of the choroid and the greater part of the ciliary body and iris and the innermost layer which is composed of the retina and the neuro-epithelia of the ciliary body and iris (Junqueira et al., 1998). The retina is the light sensitive layer at the back of the eye which converts light energy to electrical signals, and it consists of; the external limiting membrane (ELM), the photoreceptor layer (PRL), the outer nuclear layer (ONL), the outer plexiform layer, the inner nuclear layer (INL), the inner plexiform layer (IPL), the ganglion cell layer (GCL) and the retinal nerve fibre layer (RNFL), consisting of the ganglion cell axons (Figure 1.3). The final structure at the interface of the retina and vitreous body is the internal limiting membrane (ILM) which is maintained by the Müller cells (Kolb et al, 2005).

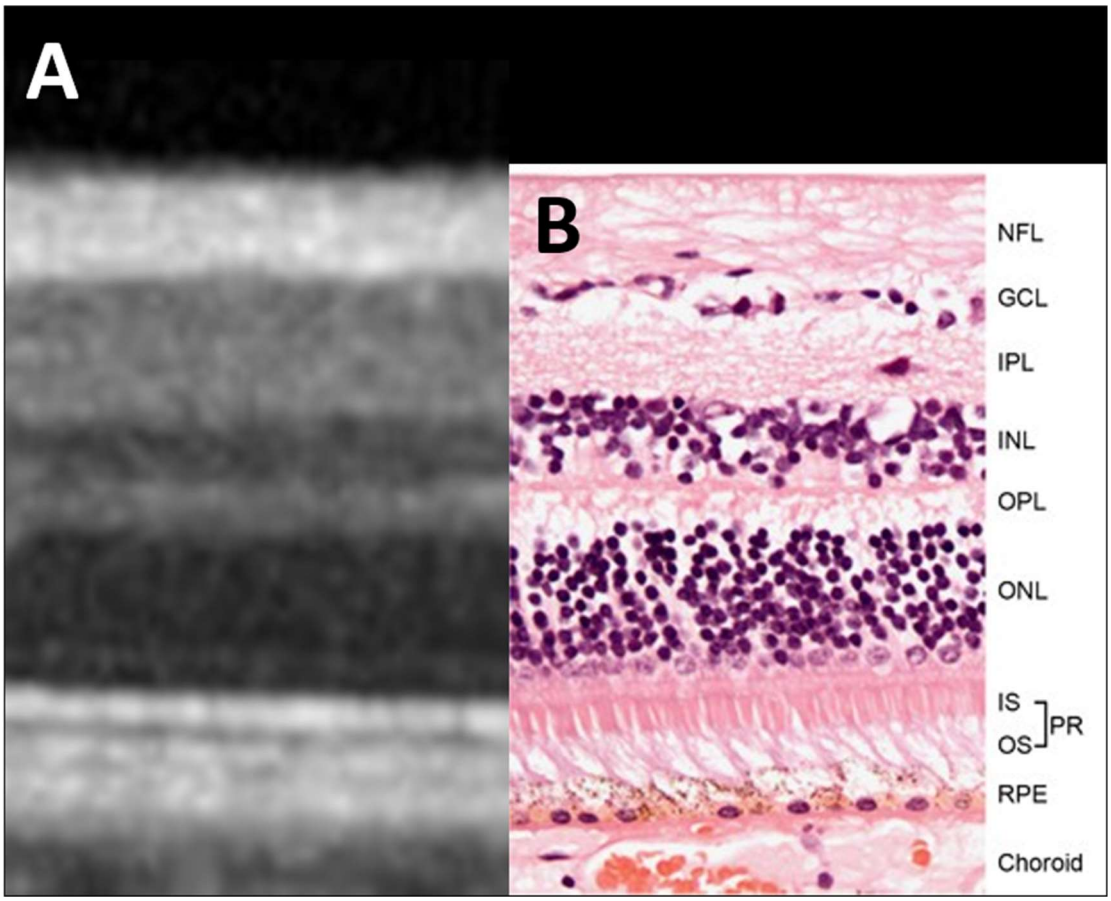

Figure 1.3: Cross-sectional histology of the human retina (B) approximately aligned with retinal layers imaged with optical coherence tomography (OCT)(A). NFL: Nerve Fibre Layer, GCL: Ganglion Cell Layer, IPL: Inner plexiform Layer, INL: Inner Nuclear Layer, OPL: Outer Photoreceptor Layer, ONL: Outer Nuclear Layer, IS: Inner Segment, OS: Outer Segment, PR: Photoreceptors, RPE: Retinal Pigment Epithelium. Adapted from Richardson *et al* (2017).

The photoreceptor layer contains the rods and cones, the photosensitive cells of the retina. Light entering the eye, on its path to the photoreceptors, must first travel the thickness of the retina, before striking and activating the photoreceptors leading to visual phototransduction, where light is converted to electrical energy. Bipolar cells found in the inner nuclear layer are responsible for vertical transmission of information from the photoreceptors to the neuropile of the inner plexiform layer, where their axon terminals connect with amacrine cells which integrate and modulate the information for the ganglion cells, and connect with the dendrites of ganglion cells themselves. The ganglion cell layer is

the innermost cellular layer of the retina and is comprised of retinal ganglion cells (RGCs) whose axons track along the retinal surface to form the retinal nerve fibre layer (RNFL) and exit the eye via the optic nerve. The optic nerve is visible through ophthalmoscopy as the optic nerve head, otherwise known as the optic disc. The optic nerve is unusual as its axons are initially unmyelinated, and only become myelinated as they exit the eye through the lamina cribrosa. Horizontal cells in the outer plexiform layer act as laterally interconnecting neurons as their dendrites connect the pedicles of cones and their axon terminals connect with the spherules of rods. The supporting cells of the retina are found throughout the neural retina and consist of a variety of neuroglia including astrocytes, microglia and Müller cells (Kolb et al, 2005). The retina is finally enclosed at the nerve fibre layer by the inner limiting membrane which separates it from the vitreous humour of the eye anteriorly. (Junqueira et al., 1998)

1.3.1 Retinal Blood Supply

The retinal circulation must provide a system which supplies nourishment and removes waste effectively without compromising vision. This requirement is satisfied by two discrete and independently formed vascular systems; the retinal and choroidal blood vessels. Functionally there is little overlap between these systems. The sources of blood to the retinal and choroidal systems are the central retinal artery, posterior ciliary artery and its muscular branches (Hayreh, 1962). The central retinal artery branches prior to emerging from the optic nerve into superior and inferior arteries (Figure 1.4). As they branch out towards the temporal retina the arteries respect the horizontal midline and therefore supply the superior and inferior hemispheres independently.

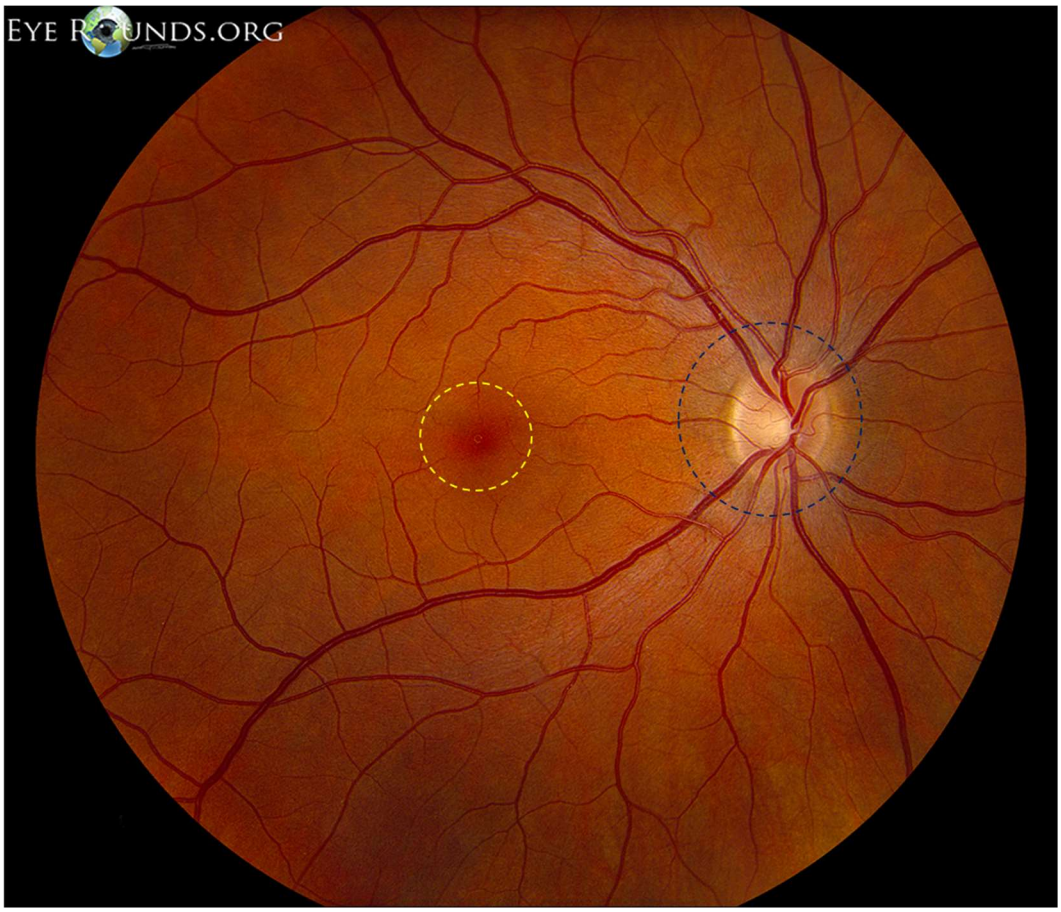

Figure 1.4: Example of a 50-degree colour fundus photograph of a healthy right eye. The optic nerve (blue dashed circle) and blood vessels radiating outwards from it are visible. Blood vessels branching toward the macula (yellow dashed circle) are also visible. Adapted from Ophthalmic Atlas Images by EyeRounds.org, The University of Iowa.

Large vessels entering and exiting the retina are embedded in the RNFL and GCL to support inner retinal function as the superficial vascular plexus. As the vascular tree descends to smaller vessels and ultimately capillaries these give rise to a laminar meshwork. Included in this are the intermediate and deep capillary plexuses, formed of a layer of capillaries above and below the INL, respectively (Weinhaus et al, 1995) (Figure 1.5). The number of layers which form the laminar mesh work depend on location, as in the periphery it merges to form only one layer and in the centre of the retina it comprises of three layers (Campbell et al, 2017). These spatial differences correspond to disparities in both tissue oxygen demand and retinal thickness in these regions.

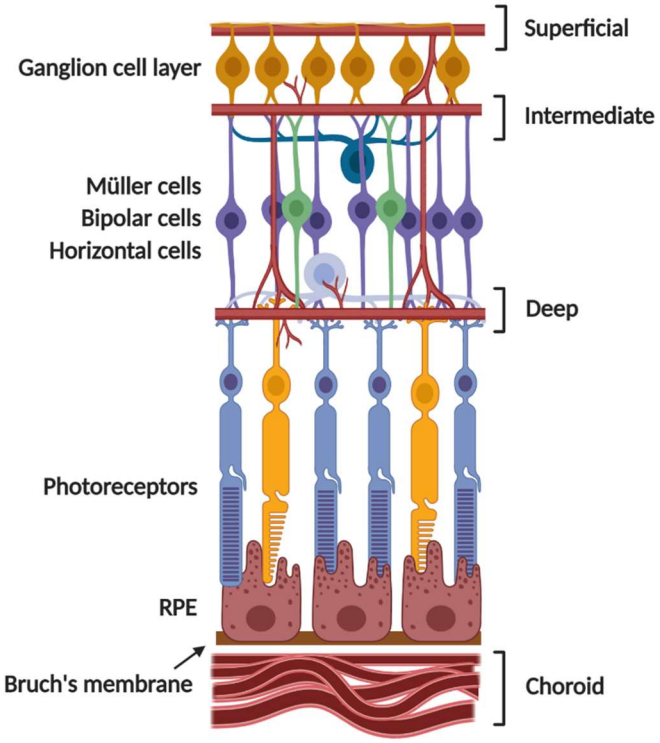

Figure 1.5: Diagram of the retinal vascular layers, including the superficial, intermediate and deep vascular plexi. The choroidal plexus is found beneath the RPE. Created with Biorender.com

Retinal capillaries are formed of a layer of endothelial cells encapsulated by a basement membrane in which pericytes are embedded. Retinal capillaries are an important element of the blood-retinal barrier (BRB), the tightly controlled boundary between the intravascular and extravascular environment in the retina (Martin et al, 2000). Pericytes are essential for contractile function, endothelial barrier integrity and endothelial cell proliferation (Martin et al, 2000). Beyond the lamina cribrosa there is no autonomic control of the retinal vasculature, therefore retinal capillaries are dependent on pericytes and smooth muscle cells for local autoregulation of blood flow. There is an approximate 1:1 ratio of pericytes to endothelial cells allowing for specific neurovascular coupling (Frank et

al, 1990). The basement membrane between pericytes and endothelial cells is also very thin, allowing for increased communication between the two.

The retinal venous system is interdigitated with the arterial vasculature and venous blood leaves the retina via the central retinal vein. The outer retina has no blood vessels and is provided with oxygen, nutrients and waste disposal functions by the choroidal circulation.

1.4 The Retina in Multiple Sclerosis

The retina is frequently affected by multiple sclerosis. Optic neuritis, inflammation of the optic nerve, is the presenting feature in 15-20% of MS patients (Arnold, 2005) and can cause long term damage to both the structure and function of the retina. Atrophy of the RNFL and GCL as measured with optical coherence tomography (OCT) has been consistently demonstrated as an indication of neurodegeneration in multiple sclerosis. The application of OCT in detecting, monitoring and understanding neurodegeneration has been established as a useful structural biomarker in the disease (Costello & Burton, 2018; Gordon-Lipkin et al, 2007; Petzold et al, 2010). OCT measurements of ganglion cell and inner plexiform layer (GCIPL) atrophy have been shown to correlate to brain atrophy from MRI derived measurements of white matter, grey matter and thalamic volume (Gordon-Lipkin et al, 2007; Saidha et al, 2015). RNFL thinning is also known to be present in each type of multiple sclerosis, regardless of history of optic neuritis (Petzold et al, 2010; Zamzam et al, 2015), demonstrating that retinal structural changes can occur in MS even in the absence of optic nerve damage. Although retinal thinning is strongly linked to clinical deterioration, retinal changes as a direct response to MS treatment are not consistently shown. A retrospective study indicated that the rate of GCIPL thinning was noticeably reduced following the use of certain MS treatments, i.e. aggressive natalizumab therapy, although this was not the case when compared to treatment with the conventional first

line therapy of glatiramer acetate and interferon (Button et al, 2017). Nevertheless, inner retinal changes can provide a direct reflection of cerebral consequences of the disease.

Retinal damage subsequent to inflammation of the optic nerve is unsurprising as the unmyelinated fibres of the optic nerve extend across the retina to form the RNFL. However, recent studies have shown it is not only the neuronal layers which are damaged in multiple sclerosis. A post mortem study suggested that retinal atrophy and inflammation in multiple sclerosis extends further into the retina, with INL atrophy seen in 40% of MS patients (Green et al, 2010). In this study, severity of retinal atrophy was negatively correlated with post-mortem brain weight and a trend was found towards an association between severe retinal atrophy and longer disease duration, suggesting global damage to the CNS and retina occurring over time (Green et al, 2010). The extent of retinal atrophy in this group also demonstrates degeneration in unmyelinated populations, implying damage is not due to demyelination alone and suggests that the disease could have effects throughout the CNS, not just at the site of pathological lesions (Green et al, 2010). The prevalence of retinal periphlebitis in MS patients also challenges this assumption of demyelination before degeneration. Retinal periphlebitis, a form of vasculitis, occurs in 10-35% of patients with MS and is associated with severity of disease (Ortiz-Perez et al, 2013). Retinal sheathing, a presenting feature of retinal periphlebitis, has been noted as a significant finding in the retinal periphery of optic neuritis patients and is associated with patients who are more likely to subsequently develop MS (Lightman et al, 1987). As the axons which form the RNFL are unmyelinated, retinal periphlebitis is a controversial issue as it suggests that there is an inflammatory process occurring in MS which precedes or is not linked to demyelination. Microglial activation, an indication of inflammation, has been directly associated with retinal cell death in experimental autoimmune encephalitis (EAE) (Horstmann et al, 2013), the foremost animal model of MS, and has been shown to precede the onset of clinical symptoms (Fairless et al, 2012). Additionally, studies in EAE have

suggested that although optic neuritis is the main trigger for RGC death it also occurs independently of histopathological changes in the optic nerve (Hobom et al, 2004), supporting the idea of a mixed model of pathogenesis.

Previous research has detected subtle but significant effects of MS on the retinal microvasculature. A study using the retinal function imager (RFI), which uses rapid full field stroboscopic illumination to image red blood cells in the retina, found increased rigidity in the retinal vessels of RRMS patients (Kochkorov et al, 2009). There was no significant difference between optic neuritis (ON) positive (+) and ON negative (-) patients, suggesting that major inflammatory events in the eye had no impact on this change. Perfusion of the retina, calculated as the retinal blood flow divided by the corresponding tissue volume, was also shown to be reduced in MS patients compared to controls (Liu et al, 2019), and both blood flow velocity and volume as measured with the RFI were reduced in the perifoveal region in MS patients (Jiang et al, 2016). However, both of these studies investigated patients with relapsing remitting MS or with clinically isolated syndrome so do not inform us of what the situation is in secondary progressive MS. This data suggests there are multiple sites of damage in the retina, and therefore possibly throughout the CNS, as a result of multiple sclerosis which are not limited in cause to demyelination. As purported effects in the retinal vasculature are subtle and subclinical, high resolution techniques must be employed to investigate both structure and function of blood vessels in these patients.

1.5 Optical Coherence Tomography

Optical coherence tomography (OCT) is a non-invasive imaging technology which allows us to distinguish individual retinal layers. OCT can be used to quantify retinal thickness as accurately as histologically derived data (Blumenthal et al, 2009), allowing us to investigate the retina *in vivo* in a similar manner. Although not strictly a form of vascular imaging, OCT

is used regularly in multiple sclerosis management and has become increasingly prominent in the diagnosis and monitoring of MS symptoms.

OCT is a form of low coherence interferometry, in which an initial light beam is split to a reference arm and sample arm. A strong interference occurs when both reflected beams recombine with an equal path length within the coherence length of the light source. The pattern of interference allows us to create a reflectivity profile, and the resulting intensity information is used to construct the OCT images. Spectral domain OCT (SD-OCT) uses frequency-based signal detection to enhance axial resolution and scanning speed (Drexler et al 2001) (Figure 1.6). Using SD-OCT we can obtain high resolution 3D volumetric scans of the retina quickly and non-invasively.

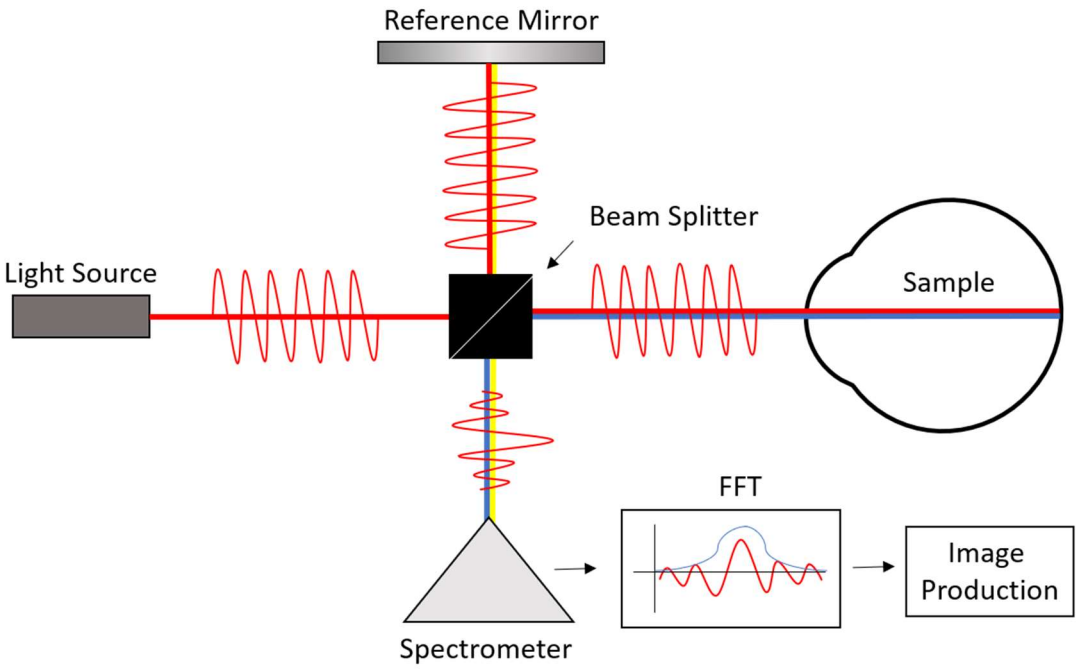

Figure 1.6: Schematic of SD-OCT. FFT: Fast Fourier Transform. Adapted from Dubis (2012).

OCT has been extensively used to study the inner retinal layers in multiple sclerosis. The lateral resolution of most commercial SD-OCT devices is 4-7µm and a retinal ganglion cell is around 5-20µm (Dacey, 1993; Hebel & Hollander, 1983), therefore SD-OCT allows us to image at a scale which reaches the cellular level in individual retinal layers. This kind of

resolution is not possible using even high-resolution T1 weighted MRI images used to measure brain atrophy, where $1mm^3$ is the smallest voxel achieved (Rocca et al, 2017). Additionally, reproducibility of SD-OCT scans is excellent (Syc et al, 2010), and standardised quality control criteria have been implemented to ensure the integrity of OCT derived data in MS (Schippling et al, 2015).

Although it also has to be considered that the retina and its activity is not a direct reflection of the CNS, there is some evidence through OCT that it provides a convenient surrogate. RNFL thickness has been associated with brain atrophy in MS (Gordon-Lipkin et al, 2007) and GCIPL loss have been shown in a longitudinal study to mirror the rate of whole brain atrophy over time (Saidha et al, 2015). RNFL thickness measured by OCT can even be used to identify patients most at risk of disability progression (Martinez-Lapiscina et al, 2016). Although not included in the 2017 revision of the McDonald Criteria, the international diagnostic definition of MS, the authors highlighted research into this field as a high priority (Thompson et al, 2017), demonstrating the potential of OCT to transform MS diagnosis and management.

The use of OCT has also been crucial in identifying previously undefined pathological processes in the MS retina. Microcystic macular oedema (MMO), a structural abnormality in the inner nuclear layer which can be seen with high resolution OCT, has a higher prevalence in MS patients. The presence of MMO is suggested to be an indicator of disability and disease progression (Gelfand et al, 2012; Saidha et al, 2012). MMO is defined as lacunar areas of hyporeflectivity with a cystic appearance (Brar et al, 2010) and although described as “oedema”, this may be a misnomer as there is much speculation as to the aetiology of MMO. There are three main causative mechanisms which have been proposed; “black holes” caused by transsynaptic degeneration (Gills & Wadsworth, 1966), disturbance of fluid homeostasis as the responsible cells die or become dysfunctional (Saidha et al,

2012), or the result of combined loss of ganglion cells and increased vitreal traction on the macula (Lujan & Horton, 2013).

OCT allows us to visualise the individual tissue layers and retinal abnormalities such as MMO non-invasively and at high resolution. The knowledge gained from OCT allows us to learn more about the cellular environment in which the vasculature operates, which we can then compare to structural and functional measures of the vasculature itself.

1.6 OCT Angiography

Different methods have been developed to detect and measure retinal blood vessels and perfusion in both invasive and non-invasive manners with varied levels of resolution. The gold standard technique for visualising retinal blood vessels in clinical ophthalmology is fluorescein angiography, which allows for real time investigation of vascular integrity. This technique is however invasive and unable to resolve individual capillary layers using standard protocols. Non-invasive techniques such as laser doppler flowmetry (LDF) and laser speckle flowgraphy (LSFG) can be used to measure retinal blood flow and perfusion, but as yet are too variable to use clinically (Avila et al, 1998; Sugiyama et al, 2010). Colour doppler imaging (CDI), although non-invasive and used clinically for measurement of retrobulbar blood flow, does not have the required resolution for retinal microcirculation (Dimitrova & Kato, 2010).

OCT angiography (OCTA) can be used to non-invasively generate volumetric images of retinal vasculature to the capillary level. OCTA forms angiographic images by comparing the signal between repeated OCT scans in order to construct a volumetric map of blood flow within the retina (Figure 1.7). OCTA is non-invasive, repeatable and able to resolve individual capillaries in separate vascular layers of the retina, making it a powerful tool for

both research and clinical practice, albeit with the potential for artefacts. It is increasingly being used in the investigation of disease and discovery of new endpoints (Bhanushali et al, 2016; Wang et al, 2019), as well as in developing a greater understanding on normal retinal vascular anatomy *in vivo* (Campbell et al, 2017). The volumetric maps are segmented into individual vascular layers, most commonly the superficial vascular plexus and deep vascular plexus in the retina. From these images vessel density (the number of pixels covered by vessels) and flow index (the vessel density compared to a normative database) can be calculated.

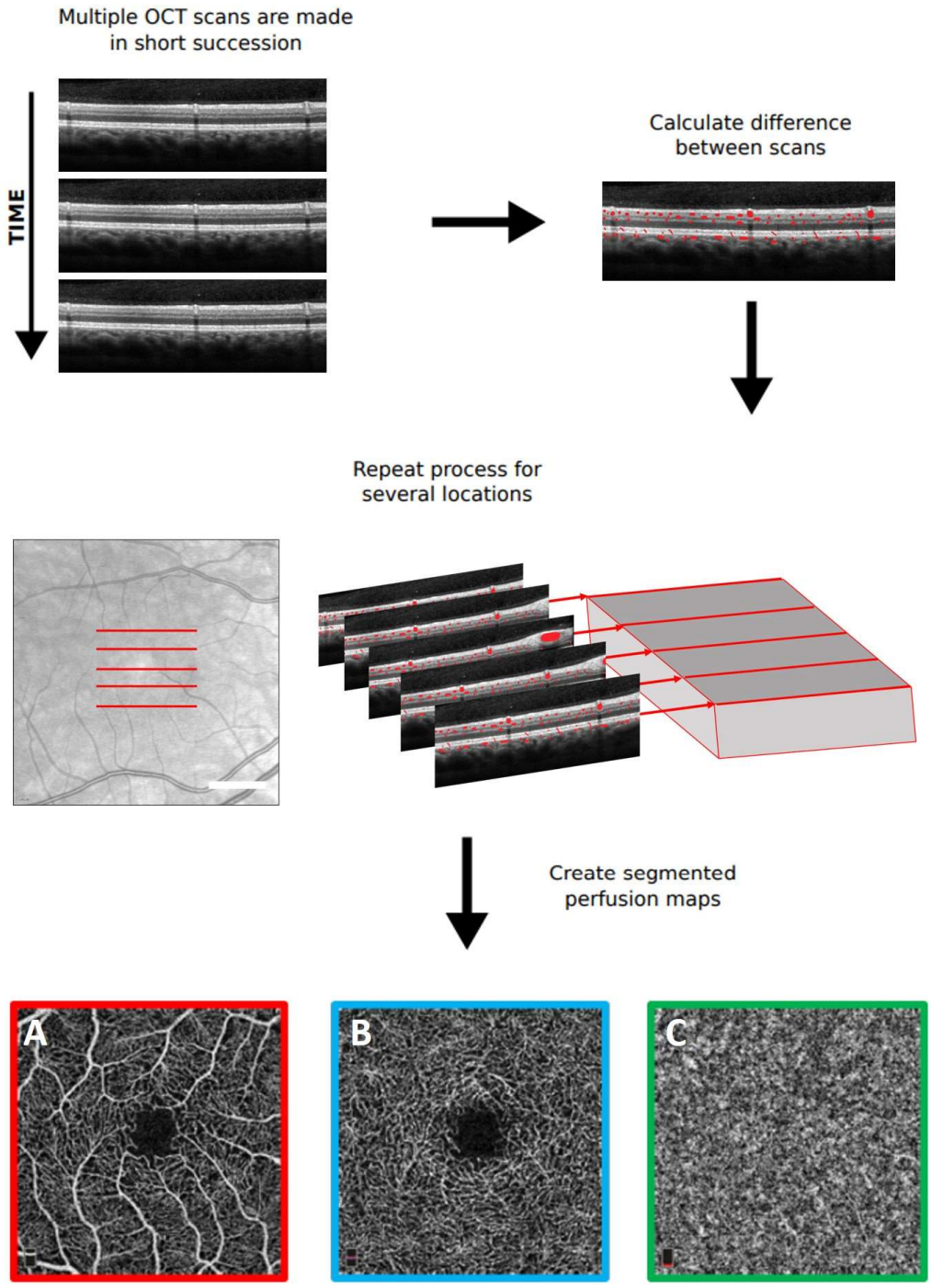

Figure 1.7: OCTA Process Diagram. OCTA images are generated by collecting multiple OCT scans in the same location (A), calculating the difference between these scans (B) and thresholding the result (C) to remove noise. This single image represents points of movement, and therefore blood flow, in this location. This process is repeated at multiple locations across a specific retinal region which allows us to generate “maps” of perfusion across the region. The perfusion maps in this diagram (E) demonstrate segmentation covering a 3x3mm region of the superficial (red), deep (blue) and choroidal (green) plexi. Scale on IR image: 1mm

OCTA studies have nearly all shown a reduction in retinal vessel density in MS patients compared to healthy control subjects in the macula (Feucht et al, 2019; Jiang et al, 2020; Lanzillo et al, 2017; Murphy et al, 2019), the optic nerve (peripapillary region) (Spain et al, 2018; Wang et al, 2014) or both (Ulusoy et al, 2020; Yilmaz et al, 2019), despite variation between OCTA devices used. However, the regions most affected by vessel rarefaction and to what extent neurodegeneration plays a role in this change is under debate. It is not consistently shown whether optic neuritis itself has a direct effect on the retinal microvasculature, with some studies reporting a reduction in vessel density in ON positive eyes and some not. It is also unclear as to whether vessel damage is constrained to the purported source of inflammatory damage, the optic nerve, or extends as far as the parafovea. There is also some debate as to whether this reduction in vessel density, or 'capillary dropout', precedes axonal and ganglion cell loss or is a result of it.

One of the largest cohort studies of vessel density in MS found a significant reduction in superficial plexus density in the macula of MS eyes while the deep vascular plexus remained unaffected (Murphy et al, 2019). Further, ON+ eyes showed a significant reduction in density compared to ON- eyes. When ON- eyes were separated and compared to control eyes, the difference was smaller but still significant. Although this was a large cohort it represented patients in a relatively early stage of MS, it does not represent results from progressive patients. Several smaller studies have also been conducted investigating density at different locations in the retina and at different stages of MS. Parafoveal vessel density is reduced across MS eyes (Feucht et al, 2019; Lanzillo et al, 2017; Ulusoy et al, 2020; Yilmaz et al, 2019) and can be correlated with clinical results in both the retina (Murphy et al, 2019) and choroid (Feucht et al, 2019). This reduction in parafoveal vessel density has also been correlated with inner retinal layer thickness in ON+ patients, indicating a close association between vessel rarefaction and cell death (Feucht et al, 2019). One study however has shown no significant reduction in parafoveal flow index in MS

patients, but a significant reduction in peripapillary flow index, although they do not report on vessel densities (Wang et al, 2014). This mounting evidence of parafoveal vessel damage in MS, even in early MS cohorts, suggests microvascular damage is occurring not only at the optic nerve head, where degeneration occurs early in MS, but further downstream also.

The studies discussed here largely either do not discriminate by subtype or use only patients from the early phases of MS (Table 1.1), therefore there is a gap in knowledge surrounding the retinal vascular architecture and function in the secondary progressive phase and whether the vasculature changes with progression between different MS disease subtypes. Regardless, these results suggest that vessel rarefaction and capillary dropout is a common feature among all stages of multiple sclerosis, and should be investigated further. If these vascular changes are widely prevalent in the MS retina, even at a subtle subclinical level, they will have profound effects on the function of retinal blood vessels and their capacity to deliver adequate oxygen and nutrients. The activity of blood vessels and the cells within cannot be measured using OCT or OCTA, therefore other techniques are required.

Authors	CIS	RRMS	SPMS	Did not distinguish
Wang et al, 2014	-	-	-	X
Lanzillo et al, 2017	X	X	-	
Spain et al, 2018	X	X	X	X
Yilmaz et al, 2019	-	X	-	
Murphy et al, 2019	X	X	-	
Feucht et al, 2019	X	X	-	
Ulusoy et al, 2020	-	X	-	

Table 1.1: MS subtypes investigated in OCTA studies

1.7 Adaptive Optics Enhanced Retinal Imaging

Adaptive optics (AO) is a technique originating from astronomy whereby image quality is improved to theoretically diffraction-limited levels by compensating optical aberrations. Correcting for these optical imperfections has allowed non-invasive *in vivo* visualisation of a number of retinal cell types. There are three main components to an ophthalmic AO imaging system: a wavefront sensor for measuring the eye's aberrations, a corrective element which is typically a deformable mirror and an imaging device. (Figure 1.8)

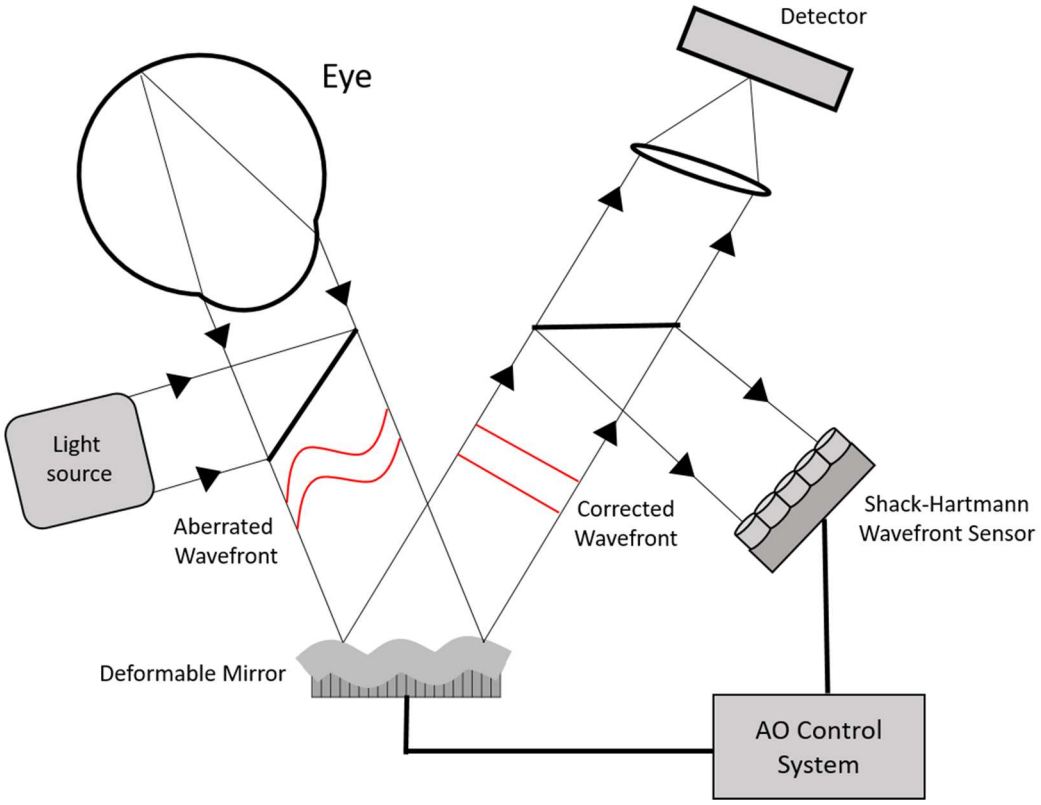

Figure 1.8: Set up of a standard adaptive optics ophthalmoscope, based on Gill *et al* (2019).

Adaptive optics has been combined with standard fundus imaging (Liang et al, 1997), OCT (Hermann et al, 2004)and scanning laser ophthalmoscopy (SLO) (Roorda et al, 2002) to enhance resolution of retinal imaging. SLO, which utilises horizontal and vertical scanning mirrors to scan a specific region and create raster images of the back of the eye, can be

coupled with AO (as AOSLO) to produce near diffraction-limited images of the retina. Confocal AOSLO has been used with great effect in ophthalmology to image photoreceptor outer segments in degenerative retinal conditions (Gill et al, 2019). However, highly scattering structures, such as blood cells and blood vessel walls, are challenging to image using confocal AOSLO as the vasculature is deeply embedded into the highly backscattering RNFL. To overcome this obstacle, several groups have looked at the optical signals present in the non-confocal signal (Chui et al, 2012; Scoles et al, 2013). The most used varieties of this non-confocal imaging are offset pinhole, dark field and split detection; all originating from histological light microscopy. Non-confocal imaging in the retina was first utilised by laterally offsetting the aperture in front of the detector, known as “offset aperture”, allowing for detection of light which is not directly captured by the system pupil. Split detection is a progression from this, where light bouncing from either side of the structures imaged is collected using two detectors, as in Figure 1.9, therefore allowing greater detection of structures which do not strongly reflect light towards a confocal pinhole, such as red blood cells and blood vessel walls.

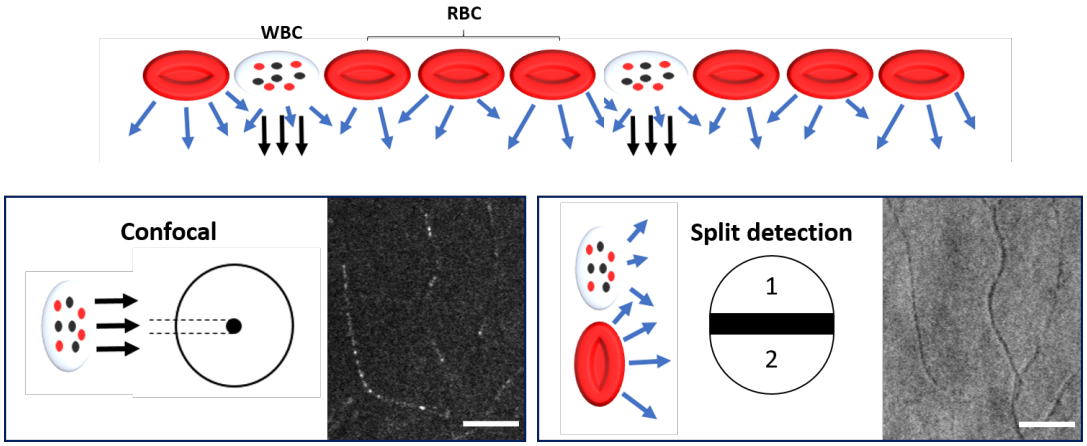

Figure 1.9: Schematic of the different components of blood cells which can be imaged using AOSLO confocal and split detection modes. Blood cells move in single file in capillaries and have diverse appearances using the two techniques. The confocal channel detects light through a small pinhole, where only light which reflects directly back, such as light reflecting off cell components, can be detected. Importantly, red blood cells (RBC) contain no nucleus or other intracellular material capable of reflection in this manner, therefore cells detected in the confocal channel are likely white blood cells (WBC) or RBCs at an angle which allows their cell membrane to be detected. Split detection, on the other hand, detects light which scatters either side of the confocal channel, meaning it can detect cell membranes of blood cells and blood vessel structure. The arrows refer to the direction of light scatter. The blue arrows refer to light multiply scattered from cells and the black arrows indicate light which is reflected directly back towards the detectors. Scale: 50µm.

Using scattered light imaging, such as split detection or offset pinhole imaging, combined with adaptive optics, the smallest capillaries and the blood cells within can be visualised in real time non-invasively (Figure 1.10). The information obtained using AOSLO could be used to calculate blood flow and perfusion in the retina more accurately than previously possible in both health and disease. Imaging techniques coupled with AO have been used to detect sub-clinical abnormalities in diabetic retinopathy (DR) (Burns et al, 2014) and hypertension (Koch et al, 2014) demonstrating the ability of this technique to identify changes never seen before with other imaging techniques, and the potential for AOSLO to do so again in MS.

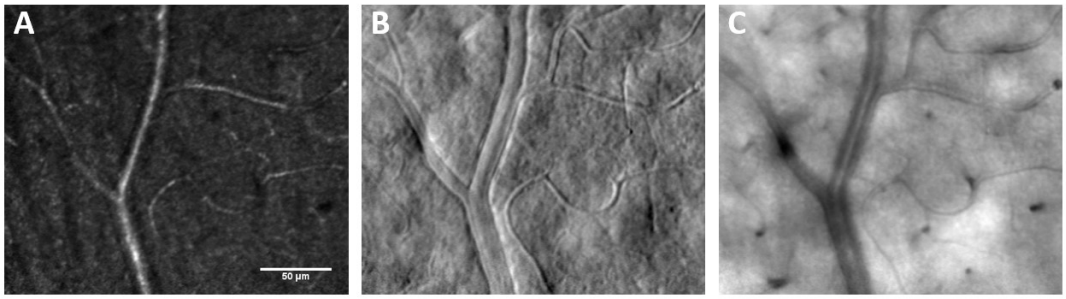

Figure 1.10: Examples of images of the superficial retinal vasculature of a healthy control subject collected using AOSLO split detection. The confocal channel (A) allows us to see material which reflects directly into the system pupil. The split (B) and average (C) images in which vascular structure is now visible are calculated from the direct and reflect channels. Scale: 50µm

1.8 Retinal Oximetry

An essential function of the microvasculature is oxygenation of tissues. Investigating retinal oxygenation in SPMS in combination with the information gained from both structural and functional imaging in the retina will allow us to decipher the interaction between tissue perfusion and metabolic need. Several methods have been used to investigate retinal oxygen saturation, however most are highly invasive or suffer from poor resolution. Direct methods of retinal oxygen saturation measurement, such as oxygen sensitive microelectrodes, are accurate but invasive. MRI based methods, such as BOLD contrast imaging, do not have the resolution required to image the retinal microvasculature. An estimation of retinal oxygenation can be made non-invasively using retinal oximetry. Oximeters such as the Oxymap Retinal Oximeter T1 (Oxymap, Reykjavik, Iceland) use spectrophotometric measurements to determine oxygen saturation in the retina. The Oxymap captures two images of the retina simultaneously using 570nm and 600nm light, which oxy- and deoxyhaemoglobin absorb differently, and determines oxygen saturation by comparing the light absorbance, or optical density, of the blood in the retinal vessels (Figure 1.11). As the ratio of optical densities (optical density ratio – ODR) between the

570- and 600nm wavelengths demonstrates a linear relationship to oxygen saturation, we can use it as an approximation of oxygen saturation within blood vessels.

Saturation values from the Oxymap can be separated into arterial and venular saturation, and one can calculate the difference between them (the arteriovenous ratio) to determine the approximate rate of oxygen uptake at the capillary level. For example, if both arterial and venular saturation is reduced in a disease group compared to controls, it is clear that not enough oxygen is being delivered to the capillary beds. However, if arterial saturation is normal and only venular saturation is increased compared to controls, it suggests that oxygen transfer or uptake is insufficient.

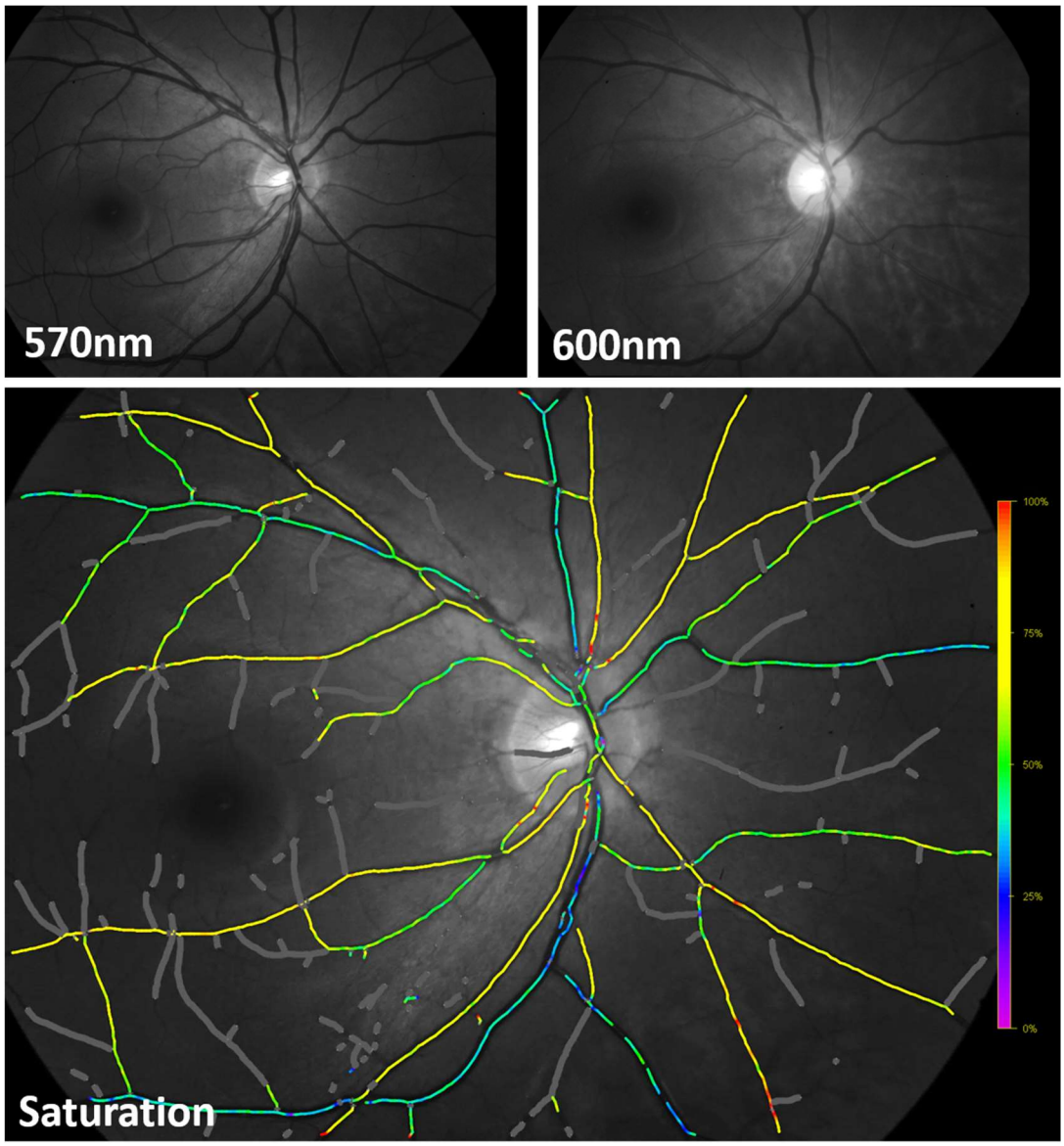

Figure 1.11: Oximetry images from a control patient taken with the Oxymap T1. The difference in light absorbance between images captured at 570nm and 600nm are used to calculate the oxygen saturation of vessels. The colour map demonstrates percentage oxygen saturation from 0% (Purple) – 100% (Red).

Insufficient oxygenation of tissues, hypoxia, has been noted in both histopathological studies and imaging studies of MS *in vivo*. Reduced oxygen saturation levels of the CNS in MS patients have been noted using near-infrared spectroscopy (NIRS), although hypoxic regions were not found in every patient (Yang & Dunn, 2015). Retinal oxygen saturation has also previously been shown to be altered in multiple sclerosis using the Oxymap. An increase in venular saturation was detected in MS patients (n = 8) compared to control

patients, demonstrating poor oxygen uptake of the retina, however the authors did not distinguish between RRMS and SPMS patients so any relation of this result to neurodegeneration could not be established (Einarsdottir et al, 2018). Although the sample size is small, this reduction in oxygen transfer at the capillary level could be explained by either a primary microvascular issue, or a lack of metabolic demand from atrophied tissue.

There are some limitations to using the Oxymap, such as inability to accurately measure small vessels, propensity for image artefacts and variability of results due to age, race and axial length. The Oxymap can only be used for vessels over six pixels (approximately >56μm) in diameter due to measurement variability in narrower vessels. Saturation value accuracy is image quality dependent, making results susceptible to artefacts caused by optical scattering, such as cataracts or vitreous infiltrates. These findings suggest the need for age correction when interpreting cross-section cohorts, but would have less effect on longitudinal studies (Hardarson 2015). The angle of gaze can have a significant impact in saturation results, therefore standardisation of image collection is essential in maintaining repeatability (Palsson et al, 2012). As the technique relies on differential light absorbance, a major contributor to light absorbance in the eye, melanin (Guo et al, 2008), will have a significant effect on results. The varied concentration of melanin pigments in eyes of different racial groups (Hu et al, 2008) mean retinal oximetry measurements vary between them (Mohan et al, 2016). Variability between healthy individuals can also be affected by high myopia (Zheng et al, 2015) and differences in ocular perfusion pressure (Geirsdottir et al, 2012). Accounting for these factors in the standardisation of imaging and careful selection of study cohorts allows for repeatable measurement of oxygen saturation in the retina.

Despite its limitations, the Oxymap is a non-invasive, user-friendly technique which produces repeatable measurements of retinal oxygen saturation. By measuring retinal

oxygen saturation in combination with retinal volume metrics we can begin to determine the relationship between them in multiple sclerosis. For example, it is possible that retrograde degeneration of the inner retina in SPMS reduces metabolic demand leading to reduced oxygen extraction from vessels, which could be investigated using the Oxymap.

1.9 Summary

The collective knowledge which could be gained using these non-invasive techniques in both structure (OCT, OCTA, AOSLO) and function (AOSLO, Oxymap) could provide new insight into the potential role of the retinal vasculature in the pathogenesis of multiple sclerosis. The combination and comparison of these non-invasive retinal imaging techniques is used in the following thesis to investigate the retinal microvasculature in SPMS.

General Materials and Methods

2.1 Imaging Methods

2.1.1 Patient preparation

Informed consent was collected from all patients participating in these studies and the studies adhered to the tenets of the Declaration of Helsinki. Ethical approval for all studies was obtained from the appropriate bodies. Where appropriate, the eyes of patients and participants were dilated with tropicamide eye drops.

2.1.2 OCT Collection and Analysis

Spectral domain optical coherence tomography (SDOCT) images of the macular region were acquired using the Heidelberg Spectralis system (Heidelberg Engineering, Germany). SDOCT scans were positioned with the centre aligned to the fovea and were acquired with automatic real-time averaging (ART) set initially at 30 and reduced if image collection time was protracted. The resulting OCT volumes were exported as AVI files, converted to 8-bit TIF stacks and cropped using ImageJ (National Institutes of Health [NIH], Bethesda, Maryland, USA) (Schneider et al, 2012) in preparation for segmentation.

Retinal layers in OCT images were segmented using the OCTExplorer Iowa Reference Algorithm (Version 4.0.0, Retinal Image Analysis Lab, Iowa Institute for Biomedical Engineering, Iowa City, IA), which is an automated retinal layer segmentation software designed to objectively define the boundaries of layers (Abràmoff et al, 2010; Garvin et al, 2009). The Iowa Reference Algorithm performs segmentation of 10 retinal layers and the choroid by analysing pixel intensities in three dimensions across the OCT image stack to determine the boundaries of adjacent retinal layers. The segmentation was corrected manually for the inner retinal layers (RNFL, GCL, IPL, INL) if required. Retinal thickness was

calculated as the mean difference of adjacent boundaries across a defined region. For this thesis, the most important section was the inner retinal layers, which were defined as the distance between the inner limiting membrane (ILM) and inner border of the inner nuclear layer (INL) (Figure 2.1).

The segmentation grid centre was adjusted per eye to lie directly over the foveal centre. The GCL-IPL ring output was utilised to segment the inner retinal layers in an annulus shape surrounding but excluding the fovea, as it has been shown to be a reliable method of measuring GCL-IPL layer thickness in healthy eyes (Mwanza et al, 2011).

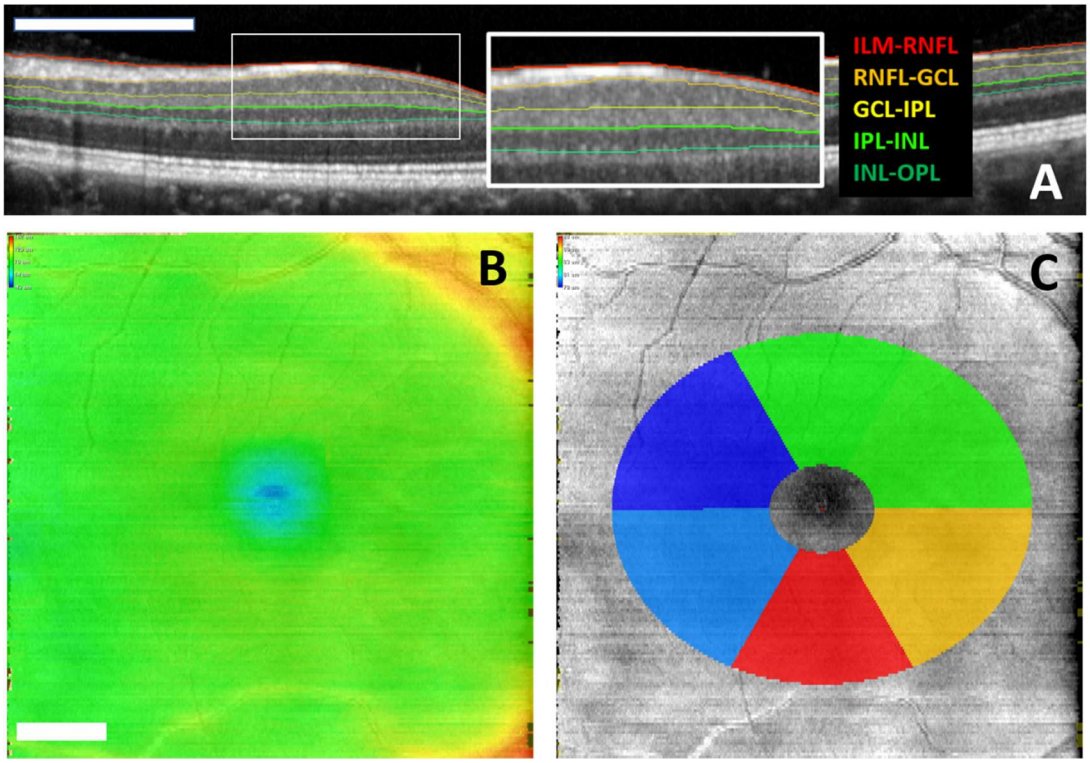

Figure 2.1: OCT Segmentation using the IOWA Reference Algorithm. Above: OCT segmentation defining the ILM (red) and the inner border of the INL (green) on a control participant, demonstrating OCTExplorer's segmenting capabilities (A). Below: OCT Segmentation Masks. 'B' demonstrates a projection of the OCT images as a representative image of a right eye. The thickness of layers may be averaged over the whole region (B) or collected from a perifoveal annulus specifically used for measuring the GCL-IPL layer (C). ILM: Inner limiting membrane, RNFL: retinal nerve fibre layer, GCL: ganglion cell layer, IPL: inner plexiform layer, INL: inner nuclear layer, OPL: outer plexiform layer. Thickness between ILM-RNFL and INL-OPL is presented in B-C. Scale: 1mm

2.1.3 OCT Angiography Collection and Analysis

OCTA images were collected from a subset of patients and healthy control subjects covering either a 3x3mm and/or a 6x6mm space, centred on the fovea, using the AngioVue system (Optovue Inc., Fremont, California, USA). Images were exported as a TIF and the resulting images of the superficial vasculature were cropped and binarized by Auto Threshold using ImageJ (National Institutes of Health [NIH], Bethesda, Maryland, USA) (Schneider et al, 2012) to allow for calculation of vessel density and fractal dimension. Images were assessed for quality before analysis, and images which contained significant movement artefacts were excluded from analysis. The superficial vascular layer, defined by boundaries pre-set on the AngioVue software as the ILM to the outer border of the IPL, was specifically selected for analysis as superficial layers comprised the most complete high-quality image set from this cohort, and because superficial layers are not impacted by projection artefacts which can often affect the deeper vascular layers using this technique (Spaide et al, 2015).

Vessel density was estimated by calculating the percentage of black pixels within the binarised image. Fractal dimension calculation was performed using the box counting method of ImageJ's in-built Fractal Box Count tool, inspired by fractal dimension analysis of OCTA images in diabetic retinopathy (Zahid et al, 2016). We intended to replicate this analysis by using the same fractal analysis tool, Fractalyse (ThéMA, Besançon Cedex, France), however analysis had to be transferred to ImageJ as the original tool was no longer being updated. Images were cropped, binarized and fractal dimension was calculated using the following ImageJ macro:

```
function action(input, output, filename) {
	open(input + filename);
	makeRectangle(24, 24, 250, 250);
	run("Crop");
	run("8-bit");
	run("Invert");
	run("Make Binary");
	run("Fractal Box Count...", "box=1,2,4,8,16,32,64,128");
	saveAs("Tiff", output + filename);
	close();
}
```

2.1.4 AOSLO

AOSLO imaging was performed using two different custom-built devices; the AOSLO specialised for photoreceptor imaging (Section 2.1.5) and the more recently acquired AOSLO specialised for vascular imaging (Section 2.1.6).

When using both devices, study participants were able to rest seated in front of the AOSLO for a minimum of approximately three minutes prior to imaging while the device was being adjusted for the individual. This resting period controls for potential variation in retinal blood flow caused by changes in blood pressure from standing to sitting (Singleton et al, 2003). Participants were advised in a similar manner for both devices to remain relaxed while on the device and take breaks as frequently as they desired.

2.1.5 AOSLO Specialised for Photoreceptor Imaging

A custom-built AOSLO was used to perform the preliminary study on the retinal microvasculature in MS (Figure 2.2, Table 2.1). The AOSLO specialised for photoreceptor imaging was built in 2013 by Alfredo Dubra from the Medical College of Wisconsin to a design by Dubra and Yusufu Sulai. It was modified to contain non-confocal capabilities in March 2014 by Adam Dubis and Drew Scoles.

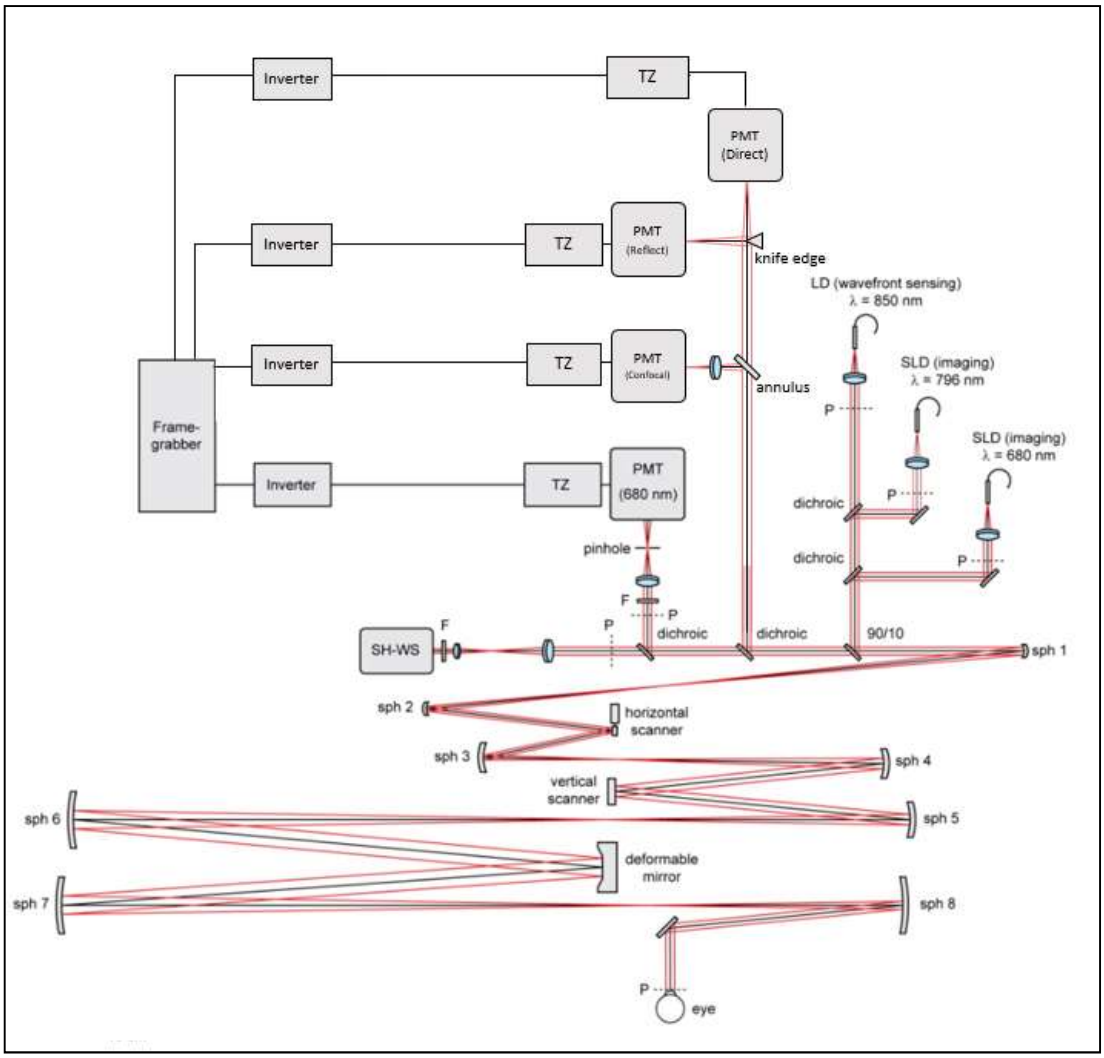

Figure 2.2: Optical Layout of the AOSLO Specialised For Photoreceptor Imaging within the Moorfields Eye Hospital Clinical Research Facility. TZ: transimpedance amplifier, PMT: photomultiplier tube, SH-WS: Shack-Hartmann wavefront sensor, LD: laser diode, SLD: superluminescent diode, P: plane optically conjugate with eye pupil, F: band pass filter. (Edited from figure by Sulai and Dubra, 2011)

AOSLO Components	Component Details
Deformable Mirror	DM97, ALPAO SAS (Biviers, Grenoble, France)
Wavefront Sensor	Custom Rolera-XR Camera, QI Imaging (Surrey, British Columbia, Canada) Lenset Array, Adaptive Optics Associates (Cambridge MA, USA)
Frame Rate	16Hz
Light sources	850nm laser diode – Qphotonics (Ann Arbor, Michigan, USA) 796nm SLD – Inphenix Inc. (Livermore, California, USA) (680nm not activated while we were imaging)
Detectors	PMTs H7422-40, H7422-50 – Hamamatsu Corporation (Bridgewater, New Jersey, USA)

Table 2.1: Components of the AOSLO Specialised For Photoreceptor Imaging

The AOSLO specialised for photoreceptor imaging contains three light sources; two for imaging (796nm and 680nm) and one for wavefront sensing (850nm) (Dubra & Sulai, 2011). It also has split detection capabilities, allowing for detailed visualisation of microvascular structures within the retina.

2.1.6 AOSLO Specialised for Vascular Imaging

In order to improve our vascular imaging quantitative abilities a new imaging system was required. In November 2018 a custom built AOSLO with adaptation for better vascular imaging was installed (Figure 2.3, Table 2.2), henceforth described as the BMC AOSLO. The modifications designed to facilitate vascular imaging were as follows. In the previous AOSLO configuration (Figure 2.2) neither the masks nor scanners could be dynamically altered, which while being acceptable for imaging photoreceptor outer segments is not ideal for blood flow imaging. The BMC AOSLO (built by Boston Micromachines Corporation (BMC), Cambridge, MA) was designed specifically to incorporate blood flow imaging capabilities, with readily adaptable pinholes, an 850nm imaging source, the ability to stop

the slow scanner on demand and an additional large field of view for navigation (2.5 x 2.5 degrees).

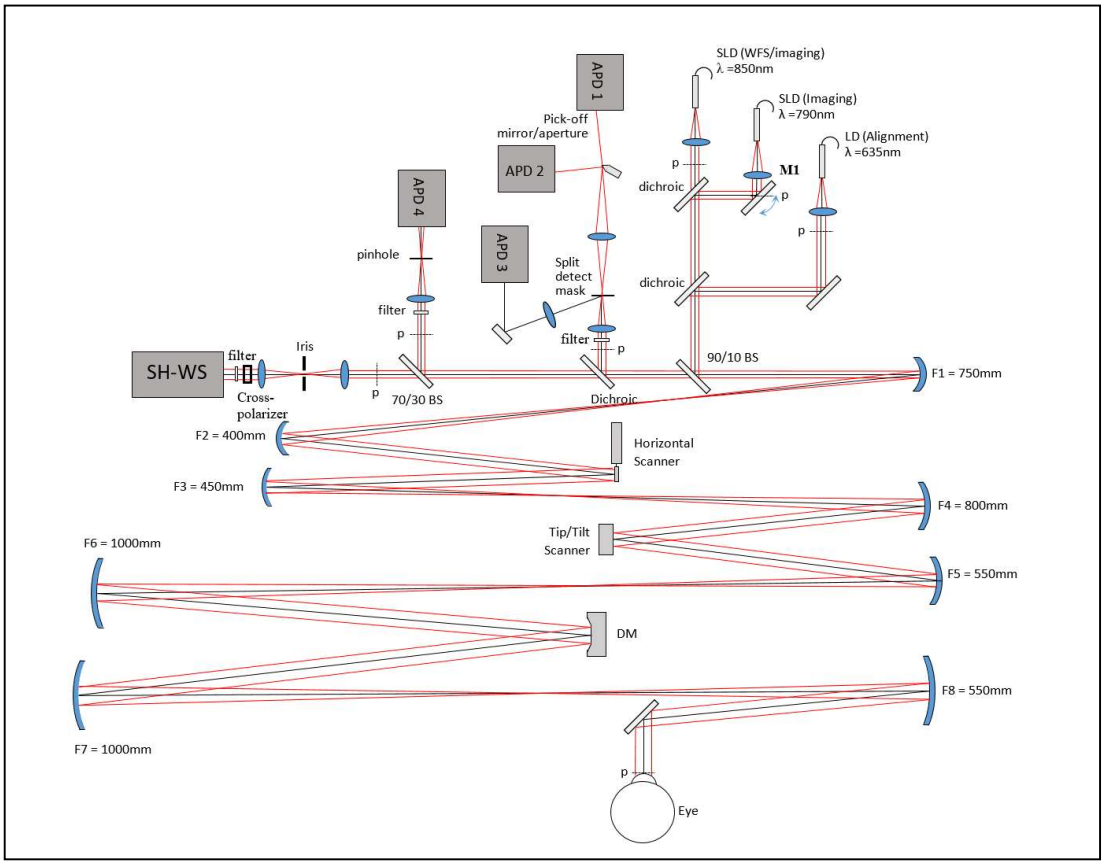

Figure 2.3: Optical Layout of BMC AOSLO. APD: Avalanche photodiode, SH-WS: Shack-Hartmann wavefront sensor, LD: laser diode, SLD: superluminescent diode, P: plane optically conjugate with eye pupil, DM: deformable mirror, BS: beam splitter.

AOSLO Components	Component Details
Deformable Mirror	Manufacturer: AlpAO DM97-15 Pupil diameter: 13.5mm
Wavefront Sensor	Shack Hartmann with CCD camera and custom lenslet array
Light sources	Two 850nm SLD sources – Imaging, wavefront sensing and calibration 790nm source – Imaging 635nm source - Alignment
Detectors	Four avalanche photodiodes (APD)

Table 2.2: Summary of BMC AOSLO components

The BMC AOSLO consists of four afocal telescopes formed by pairs of off-axis spherical mirrors in a non-planar arrangement. The two spectrally separated imaging beams are scanned onto the retina using two scanners; a fast resonance scanner to move horizontally and a slow, tip-tilt scanner to move vertically. In this system, the second spectral imaging beam (850nm) was used for both wavefront sensing and AOSLO imaging. As before, a Shack-Hartmann wavefront sensor is used for wavefront phase measurement and a deformable mirror is used for phase control. With its use of mechanical stages, the device also allows for real-time user interaction with the masks of the device from the imaging interface, allowing dynamic control of the type of imaging performed, e.g. offset pinhole or split detection. The use of an annulus mask anterior to the offset aperture mask also allows us to collect confocal images while maintaining offset pinhole image quality. This allows us to use these confocal images as reference frames during image registration, which are preferred references due to their high contrast. Inline desinusoiding can also be performed using this device, negating the need for desinusoiding post-collection.

The ability to dynamically interact with the tip-tilt mirror also allowed us to perform XT (X time) imaging, where the slow mirror is paused at a specified point in the image, allowing for imaging collection only from the fast scanner. XT imaging can be used to directly measure blood cell velocity in arterioles and venules, which is described in detail later in this thesis (Chapter 4, Section 4.2.6).

2.1.7 Vessel Thickness Estimation

The smallest retinal capillaries may be imaged using AOSLO split detection and their width could be used as a biomarker of microvascular pathology. Therefore, an objective measurement of capillary thickness was established and tested using split detection images previously collected. Manual measurements have been used previously with adaptive

optics to measure vessel width (Burns et al, 2014) although this is prone to variation caused by measurement error and image quality. Small (<10µm diameter) vessel images collected by AOSLO split detection display a characteristic intensity profile across the vessel (Figure 3.4) with peaks at either edge of the vessel. As the observed vessel changes may also be small, it is even more crucial that this change is detected repeatably and reliably. A semi-automated method was tested and found to be a repeatable and more reliable method of measurement than manual estimation of vessel size.

2.1.8 Retinal Oximetry

Retinal oximetry was performed using the Oxymap T1 (Oxymap ehf., Reykjavik, Iceland), a dual wavelength, non-invasive spectrophotometric oximeter. The oximeter consists of a standard fundus camera with two separate digital cameras allowing for simultaneous retinal imaging using two different wavelengths; 570nm and 600nm. Oximetry results from both eyes were analysed using the specialised analysis program for Oxymap T1, the Oxymap analyser (Version 2.4.2). Following vessel selection, results were exported as a CSV file containing the pixel location, width and oxygen saturation of vessel segments. The results were then subsequently analysed in Matlab using the technique described in Section 5.2.4.

2.2 Retinal Vessel Classification

Where used in this thesis, the term “retinal vasculature” refers to all vessels within the retina, and “retinal microvasculature” specifically refers to the interconnected laminar network of capillaries within the retina.

2.3 Statistical Analysis and Figure Preparation

Statistical analyses were performed using GraphPad Prism (version 7.0, GraphPad Software Inc.). Values were considered statistically significant if $p < 0.05$. Figures were prepared using ImageJ, GraphPad Prism, Adobe Photoshop (v2020), Tableau (v2018.2, Tableau Software), Biorender (v2020), Inkscape (v1.0.1) and Microsoft PowerPoint (v2016). Where included, error bars on bar charts indicate standard deviation of the mean. In box and whisker plots, the whiskers indicate the minimum to maximum values.

Preliminary Study on the Retinal Microvasculature in Multiple Sclerosis

3.1 Introduction

Little is understood about retinal microvascular pathology in SPMS. With the advent of new technologies allowing for *in vivo* imaging of the microvasculature, we can delve deeper into potential retinal microvascular dysfunction in SPMS. In this chapter we investigate both structure and function of the microvasculature in control subjects and MS patients of different stages of the disease to evaluate the utility of microvascular imaging techniques in MS and to understand more about how the retinal microvasculature changes throughout this disease.

Ophthalmic consequences of MS are common in patients and ubiquitous in post-mortem studies of MS (Toussaint et al, 1983). The inner retina and the brain are intrinsically linked, as axons of retinal ganglion cells lie on the inner surface of the retina where they form the retinal nerve fibre layer. These nerve fibres then converge to form the optic nerve that projects into the brain. With the advent of OCT, it has become possible to visualise the individual layers of the retina, allowing us to quantify neural loss in the eye and relate it to clinical parameters in MS. Atrophy of the RNFL and GCL, as measured with OCT, has been consistently demonstrated as an indication of neurodegeneration in multiple sclerosis with OCT measurements of ganglion cell - inner plexiform layer (GCIPL) atrophy correlating with brain atrophy from MRI derived measurements of white matter, grey matter and thalamic volume (Gordon-Lipkin et al, 2007; Saidha et al, 2015). OCT measurements of the inner retina have been established as reliable biomarkers in the disease in detecting, monitoring and understanding neurodegeneration (Costello & Burton, 2018; Gordon-Lipkin et al, 2007; Petzold et al, 2010).

Although retinal neurodegeneration is a common feature of multiple sclerosis, the aetiology of retinal neurodegeneration in MS has not been well defined. The optic nerve can be directly damaged by optic neuritis, but injury to afferent fibres can also cause transsynaptic degeneration downstream. Retrograde axonal degeneration causes pathological changes in the cell body proximal to the point of injury along an axon, such as degeneration of ganglion cells due to an optic nerve injury, whereas anterograde or "Wallerian" degeneration results from a "dying-forward process", where the axon separates from the cell body, causing degeneration distal to the injury. The reported rate of neural degeneration in the retina throughout the disease is also inconsistent, with reports that the progressive phase of the disease amplifies the process (Sotirchos et al, 2020) and causes damage extending as far as the inner nuclear layer (Green et al, 2010). All of these factors challenge the traditional view of neurodegeneration in MS, as purely a result of past inflammatory events and the remaining low-level inflammation of the secondary progressive phase. One potential explanation for this long-standing damage is microvascular impairment, either as a cause of neurodegeneration or a result of reduced metabolic demand. In order to understand the aetiology of retinal degeneration and potential link to microvascular damage, direct visualisation of retinal layers is required and OCT serves as a valuable tool to visualise the cross-sectional structure in which the vasculature sits.

The retinal microvasculature in MS has been investigated with both conventional OCT and OCTA, showing changes at all stages of the vascular tree. Using conventional OCT, Bhaduri *et al* demonstrated that MS eyes had a lower blood vessel diameter and count around the optic nerve (Bhaduri et al, 2016), demonstrating not only a reduction in the number of vessels but also a rarefaction of the remaining vasculature. Vessel density around the optic nerve and in the parafoveal region has also been investigated using OCTA. Wang *et al*, using OCTA, showed lower optic nerve head blood flow in patients with a history of ON

compared to other MS patients and controls, suggesting the reduced flow was related to ganglion cell loss and drop in metabolic demand. Parafoveal blood flow was not found to be significantly different between control and MS patients across all subtypes (Wang et al, 2014) suggesting reduced flow is only due to degeneration at the optic nerve site, although other studies have shown a reduction in vessel flow in the parafoveal region in MS (Feucht et al, 2019; Lanzillo et al, 2019), suggesting greater complexity. Although these studies demonstrate changes at all stages of the vascular tree in MS, there is little information available specific to disease subtypes, particularly for SPMS. The studies discussed here either do not discriminate by subtype or use only RRMS patients (see Table 1.1), therefore there is a gap in the knowledge surrounding the retinal vascular architecture and function in SPMS and whether the vasculature changes with progression between different MS disease subtypes.

OCTA provides us with a tool to rapidly map blood flow at a capillary level, however it cannot resolve vessel structures which are static, such as vessel walls. One form of ophthalmic imaging which allows us to do both, and has not yet been used to investigate the retinal microvasculature in MS, is adaptive optics ophthalmoscopy. AO, as an add-on to other imaging techniques, allows us to visualise the retina *in vivo* at a magnification previously unattainable using non-invasive technologies. Although it is a technically demanding and time-intensive technique, it can be used to construct more detailed images of the retinal microvasculature than OCTA (Mo et al, 2016). AO, specifically coupled to scanning laser ophthalmoscopy, can integrate a number of image modes simultaneously (e.g. confocal and non-confocal [split detection, dark field, offset aperture]) meaning as a technology it lends itself well to the study of the microvasculature. The microvasculature contains both directly reflective components, such as leucocytes, and highly scattering components, such as blood vessel walls, which can be visualised at physiologically relevant speeds in real time using AOSLO. AO equipped devices have previously been used to reveal

subclinical abnormalities in the retinal vasculature in vascular disorders such as diabetic retinopathy, at a stage where vascular abnormalities were thought to be undetectable (Burns et al, 2014). Microvascular abnormalities such as hairpin loops, ghost vessels and microaneurysms have been identified and described with AO imaging, and their appearance in diabetic retinopathy has been monitored over time (Chui et al, 2016). A study to systemically investigate changes to blood vessels using AO has not yet been performed in multiple sclerosis and could detect subclinical alterations in both blood vessels and the retinal environment surrounding vessels. Using a highly sensitive technique such as AOSLO we could learn more about the impact of multiple sclerosis in the retina before it becomes clinically detectable.

This chapter describes a study investigating the retinal microvasculature in control subjects and in patients with MS at different stages of disease using numerous ophthalmic imaging techniques in order to ascertain if a significant change in the microvasculature can be detected in MS and if so, which are the most appropriate techniques and endpoints to use in future studies to detect and monitor these changes.

3.1.1 Aims of Study

The aim of this study was to compare the retinal microvasculature in patients with relapsing remitting and secondary progressive multiple sclerosis to healthy control patients using OCT, OCTA and adaptive optics. A secondary aim was to develop new methods of vascular measurement using adaptive optics technology.

3.2 Materials and Methods

3.2.1 Declaration of Collaborator Roles Within Chapter

The data in this chapter were collected by Dr Adam Dubis, Sarah Houston, Dr Angelos Kalitzeos, Vincent Rocco and Monica Clemo. The data were analysed by Sarah Houston, apart from the abnormality grading which was performed by Sarah Houston, Vasileios Theofylaktopoulos and Dr Meriam Islam. Prof Richard Nicholas and Dr Ashwini Nandoskar identified MS patients to be recruited for the study. All videos included in this chapter were prepared by Sarah Houston.

3.2.2 Cohort Development

Patients with multiple sclerosis and healthy control participants were recruited as part of the ACAD (Advanced OCT and Adaptive Optics Imaging in Retinal Disease) study. The primary objective of the ACAD study was to understand the level of agreement between different types of OCT devices across a variety of retinal diseases, however a secondary objective of the study was to use adaptive optics to image the microvasculature in eyes with retinal and choroidal disease. The study was approved by the North Thames Clinical Research Network Ethical Review Board (15/LO/0440) and was registered with ClinicalTrials.gov (NCT02828215).

Written informed consent was collected from participants and the study adhered to the tenets of the Declaration of Helsinki. Healthy control patients were recruited from staff and students at UCL Institute of Ophthalmology and had no reported history of ophthalmic disease or trauma. MS patients were identified and evaluated at neurology clinics at Imperial College Healthcare NHS Foundation Trust, and were included on the basis they had no other history of ophthalmic disease or trauma other than MS-related optic neuritis.

Recent measurements of disability, such as the Enhanced Disability Status Scale (EDSS), were collected by the patient's neurologists and included in their referral to us for this trial. All patients underwent retinal imaging using OCT, OCTA and AOSLO at the Clinical Research Facility of NIHR Moorfields Biomedical Research Centre as part of this trial.

3.2.3 OCT Collection

Spectral domain optical coherence tomography (SDOCT) images were acquired using the Heidelberg Retina Angiograph Spectralis system (Heidelberg Engineering, Germany). SDOCT scans were acquired with ART set at approximately 29 (Average: 26, Range: 9-30). The scanned area covered the central 20° (1024 x 496 pixels) and consisted of 49 horizontal B-scans.

Retinal layers were segmented as discussed previously using the Iowa Reference Algorithm (Garvin et al, 2009) (Section 2.1.2). The inner retina and the inner nuclear layer were considered separately, due to the potentially divergent impact of MS on their thickness. Inner retinal thickness (IRT) was defined as the mean distance between the ILM and the inner border of the INL and INL thickness was defined as the mean distance between the top border of the INL and the bottom border of the INL over the 20-degree measurement region.

3.2.4 OCT Angiography Collection

OCTA images were collected from a subset of patients and healthy control subjects as previously described (Section 2.1.3) of either a 3x3mm and/or a 6x6mm space centred on the fovea, using the AngioVue system (Optovue Inc., Fremont, California, USA). There was some disparity in imaging protocol as a result of changes to the scope of the ACAD study,

individual variation between the ability of study participants and device issues leading to loss of data.

3.2.5 OCTA Analysis

The retinal vasculature can be seen as a fractal structure, where a repeating pattern is displayed at every scale. Fractal dimension (FD) analysis can be used in OCTA to gain a quantitative measurement of overall retinal microvascular structure. Fractal dimension was calculated using the standard box counting method using ImageJ Fractal Box Count tool (Figure 3.1).

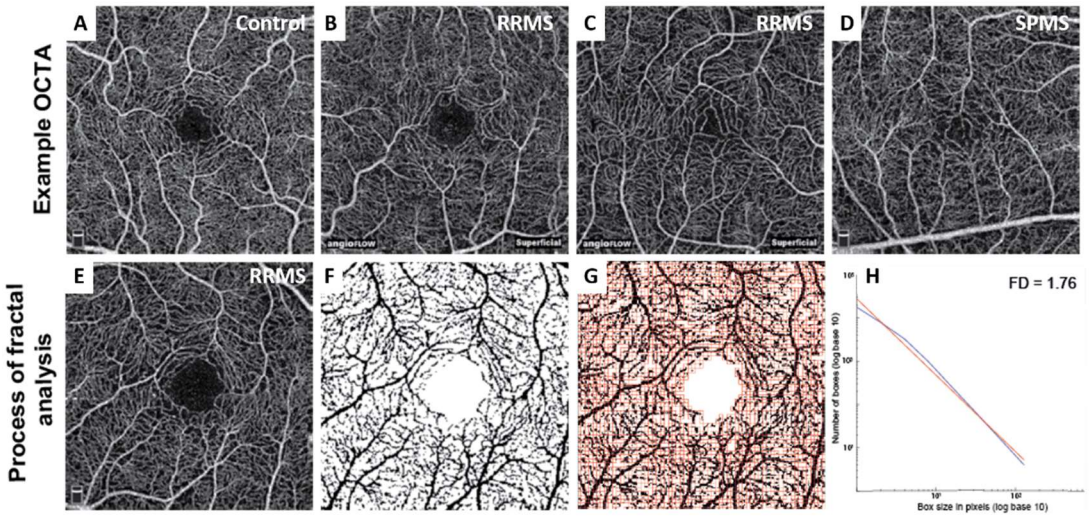

Figure 3.1: Examples of OCTAs in both control and MS patients (A-D), and a diagram demonstrating the process of fractal analysis in OCTA images (E-H). OCTA images are converted from their grayscale format (E) to binary images (F), on which fractal analysis using the box counting method (G) is performed. The fractal dimension (FD) is calculated by plotting the number of boxes used in the box counting method to the box size in pixels on a log:log scale and calculating its slope (H).

3.2.6 AOSLO Imaging Procedure

Healthy volunteers and MS patients were imaged using a custom-built AOSLO (Section 2.1.5). Prior to imaging, participant's pupils were dilated and cycloplegia induced with one drop of 1% tropicamide. The participants were aligned and stabilised with the use of a disposable dental impression on a bite bar. Spherical error corrected for by adjusting the deformable mirror and sequences of 150-300 images were recorded using both 1- and 1.5-degree fields of view. Sequence settings varied throughout the course of the trial as it became apparent the video length needed to be longer to gather long consecutive sequences of blood flow following registration. During imaging, patients were asked to fixate on a plus sign shaped fixation target which was projected into their field of view using a digital light projector. The target was moved at one-degree increments in order to collect overlapping images and build a continuous montage of the area imaged.

3.2.7 Image Processing

There are a number of factors which can result in distortion of AOSLO images, including the resonance scanner's sinusoidal velocity pattern, mirror buckling and involuntary eye movements. In order to account for these large distortions, the images must be corrected by stabilisation and registration. The sinusoidal motion of the resonance scanner results in image warping which must be corrected for before the image may be registered. The average degree of warping may be measured using a Ronchi grating, which is an optical target made of etched glass. It was used in this case as a calibrated grid to measure sinusoidal warping caused by the resonance and tip/tilt scanners. Directly following an imaging session, a short series of images (10 frames) of a Ronchi grating were collected and the distortion of these images was calculated by resampling the images over a grid of equally spaced pixels. The resulting "fringe period" was accounted for during image

processing. The fringe period refers to the distance (in pixels) between white bars of the grating, therefore providing an index of the sampling frequency. To increase signal to noise ratio, the image distortion due to eye motion was removed and then a number of registered frames were averaged as previously described.

A reference frame was chosen manually and was used as a template to register all subsequent frames. Some frames are discarded in this process due to severe distortion, sudden drop in intensity or discarded if they did not overlap with the reference frame. All frames with the normalised cross correlation above a designated threshold when compared against a manually selected reference frame were retained and motion stabilised via registration. The goal of this process was to create the stabilised videos of blood flow for further analysis of object tracking and capillary measurement.

3.2.8 Vessel Thickness Estimation

The smallest retinal capillaries may be imaged using AOSLO split detection and their width could be used as a biomarker of microvascular pathology. For this reason, an objective measurement of capillary thickness was developed and validated using split detection images previously collected.

AOSLO split detection videos of retinal vasculature from both MS patients and healthy controls were processed and 28 segments were collected to trial this thickness measurement algorithm. ImageJ was used to double the size of the image using bicubic interpolation to make it easier to place markers accurately. Segments were selected based on their morphology (Figure 3.2) to ensure they were as close as possible in appearance to capillaries. Vessels larger than capillaries (Figure 3.2, blue box) have a distinctively different intensity profile which would not be accurately measured using this technique and so were excluded based on their appearance.

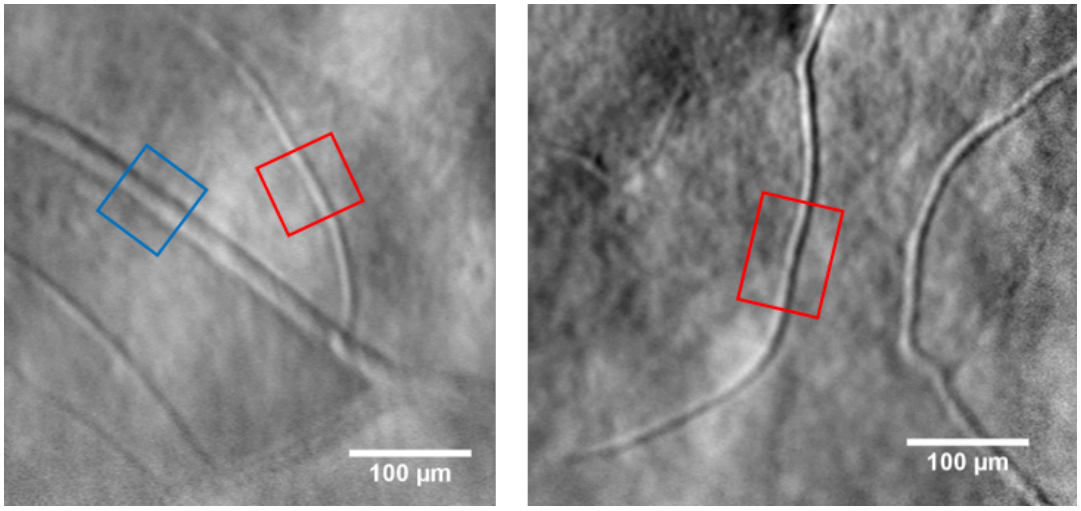

Figure 3.2: Examples of vessel segments included in thickness measurement as imaged using AOSLO split detection. Vessel segments such as those in the red boxes were included. The vessel segment in the blue box would have been excluded based on its morphology as a clear vessel wall structure is visible.

The ImageJ line width tool was adjusted to 100 lines wide (using an in-built ImageJ function), and ImageJ used to manually draw a line perpendicular to the vessel and the Line Profile function was used to measure average pixel intensity along the line (Figure 3.3). Speckle noise in split detection imaging causes the pixel intensity to vary widely from line to line, and averaging over a number of lines reduced the effect of this noise. A series of measurements were made to estimate how wide the line should be for calculation. One hundred lines was used as it allowed for increased signal to noise ratio whilst not making the line too wide to possibly cross over other vessels.

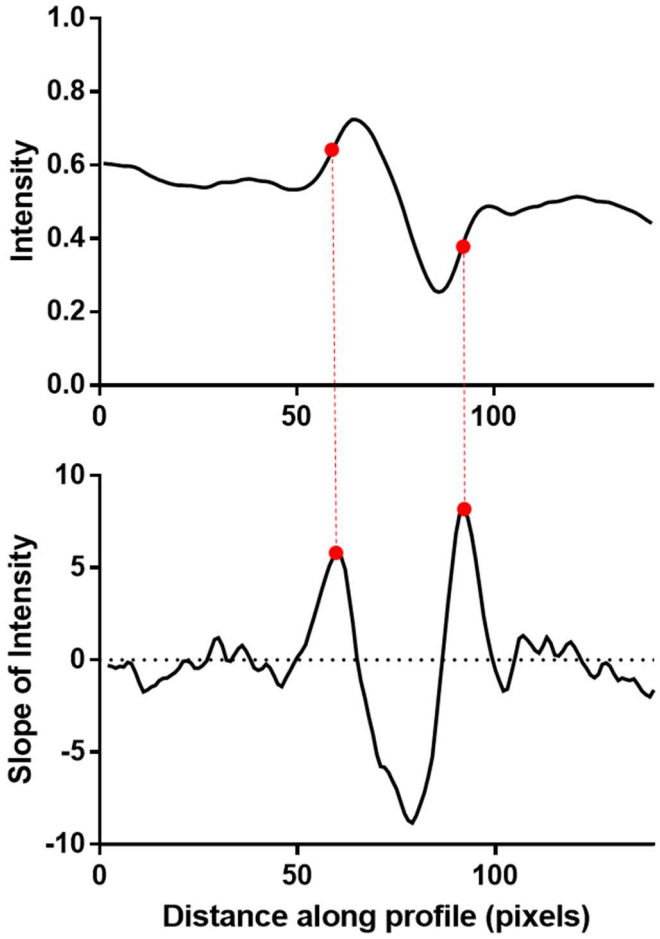

Figure 3.3: Intensity profiles of semi-automated capillary measurements. An intensity profile was extracted from an average of 100 cross section lines and filtered. The slope profile was determined by calculating the slope at each point along the intensity profile and the vessel edges were extracted from these data. The largest peaks on either side of the largest trough were considered the left and right edges of the vessel.

The resulting intensity plot was then read into MATLAB® (R2013b; The Mathworks Inc., Natick, MA, USA), a high-level language and data processing software. A smoothing filter was applied using the moving average method along each pixel. The slope of each point along the profile was then calculated and plotted and a function was used to find the peaks and minimum values of the plot. The two largest peaks on either side of the largest trough were automatically detected and taken as the vessel edges. The measurement process is described in brief in Figure 3.4.

Figure 3.4: Semi-automated measurement vessel thickness measurement pathway

Vessel segments were chosen based on their morphology and image quality. Vessel segments which had a relatively uniform background were also selected as the background could have a significant impact on the baseline of the intensity profile. Vessel segments also could not be proximal to- or cross with other vessels as it would be impossible to measure a uniform background either side of the vessel and to ensure only the vessel selected was measured. Segments were measured twice both manually using the ImageJ line drawing tool and using the semi-automated tool in order to compare their repeatability.

3.2.9 Microvascular Morphological Grading

In order to investigate the presence and spread of microvascular abnormalities in the inner retina, split detection videos were manually graded and given scores based on the presence of certain structures previously described as microvascular anomalies, namely erythrocyte aggregates, hairpin loops and inner retinal cysts.

Grading was performed by two masked trained graders and graders were trained on a subset of images which were not present in the final test set. Videos were masked by an independent observer and eight videos of each patient were graded. The regions chosen for grading were located 1-4 degrees temporal and 1-4 degrees superior to fixation (1 video per degree, 1-degree field of view) (Figure 3.5), as most of the sample had these videos available. Raw videos were visually graded frame by frame to ensure the whole region the

patient fixated in was visible. Sixteen MS patients (10 RRMS, 6 SPMS) and seven controls were graded based on image quality and retinal locations imaged.

Figure 3.5: Locations of videos graded (black boxes) in an example infrared image of a right eye. Regions 1-4 degrees temporal to fixation (blue boxes) and regions 1-4 degrees superior to fixation (red boxes) were imaged. Each box corresponds approximately to a 1x1 degree region. Scale: 1mm.

Graders first graded the images on quality (Figure 3.6) and images of insufficient quality (i.e. “Ungradable”) were excluded from analysis. Good quality videos were defined by clear vessel margins, clear erythrocytes in vessels and minimal eye movements. Medium quality videos were still graded, but may have had additional movement artefacts or reduction in clear vessel margins. Ungradable videos were those in which vessel margins and erythrocytes were not in focus or visible and were therefore excluded from further grading.

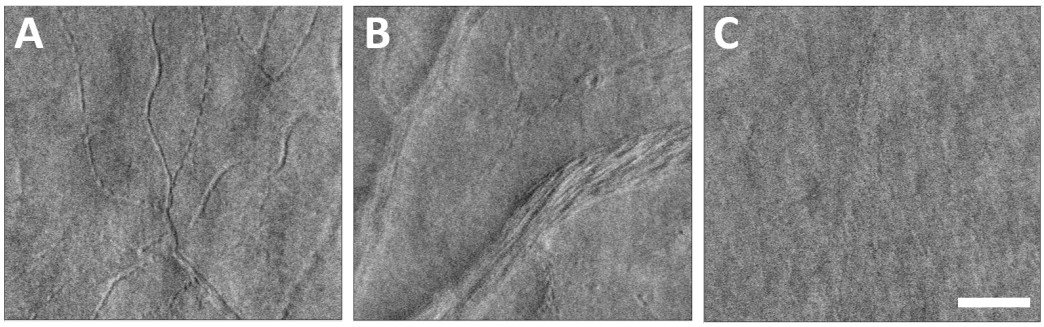

Figure 3.6: Examples of images used to train graders on quality metric. Good quality (A) and medium quality (B) images were used in the analysis. Ungradable images (C) were excluded. Scale: 50µm

Initial videos of all locations were reviewed manually to determine if there were any abnormalities which could be graded. Hairpin loops, purported to be formed by recanalization of a vessel wall (McLeod et al, 1993) were included. Inner retinal cysts were also identified in image review and included in analysis. Microaneurysms were also originally considered as part of the analysis, however due to our image quality and narrow axial slice it was difficult to determine if it was a true microaneurysm (i.e. swelling of vessel walls) or normal vessel branching seen at an angle which appears as a microaneurysm.

Raw split detection images of the retinal vasculature were graded by two masked graders on the presence or absence of erythrocyte aggregates (Figure 3.7), hairpin loops (Figure 3.8) and inner retinal cysts (Figure 3.9).

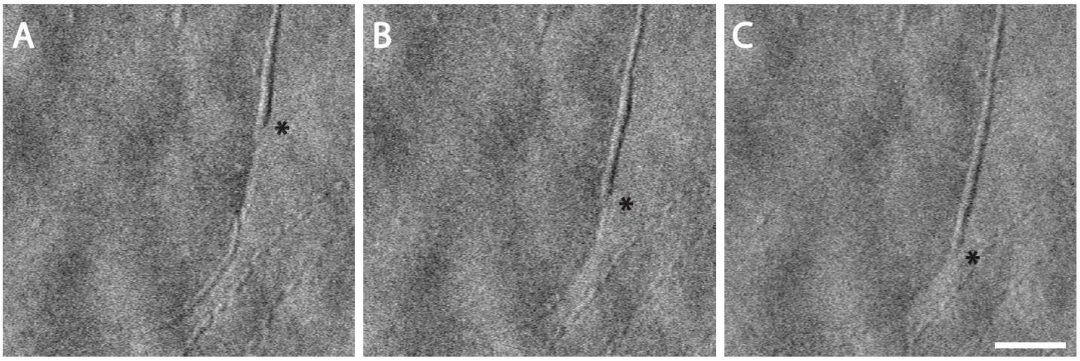

Figure 3.7: Erythrocyte aggregate example. The black asterisk indicates the leading edge of the aggregate. A, B (+0.06s) and C (0.13s) are sequential frames captured using AOSLO split detection with a 1-degree field of view. Scale: 50µm. An additional example is shown in Video 1 (https://youtu.be/9OHg2_JSkb4).

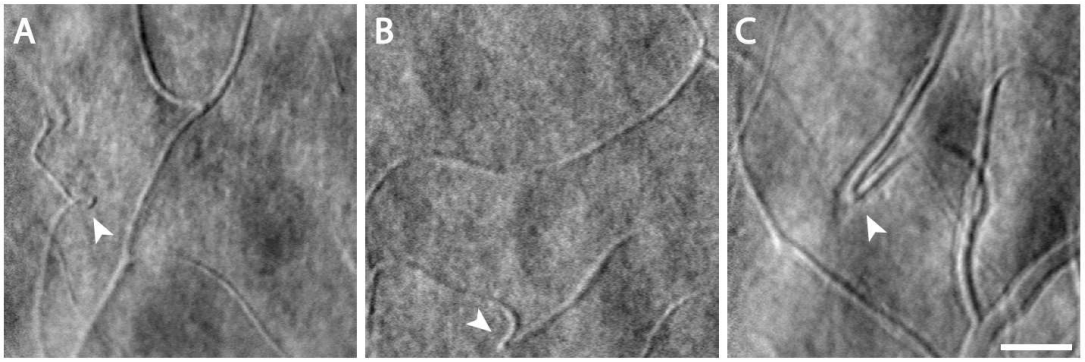

Figure 3.8: Examples of hairpin loops captured by AOSLO split detection, indicated by white arrows. Scale: 50µm. The hairpin loop in image C can be viewed in Video 2 (https://youtu.be/62DZP56mbNA).

Inner retinal cysts were further classified according to their size. Cysts were divided into small discrete cysts, medium sized (>40 pixels) cysts and large patches of 3 or more large cysts (Figure 3.9).

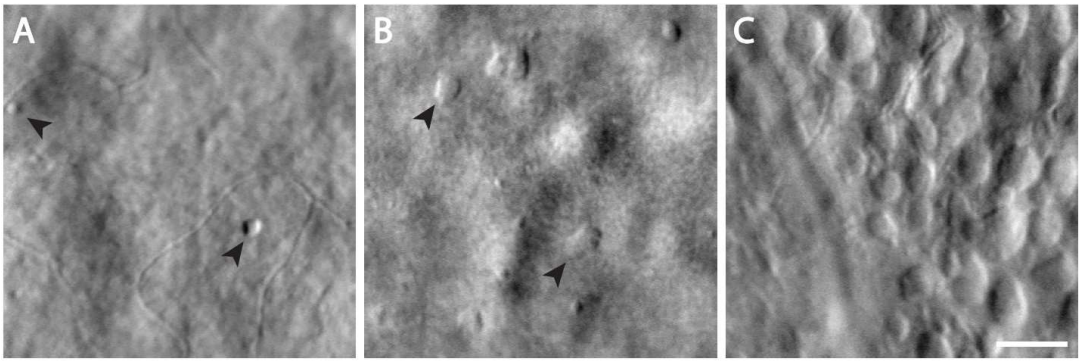

Figure 3.9: Examples of cyst morphology as imaged by AOSLO split detection. Cysts of less than 40 pixels (A, black arrows) were defined as small discrete cysts. Cysts of 40 pixels and above (B, black arrows) were defined as large cysts. An area of 3 or more large contiguous cysts (C) was defined as a patch of cysts. Scale: 50μm

3.2.10 Erythrocyte Aggregate Speed

Erythrocyte aggregates (ECAs) or "rouleaux" are stacks of erythrocytes which form due to the unique discoid shape of the cells and they are easily identifiable in capillaries due to single cell flow (Baskurt & Meiselman, 2013). For this experiment, stabilised videos were used to measure aggregate speed. The speed of erythrocyte aggregates in MS and control patients were measured over 3 frames using the Manual Tracking Plugin (ImageJ) (Figure 3.10). ECAs from MS patients and controls were selected to be measured by quality criteria; if the image quality was high, if a leading edge was easily identified and if the vessel segment which the ECA moved through did not contain any large angles. In order to ensure video segments used for ECA tracking were continuous and had not "lost" frames in the registration process, a video with frame numbers labelled on each slice was co-registered with the AOSLO video and used to check for continuity. Three consecutive frames were measured in order to obtain an average of two consecutive velocities.

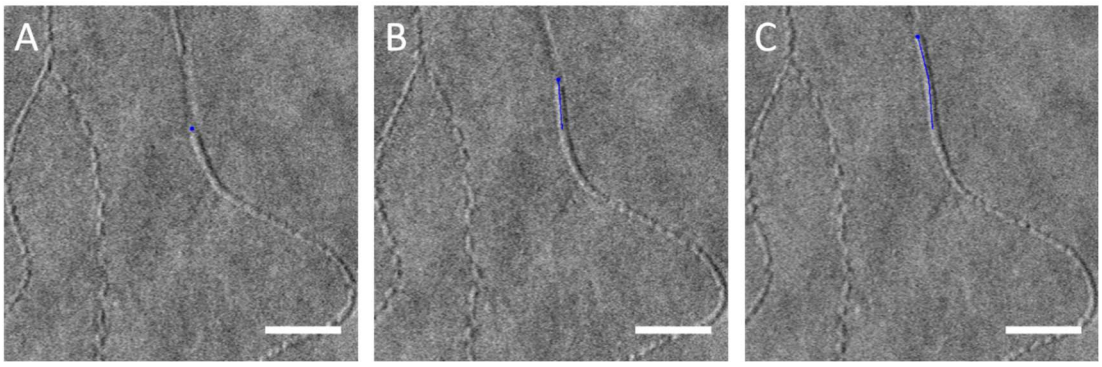

Figure 3.10: Example of measurement of an erythrocyte aggregate using the ImageJ Manual Tracking Plugin as imaged by AOSLO split detection. The marker was placed on the leading edge of the aggregate over 3 consecutive frames. The blue line indicates the distance the aggregate travelled in 3 consecutive frames (A, B, C) with 60ms intervals. Scale: 50μm

3.2.11 Vessel Stiffness Measurement

As an erythrocyte aggregate moves through a capillary, a noticeable change in vessel thickness occurs as the vessel wall stretches to accommodate to larger block of cells (Figure 3.11). It was hypothesised that vessel stiffness as a result of multiple sclerosis could be measured by how compliant the vessel is to these aggregates moving through.

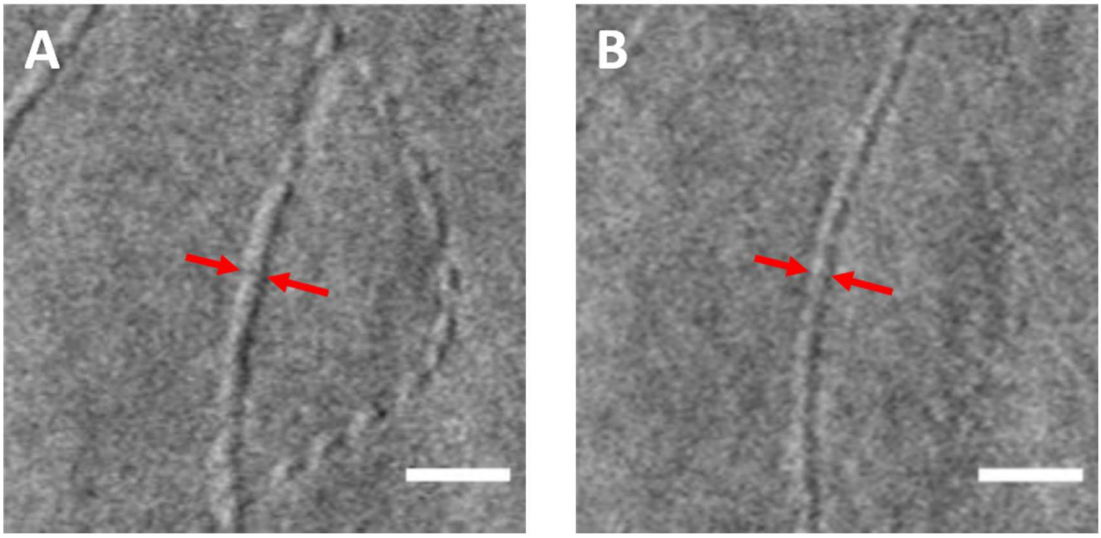

Figure 3.11: Example of how capillary thickness changes in the presence of an erythrocyte aggregate (A) compared to at rest (B) as imaged using AOSLO split detection. Scale: 20µm.

The compliance of small vessels was measured as the ratio between vessel thickness in the presence of the aggregate and vessel thickness at rest (Equation 3.1), which will be described as the EC ratio.

$$\text{EC Ratio} = \frac{\text{Vessel thickness during ECA}}{\text{Vessel thickness at rest}} \qquad \text{Equation 3.1.}$$

3.3 Results

3.3.1 Patient Demographics

There were more females in the MS patient group (69%) compared to the control group (43%) (Table 3.1). There was no significant difference in age (t-test, p = 0.16) between control and patient groups.

	Controls (n = 7)	MS (n = 16)	
Mean Age in Years (Range)	40 (26-53)	47 (31-66)	
Sex (% Female)	43%	69%	
EDSS Range		RRMS	1-6
		SPMS	6-6.5
Type of MS		RRMS	n = 10
		SPMS	n = 6

Table 3.1: Patient demographics of the ACAD cohort

The number of patients and participants used in each individual portion of the trial is highlighted in Figure 3.12.

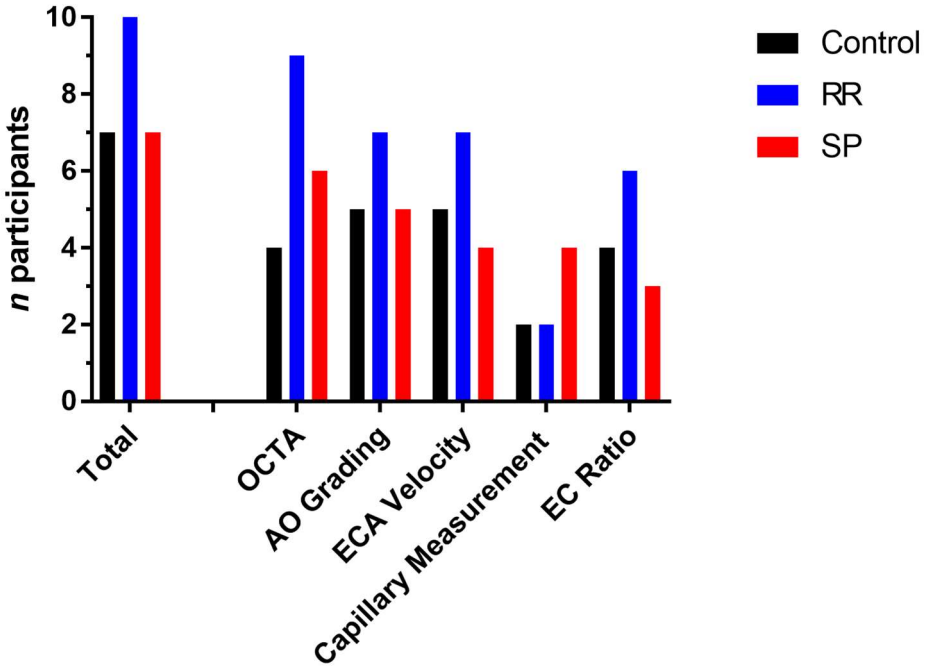

Figure 3.12: Clustered bar chart of number of participants used in individual studies. RR: relapsing-remitting, SP: secondary progressive.

3.3.2 Optical Coherence Tomography

Firstly, OCT measurements of retinal thickness were measured as retinal thinning is a widely reported finding in MS. Inner retinal thickness (IRT) values and INL thickness values were normally distributed, as assessed by Shapiro-Wilk test (P>0.05 for both). Right eyes only were assessed for each patient and control subject.

IRT was significantly thinner in SPMS and RRMS than control, as has been reported previously in studies of larger sample sizes, suggesting this sample is reflective of a standard MS population (Figure 3.13) (One-way ANOVA, p = 0.002). Tukey's multiple comparison test showed significant difference between control group and RRMS (p = 0.01) and control and SPMS groups (p = 0.003). There was no significant difference in inner nuclear layer thickness between the three groups as determined by one-way ANOVA (p = 0.697) (Figure 3.13). Similar results were achieved when comparing groups by EDSS. IRT was significantly thinner in high EDSS and low EDSS patients than control patients (One-way ANOVA, p = 0.002) and Tukey's multiple comparison test showed significant difference between controls and low EDSS (p = 0.02) and controls and high EDSS (p = 0.002). There was also no significant difference in INL thickness between the three EDSS ranked groups as determined by one-way ANOVA (p = 0.61) (Figure 3.13, second panel). We have found atrophy in inner retinal layers in MS which worsens with disease progression; however, the inner nuclear layer remains at a similar thickness throughout.

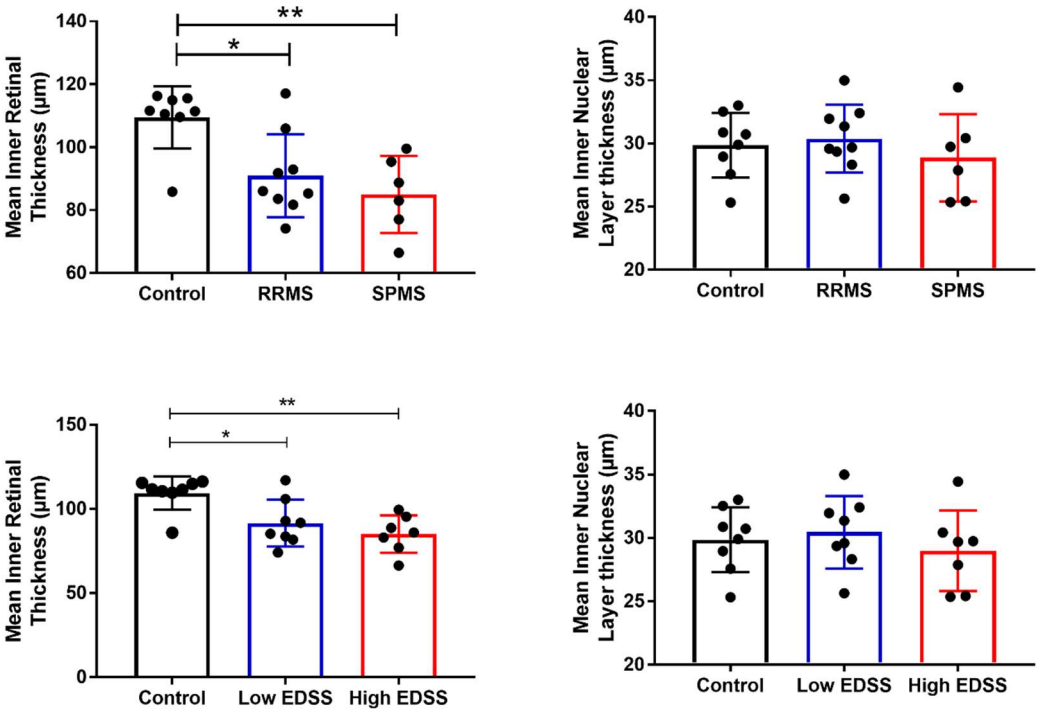

Figure 3.13: Retinal thickness measurements by OCT in each patient group and by EDSS score. Groups were compared using one-way ANOVA and Tukey's multiple comparisons test. *P<0.05; **P<0.005.

3.3.3 Optical Coherence Tomography Angiography

OCTA was performed on thirteen participants using the AngioVue device. Other participants were excluded from OCTA analysis due to loss of data (n=1), poor image quality (n=4), change in study protocol (n=5) or inability to access machine (n=1). There were no subjective differences in microvascular structure in either the 3mm or 6mm scans (Figure 3.14). Due to low sample size we cannot say with any certainty but it appears that gross vascular structure is unchanged in MS (Table 3.2, Table 3.3) as measured with both vessel density and fractal dimension (Figure 3.15).

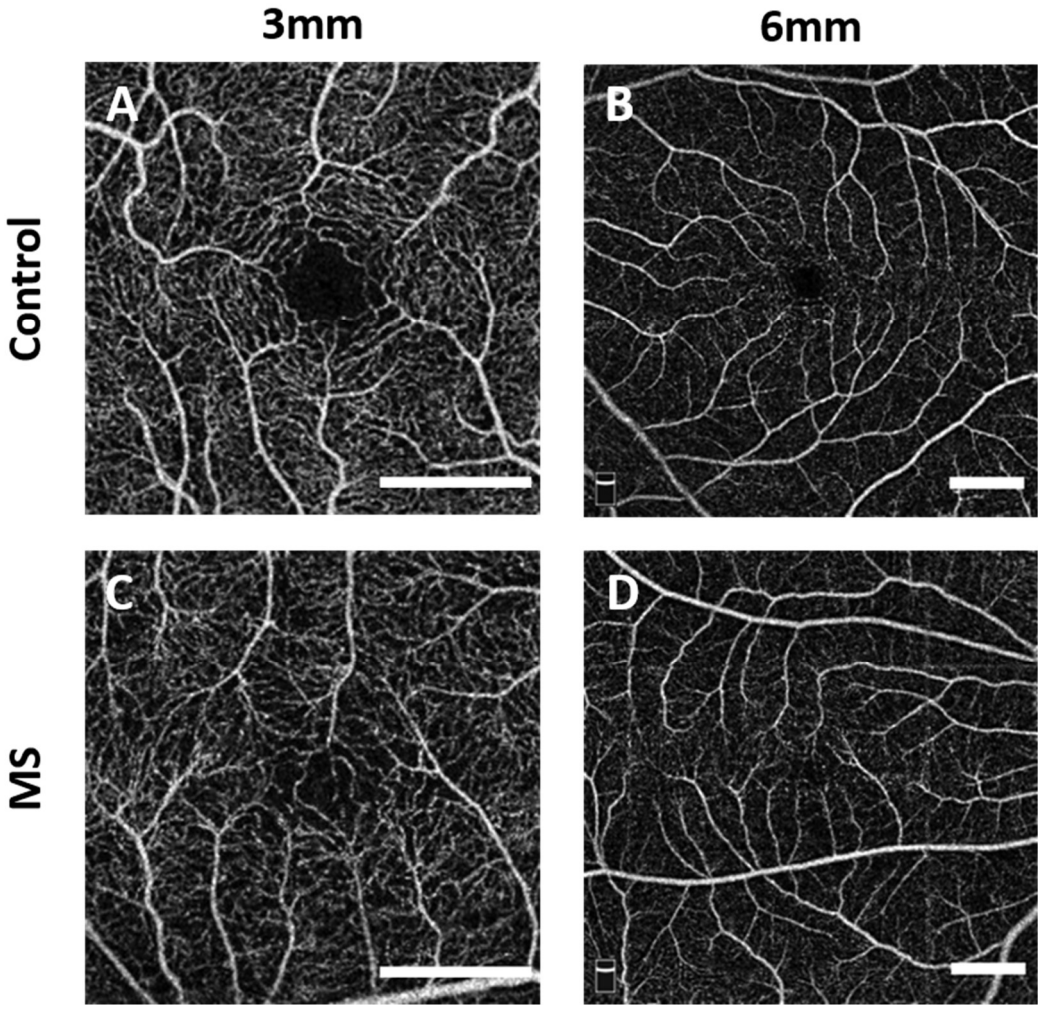

Figure 3.14: Examples of OCTA images used in this analysis. Images A and B are from two different controls, and C and D are from the same MS patient. Scale: 1mm.

		Fractal Dimension		Vessel Density	
	N	**Mean**	**SD**	**Mean**	**SD**
Control	3	1.734	0.033	0.780	0.026
RRMS	5	1.672	0.059	0.821	0.037
SPMS	2	1.701	0.059	0.806	0.029

Table 3.2: OCTA results from the superficial retinal vasculature over a 6x6mm area

		Fractal Dimension		Vessel Density	
	N	**Mean**	**SD**	**Mean**	**SD**
Control	4	1.744	0.071	0.742	0.007
RRMS	5	1.746	0.029	0.773	0.033
SPMS	4	1.754	0.024	0.747	0.027

Table 3.3: OCTA results from the superficial retinal vasculature over a 3x3mm area

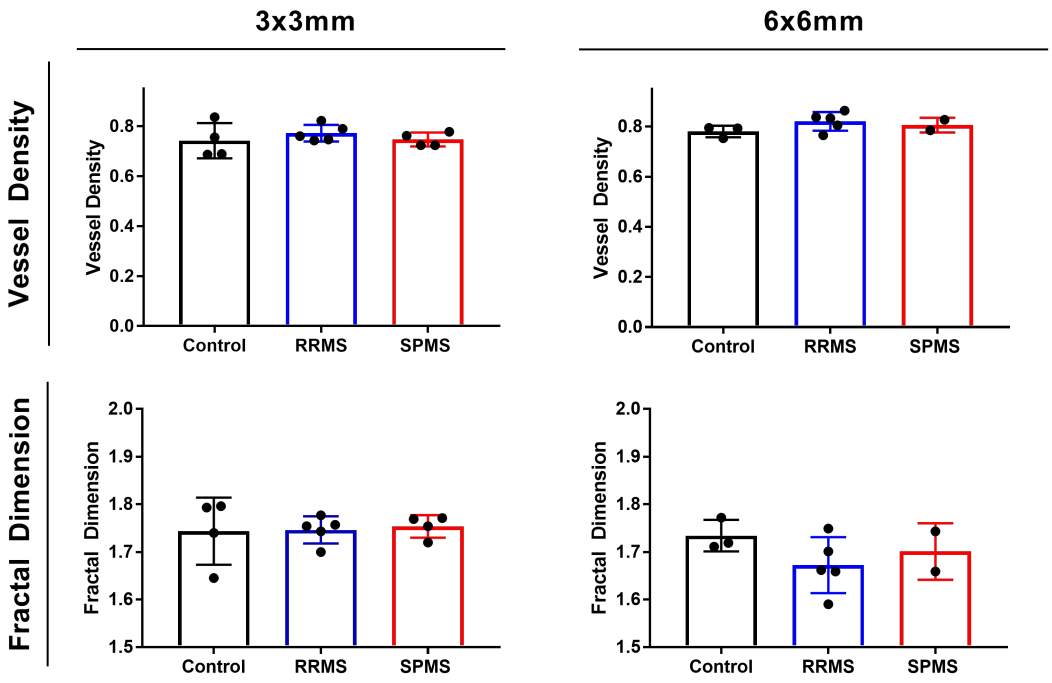

Figure 3.15: Bar charts showing OCTA density and fractal dimension results from control and MS patients over a 3x3mm region and a 6x6mm region. There was no clear difference in vessel density or fractal dimension between groups.

3.3.4 Abnormality Grading of AOSLO images

As it was considered categorical data, the results of adaptive optics grading were analysed using non-parametric techniques frequently used for analysing this class of data. For microvascular grading, graders had a fair agreement on hairpin loops (K = 0.368 (95% CI= 0.198, 0.538)) and good agreement for IRC (K = 0.627 (95% CI = 0.537, 0.717)) as assessed using Cohen's κ. Examples of abnormalities on which graders agreed and disagreed are included in Figure 3.16. Abnormality data, as they are categorical and not continuous, were analysed using non-parametric techniques.

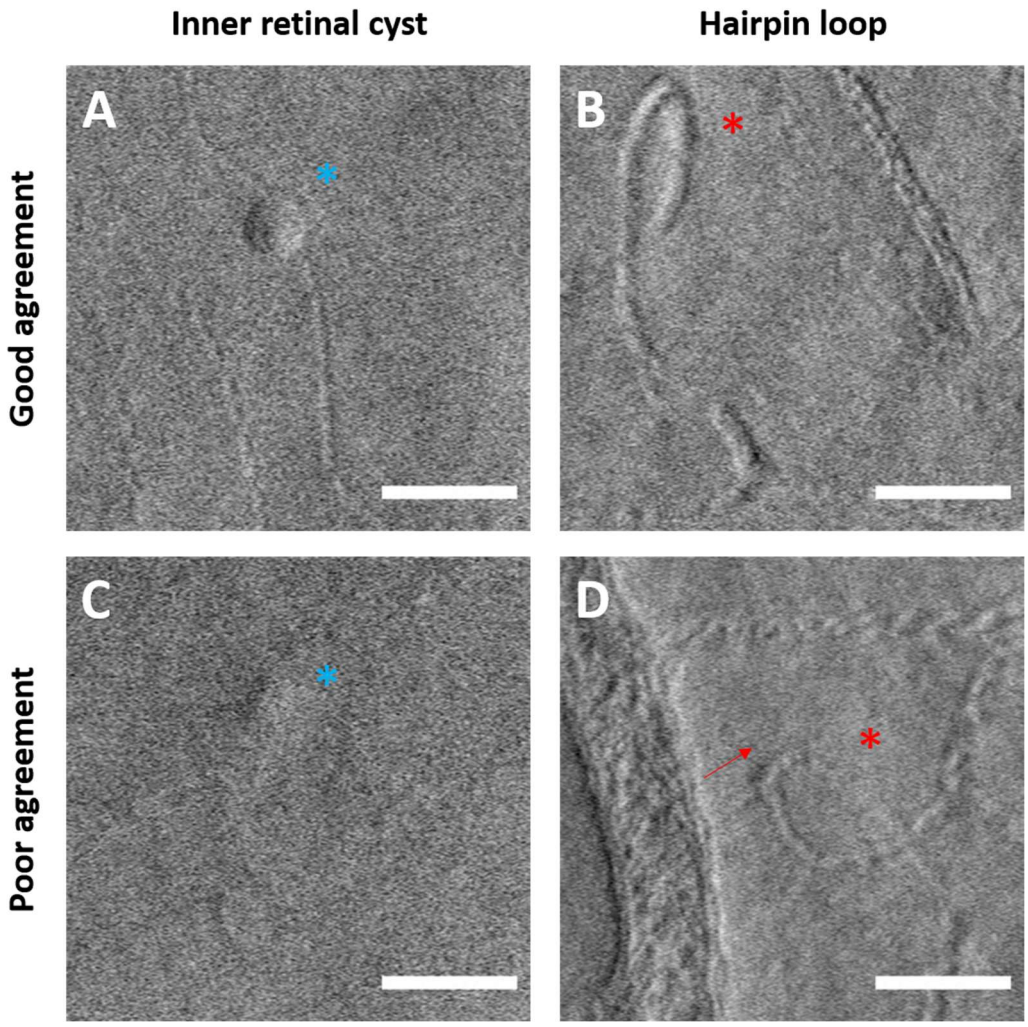

Figure 3.16: Examples of good and poor agreement between graders in abnormality grading. For intraretinal cysts, grading had good agreement in cases where the cyst was large and clearly defined (A), but regions of the retina containing small divots (C) where the edges are not clearly defined could be misinterpreted as cysts. For hairpin loops, graders agreed well on large loops where the path of blood flow could be easily traced (B). There was disagreement in cases where vessels did appear to loop, but actually had a small feeder vessel (D, red arrow) which meant it could not be defined as a hairpin loop. Scale: 50µm.

One expert grader was selected for abnormality assessment and one eye only for each patient and control is shown here. Erythrocyte aggregates, as they were not strictly vascular abnormalities, were not considered as part of the abnormality analysis and the locations were used to determine high quality aggregates for velocity measurement.

The Kruskal-Wallis H Test showed that there was a significant difference in number of regions positive for abnormalities between the three groups ($p = 0.047$). Dunn's multiple

comparison tests showed there was a significant difference in abnormalities between controls and SPMS (p = 0.042) but not controls and RRMS (p = 0.542) (Figure 3.17).

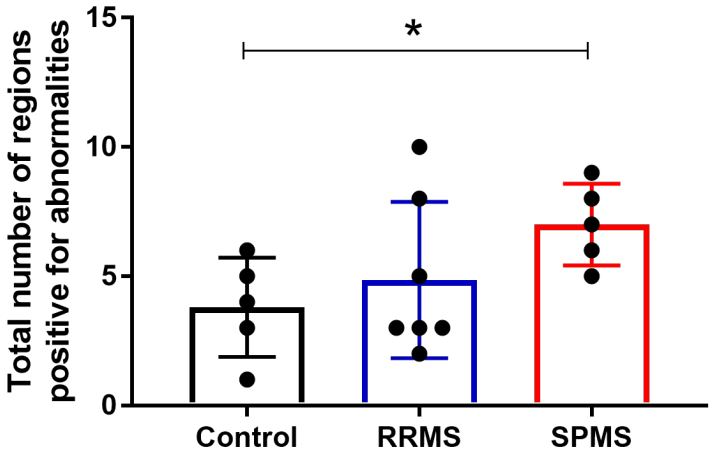

Figure 3.17: Bar charts indicating the number of regions which were graded positive for the presence of abnormalities in each of the three groups. The error bars indicate mean and standard deviation. A Kruskal Wallis test and a Dunn's multiple comparisons test was performed. * : P<0.05.

Following intraretinal cyst classification, it was found that large patches of cysts were only found in MS patients. There was no significant difference in the number of small or medium sized cysts in control and MS patients as assessed by Kruskal-Wallis H Test (p = 0.372) (Figure 3.18).

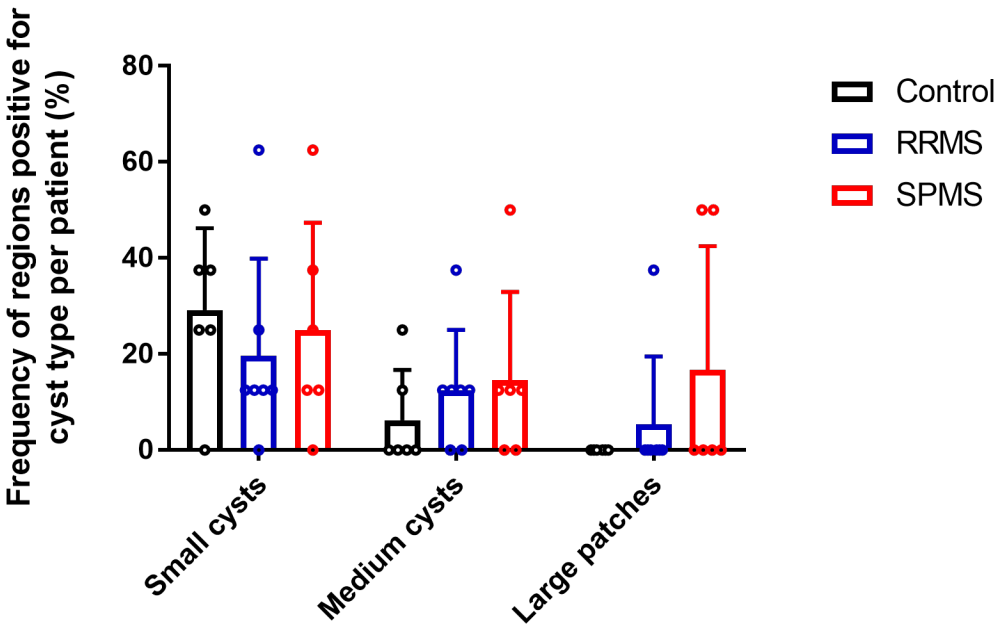

Figure 3.18: Clustered bar chart with scatter plots overlaid indicating the frequency of regions containing cysts in patient groups (number of regions graded positive for cysts divided by number of regions graded). There were no large patches of cysts identified in the control group.

Microvascular defects are often a cause or a result of tissue damage in the retina, therefore we sought to investigate if there was any correlation between the retinal thickness metrics and the results of abnormality grading. The location of cysts was compared to their cross-sectional OCT in order to identify which retinal layer they belong. However, even in locations containing large patches of cysts on AOSLO the cysts could not be identified on the OCT image (Figure 3.19).

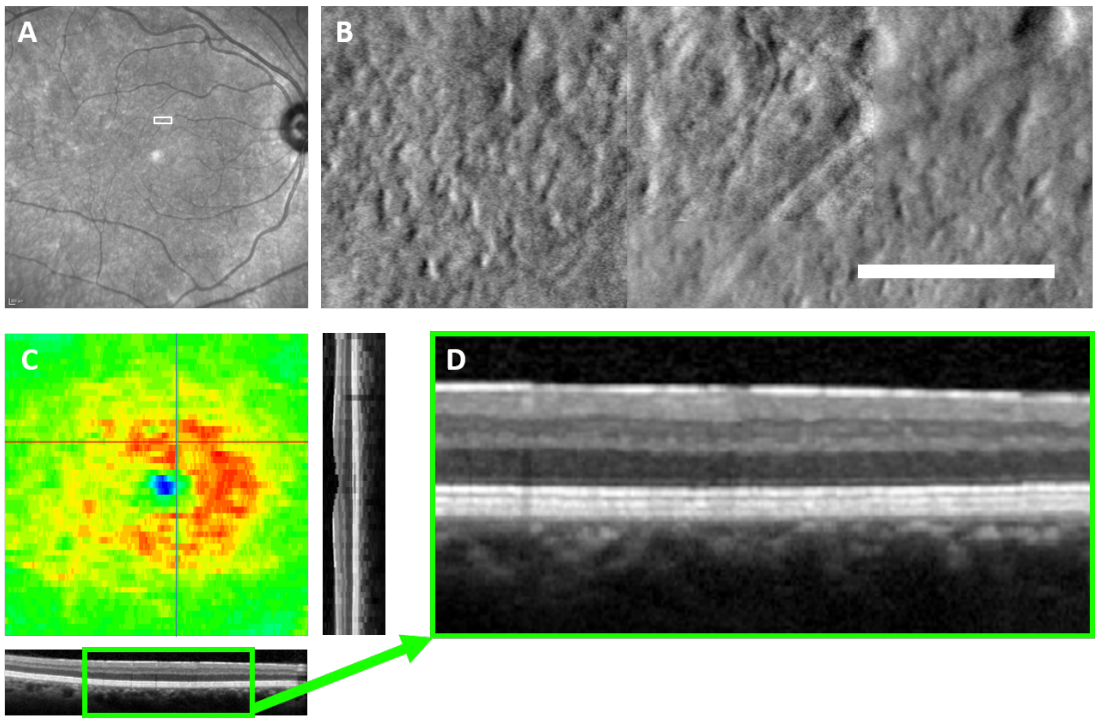

Figure 3.19: Analysis of retinal region in the presence of large patches of inner retinal cysts. The region indicated using the white box in the infrared image (A) was imaged using AOSLO (B) and demonstrates a large region of inner retinal cysts. However, when examining this specific region using OCT (D) no clear abnormalities are seen. However, there is patchy thickening seen in the region in on the retinal thickness map (C).

A one-way ANOVA showed no significant difference between inner retinal thickness between abnormality groups in MS patients ($p = 0.09$), however in post-hoc testing there was a significant linear relationship ($R^2 = 0.20$, $p = 0.03$) between abnormality score grouping and mean inner retinal thickness (Figure 3.20).

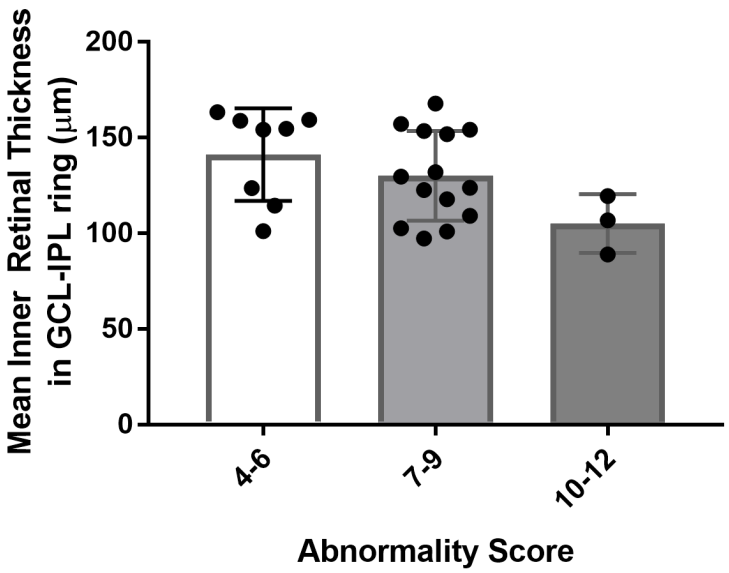

Figure 3.20: Bar chart showing relationship between abnormality score grouping (4-6, 7-9, 10-12) and mean inner retinal thickness in MS patients. A one-way ANOVA showed no significant difference between the groups, but a linear relationship between inner retinal thickness and abnormality score (p = 0.03) was found in post-hoc testing.

We sought to investigate if thickness could predict abnormality. Using two-way ANOVA we found that there was no significant interaction between abnormality score and patient group on OCT thickness (p = 0.23). There was no significant effect of abnormality status on OCT thickness (p = 0.97), but there was a significant effect of patient group (p = 0.02). Tukey's multiple comparisons tests revealed no significant interactions between individual groups (Figure 3.21).

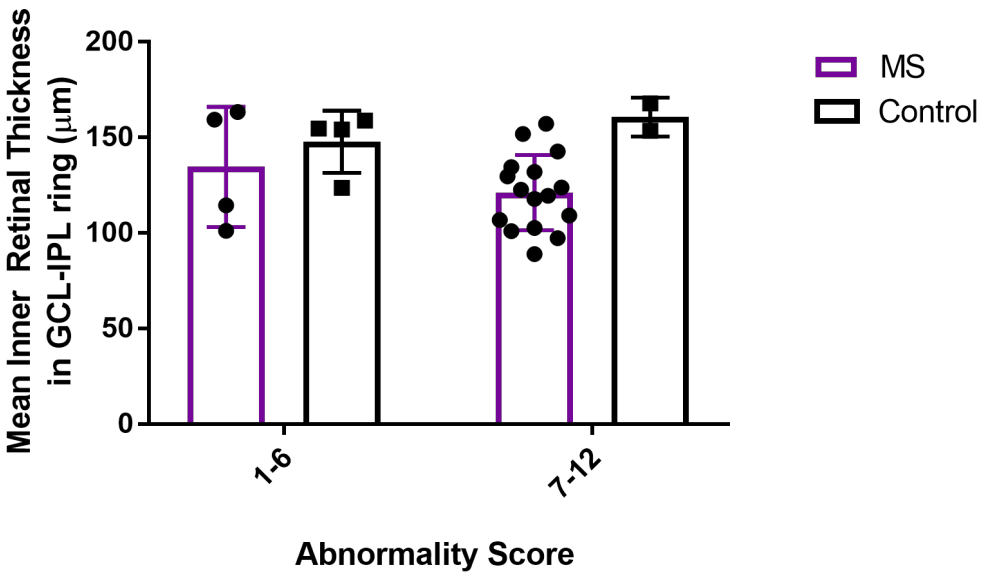

Figure 3.21: Clustered bar chart showing relationship between abnormality score grouping (1-6 or 7-12) and mean inner retinal thickness in MS and control patients.

Presence of large patches of cysts was compared to inner retinal thickness and inner nuclear layer thickness both in the perifoveal ring (A) and in the superior segment of the ring (B), as all the large patches of cysts were found in regions superior to fixation (Figure 3.22).

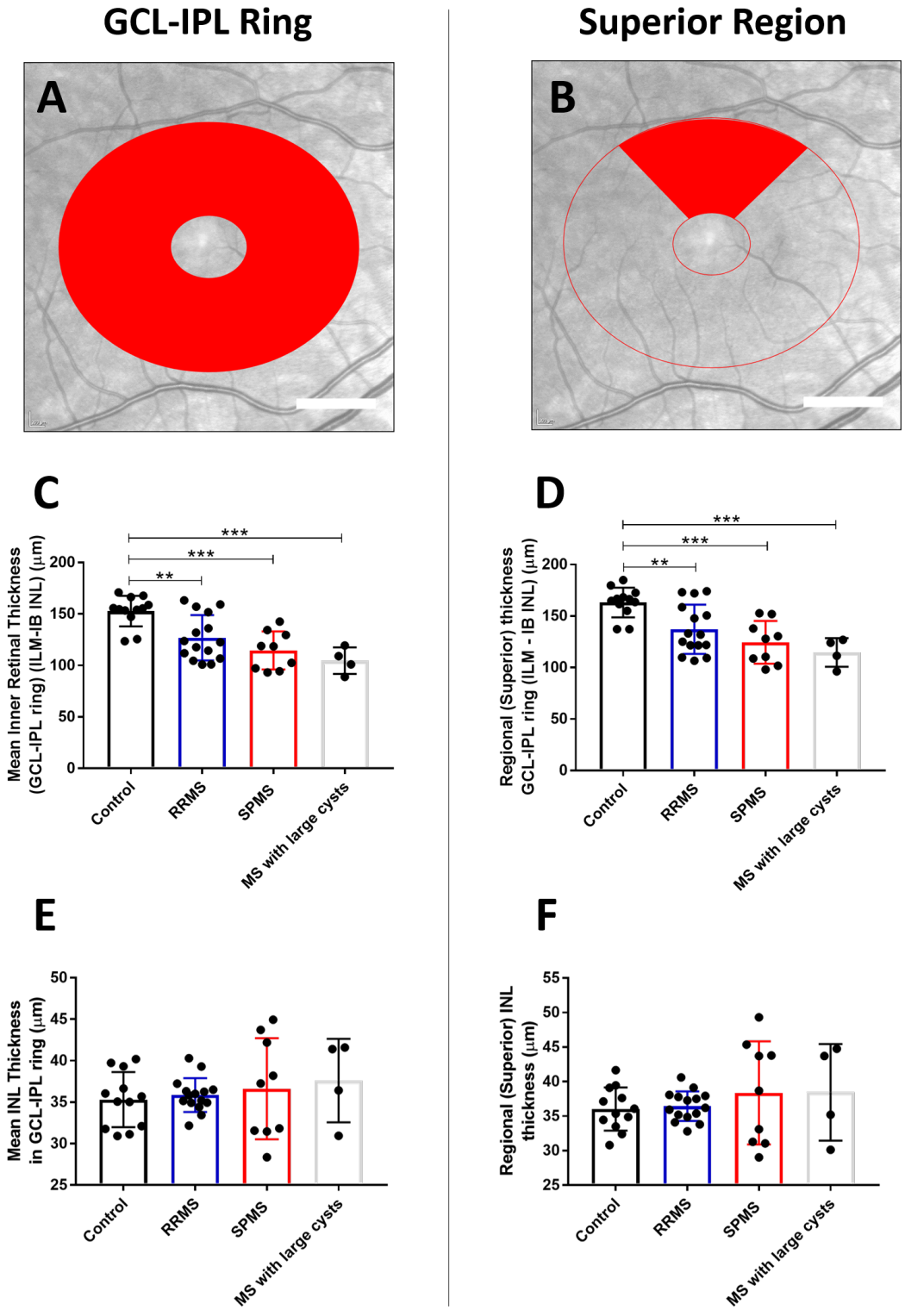

Figure 3.22: Bar charts of inner retinal thickness in the GCL-IPL ring (A) and the superior region of the ring alone (B) in control, RRMS, SPMS and eyes of patients containing Type III cysts. Groups were compared using one-way ANOVA and Tukey's multiple comparisons tests. There was a significant difference in IRT between groups when comparing both the whole GCL-IPL ring (C) and the cyst-specific superior region (D). There was no significant difference in inner nuclear layer thickness between groups for either regions (E, F).
** : P<0.005, *** : P<0.0005. Scale bar: 1mm.

Inner retinal thickness was measured in regions of cystic activity to determine whether there was a correlation between thickness and presence of cysts. A significant difference was found in inner retinal thickness in the GCL-IPL ring between groups (control, RRMS, SPMS, MS eyes with large patches of cysts) for both the whole GCL-IPL ring and superior regional thickness alone ($p < 0.0001$, $p < 0.0001$ respectively) using one-way ANOVA. Tukey's multiple comparisons tests showed a significant difference in inner retinal thickness between the control group and RRMS ($p = 0.004$), SPMS ($p = 0.0003$) and MS with large patches of cysts ($p = 0.0004$). There were also significant differences within the superior region between control and RRMS ($p = 0.009$), SPMS ($p = 0.0005$) and MS with large patches of cysts ($p = 0.0009$). There were no significant differences between other groups, including between MS groups for both ring thickness and regional thickness. A post hoc test for linear trend between left to right columns showed a significant trend for inner retinal thickness in both the whole ring region ($p < 0.0001$) and in the superior region ($p < 0.0001$) (Figure 3.22).

We wanted to discern whether the INL or overlying areas were most affected by the presence of microcysts. The presence of large patches of cyst both regionally and within the whole GCL-IPL ring is associated with atrophy of the RNFL-GCL-IPL layers. On the contrary, we found that INL thickness is variable in the later stages of disease and is thicker or at least maintained in the presence of cysts (Figure 3.22). There was no significant difference between groups for INL thickness in both the whole ring region ($p = 0.74$) and the superior segment ($p = 0.59$) as measured with one-way ANOVA. Overall, we did not see a significant difference in inner retinal thickness in patients with a higher rate of abnormalities, however there is a negative association between the frequency of abnormalities and thickness.

Other reported abnormalities were also seen infrequently in MS patients and so were not included in the abnormality grading. In one patient, a waxy membrane was seen (Figure 3.23).

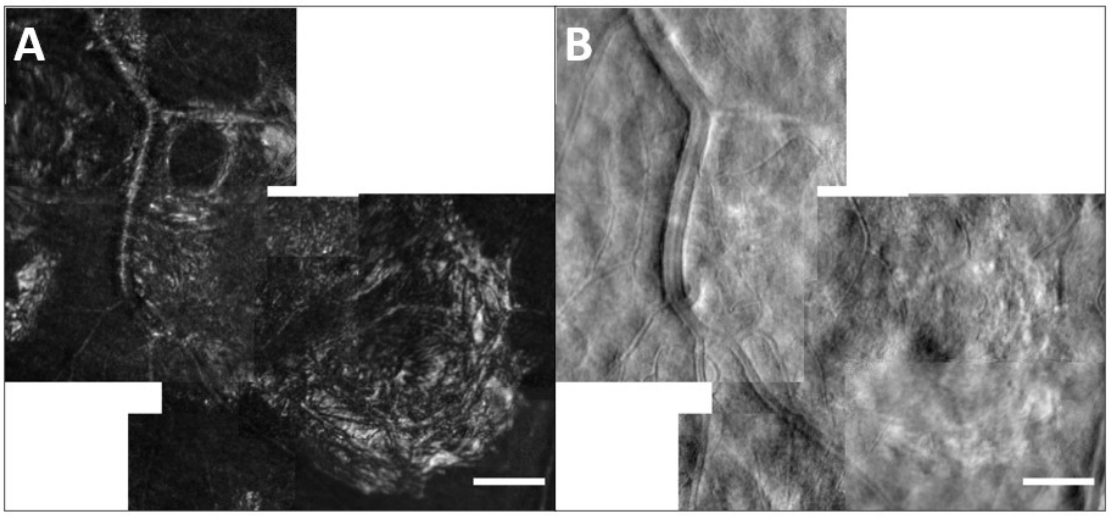

Figure 3.23: Example of a waxy membrane structure seen in an SPMS patient in both the confocal (A) and split detection channel (B) using AOSLO. Scale: 100µm

3.3.5 Dynamic Changes in the Retinal Microvasculature

3.3.5.1 Capillary Thickness Measurements

Twenty-eight vessel segments were collected from AOSLO split detection registered image sequences. Thickness ratios were collected from erythrocyte aggregates from control (n = 10), RRMS (n = 9) and SPMS (n = 10) patients. EC ratio values were not normally distributed, as assessed by Shapiro-Wilk test (p=0.01). The results of both manual and semi-automated measurements (Table 3.5) were plotted on Bland-Altman charts to measure repeatability of the techniques (Figure 3.24).

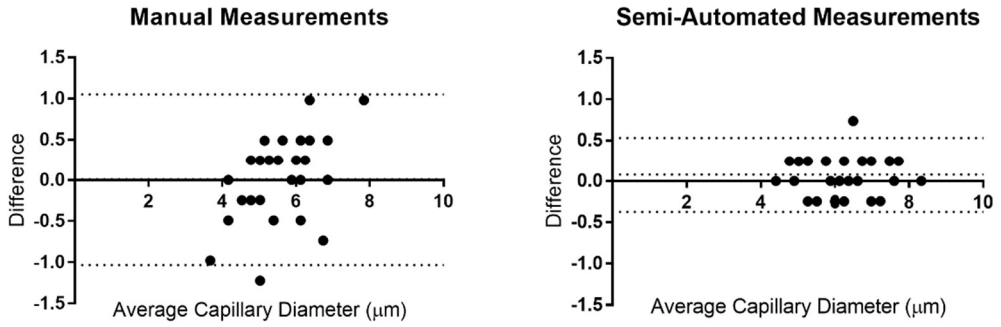

Figure 3.24: Bland Altman plots showing agreement between repeated measures of manual and semi-automated techniques.

For both manual and semi-automated methods, the bias between repeated measures was minimal at 0.01µm (SD 0.53µm) and 0.08µm (SD 0.23µm), respectively. The 95% confidence intervals were larger for the manual method at -1.03µm to 1.05µm, whereas for the semi-automated method they were -0.38µm to 0.53µm. It has to be considered, however, that this implies the manual method would only incur an error of up to 2µm, which depending on the study question may not be a concern. The semi-automated method was preferable for us for the measurement of EC ratio (Section 3.2.11), as small changes in diameter needed to be detected.

There was some error in the semi-automated measurements, likely due to variation in the placement of the line. Automated measurements despite this error were much more repeatable. Examples of good and poor agreement between the techniques are given in Figure 3.25.

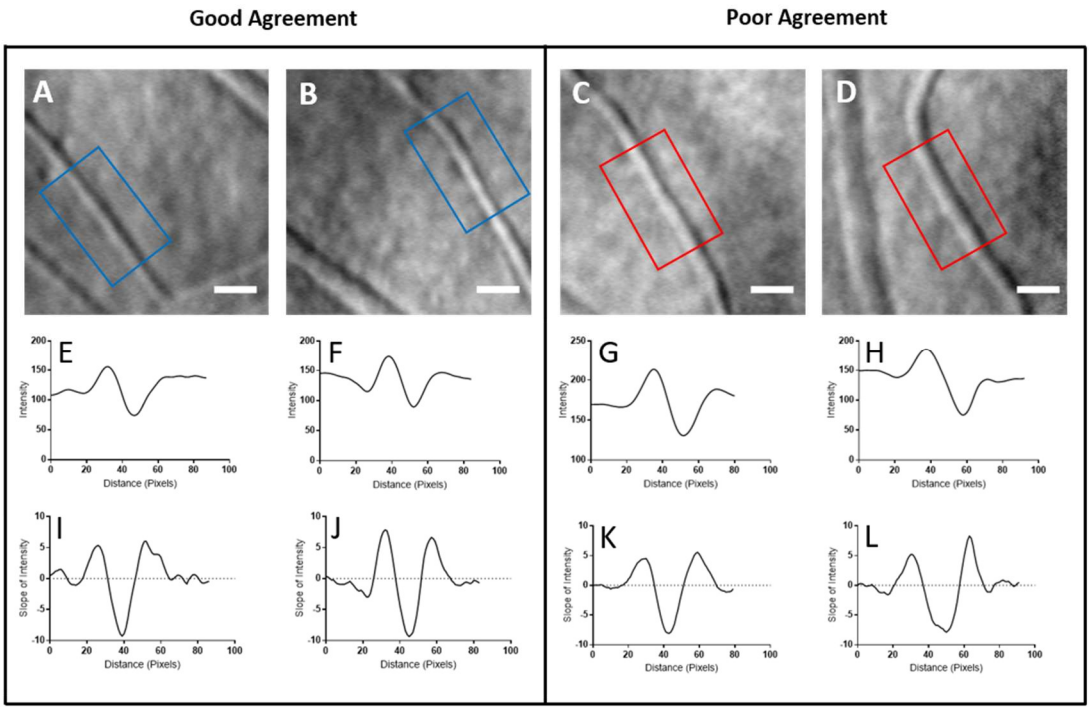

Figure 3.25: Examples of good and poor agreement between manual and automated methods of capillary measurement. There are minimal differences between vessel segments which performed well on automated measurements (A, B) and those which did not (C, D). Vessels segments for which manual and semi-automated measurements agreed perfectly (E and I, F and J) do not appear qualitatively different to those which agreed poorly in intensity profile (G, H) or slope of intensity (K, L). This difference is therefore likely to due to measurement error. Scale: 15µm.

The mean capillary thickness found in this study (Table 3.4) was similar to that seen in other studies (5.1 +/- 1.4µm using AO-OCT (Wang et al, 2011), 4.15 +/- 0.69µm using histology in the macaque retina (Weinhaus et al, 1995)).

	Capillary Thickness (µm)	
	Mean	**Standard Deviation**
Manual	5.60	0.99
Semi-automated	6.29	0.96

Table 3.4: Results of both manual and semi-automated thickness measurements.

3.3.5.2 Erythrocyte Aggregate Velocity

ECA velocity was originally measured over three frames and two velocity values averaged, however there was no significant difference in values collected in the first frame than in the second in a random sample of measurements (n = 20, paired t-test p = 0.695), therefore two frame sequences were used to increase sample size. ECA velocity was collected from aggregates in seven controls (n = 17 aggregates), including two additional control patients who were collected for this study (n = 2) who were not age matched, as there is no current literature suggesting that age has an impact on ECA velocity. Videos from eight RRMS patients (n = 24 aggregates) and four SPMS patients (n = 14 aggregates) were also used in this study.

ECA velocity values were normally distributed as assessed by the Shapiro-Wilk test (p>0.5). ECA velocity was significantly reduced in the MS group compared to controls (t-test, p = 0.048). There was a significant difference in velocity in the three groups separated as determined by one-way ANOVA (p = 0.039). Tukey's multiple comparisons test showed a significant difference between the RRMS and control group (p = 0.044) (Figure 3.26, Table 3.5).

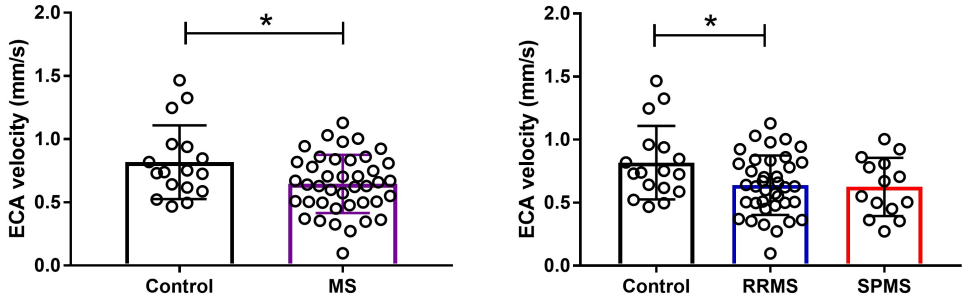

Figure 3.26: Bar charts with overlaid scatter plots comparing ECA velocity between patient groups. The error bars indicate mean and standard deviation. Groups were compared using t-test, one-way ANOVA and Tukey's multiple comparisons tests. * : P<0.05.

ECA Velocity (mm/s)		
	Mean	**Standard Deviation**
Control	0.817	0.292
MS	0.639	0.236
RRMS	0.646	0.244
SPMS	0.625	0.230

Table 3.5: Erythrocyte velocity results

3.3.5.3 EC Ratio

Thickness ratios were collected from erythrocyte aggregates from control (n = 10), RRMS (n = 9) and SPMS (n = 10) patients. EC ratio values were not normally distributed, as assessed by Shapiro-Wilk test (p=0.01). There was no significant difference between vessel sizes between MS and control registered images (Mann Whitney test, p = 0.66) suggesting that the sample was uniform and vessel size is likely to not have impacted the result. There was no significant difference in ratio between MS and control groups (Mann-Whitney test, p=0.08). When the MS group was divided into RRMS and SPMS and compared to controls, a Kruskal-Wallis test found no significant difference between groups (p=0.232). A trend was seen towards patients with SPMS having capillaries with poorer compliance than control participants, however a large amount of variability was seen in the RRMS population. (Figure 3.27)

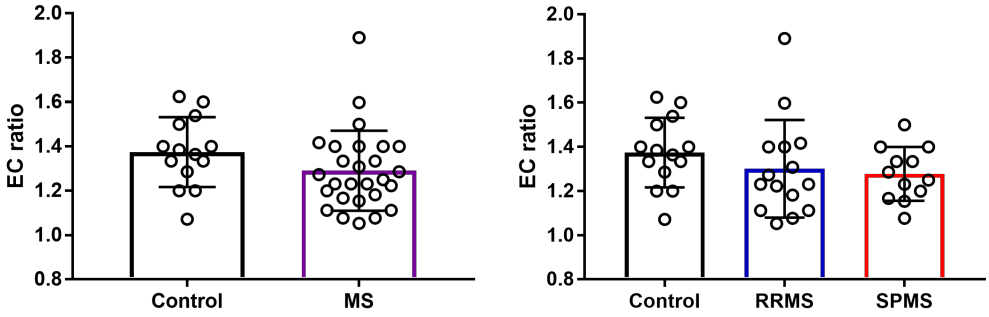

Figure 3.27: Bar charts with overlaid scatter plots comparing EC ratio between both the whole multiple sclerosis cohort and between control and RRMS and SPMS groups. There was no significant difference between the groups as measured with Mann Whitney test (Control vs MS) and Kruskal-Wallis test (Control vs RRMS and SPMS).

3.4 Summary

In this chapter we have used OCT, OCTA and adaptive optics to investigate retinal structure, vessel compliance and aggregate speed in MS patients and healthy controls. A method for measuring retinal capillary diameter was also developed and validated. We have shown a higher rate of tissue and microvascular retinal abnormalities in patients with multiple sclerosis compared to healthy controls.

3.4.1 Retinal Lamination

Neural layers of the eye are frequently impacted by multiple sclerosis; especially as optic neuritis is often the presenting feature. Our results demonstrate that measurements of inner retinal thickness collected in this study were consistent with patterns published previously, where patients further in their disease course (with SPMS, or with higher EDSS) show significantly reduced inner retinal thickness compared to earlier in the disease (Behbehani et al, 2017).

However, the retina may be undergoing additional changes besides thinning alone. Gliosis and perivascular inflammation may also lead to increased thickness of retinal layers (Green et al, 2010). This in turn may lead to incorrect interpretation of inner retinal layers as being of normal thickness despite extensive cellular loss. Costello *et al* have argued that inner retinal thickness should not be viewed in isolation as a pure estimate of anterior visual pathway health (Costello & Burton, 2018). Inflammation and gliosis may also alter the backscattering of low-coherence infrared light in OCT (Green et al, 2010) causing loss of lamination, making segmentation based on intensity alone unreliable.

History of optic neuritis is a confounding factor in measuring the inner retinal volume in these patients as it will have a profound and direct impact on retinal axons. Unfortunately,

the full ophthalmic history of these patients was unavailable therefore we are unable to consider this in our analysis. For subsequent studies we decided to collect more information on their disease course, such as visual acuity, a detailed history of optic neuritis and a detailed history of their multiple sclerosis (length of disease, time since transition to progressive phase, treatment history) in order to stratify patients more effectively. As this was only a methodological refinement study, these factors were not essential to this work, but they should be more carefully obtained in future work.

3.4.2 Retinal Vascular Assessment by OCT and OCTA

We were unable to confirm if central retinal OCTA measurements are impacted in multiple sclerosis due to small sample size, but qualitative assessment of the images suggests there is no obvious change in retinal architecture. Our study agrees with previous research which had found parafoveal vessel density to be unaffected in MS (Wang et al, 2014), however other studies have noted a significant reduction of vessel density in this region especially when differences in retinal thickness are taken into account (Feucht et al, 2019).

The optic nerve has been highlighted as a location where significant changes in vessel density occurs in MS (Bhaduri et al, 2016; Wang et al, 2014). We have not investigated optic nerve head flow in the current dataset due to the constraints of the study protocol, but look to compare patients with a history of optic neuritis to those without and correlate OCTA metrics to inner retinal thicknesses in future work.

We did not see a significant difference in fractal dimension of OCTA images of MS and control patients in this cohort, however there are potential issues surrounding the use of fractal analysis in the retina. Although it has been shown to differentiate between diabetic retinopathy and control eyes (Zahid et al, 2016), the use of fractal analysis of the retina is still in its infancy, and it is as yet unclear what factors could impact the result. For example,

OCTA is prone to imaging artefacts, which are confounded by disease processes in MS and therefore could have a profound impact on fractal analysis (Iftikhar et al, 2019).
As history of optic neuritis was not available in this cohort and due to the small cohort sizes, multivariate analyses to improve the sensitivity of OCTA metrics could not be performed. Combining structural OCT parameters and OCTA measurements has been shown to be effective in distinguishing ON+ from ON- eyes previously (Feucht et al, 2019; Spain et al, 2018). Reduced retinal perfusion has also been demonstrated in ON+ eyes following full visual recovery compared to fellow eyes measured using OCTA (Higashiyama et al, 2017). However, fellow eyes of ON+ patients still present with neural degeneration despite being asymptomatic (Fisher et al, 2006), therefore investigation of retinal vessel architecture into fellow eyes and ON- patients is essential. We decided from this to investigate both ON+ and ON- eyes in future studies to allow for a more complete picture of retinal vessel architecture in MS.

3.4.3 Abnormality Grading

The use of AO-coupled techniques in research and clinical centres has expanded as technical advances, expertise and understanding of its potential has grown (Miller et al, 1996). Techniques for imaging the retinal microvasculature with AOSLO have continually improved (Chui et al, 2012; Gu et al, 2018). As imaging of the smallest retinal capillaries has become possible using non-confocal methods of adaptive optics imaging (Chui et al, 2012), its value in gaining a deeper understanding of retinal vascular disease has been noted. Sub-clinical abnormalities in diabetic retinopathy (Burns et al, 2014) and hypertension (Koch et al, 2014) have been identified in the microvasculature using AO imaging.

Abnormalities identified in these previous studies of microvascular disease, hairpin loops and inner retinal cysts, were found in this study to be more frequent in MS patients than

controls. Regions containing microcysts were found at a significantly higher rate in SPMS patients. This is the first report of retinal microcyst imaging in MS using split detection AOSLO. Microcysts have been noted using other AOSLO designs in choroideremia (Morgan et al, 2014), diabetic retinopathy (Karst et al, 2018) and using AO-OCT in glaucoma (Wells-Gray et al, 2018). One reported abnormality in multiple sclerosis, which could explain the cystic changes seen, is microcystic macular oedema (MMO). MMO is a noted retinal abnormality in multiple sclerosis (Gelfand et al, 2012) visible with OCT and mainly found within the inner nuclear layer in the perifoveal ring region. There is much speculation as to the aetiology of MMO. There are three main causative mechanisms which have been proposed; “black holes” caused by transsynaptic loss of cells, disturbance of fluid homeostasis as the responsible cells die or become dysfunctional, and the result of combined loss of ganglion cells and increased vitreous traction on the macula.

None of the large patches of cysts were visible on OCT. Despite there being a higher number of regions positive for microcysts in relapsing remitting and secondary progressive patients, the inner nuclear layer thickness in these patients was not significantly different to controls. When investigating the specific regions in which the large microcysts are present we also do not see any changes in inner nuclear layer thickness compared to surrounding regions, which suggests the cysts are not the result of fluid leakage into the intracellular space but perhaps an evacuated space where cells have degenerated. This is supported by evidence that the overlying inner retinal layers in the region where the cysts were found was significantly thinner. A greater sample size and longitudinal study would be required to determine the exact aetiology of these cysts, and to be able to correlate them to metrics of disease. The inability to detect cysts on OCT may have been due to the distance between slices used in our OCT technique, which may not have traversed the thickness of cysts. Using 49 slices over an area of 6x6mm, the space between slices was 125µm, larger than a typical contiguous patch of three large cysts. This could be rectified in

further studies by performing more densely packed OCT scans with smaller distances between slices, allowing us to detect small spaces between layers and not overlook potential cystic space.

There were some abnormalities seen in the ACAD cohort which were not included in the grading scheme as they appeared too infrequently or were difficult to characterise accurately. Potential microaneurysms were seen as small bulges either in a vessel segment (focal bulge) or at vessel junctions (saccular/fusiform microaneurysms) (Dubow et al, 2014). However, due to the *en face* nature of AOSLO it was difficult to exclude the possibility that these were in fact vessels projecting at an angle towards the imaging beam then diving into the underlying retinal tissue, appearing as a microaneurysm. This could have been investigated using our device by adjusting focus to image above and below the potential microaneurysm. This phenomenon could also have been investigated by using AOSLO fluorescein angiography, which has been used before to identify and classify microaneurysms (Dubow et al, 2014), however this was unavailable to us.

A “waxy membrane” was also seen in one MS patient, similar to that reported before using confocal AOSLO (Scoles et al, 2014), with a strong specular reflection, scalloped edges and large circular gaps within the structure. It was proposed this could be an epiretinal membrane, which have been associated with uveitic complications of multiple sclerosis (Kaya et al, 2014), but can also be an incidental finding (Stevenson et al, 2016) especially in patients within the age range of SPMS. However, it appeared only in one patient, and could not be directly related to microvascular insult it was not included in the final grading scheme.

This study is also limited by the small region covered by graded videos (Figure 3.6). Retinal periphlebitis, vasculitis of the peripheral retinal vasculature, is an ophthalmic consequence of multiple sclerosis associated with disease severity (Ortiz-Perez et al, 2013). Although all

patients with uveitis were excluded from the study, by covering only a small region of the retina with AOSLO and OCTA, it is likely that we would miss peripheral abnormalities which may be more prevalent in our population.

We have, however, also noted some 'abnormalities' in control patients which have not been reported in control groups of AO studies previously. Both hairpin loops and inner retinal cysts were identified in control patients with no history of ophthalmic disease at a lower frequency than MS patients. Hairpin loops have been identified in a paediatric control population previously using fluorescein angiography, where the authors suggested that in this circumstance they were not pathological and that they may be a long-standing remnant from the embryonic retinal vascular bed (Penman et al, 1994). Unlike hairpin loops, there are no published reports to date on the prevalence of microcysts in healthy populations, although the lifecycle of one retinal cyst in a control participant imaged using AO has been described, albeit focussing mainly on the negligible effect of that cyst on the underlying photoreceptor mosaic (Meadway et al, 2020). Both hairpin loops and small inner retinal cysts could be seen as elements of normal variation in the healthy retina, which in the presence of conditions such as diabetic retinopathy may become more frequent and severe (Chui et al, 2016). Understanding what can be defined as normal and abnormal is essential to the further analysis of AOSLO vascular images and a prospective study of control patients should be performed to define normal values for these vascular anomalies. As the largest type of inner retinal cysts were only present in multiple sclerosis, we can suggest that these are pathological but we would require more samples of both MS and control patients to confirm this.

It is also unclear how dynamic these retinal abnormalities are. Using AOSLO, hairpin loops in DR have been shown to evolve and resolve as shown by Chui *et al* (Chui et al, 2016). Microcysts in their study, like our sample, were also not visible on SD-OCT and in one

patient appeared within a six-week period, suggesting that is a suitable time frame to see dynamic change in these anomalies. On the contrary, similar large patches of cysts have been shown using confocal AOSLO in dominant optic atrophy and remained unchanged in the patient 13 months after initial imaging (Scoles et al, 2014). Studying the lifecycle of these cysts would allow us to further discriminate between them and may hold clues to their aetiology. Longitudinal monitoring of both microcysts and hairpin loops would allow us to investigate if they are a dynamic process. If cysts are seen to resolve on AOSLO we can then examine the OCTs collected of that individual and may be able to determine if they are a consequence of cell death or simply a benign space.

Overall, it has been determined that abnormalities are found at a higher rate in the SPMS retina and their presence is related to inner retinal thinning. However, by investigating abnormalities which are static during imaging we are not utilising AOSLO to its full potential. As images are collected in short bursts, we can observe blood cells which are constantly moving and the effect these cells have on blood vessels.

3.4.4 Dynamic Measurements – ECA tracking

We showed reduced ECA speed in MS patients, which can be explained by a number of inflammatory and haemorheological pathologies previously reported in MS. There are, however, a number of issues with measuring erythrocyte aggregates as a surrogate for blood flow which have to be considered.

Aggregate speed has previously been measured indirectly using the shadows of aggregates while focusing on the underlying photoreceptor layer, either as “plasma gaps” (Martin et al, 2005) or “dark tail” flow (Arichika et al, 2013). Using scattered light AOSLO imaging, we can image these aggregates directly, unimpeded by optical aberration caused by relying on

shadows of the aggregates. The range of speed of erythrocyte aggregates measured in our sample is similar to that reported previously for aggregate measurements (Table 3.6) and of single cell erythrocytes of 0.5mm/s to 2.5 mm/s (Bedggood & Metha, 2012; Tam et al, 2011). We were unable to align speed measurements to patient's cardiac cycle, which confounds our results as it has been reported that erythrocyte speed in capillaries can change as much as 1mm/s during diastole (Gu et al, 2018; Tam et al, 2011).

Study	Type of flow	Result
Arichika et al 2013	Dark tail	1.49 ± 0.36 mm/s
Martin and Roorda 2005	Leucocyte flow	1.37 mm/s
Uji et al 2012	Leucocyte flow or plasma gaps	1.34 ± 0.42 mm/s
ACAD	Direct aggregate measurement	0.82 ± 0.29 mm/s

Table 3.6: Published measurements of erythrocyte aggregate velocity using AOSLO

The slowing of aggregates seen in our cohort could be explained by a number of inflammatory and haemorheological pathologies previously reported in MS. The binding of leucocytes to CNS endothelial cells and subsequent migration through the blood-brain barrier is an essential step in the pathogenesis of brain inflammation in MS (Prat et al, 2002). This step is mediated by adhesion molecules on the surface of the endothelium, allowing for immune cell adhesion and entry. The shed form of these adhesion molecules are found at a higher concentration in the plasma of MS patients (Elovaara et al, 2000), suggesting the CNS endothelium as a whole may be more susceptible to this cell sticking process. This may produce the friction required to slow leucocytes down, resulting in a blockage which causes an upstream increase in erythrocyte aggregation and a decrease in velocity.

Oxidative stress, a major component in the pathogenesis of MS, can have a direct effect on the erythrocyte membrane through lipid peroxidation leading to poor erythrocyte deformability (Ljubisavljevic et al, 2014; Polidoro et al, 1984). Poor erythrocyte

deformability can cause a number of issues within the microvasculature, exemplified by sickle cell retinopathy, a condition where aggregation of abnormal haemoglobin causes loss of erythrocyte deformability leading to stagnant blood flow in the pre-capillary arterioles, thrombosis and finally ischaemia (Elsayed et al, 2019). Aggregation is important as a haemorheological factor in microcirculatory problems as well as its direct impact on blood viscosity. However, reports on the levels of total blood viscosity and erythrocyte deformability in MS, as measured with classic filtration analysis, are contradictory (Brunetti et al, 1981; Pollock et al, 1982; Simpson et al, 1987).

There are some discrepancies in the understanding of the nature of erythrocyte aggregates. Some have determined that aggregates are formed by a white blood cell due to their larger size blocking the path of red blood cells downstream (Arichika et al, 2013). It has not been clearly stated whether there is a spectrum of erythrocyte aggregation – whether in disease aggregates appear slower or more frequently than in health. Although we did not systematically investigate this, we did not see any significantly higher number of aggregates in our MS patients. Further studies in erythrocyte aggregates should look at classic haemorheological diseases, such as sickle cell retinopathy which is likely to have increased aggregation even during an inactive phase of the disease, to determine if increased aggregation can be detected using AOSLO and if it could be correlated to disease parameters.

Similar to measuring ECA velocity, “dark tail velocity” has been measured using AOSLO (Arichika et al, 2013; Arichika et al, 2014a; Arichika et al, 2014b). The “dark tail” refers to the shadow that an erythrocyte aggregate causes on the underlying photoreceptors when both are in focus using confocal reflectance. With the imaging protocol used we are unable to visualise this dark tail as the set axial slice on the confocal channel (~60µM) was too narrow to capture both layers at once in most patients. A more useful metric would be that

of single cell velocity which has been investigated by other groups using AOSLO (Gu et al, 2018; Guevara-Torres et al, 2016; Zhong et al, 2008). Whilst we did investigate the possibility of tracking erythrocytes, we are unable to track individual erythrocytes with the AOSLO used as the frame rate (16Hz) would lead to an expected measurement error of approximately 47% for an object at 1.5 mm/s (Tam & Roorda, 2011). The similar appearance of adjacent erythrocytes also makes identification and matching of cells between frames nearly impossible. This caused us to move towards alternative AOSLO designs to allow for further investigation into the retinal microvasculature, such as systems which use a dual beam method to allow for substantially faster capture rate and therefore lower error with an elegant design adjustment (de Castro et al, 2016). Many of the reported measurements of aggregate velocity have also been made in the vessels surrounding the foveal avascular zone, which is understandable due to its singular lamination and clear capillary structure. However, this is likely not representative of the whole retina.

ECA speed may be confounded by a number of factors, such as geometric shape of vessel, distance of vessel segment from its branches and likely variation of ECA speed across the cardiac cycle. The variation seen in erythrocyte aggregate velocity could be due to a number of factors. Firstly, as mentioned we have not accounted for pulsatile flow in our measurements. Secondly, despite categorising capillaries as single file flow vessels, there can also be variation in this also, where some vessels are much more prone to aggregation than others suggesting they may be slightly larger than the average capillary despite demonstrating single file flow. Thirdly, aggregation velocity likely reflects the average velocity on the capillary in which it is found, and individual capillary velocity is known to be variable in small regions of healthy subjects (Bedggood & Metha, 2012; de Castro et al, 2016). Finally, blood cells can form aggregates of different lengths, according to the number of red blood cells stacked together, and the aggregate lengths could influence

these speeds. The leading edge in our case was always measured for velocity but unfortunately the lagging edge of the aggregate was not always possible to measure because of our small field of view (1 x 1 degree). The length of the aggregate was also seen to vary during measurement, which is understandable if they are formed by a continuous "backing up" of erythrocytes behind a slowed rolling leucocyte. Due to its limitations, tracking of erythrocyte aggregates was no longer pursued and a non-invasive method of measuring erythrocyte velocity in a range of vessel sizes was sought.

3.4.5 Dynamic Measurements – EC ratio

We did not see any significant difference in patients regarding vessel stiffness as measured by the EC ratio, however the smallest vessels may not be appropriate for us to test as the structure of the retinal capillary wall does not contain material such as elastin which could be damaged in MS leading to stiffening (Hogan & Feeney, 1963). Basement membrane thickening may cause reduced compliance in these vessels, which although not shown in MS to date, has been demonstrated in cerebral microvessels in Alzheimer's disease (Mancardi et al, 1980) and it could be investigated in future using high resolution AOSLO.

Previous research in MS focussed on stiffness of larger vessels (Kochkorov et al, 2009) which are perhaps more likely to show changes in compliance due to the difference in components of vessel walls as you move down the vascular tree (Hogan & Feeney, 1963). Vascular compliance is usually measured by calculating the relationship between ocular compliance, pulse pressure and intraocular pressure (Villamarin et al, 2012), requiring relatively invasive procedures. In future, the pulsatility of larger vessels could be measured with AOSLO as an index of vessel stiffness.

3.4.6 Other Limitations

Axial length measurements were unavailable for this study, therefore a set axial length was used to scale images. This could have affected both cyst measurements and ECA velocity, however MS is not known to be related to alterations in axial length so it is unlikely to cause a systematic error in results. The possible error incurred by axial lengths of 22 to 26 mm was calculated as substantially lower than the possible measurement error on images, therefore this was considered to have a limited impact on the result. The difference between image scale for a 22mm eye (0.45µm/px) and a 26mm eye (0.53µm/px) when measuring an object of 20 pixels wide such as a cyst, would cause a difference in measurement of 1.63µm. This is within the range of possible measurement error for manual measurements such as cyst measurement, capillary measurement and selection of erythrocyte aggregates for velocity measurement.

3.4.8 Summary of Chapter

In this preliminary study we have identified significant anatomical changes in the inner retina as well as functional changes to the retinal microvasculature in MS (Table 3.7). We have developed microvascular imaging protocols for use in MS and identified areas of interest for further investigation in the disease.

Parameter	Effect on disease subtype		Figure Number
	RRMS	SPMS	
IRT	↓	↓↓	3.13
INL Thickness	ND	ND	
OCTA Metrics	ND	ND	3.15
Inner Retinal Abnormalities	ND	↑	3.17
Type 3 Cysts	Present		3.18
ECA Velocity	↓		3.26
EC Ratio	ND	ND	3.27

Table 3.7: Summary of Chapter 3 results. The number of arrows indicates the significance level of difference between the MS subgroup compared to age-matched control subjects. One arrow, *P<0.05*; two arrows, *P<0.005*. ND: No difference, IRT: Inner retinal thickness, INL: Inner nuclear layer, OCTA: Optical coherence tomography angiography, ECA: Erythrocyte aggregate, EC ratio: Erythrocyte aggregate ratio.

Development of Techniques used in AOSLO Microvascular Imaging

4.1 Introduction

The retina is one of the most metabolically active tissues in the body, and as such is very sensitive to changes in blood flow. The anatomy of the retinal microvasculature is well understood. The architecture of the retinal circulation is largely planar, with the vasculature being stratified into three main capillary layers; the superficial vascular plexus embedded in the RNFL and GCL, and the intermediate and the deep vascular plexi, which are found above and below the inner nuclear layer respectively. The inner retina is fed by the central retinal artery, branching to arterioles which deliver blood to capillaries rich with oxygen and nutrients, which are then exchanged at the capillary level for carbon dioxide and waste products. These waste products are then carried back by venules to the central retinal vein. Functional characterisation of the microvasculature, in velocity and flow of blood, is less well defined as functional measurements of retinal capillaries are limited to techniques which can only be performed using invasive dyes.

Standard colour fundus photographs can resolve vessels ~75-150µm in diameter, however the critical activities of the vascular system take place at the capillary level (5-10µm diameter) and in the vessels adjacent to it. There is increasing evidence to suggest that in SPMS there is a subtle and long-standing insult to the microvasculature which would be best visualised at the capillary level. Capillary flow is reliant on flow through branches of the arteriolar tree, therefore measurement of velocity and flow through these vessels should give us an indication of the health of the capillary bed. Different methods have been developed to detect and measure retinal perfusion in both invasive and non-invasive manners with varied levels of resolution. Non-invasive techniques for measuring retinal blood flow either suffer from high rates of variability such as laser Doppler flowmetry and laser speckle flowgraphy (Avila et al, 1998; Sugiyama et al, 2010), or are constrained to

certain vessel sizes, as some are limited to small vessels, such as the retinal functional imager (Grinvald et al, 2007) or to large vessels, such as colour Doppler imaging (CDI) (Dimitrova & Kato, 2010) and Doppler OCT (Harris et al, 1998).

The resolution of standard ophthalmic imaging is inhibited by two main factors; low contrast of the smallest vessels and scatter caused by optical aberrations of the eye. Contrast of individual vessels can be improved by providing intravenous or oral dye such as in fluorescein angiography (Yang et al, 1997), however this technique is invasive, there is a risk of allergic reaction and it can only provide "bulk" velocity measurement. Optical aberrations of the eye can be corrected using adaptive optics coupled techniques which, as previously shown, can resolve vessels at all levels of the vascular tree. Numerous techniques using AO-coupled technologies have been proposed for measurement of retinal microvascular velocity. Direct measurements of leucocyte velocity have been achieved by tracking the shadows of leucocytes (and likely, erythrocyte aggregates) (Martin et al, 2005; Martin & Roorda, 2009; Tam & Roorda, 2011) and the "dark tails" of erythrocyte aggregates (Arichika et al, 2013) on the underlying photoreceptor layer. These techniques measure aggregate velocity and, although useful in estimating capillary flow, are limited due to inherent variations in pulsatile flow and haemorheology.

The use of AOSLO in imaging blood flow directly is often limited by the frame rate of devices, as imaging blood flow below a certain speed results in an inability to track individual moving cells and "aliasing" of these cells. An alternative strategy for measuring blood velocity which does not require an extremely fast frame rate, is to utilise the fast-horizontal scanning capability of the AOSLO by "freezing" the vertical position of the beam, so the rapid resonance scanner can be used to image one specific line repeatedly (at a kilohertz rate), allowing for accurate measurement of cell velocity in that region. As the laser scans across the retina, it can also be stopped at a specific Y position, allowing for

repeated scanning at one specific plane. This results in an image which is part XY, representing structural imaging, and part XT, representing speed of cells. As blood cells move through this plane they appear as “streaks” which are seen at different angles to the scan line, depending on their speed. The measured angle can then be converted to velocity. Using this “XT” technique, AOSLO can be used for non-invasive visualisation of cell speed and calculation of flow across the complete hierarchy of the retinal vascular tree.

Previously published reports on XT imaging use a manual method of measurement (Palochak et al, 2019; Zhong et al, 2012; Zhong et al, 2008; Zhong et al, 2011), which involves measuring the angle between the streak and the scan line in triplicate and averaging the result (Zhong et al, 2011). As blood velocity is pulsatile in nature, in order to measure blood velocity accurately it must be measured across the cardiac cycle and averaged over a number of cycles. This increasing number of measurements quickly become time consuming and impractical, therefore this technique would benefit from automation.

As this process is relatively time consuming, some researchers have taken a reductionist approach in measuring the cardiac cycle, identifying the frames which appear to represent the peak and trough of the cycle and measuring them in isolation to calculate the average flow (Palochak et al, 2019). This technique, although efficient, may be prone to subjective error and disregards information which could be gleaned by studying the morphology of the whole cardiac cycle. An automated method of velocity measurement has been developed for XT-type images using the Radon transform (Joseph et al, 2019), although it was specialised for images acquired from anaesthetised mice which do not present the same challenges of acquisition as awake human subjects. Similar approaches, such as using the Fourier transform, could prove ideal in the automated measurement of streaks.

The Fourier Transform converts image information from the time domain to the frequency domain and the resulting Fourier spectrum can be analysed to extract information on both the frequency of components within an image and their orientation. As the Fourier Transform has been used previously for AOLSO image analysis (Cooper et al, 2013) it makes an ideal candidate for the automated analysis of streak orientation in XT images. The aim of this study was to evaluate the comparability of manual measurements of XT imaging to an open source Fourier transform based plugin (Directionality, v2.0, Fiji).

In order to measure the microvasculature in detail we needed to utilise emerging techniques in AOSLO to investigate blood vessel structure and function at all levels of the vascular tree. In the previous study, we did not have the hardware or software in place to perform XT imaging or analyse it effectively. We subsequently obtained a new custom-built AOSLO device that gave us the capacity to develop vascular imaging and analysis techniques which would help answer the question posed. In this chapter we discuss the development and validation of tools to analyse XT imaging in a cohort of control patients for both the current study and future studies in retinal microvascular disease.

4.2 Materials and Methods

4.2.1 Declaration of Collaborator Roles Within Chapter

The ophthalmic data in this chapter were collected by Sarah Houston, Dr Adam Dubis and Vasileios Theofylaktopoulos. Ethical approval was applied for and received by the UCL Research Ethics Committee in April 2019 (Approval Number 11353/004). The XT pre-processing analysis script was written by Dr Joan Nuñez Do Rio and adapted by Sarah Houston to make it more user-centric. All analysis for the pilot study undertaken at Moorfields Eye Hospital was completed by Sarah Houston. All videos included in this chapter were prepared by Sarah Houston.

4.2.2 Subjects

Seven healthy volunteer subjects were identified. This study adhered to the tenets of the Declaration of Helsinki. Each subject was dilated with 1% tropicamide. Control participants were recruited to this study on the basis of the following inclusion and exclusion criteria (Table 4.1).

Inclusion Criteria
Aged 18-80 years old
Exclusion Criteria
History of ophthalmic disease or trauma
History of photosensitive epilepsy
History of migraines
Any form of statin treatment

Table 4.1: Summary of inclusion and exclusion criteria for the Pilot Study of Non-Invasive Retinal Vascular Flow Imaging

4.2.3 BMC AOSLO Instrumentation

In order to improve our vascular imaging quantitative abilities a new AOSLO system was installed (BMC AOSLO (Section 2.1.6)), with the capability to perform XT imaging. Healthy volunteer subjects were used in this study to develop and validate new techniques and protocols for this device.

4.2.4 AOSLO Imaging Protocol

4.2.4.1 Vessel Identification

The participant's right eye was used as default and only changed to left eye if requested by the subject. In this particular study it was not possible to use infrared images to distinguish arteries from veins, however when using a wide field of view (2x2 degrees) on large vessels using the AOSLO it is possible to identify them visually based on their reflectance as arteries appear lighter than veins because of the high concentration of oxyhaemoglobin in arterial blood, which is red in colour (Figure 4.1). Larger arteries could therefore be identified and traced downwards to measure velocity in a range of vessel sizes.

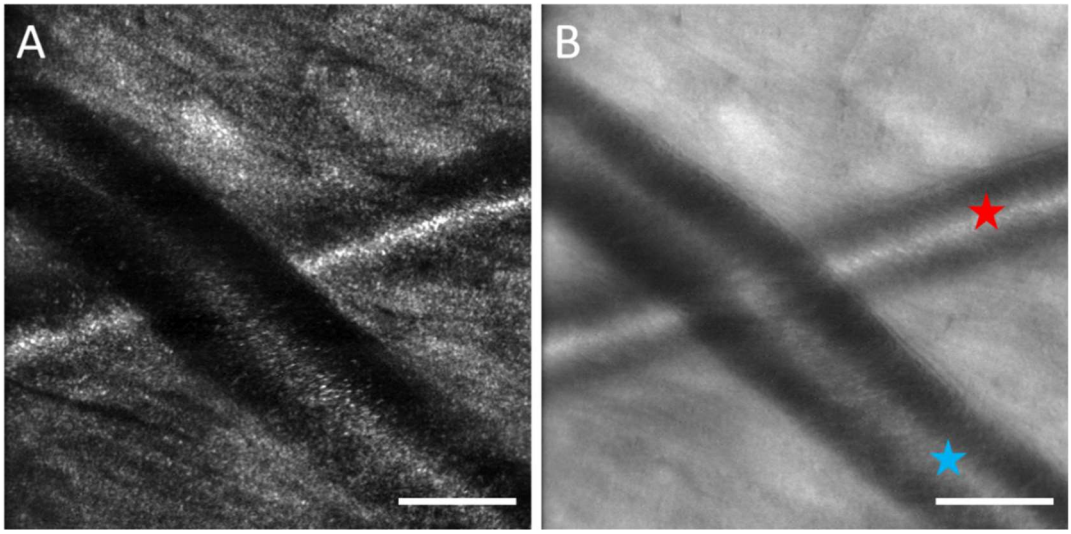

Figure 4.1: Images demonstrating how arteries and veins appear on AOSLO confocal (A) and Offset Aperture 790nm (B) images in order to differentiate. The red star indicates an artery and the blue star indicates a vein. Scale bar: 200µm

4.2.4.2 Imaging Sequence

To investigate vascular function at different levels of the vascular tree four locations along an individual arterial branch were identified which would subsequently be used for imaging (Figure 4.2). Each image contained 50% XY imaging and 50% XT imaging to ensure that the blood vessel measured was always in view and videos of 300-500 frames in length were collected. Measurements were limited to arteries and arterioles as the cardiac pulse is significantly dampened in venules and veins, resulting in less variation of speed and therefore a limited range of streak angles across a cardiac cycle, as demonstrated in other AOSLO investigations of retinal blood flow (Joseph et al, 2019). All images analysed in this experiment were collected using 790nm offset pinhole imaging by utilising the interactive stages on the BMC AOSLO device to move a 700µm aperture in front of the 790nm detector 300-500µm to the right. The pinhole position was optimised to remove directly reflecting structures, while allowing sufficient signal to visualise the multiple scattered structures. The size of displacement depended on the resulting image quality in individual participants but remained relatively consistent throughout imaging. This offset-pinhole scattered light imaging allowed for enhanced definition of vascular structures in the XY portion of the image and increased visibility of cell streaks within the XT portion of the image compared to confocal imaging (Video 3: https://youtu.be/BtXfGAtNsZM) used in the development of the XT technique (Zhong et al, 2008; Zhong et al, 2011).

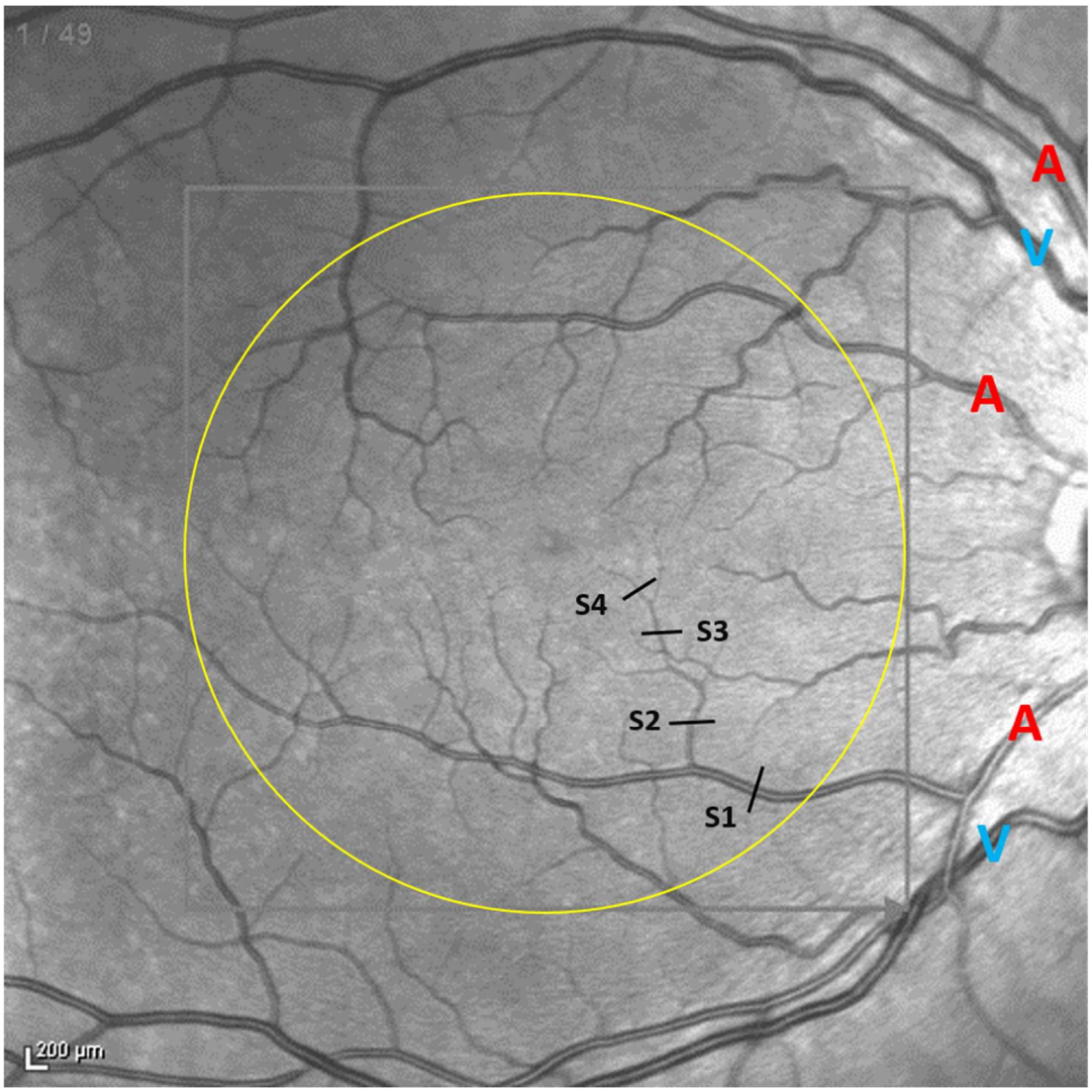

Figure 4.2: Example of 30° infrared retinal image describing the XT imaging protocol. The yellow circle indicates an approximate 10-degree radius circle area where fixation could usually be directed. “A” indicate the typical appearance of arteries and “V” indicate the typical appearance of veins. S1/S2/S3/S4 indicate the typical vessel segments selected for XT imaging. Scale: 200µm

4.2.5 Blood vessel diameter analysis

Wall and lumen diameter measurements were performed using ImageJ. Using the line tool, three separate measurements were made of the whole diameter of vessel including the walls and of the lumen alone. These three measurements were then averaged, and the wall measurement was calculated by subtracting the average lumen measurement from the

average whole vessel diameter. The resulting wall thickness therefore represents both sides of the vessel wall. This was deemed appropriate for AOSLO measurements as vessel walls often appear asymmetrical in scattered light imaging (Figure 4.3).

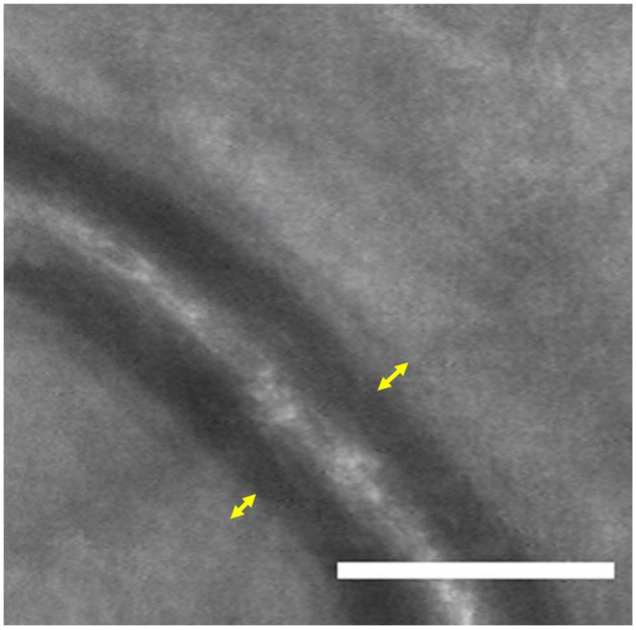

Figure 4.3: Example of arteriole with asymmetrical vessel walls likely due to the directional nature of off-pinhole imaging. Scale bar: 100µm

4.2.6 Development of AOSLO XT Analysis

4.2.6.1 Introduction

AOSLO XT Imaging can be used to measure the velocity profile in real time in vessels as small as pre-capillary arterioles and venules as well as large arteries and veins of the retina. As the laser scans across the retina, it can also be stopped at a specific Y position, allowing for repeated scanning at that position. This results in an image which is part XY, representing structural imaging, and part XT, representing speed of cells. As blood cells move through this plane they appear as a streak. Cells will appear at different angles to the

scan line, depending on their speed. The measured angle can then be converted to velocity (Figure 4.4).

Calculation of cell velocity is performed firstly by calculating speed of erythrocyte in the vessel lumen by the measured streak angle θ ($0 < \theta < \pi/2$) against the scanning line. The horizontal vector of velocity (Vp) is then calculated by the equation given below (Figure 4.4, D), where *f* is the horizontal frame rate and *k* is magnification. Velocity along the axis of the vessel must then be calculated by taking into account the angle of the blood vessel to the scanning line, α.

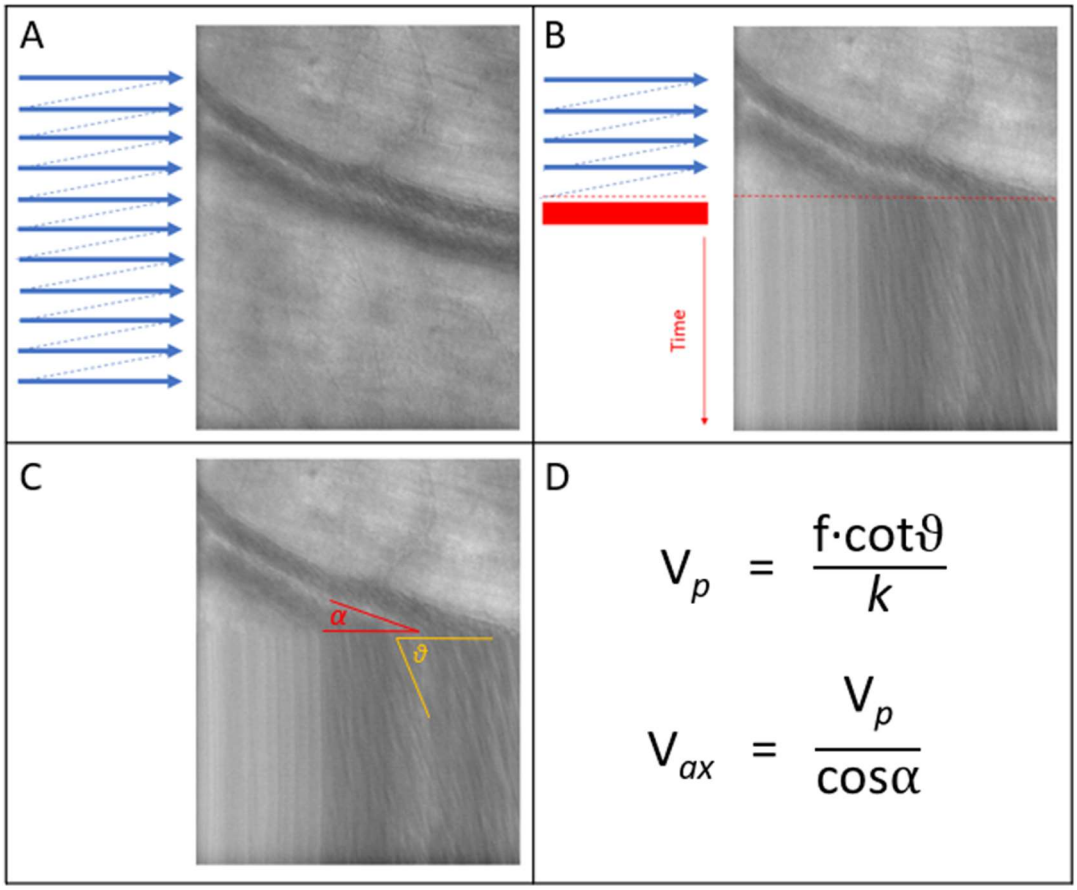

Figure 4.4: Schematic of XT imaging collection and analysis. In AOSLO imaging, a fast scanner moves the laser from left to right and a slow scanner moves it to the next line to repeat the process until a full XY image is formed (A). In XT analysis, the slow scanner is paused at a prespecified Y location and the fast scanner repeatedly scans the same location to create an image which is part XY and part XT (B). The XT portion of the image contains cell "streaks" whose slope angle to the scanning line (θ) can be used to calculate speed of cells in the scanning direction (V_p) (C, D). This must then be adjusted using the angle of the vessel to the scanning line (α) to calculate the velocity of cells along the vessel axis (V_{ax}). f: horizontal scan frequency, *k*: system magnification.

The current published method of measurement of these streaks involves manually measuring the angle between the streak and the scan line in triplicate and averaging the result (Zhong et al, 2011). Due to large volumes of data required, semi and fully automated methods were investigated.

4.2.6.2 Analysis Development

As the Fourier transform can be used to calculate orientation of objects within an image, this could be a highly effective and efficient method of analysis for XT images. Although efficiency in measurement is important, accuracy of results is crucial. When all possible streak angles are plotted against the resulting velocity for a number of vessel angles, there is clear indication that measurement error is not equally distributed across the angles (Figure 4.5). For an 80-degree measurement, a measurement error of 5 degrees will result in a velocity difference of 1.47 mm/second. However, for a 20-degree measurement which reflects the faster components of a cardiac cycle, a measurement error of 5 degrees will cause a much more significant difference in velocity of up to 15.81mm/second. It is therefore important for both efficiency and accuracy of data collection that an automated method of measurement is sought. The aim of this experiment was to evaluate the comparability of manual measurements to an open source Fourier transform based plugin (Directionality, v2.0, Fiji).

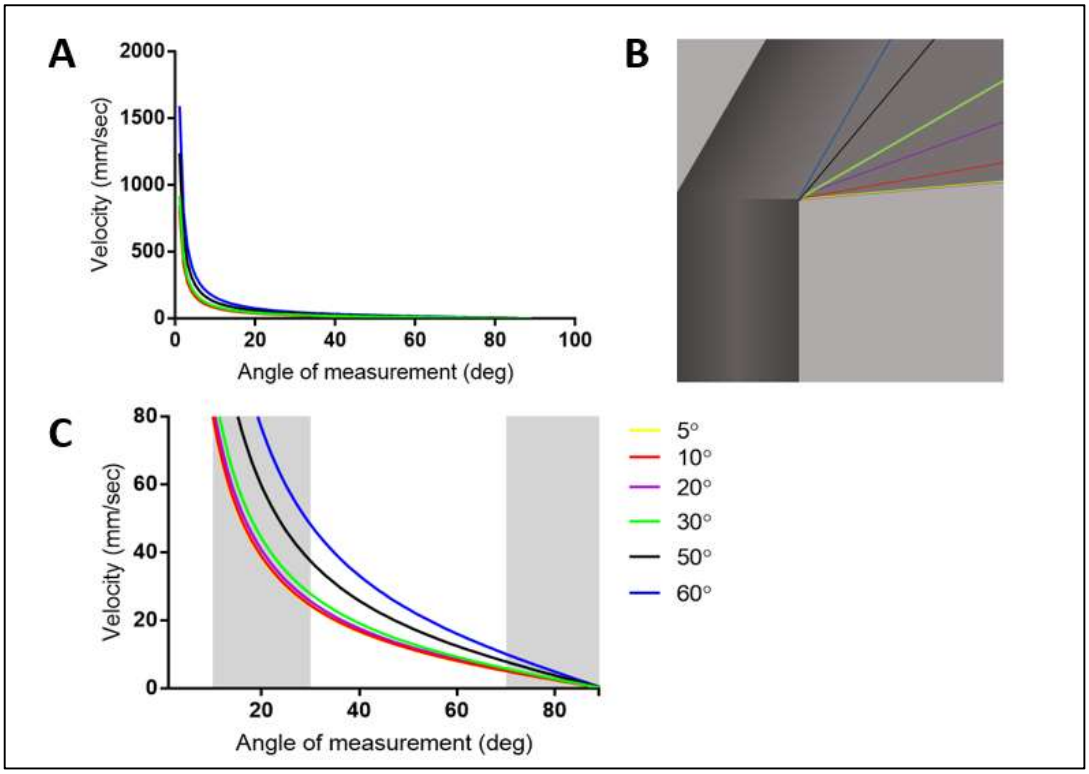

Figure 4.5: XT Measurement Error. The relationship between velocity and angle of measurement (A) shows us that there is a narrow range of velocities that can be accurately measured using XT analysis and there is significant overlap of measurements based on the angle of vessel to the scanner, the angles investigated are represented in B. The results from A are magnified in C, and a distinct separation of slopes are seen at velocities <80mm/s. The risk of measurement error from 10-30 degrees (shaded area) is much greater than at 70-90 degrees (shaded area), as the slope is larger at narrow angles.

4.2.6.3 Pre-processing of Videos for Directionality

The structural component of the image (XY) contains other directional elements, such as the blood vessel walls or the retinal nerve fibre layer, which would be detected by the Directionality software and therefore needed to be removed. Straight lines either side of the vessel column representing elements in the line scanning which were not moving also need to be excluded from the image as they could cause inaccuracies in analysis. In order to account for this, images were processed through Matlab (R2017b) to crop out the structural component. This was performed by manually selecting the left and right side of the XT profile in each frame, based on where straight lines representing static objects began. Frames which contained blinks, indicated by a sudden drop in intensity, or eye

movements, indicated by image warping, were also removed from the image stack at this stage and replaced with black frames to maintain image order.

Although the Directionality plugin is automated, using the plugin requires some pre-processing of images. The time taken to pre-process images is an important consideration when comparing these two measurement techniques. The length taken to complete manual measurement of frames was measured using an external stopwatch, and pre-processing of data was measured using the Run and Time functionality within Matlab.

4.2.6.4 XT Measurement

Retinal cell velocity was measured in videos of equal length (100 frames) of separate vessel segments. Angles were measured using both the reported manual technique (Zhong et al, 2011) in triplicate using the Line Tool in ImageJ and using the Directionality plugin (Video 4: https://youtu.be/OwodyE87B-I). Direction (in degrees) was measured between -5 and -65 degrees, or 5 and 65 degrees depending on direction of flow using 60 bins of measurement. This interval was selected based on expected angles of streaks, and to avoid measurement of purely horizontal and vertical artefacts within the images. Results from the Directionality plugin were also post-processed in Microsoft Excel to remove any outliers i.e. filtering angle from 5-65 degrees, filtering Amount >0.1. (Figure 4.6)

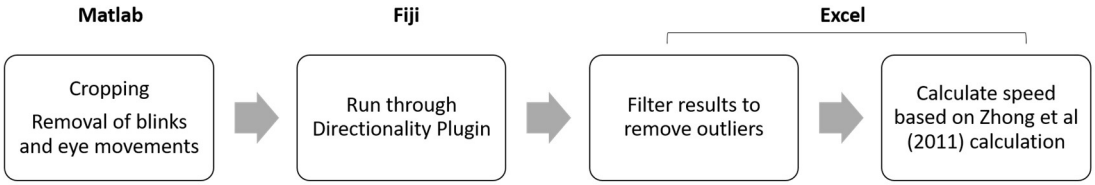

Figure 4.6: Process of measuring velocity using Directionality plugin.

4.2.6.5 Measurement of cardiac cycles

As there is some physiological variability in cell velocity from cycle to cycle, I created a MATLAB script to analyse the resulting cell velocity curves and produce an averaged result representative of the whole cycle. In the MATLAB script, the curves are read by the script and plotted as Frames versus Velocity. The user then identifies the first three acceptable velocity curves. The acceptability of the curves is based on their morphology, whether they appear similar to what is expected (Figure 4.7) and whether they appear similar to the other curves in the plotted cycles in both morphology and size. Curves must also be continuous in the critical regions of peaks and troughs, if more than one frame is missing in these regions that cycle should not be selected. Missing frames in other parts of the cycle, such as the descending wave, are acceptable if the other criteria for acceptability are still met. Once these curves are identified the user selects the peaks and troughs of each cycle. The peak and trough of each cycle are then averaged, then the difference between consecutive peaks and troughs are averaged together to create the Vax Average. The three peaks of each cycle are averaged to create the Average Peak Velocity.

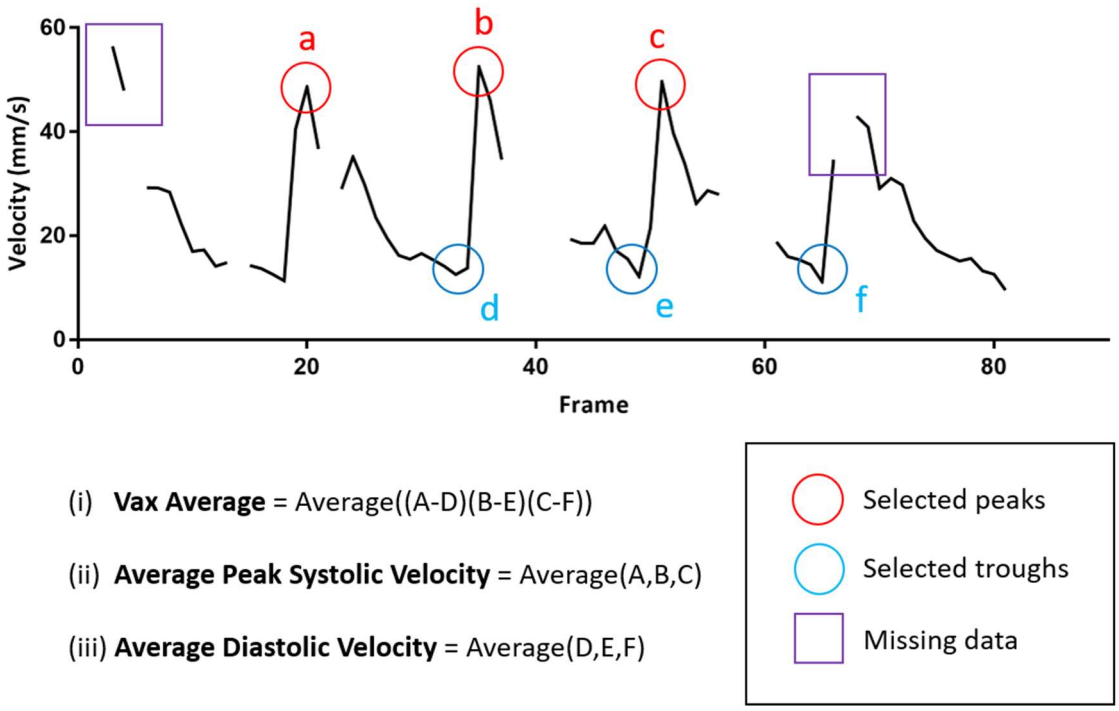

Figure 4.7: Methods of XT derived cardiac cycle measurement and analysis. Examples of cycles which would not have met the inclusion criteria are highlighted in purple squares, and suitable peaks and troughs are featured in red and blue circles respectively. Equations describing methods of cycle analysis are included also.

4.2.7 Grading of Result Quality

The quality of results derived from Directionality measurements was determined by comparing them to results from averaged manual measurements. Directionality results were overlaid with manual measurements and results were graded based on these comparisons. Poor quality videos were identified based on number of angles identified by the software (less than 20 frames) and clear variation from manual measurement. Medium quality videos were identified based on number of significant outliers from the manual measurements (less than 5). Significant outliers were defined as velocity measurements which did not follow the morphology of the cardiac cycle and were approximately two standard deviations from the mean. High quality videos were classed according to good subjective overlay on manual measurements.

4.2.8 Cycle Averaging

In order to ensure repeatability of velocity measurement, we also had to determine the number of cycles which should be measured to produce an “average” velocity measurement. There is variation in the number of cycles measured and averaged using different techniques, and there was noticeable variation in peak velocity in our results, therefore it was important for us to determine the number of repeated measures required to obtain a representative average velocity for the vessel segment. Twenty-eight videos from six control subjects (3-8 videos per subject) were analysed for this part of the study.

4.3 Results

4.3.1 AOSLO Image Modality Selection

Velocity results from split detection videos were comparable to that of confocal videos, and a higher number of frames were measurable (Figure 4.8), therefore split detection and other scattered light imaging were used henceforth to measure velocity.

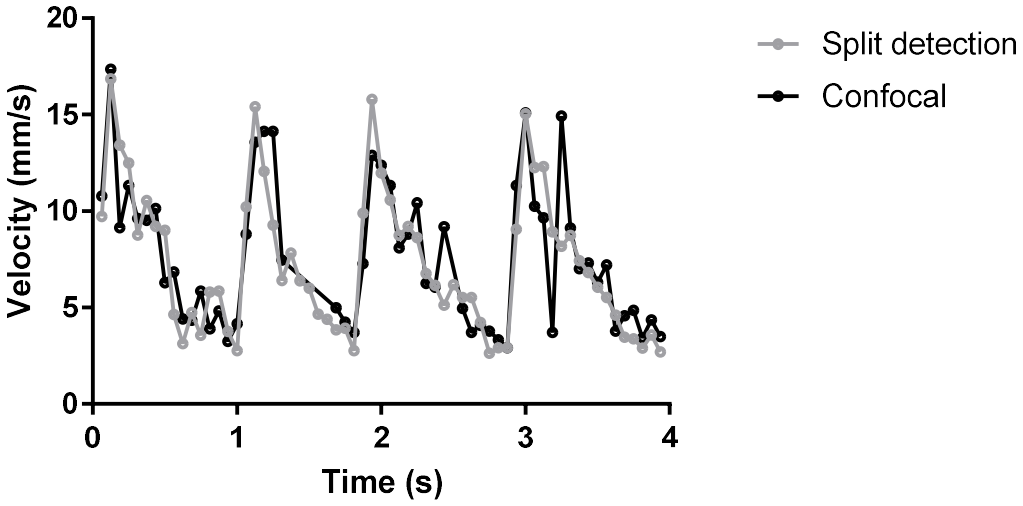

Figure 4.8: Comparison of velocity measurements made manually from simultaneous confocal and split videos of the same vessel segment.

4.3.2 Cycle Averaging

Next it was important to determine the number of repeated measures to average to obtain a representative velocity for the vessel segment. Figure 4.9 shows the change in velocity measured from 28 videos over 1, 3 , 5, 8, 10 and 15 cycles. There is no more than 20% change across any of the videos measured.

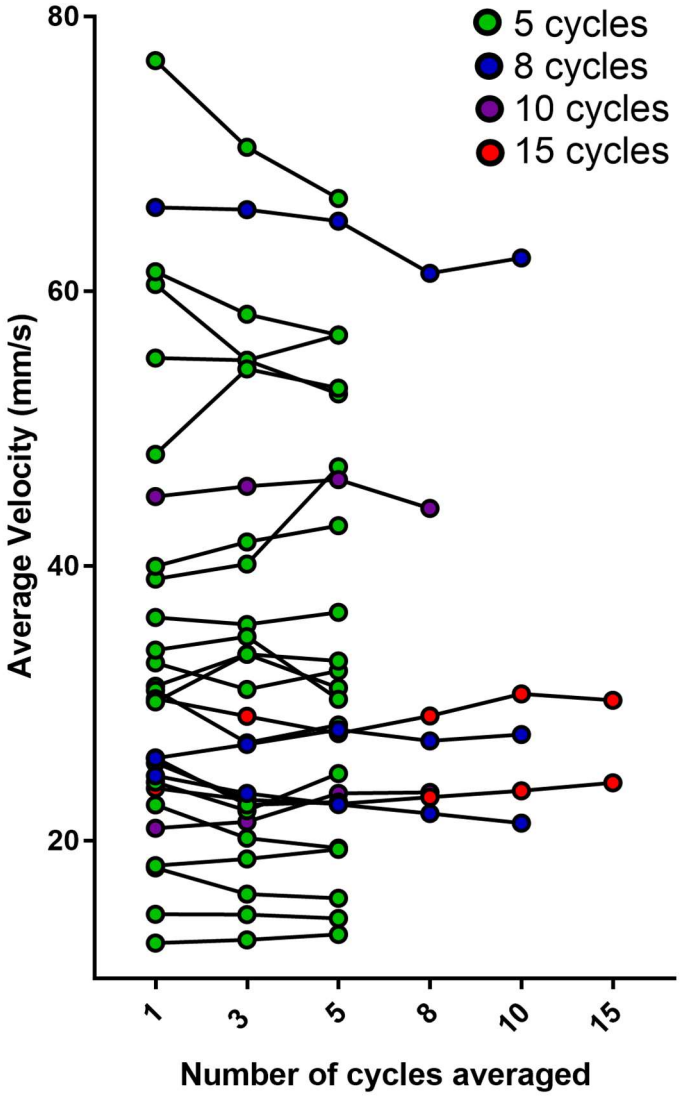

Figure 4.9: Before-after plot of the average velocity of individual videos. Twenty-eight videos from six control subjects (3-8 videos per subject) were measured over 3, 5, 8, 10 or 15 cycles, depending on the length of continuous usable cycles, to determine the general magnitude of change as measurements were continuously averaged.

Five videos were measured over 10 cycles to calculate the average percentage change from the first cycle to averages of three, five, eight and ten cycles. The percentage difference of the initial (first peak velocity) measurement from the average of repeated measurements (3, 5, 8 and 10) was calculated. Intrasession variability of retinal blood flow has not yet been reported using XT analysis, however intrasession variability of retinal arterioles as measured using the RFI has been reported as 8.4 ± 4.8% (Christian et al, 2010), therefore an expected variability for measurements of arterioles using the AOSLO could be estimated at

10%. The measurements were consistently below the expected variability of 10%, therefore an average of three measurements was used henceforth (Figure 4.10).

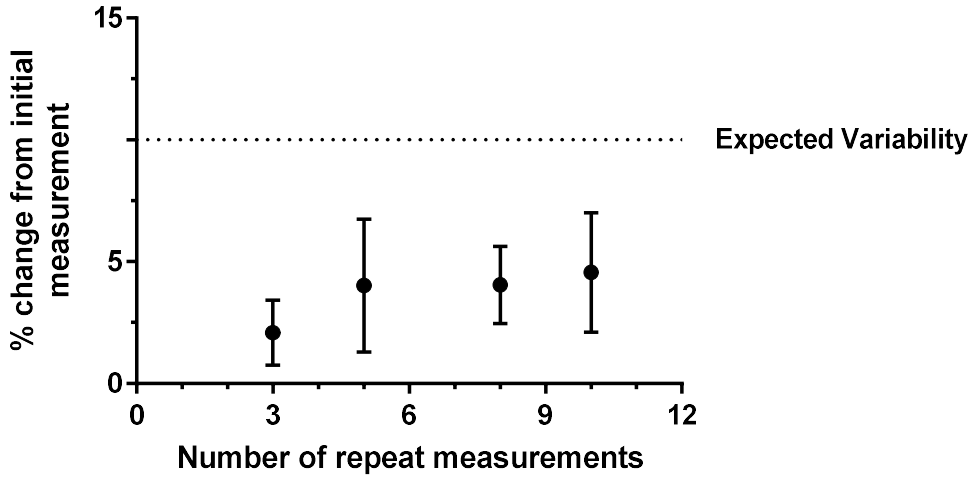

Figure 4.10: Plot demonstrating percentage change from first cycle measurement for averages of 3, 5, 8 and 10 cycles for five videos.

4.3.3 Development of Semi-Automated Streak Measurement

4.3.3.1 Video Selection

For development of semi-automated methods of angle measurement, 21 videos from separate locations in six control patients were used. Approximately 2-5 videos from each subject were used for this study (Table 4.2).

Subject ID	Subject 3	Subject 4	Subject 6	Subject 10	Subject 12	Subject 18
Number of videos used	4	2	4	3	3	5

Table 4.2: Number of videos from each subject used for this study.

4.3.3.2 Manual Measurement Error

One video of 200 frames was measured twice for this preliminary analysis. One video, although limited in its variation in terms of vessel diameter and general image quality, can accurately represent a range of possible results due to the pulsatile nature of blood flow

and variation in image quality and location caused by eye movements. The velocities calculated from repeated manual measurements were compared using a Bland-Altman plot to determine their repeatability (Figure 4.11). The bias was -3.28mm/s (SD 15.11) and the 95% limits of agreement were 32.9mm/s to 26.33mm/s. Similarly, manual measurements demonstrated a mean within-subject standard deviation of 2.01 to 5.36 degrees between three different measurements.

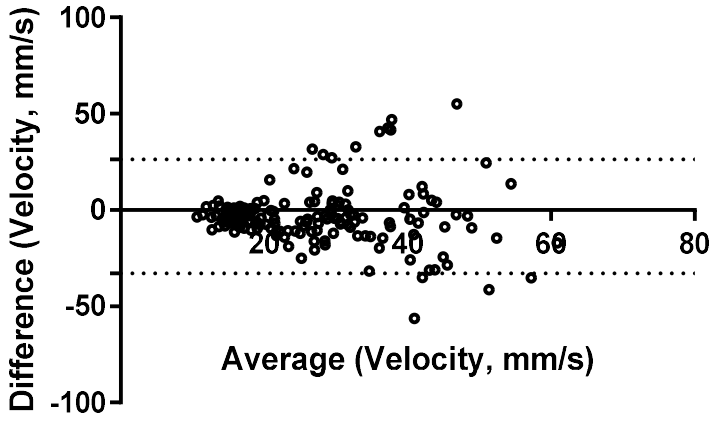

Figure 4.11: Bland-Altman plot of repeatability of manual measurements. Bias = -3.28mm/s (SD 15.11), LOA -32.9mm/s to 26.33mm/s.

4.3.3.3 Grading of Result Quality

We wanted to compare the quality of results over a number of cardiac cycles from the manual method and Directionality tool, and determine if vessel diameter had an impact on quality (Figure 4.12). Narrow vessels at a wide angle to the scanning line produced worse results on Directionality than wide vessels at a narrow angle (Table 4.3). At wide angles there is less variation in cell streak in response to speed, therefore it is difficult to detect this change. Cell streaks at this vessel angle tend to be consistently wider in the velocity range relevant for retinal vessels, consequently they may be difficult to differentiate from 90-degree angles, which are excluded as part of this analysis. Directionality is therefore not recommended for small vessels at wide angles (>40 degrees) to the scanning line.

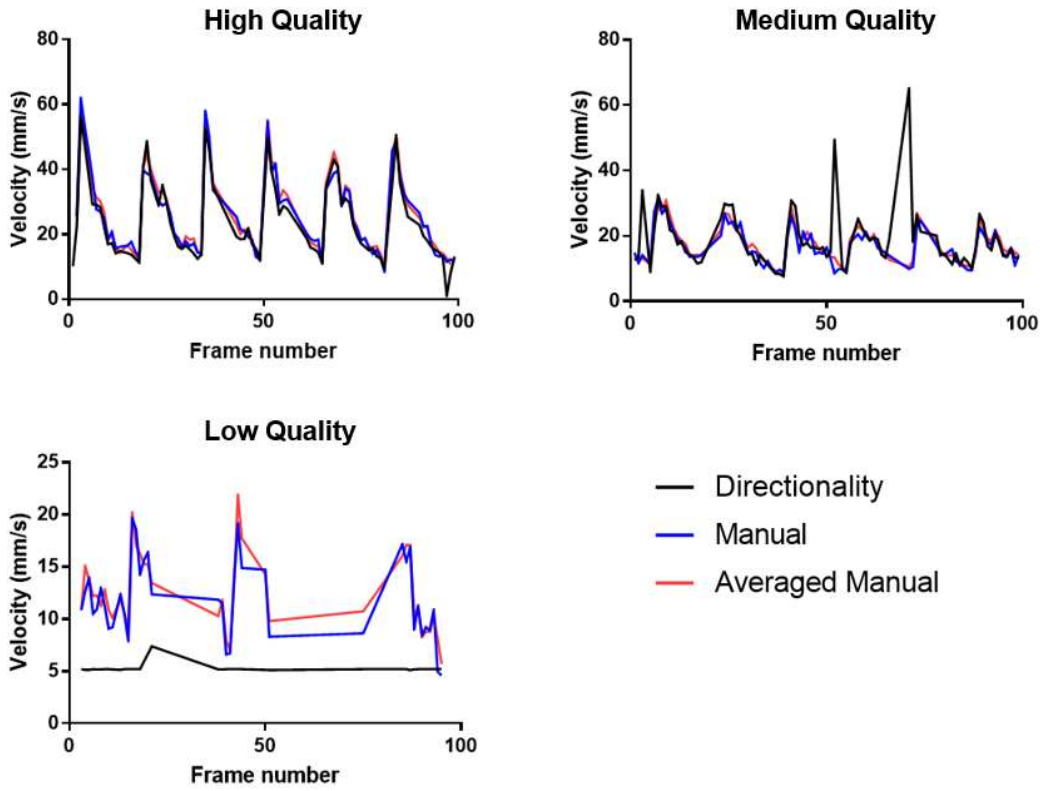

Figure 4.12: Variation in quality of results from the semi automated measurement (Directionality) compared to velocity measured once manually (Manual) and velocity measured three times and averaged (Averaged Manual).

Category	Number of videos in category	Diameter (Mean, µm)	Diameter (Range, µm)
High Quality	12/21	105.5	70.4-149.9
Medium Quality	5/21	87.1	42.3-125.1
Low Quality	4/21	38.9	27.0-70.8

Table 4.3: Summary of quality assessment results for comparing semi-automated to manual measurement of velocity.

4.3.3.4 Averaged Manual Measurements versus Directionality

In order to compare results from Directionality to manual measurements, we had to examine results from each method in three different ways. Firstly, we had to compare the angle measurements from each method which form the raw data used to calculate

velocity. Next, we had to compare the resulting velocities due to the varied impact of measurement error on different angles, as shown in Figure 4.5. Finally, it was important to compare results from each method on the most commonly reported metric of retinal blood flow, average velocity, as this would be an endpoint of future studies of retinal blood flow.

Comparability of angle measurements made using manual techniques and Directionality were assessed using a Bland-Altman plot (Figure 4.13). Six videos were excluded from Bland Altman analysis based on poor quality and the results from remaining individual frames (n = 1141) were compared. Firstly, the angle (in degrees) measured using averaged manual methods was compared to results from Fourier analysis (Figure 4.13). The bias at 2.99 degrees (SD 7.38) indicates there is a very small difference between manual and Directionality methods in measurement of velocity. The 95% limits of agreement are narrow at -11.48 degrees to 17.46 degrees. Results appear to be more comparable at the smaller angles (20-30 degrees) than at larger angles (40-80 degrees) when assessed using Bland-Altman. However, as seen previously (Figure 4.5), measurement error at larger angles has a less detrimental effect on the result.

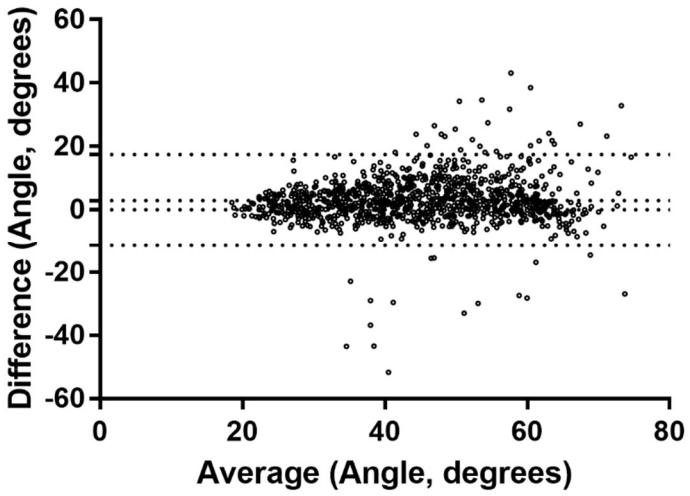

Figure 4.13: Bland-Altman plot of comparability of manual to semi-automated measurement (Directionality) of individual frames (angle, degrees). Bias = 2.99 degrees, LOA = -11.48 degrees to 17.46 degrees.

Next it was important to determine in these images the comparability of manual and automated methods on the overall velocity result, as the results may be confounded by a number of other metrics for this value, such as angle of vessel to scanning beam. The bias was -2.01mm/s (SD 5.43) indicating there is no significant difference between manual and Directionality methods in measurement of velocity (Figure 4.14). This bias is even less than that seen for comparability of repeated manual measurements (Figure 4.11). The 95% limits of agreement were narrow at -12.71mm/s to 8.56mm/s, demonstrating the potential error when using the automated method is limited.

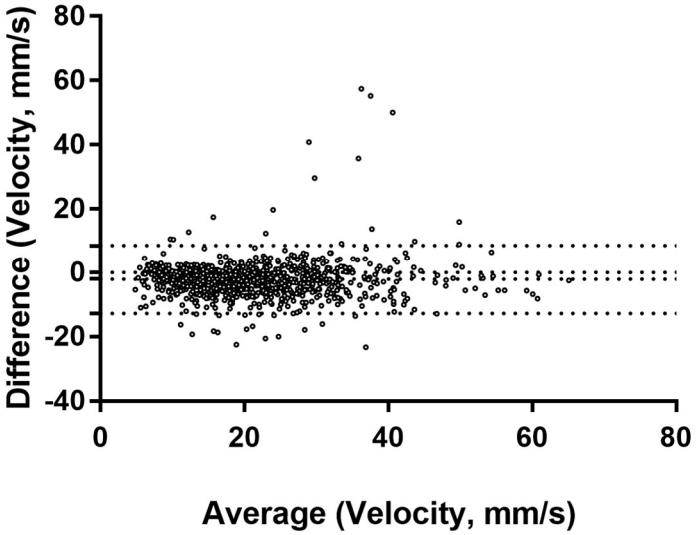

Figure 4.14: Bland-Altman plot of comparability of manual to semi-automated measurement (Directionality) of individual frames (velocity, mm/s). Bias = -2.01mm/s (SD 7.38), LOA = -12.71mm/s to 8.56 mm/s.

Although assessment of individual frames is critical to success of the technique, we also needed to determine the comparability of the most widely reported endpoint of retinal blood flow, the average velocity. Thirteen videos from seven subjects were also used to compare manual and Directionality velocity measurements of cycles. The difference between peak systolic velocity and lowest systolic velocity for three cycles were averaged for each video measured both manually and using Directionality, and compared using a

Bland-Altman plot (Figure 4.15). The bias was minimal at 0.275mm/s (SD 4.31) and limits of agreement were narrow at -8.18mm/s to 8.73mm/s. There also does not appear to be any systematic error in measurement, all average velocities appear to be equally susceptible to this small difference in results.

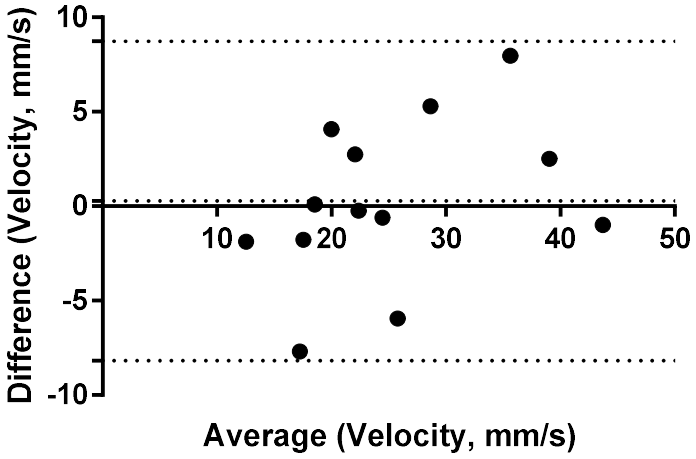

Figure 4.15: Bland-Altman plot of repeatability of comparability of manual to semi-automated measurement (Directionality) of cycles. Bias = 0.275 (SD 4.31), LOA = -8.18mm/s to 8.73mm/s.

4.3.3.5 Measurement Time

Both manual measurement and semi-automated pre-processing steps were timed in fourteen videos. It was significantly faster to complete pre-processing steps than the manual technique of velocity measurement as measured using a two-tailed Mann Whitney test ($p<0.0001$) (Table 4.4).

Measurement Technique	Time to Complete (seconds)	
	Median	IQ Range
Manual	238	76
Directionality	83	13

Table 4.4: Summary of results comparing measurement time of manual method of analysis to Directionality analysis.

4.4 Summary

This chapter has demonstrated the repeatability of an open-source, semi-automated method of velocity analysis (Directionality) to improve accuracy and efficiency of AOSLO XT measurements. We developed methods of pre-processing to increase accuracy of the plugin, compared the results from manual measurement to those generated by automated analysis and were able to identify vessels with specific features which perform poorly and should therefore be excluded. Although use of Directionality does require some pre-processing, we have been able to demonstrate that it is still significantly faster (approximately 3x) to perform. There is also minimal training required and the process could be integrated directly with the pre-processing step. As the software is open source (https://github.com/fiji/Directionality/releases/tag/Directionality_-2.0.2), it can also be adapted for individual lab's needs. Increased efficiency of analysis may make XT imaging a more attractive concept for other researchers and allow expansion of the field.

There is an alternative strategy for measuring orientation of streaks within XT images. Automated analysis of velocity visualised using XT imaging has been presented in the mouse eye (Joseph et al, 2019) using the Radon transform. This method is open source (https://github.com/elifesciences-publications/single_cell_blood_flow) and could serve as a suitable alternative to Fourier transform analysis. Although this technique is promising for fully automated analysis of XT images, it was developed using anaesthetised mice, which would not present the same challenges as imaging awake humans, such as image warping from involuntary saccades or fixation fatigue. The analysis technique presented in this chapter requires some pre-processing but otherwise can be used in its published format to analyse human XT images with no additional filtering, making it more accessible for those with limited computational training. Additionally, as most AOSLOs are custom built and results can be variable on a lab to lab basis, it would also be important for individuals to

assess this process on their own datasets or devices before integrating it into their analysis pipeline.

There is currently only one published study where XT imaging was used to investigate blood velocity in a diseased state. In order to investigate blood velocity and flow in diabetic retinopathy, Palochak *et al* measured the peak and trough of the cardiac cycle by subjectively selecting XT frames with the narrowest and widest angles (Palochak et al, 2019), then using only these frames to measure and calculate mean velocity across the cycle. This limited analysis may have been due to the time-consuming nature of manual streak measurement, and although it is efficient, it would be prone to error in identifying correct peaks and troughs as the full cardiac cycle would not be represented. Furthermore, pathological features of the cardiac cycle cannot be identified and explored with such a reduced method. As the use and applicability of XT imaging expands, the reliability of metrics used in this technique must be considered.

There are limitations to the method proposed here. This technique is also not fully automated and requires processing of images before use. Automation of this pre-processing step is possible and could be integrated with the open-source Directionality program to create a fully automated pipeline for analysis of XT videos. Additionally, as the orientation of the scanning beam was static, we were limited to vessels which could be measured at an angle less than 50 degrees to the scanning beam. Ideally, the beam could be rotated to allow for measurement of the vessel at the narrowest angle, which would improve image quality especially for the smallest vessels where a narrow angle, and therefore a wide XT portion, is crucial for accurate measurement of velocity. Directionality cannot be reliably used for small vessels where the vessel in question is under 40 micrometers because of the impact of persistent artefacts on these images. Removal of images with motion artefacts is straight forward, however all images will have some form

of small horizontal artefact due to the horizontal scanning element of imaging. Analysis of low-quality images is also not recommended using this technique as the program shows poor detection of these streaks. However, in these cases it may still be possible to detect cell streaks manually and as there is no significant bias between Directionality and manual measurements, they can be used in conjunction with each other.

This technique may also be useful to study the haemorheology of retinal diseases, as XT imaging allows us to analyse flow across the retinal vessel. Detecting velocity not only in the centre of the lumen, as has been performed here, but also at vessel walls will allow us to visualize altered rheology *in vivo* across the whole vessel profile and assess its downstream effects. This kind of analysis is very time intensive to complete manually, therefore automated detection such as this is a boon. This technique could also be used on veins and venules, but they are not examined using this technique as the cardiac pulse is dampened significantly in these vessels and would therefore not present the same range of velocities as an arteriole.

Validation of Directionality and post-processing analysis of velocity results from retinal vessels grants us the capacity to use this technique on a large number of images, collected as part of this thesis to investigate the retinal microvasculature at all levels of the vascular tree. Processing and analysis of adaptive optics images is a significant constraint in the translation of adaptive optics imaging to the clinical setting and its perception as a clinically useful technique, therefore automation of measurement such as this is essential to the growth of the field.

Retinal Vascular Structure and Function in SPMS

5.1 Introduction

Multiple sclerosis has traditionally been viewed as a chronic inflammatory disease, where cycles of neuroinflammation and neurodegeneration lead to accrual of disability. There is, however, increasing evidence to suggest that the microvasculature plays a significant role in the pathophysiology of multiple sclerosis, especially in progressive stages of the disease.

The primary function of the microvascular system is adequate perfusion and sufficient transfer of nutrients and oxygen to tissues. In MS patients many studies have described the presence of hypoperfusion, failure to deliver sufficient blood volume, and hypoxia, failure to sufficiently oxygenate tissues, in the CNS using clinical, radiological and histological methods. Histological studies have shown that lesions tend to form in watershed regions of the brain, where tissue is supplied by the most distal branches of two arteries and are therefore most at risk of persistent hypoperfusion, suggesting an early role for the vasculature in lesion formation (Desai et al, 2016; Haider et al, 2016). Cerebral type-III MS lesions histologically resemble an hypoxic insult (Haider et al, 2016) and expression of vascular factors associated with hypoxia (HIF-1α, (Stadelmann et al, 2005)), have also been identified in sclerotic lesions. Reduced cerebral blood flow has been demonstrated in all subtypes of MS (Adhya et al, 2006; D'Haeseleer et al, 2013; Law et al, 2004; Rashid et al, 2004), even in the absence of structural damage (Varga et al, 2009), suggesting hypoperfusion is not strictly a result of neurodegeneration and subsequent lack of metabolic demand. Cerebral circulation time is also increased in all types of MS (Monti et al, 2015), indicating that decreased blood velocity is an early component of the disease. Haemoglobin saturation levels are also shown to be reduced in MS patients using near infrared spectroscopy (Yang & Dunn, 2015), suggesting the impact of insufficient blood delivery could be compounded by a reduction in oxygen carrying capacity of the blood. This

is supported by evidence from haematology; haemoglobin levels are significantly reduced in MS patients (Hon et al, 2011) and the presence of anaemia doubles the risk of developing MS (Koudriavtseva et al, 2015) and increases the risk of relapse (Tettey et al, 2016). Although hypoxia and hypoperfusion are increasingly being recognised as important factors in the progression of MS, there is still controversy regarding their role in the process.

The anterior visual pathway, consisting of the RGCs, RNFL and optic nerve, is now widely understood to reflect the overall degenerative status of the brain in MS. As the retina demonstrates a strong link with the brain in its neurodegenerative processes and as they share similar microvascular traits, it is likely that any vasculopathy in the brain will also be reflected in the retina. Homology between the cerebral and retinal microvasculature in both structure and function, as well as the accessibility of the retinal microvasculature, suggests the retina would be an ideal location to observe the cerebral vasculature in health and in disease. Indeed, retinal microvascular abnormalities have been noted in MS patients at all stages of the disease. OCTA measurements of retinal perfusion, as mentioned previously, have demonstrated altered retinal perfusion in multiple sclerosis in both early and late stages of the disease (Feucht et al, 2019; Wang et al, 2014), and studies using the retinal function imager have found both structural and functional abnormalities in MS, in reduced retinal perfusion (Liu et al, 2019) and velocity (Jiang et al, 2016). There are, however, no studies investigating retinal vessels in SPMS specifically, as studies either only investigate the earlier RRMS stage or do not differentiate by subtype. There is also limited information available on vessel wall structure in SPMS, which could be extremely informative on the disease process. Investigation of both structure and function of retinal vessels in SPMS is essential to understanding the wider vascular impact of MS. This could be achieved with AOSLO which can investigate both structure of retinal vessels, in measuring wall and lumen thickness, and function of vessels, in measuring blood velocity.

Wall to lumen ratio can be used to examine the impact of SPMS on the microvasculature in more detail. The walls of blood vessels co-vary with vessel size, where vessels with larger lumen require larger walls to maintain vessel tone. This measurement is typically expressed as wall to lumen ratio (WLR) and has been used extensively with a number of retinal imaging techniques to gather insights on retinal and systemic disease in the microvasculature. As the retina contains a range of more than a log unit of lumen diameters it is possible to fit a relation between vessel diameter and wall thickness. This relationship is consistent between normal eyes, therefore it can be a useful tool to compare healthy to diseased eyes (Hillard et al, 2016). There is currently a paucity of clinically available techniques for measuring WLR across a range of vessel sizes *in vivo*. Scanning laser doppler flowmetry (SDLF) can be used to measure wall thickness (Michelson et al, 2007), but it is limited to larger vessels where changes are likely to occur later in a primarily microvascular disease. AOSLO can instead be used to image a wide range of vessel sizes, from the main branches at the optic nerve down to the capillary level. WLR as measured using AO-based techniques has been associated with a number of conditions, such as hypertension (Hillard et al, 2016), diabetic retinopathy (DR) (Burns et al, 2014), and has even been used to detect structural changes in subclinical DR (Zaleska-Zmijewska et al, 2017).

Measurements of cell velocity in retinal blood vessels can be made using a number of different techniques, yet these are also limited in the range of vessel sizes they detect. AOSLO XT imaging allows visualisation of cell speed and calculation of flow across all stages of the retinal vascular tree. XT imaging, as a part structural, part functional imaging modality (Section 4.2.6) allows us to integrate information about vessel size and cell speed in order to calculate vessel flow (Zhong et al, 2008). The relationships between diameter, velocity and flow have been investigated in DR using XT imaging, and it was found that different forms of DR displayed different relationships between these factors (Palochak et

al, 2019). Techniques previously used to study the retinal microvasculature in MS have been limited in scope to either small, low flow vessels or large, high flow vessels and this may restrict observations on interactions across the whole vascular tree in MS.

Another essential function of the microvasculature is in oxygenation of tissues. Facilitation of oxygen transfer is an essential role of blood vessels, and can be altered independently of changes to vessel structure or flow. As previously described, retinal oximetry has been used to demonstrate significant reduction in oxygen transfer in a heterogenous group of MS eyes compared to controls, which was purported to be linked to inner retinal atrophy and subsequent reduction in metabolic need (Einarsdottir et al, 2018), however structural measurements of the retina in this case were not compared to saturation levels. There are no published findings focussing on retinal oxygenation in SPMS. Whether microvascular dysfunction is a result of atrophy, alterations in perfusion or insufficient oxygen transfer is yet to be determined in MS and could be investigated in detail in the retina.

Previously, we have examined the microvasculature in both RRMS and SPMS patients at a superficial level to develop methodologies and hypotheses regarding the microvascular state in SPMS. As there was no significant difference in overall microvascular structure in MS patients, a closer look at vascular structure was required. In Chapter 3, we also found a significant reduction in velocity of erythrocyte aggregates in MS patients, which would indicate a slowing of flow upstream from capillaries. Measurements of aggregate velocity are however impacted by a number of external factors which could not be controlled for using our techniques, therefore an alternative method of blood velocity measurement was sought in XT imaging, which we can use to further explore the functional microvascular changes seen in Chapter 3.

We have investigated the overall structure of the microvascular tree, the function of small capillaries and the cellular environment in which they sit. We were initially unable to look

at retinal blood velocity in a range of vessel sizes using the techniques available to us at the time. The potentially subtle alterations of the retinal microvasculature in SPMS require a multifaceted approach to investigate their aetiology, and to identify specific biomarkers which could be utilised by clinical trials in future. The sensitivity of AOSLO to changes in both structure and function at all levels of the vascular tree makes it is a powerful tool in detecting vascular disorder in the retina. In this chapter we examine both vascular structure, using wall and lumen metrics, and function, in velocity, flow and oxygen saturation in SPMS. We also look at the wider impact of vascular function and retinal structure in SPMS.

5.2 Materials and Methods

5.2.1 Declaration of Collaborator Roles Within Chapter

The ophthalmic data in this chapter were collected by Sarah Houston, Dr Adam Dubis, Vasileios Theofylaktopoulos and Sevim Ongun. Recruitment and data collection for the MSOpt trial at the Institute of Neurology was carried out by Dr Rosanna Cortese, Dr Alessia Bianchi, Hannah Wood and Leilani Cabreros. Application for the MSOpt study was completed by the MSOpt Study Team including Sarah Houston and Adam Dubis. Application for the pilot study, recruitment and data collection was performed by Sarah Houston in this trial. Data analysis for both the pilot study and baseline results of the MSOpt retinal imaging results was completed by Sarah Houston. All videos included in this chapter were prepared by Sarah Houston.

5.2.2 Cohort Development

5.2.2.1 Control Patients

A pilot study of retinal vascular imaging was performed in order to investigate normal variation in retinal vascular measurements, such as metrics of vessel diameter, blood velocity and flow and oxygen saturation. It was also performed to compare results from the MSOPT study to those of young and age-matched controls, and develop the analysis techniques used in this thesis.

Ethical approval was applied for and received by the UCL Research Ethics Committee in April 2019 (Approval Number 11353/004). Twenty-four volunteer participants were recruited to the study. All participants provided written informed consent and the study adhered to tenets of the Declaration of the Helsinki. Control participants were recruited to

this study on the basis of the following inclusion and exclusion criteria (Table 5.1). During this study, AOSLO imaging and retinal oximetry were performed.

Inclusion Criteria
Aged 18-80 years old
Exclusion Criteria
History of ophthalmic disease or trauma
History of photosensitive epilepsy
History of migraines
Any form of statin treatment

Table 5.1: Summary of inclusion and exclusion criteria for the Pilot Study of Non-Invasive Retinal Vascular Flow Imaging

5.2.2.2 SPMS Patients

Ten SPMS patients were recruited as part of the MSOpt study, a randomised controlled trial of simvastatin in the treatment of SPMS. Their baseline results prior to treatment are presented in this thesis. In this chapter we used control subjects (recruited via the study detailed in Section 5.2.2.1) and SPMS patients from the MSOpt study prior to treatment to develop post-acquisition methodologies, compare differences between controls and patients, and enable us to establish baseline parameters of the retinal vasculature in SPMS. The study was approved by the Brighton and Sussex Research Ethics Committee (17/LO/2088) and was registered with ClinicalTrials.gov (NCT03896217).

The ten patients in this study recruited as part of the larger MSOpt study were selected on the basis of the following inclusion and exclusion criteria (Table 5.2), which has been summarised for relevance to this chapter. Further detailed information on the recruitment criteria for the MSOpt study is available in the Appendix.

Relevant Inclusion Criteria
Confirmed diagnosis of multiple sclerosis according to revised Mc Donald criteria and have entered the secondary progressive stage. Steady progression rather than relapse must be the major cause of increasing disability in the preceding 2 years.
EDSS 4.0 – 6.5 (inclusive).
Male and Females aged 18 to 65
Willing and able to comply with the trial protocol (e.g. can tolerate MRI and fulfils the requirements for MRI, e.g. not fitted with pacemakers or permanent hearing aids) ability to understand and complete questionnaires
Willing and able to provide written informed consent
Relevant Exclusion Criteria
The use of immunosuppressants (e.g. azathioprine, methotrexate, cyclosporin) or disease modifying treatments (avonex, rebif, betaferon, glatiramer, dimethyl fumerate, fingolimod) within the previous 6 months
If the patient reports any ophthalmic conditions such as glaucoma, ocular trauma or degenerative eye disease

Table 5.2: Relevant inclusion and exclusion criteria for the MSOpt trial. The full list of inclusion and exclusion criteria is included in the Appendix.

5.2.2.2.1 MSOPT Trial Protocol

The baseline visit of the MSOPT study occurred over two days. Day One consisted of screening for the trial, including safety blood tests and an MRI to determine suitability for the trial. They also had disease specific functional tests performed by a qualified neurologist. They were provided with the study drug at the end of Day One but were informed not to take the drug until the end of Day Two. Day Two of the MSOPT trial occurred at Moorfields Eye Hospital, where baseline retinal imaging was performed (Figure 5.1).

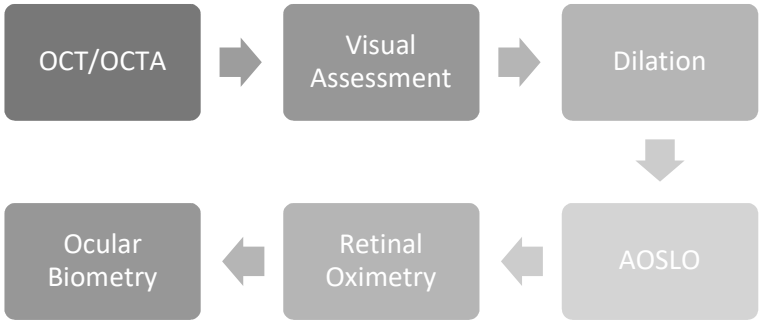

Figure 5.1: Flow diagram of the general patient pathway through the baseline visit to MEH of the MSOPT trial

5.2.3 AOSLO Imaging Protocol

To facilitate time management and due to the high degree of interocular symmetry, one eye from each patient was selected as a study eye for AOSLO imaging. In the control cohort, the participant's right eye was used as default and only changed to left eye if requested by the subject. In the SPMS group, if a patient had no history of optic neuritis in either eye, then the right eye was used as default. If a patient did have a history of optic neuritis, the non-diseased eye or the "better" eye as determined by visual acuity and general assessment of performance on OCT, was used. This was to ensure that the patient had the best possible visual fixation for AOSLO imaging. All subjects were dilated using one drop of 0.5% tropicamide.

In SPMS patients, arteries suitable for imaging were identified using the infrared image provided alongside the macular volume scan collected earlier, using the different reflectance of vessels as a guide (Figure 4.2). In the control cohort, OCT images were unavailable so arteries and veins were identified using the same method as in the previous chapter based on their reflectivity on AOSLO (Figure 4.1), as large arteries (in the peripapillary region) are distinctly lighter in colour than large veins.

Two arteries, a pair on either side of the equator, were identified for XT imaging. AOSLO XT imaging was performed in a minimum of four locations in two separate arteries. Before imaging, four locations each along a branch of two individual arteries were identified which would subsequently be imaged. In MS patients, the infrared image was marked to show the estimated location of measured vessels. The field of view used varied from 1-2 degrees depending on image quality and the participant's fixation stability. In both MS and control subjects the location of the fixation target was also saved at each video capture for future reference.

5.2.3.1 Analysis of Blood Vessel Diameter

Wall and lumen diameter measurements were performed in triplicate using the ImageJ line tool. Wall cross sectional area (WCSA), wall thickness (WT) and wall to lumen ratio (WLR) were calculated according to the following equations used previously in AOLSO study of the microvasculature (Hillard et al, 2016). Inner Diameter (ID) denotes lumen thickness and Outer Diameter (OD) denotes whole vessel thickness.

$$\textbf{WCSA} = (\pi (OD^2 - ID^2)) / 4 \qquad \text{Equation 5.1.}$$

$$\textbf{WT} = (OD\text{-}ID) / 2 \qquad \text{Equation 5.2.}$$

$$\textbf{WLR} = (OD\text{-}ID) / ID \qquad \text{Equation 5.3.}$$

5.2.3.2 Analysis of XT Imaging

XT images used to calculate cell velocity and flow in control and SPMS patients were analysed using Directionality processes where possible. When videos did not meet the quality criteria for Directionality measurement, or the results from semi-automated measurement did not reach quality standards, manual measurement of velocity (as previously described) was performed.

For analysis of XT imaging, I utilised the MATLAB script developed for cycle measurement of XT results (Section 4.2.6.5). For this study, I also calculated additional measurements of flow dynamics to develop our understanding of retinal microvascular function in MS. As previously described, the user selects the peak and trough of three "acceptable" cycles, which are then averaged and the difference between consecutive peaks and troughs are averaged together to create the Vax Average. The resistive index (RI) was also calculated from the resulting peak and trough results. The RI is a measurement of pulsatile flow that reflects the resistance of microvascular beds downstream to blood flow (Nichols et al, 2011). It is calculated by dividing the difference between the lowest diastolic velocity and the peak systolic velocity by the peak systolic velocity.

$$\text{Resistive Index} = \frac{\text{Average Peak Systolic Velocity} - \text{Average Diastolic Velocity}}{\text{Average Peak Systolic Velocity}} \qquad \text{Equation 5.4.}$$

From calculating velocity and vessel diameter, it was also possible to calculate flow in the vessel.

Vessel flow (Q) was calculated based on the following equation reported by Zhong et al (2011), where Dv is the average lumen diameter and Vax is the average velocity (Equation 5.5). Velocity measurements were corrected for retinal magnification based on axial length (IOLMaster 500/700 – Zeiss, Jena, Germany) for SPMS patients but not controls as it was unavailable.

$$Q = \frac{Vax \cdot \pi \cdot Dv^2}{4} \qquad \text{Equation 5.5.}$$

5.2.3.3 Statistical Analysis

Linear regressions were performed in Prism (v7, GraphPad) and post-hoc analysis was used to investigate differences between elevation of lines if the slopes were equal. Prism calculates the difference in elevation based on Analysis of Covariance (ANCOVA) (Zar,

2010), where the intercepts of lines are compared after "sharing" the slope parameter between the lines to make them equal. The difference in intercept, and therefore elevation, between lines demonstrates whether two lines are identical or not.

5.2.4 Retinal Oximetry

5.2.4.1 Retinal Oximetry Collection

Retinal oximetry was performed using the Oxymap T1, a dual wavelength, non-invasive spectrophotometric oximeter. The oximeter consists of a standard fundus camera with two separate digital cameras. Images of the retina are collected simultaneously using two different wavelengths, 570nm and 600nm. One image in each eye was collected at 50° FOV, centred on the optic disc and focussed on the retinal vessels.

5.2.4.2 Retinal Oximetry Analysis

Oximetry results from both eyes were analysed using the specialised analysis program for Oxymap T1, the Oxymap analyser. Images which did not meet the quality standards (i.e. optic nerve not in central third of image, vessels not clearly visible) were excluded.

Oxygen saturation was measured in all major retinal vessels found within two concentric circles placed at 1.5- and 3-disc diameters from the optic disc (Figure 5.2, A), for two reasons. Firstly, this method of measurement had been performed in previous studies using the Oxymap (Eliasdottir et al, 2017; Nakano et al, 2016; Nitta et al, 2017) and the location of measurement allows us to ensure consistency as the vessels in this region were of greatest clarity. Vessels whose diameter was below eight pixels were excluded due to reported errors in results using vessels of this calibre (Geirsdottir et al, 2012). Individual

vessel values from each eye were averaged to determine the mean arteriolar saturation and mean venular saturation.

Complete results from each eye detailing saturation values and locations were analysed in Matlab (R2013a) to determine arteriolar and venular saturation, as detailed in a study by Paul *et al* (2013). Briefly, saturation values are read into Matlab and plotted in a histogram format (Figure 5.2, B and C).

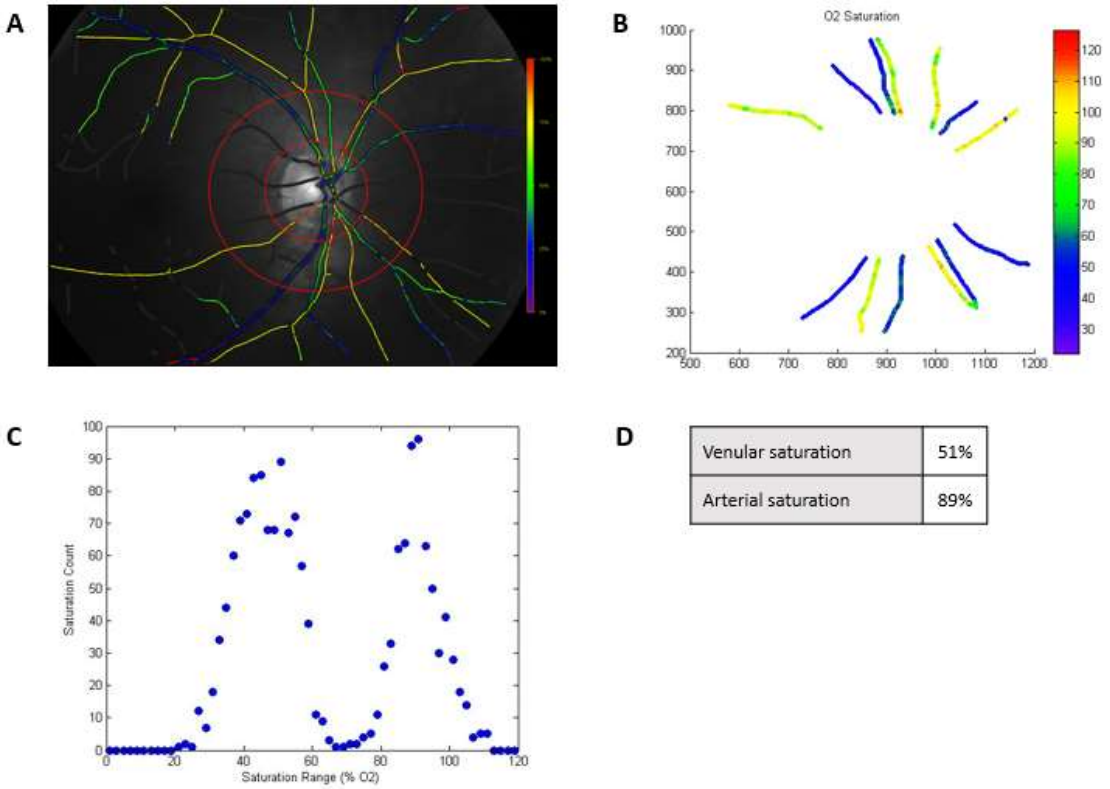

Figure 5.2: Oxymap Analysis Process. Vessel segments are extracted from the Oxymap image using two concentric rings centred over the optic disc, 1.5 and 3 disc diameters in size. The resulting segments are read into Matlab (B) and plotted as a histogram (C) to determine the venular and arterial saturation peaks (first and second peaks, respectively) (D).

The X location of the first peak (at a lower saturation) is collected as venular saturation and the second peak (at a higher saturation) is taken as arterial saturation. Data were also analysed based on vessel diameter, as different vessel diameters are known to produce

different saturation curves (Paul et al, 2013). The arteriovenous difference was calculated as the difference between arteriolar and venous saturation.

5.3 Results

5.3.1 Normality Calculation

Vessel diameter values and blood velocity measurements were not normally distributed as measured by the Shapiro-Wilk test ($p<0.0001$, $p<0.0001$ respectively), as they were skewed towards smaller vessels. Flow measurements were normally distributed as measured by Shapiro-Wilk test ($p = 0.84$).

5.3.2 Structural Metrics of Retinal Blood Vessels

5.3.2.1 Subjects

Ten SPMS patients and twelve sex- and age-matched controls were used in this section. One eye from each patient was used in the analysis (Table 5.3).

	Controls (n = 12)	**SPMS (n = 10)**
Age in Years (Range)	52.3 (38-64)	53.5 (36-64)
Sex (% Female)	60%	58.3%

Table 5.3: Summary of patient demographics.

5.3.2.2 Structural Metrics Results

Using AOSLO, vessel walls were clearly visible in all of our SPMS and control subjects (Figure 5.3).

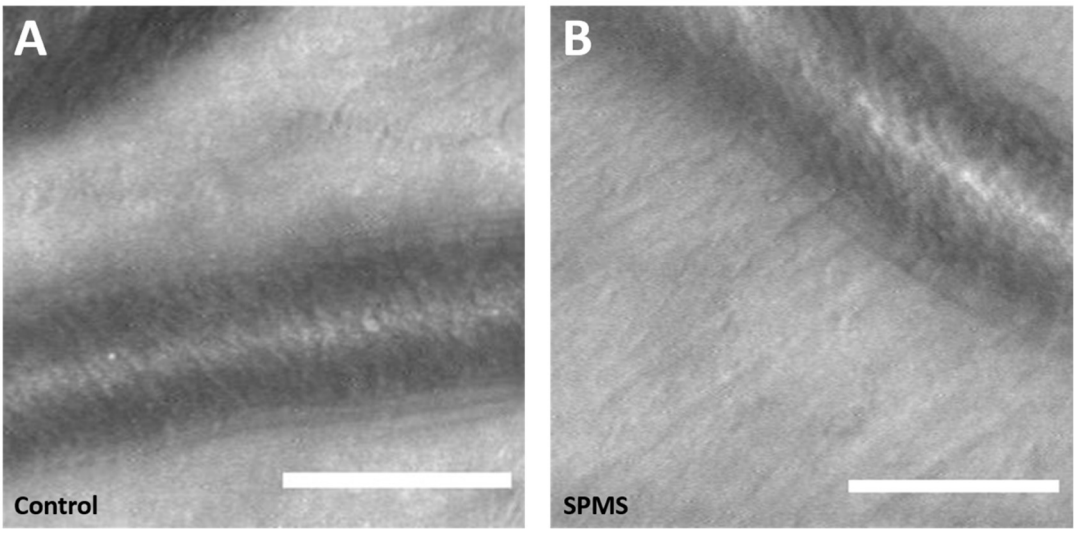

Figure 5.3: AOSLO images of retinal arteries to demonstrate the clarity of vessel walls using this technique, from both a control participant (A, Vessel Diameter: 122.7µm, WLR: 0.39) and SPMS patient (B, Vessel Diameter: 116.7µm, WLR: 0.41). Scale: 100µm

As predicted, we found a significant correlation between mean lumen diameter and mean wall thickness in arterioles, where wall thickness increased with increasing lumen diameter (Figure 5.4). To establish whether there was a difference between SPMS and control subjects, linear regression coefficients (r) were calculated giving values of 0.36 for SPMS patients and 0.58 for controls, and when compared revealed a significant difference between slopes ($p = 0.017$). This indicated that the relationship between lumen and wall diameter is affected by SPMS. In the MS patients the difference appeared to be due to the vessel wall being thickened for a given lumen diameter compared to control participants.

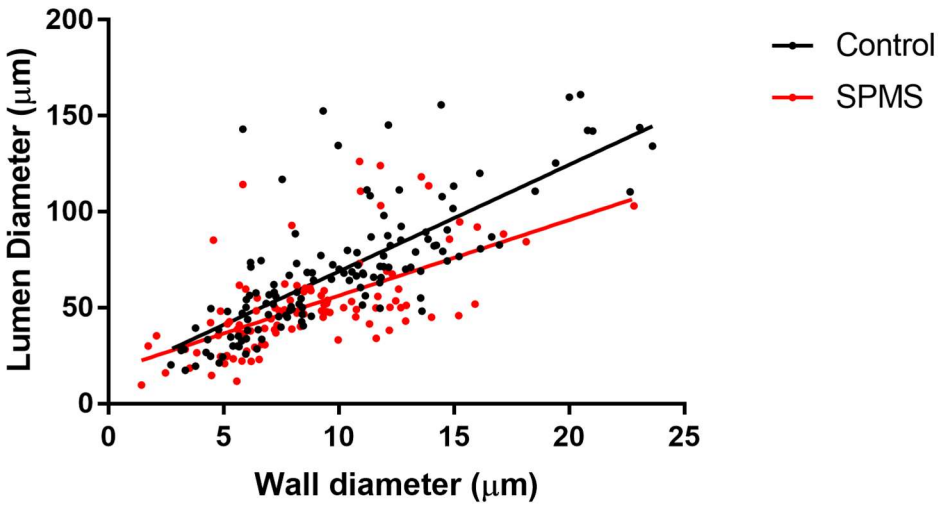

Figure 5.4: Relationship between wall diameter and lumen diameter in arterioles of SPMS patients and age-matched controls. Linear regression coefficients (r) were 0.36 for SPMS patients and 0.58 for controls. There was a significant difference between slopes (p = 0.017).

When vessels were grouped by diameter, WLR was significantly larger in vessels 50-99µm (p = 0.0001) in SPMS patients, as measured with Mann-Whitney tests, indicating vasoconstriction and lumen narrowing of these vessels (Figure 5.5). There was no significant difference between SPMS patients and controls in WLR in vessels <50µm (p = 0.13) and between 100-150µm (p = 0.61).

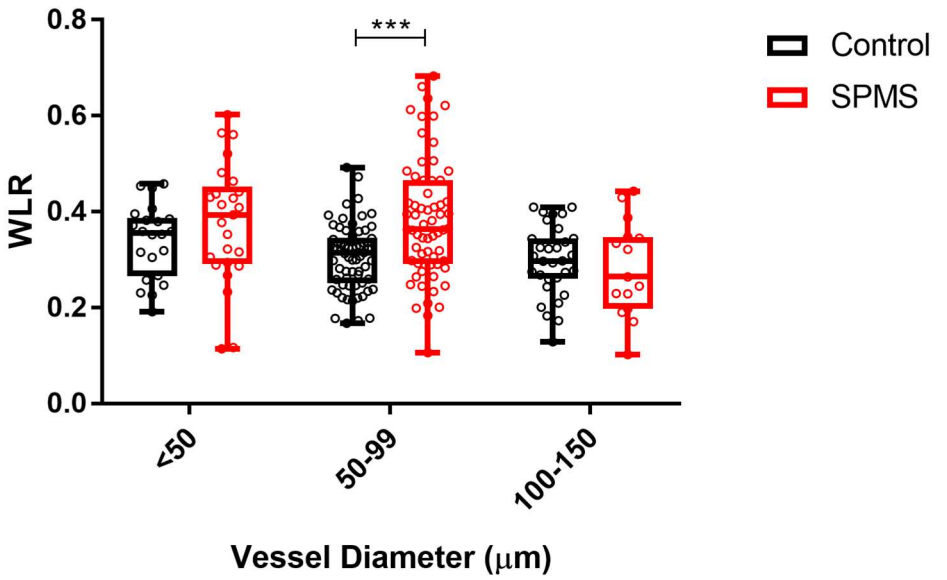

Figure 5.5: Box and whisker plots with overlaid scatter plots of vessel diameter versus wall to lumen ratio (WLR) in three vessel size groups. There was a significant difference between SPMS patients and controls in WLR in vessels 50-99μm diameter (p = 0.0001) as measured with Mann-Whitney tests. There was no significant difference in WLR in vessels less than 50μm (p = 0.13) and from 100-150μm (p = 0.61) in diameter. ****P*<0.0005.

This increase in WLR could be caused by generalised vasoconstriction or by a genuine increase of parietal thickness in retinal vessels. This can be further explored by examining the relationship between the inner diameter (lumen) and outer diameter (whole vessel thickness) (Figure 5.6). The close relationship between inner and outer diameters was confirmed using linear regression coefficients (r) (0.98 for SPMS patients, 0.96 for controls). There was no significant difference between slopes for SPMS and controls (p = 0.61), but there was a significant difference in elevations between slopes (p = 0.04) indicating the relationship between inner and outer diameter is maintained but SPMS vessels tend to have smaller lumen diameters than control vessels across all vessel sizes.

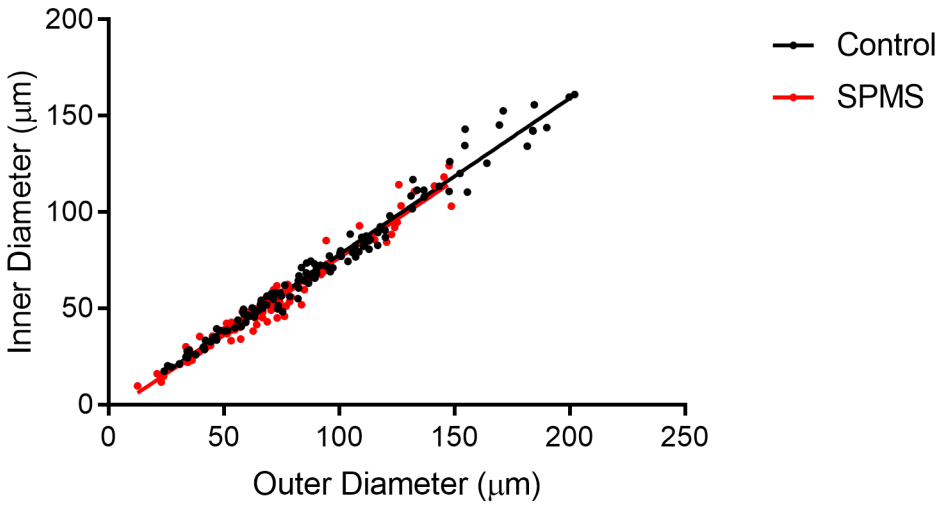

Figure 5.6: Relationship between outer diameter and inner diameter (i.e. lumen diameter) in arterioles of SPMS patients and age-matched controls. Linear regression coefficients (r) were 0.98 for SPMS patients and 0.96 for controls. There was no significant difference between slopes (p = 0.61), but there was a significant difference in elevations between slopes (p = 0.04)

In order to further interrogate the results, vessels were grouped according to vessel size (Figure 5.7, Table 5.4). The results indicated that this elevation between slopes seen previously was mainly due to differences in vessels 50-99μm in diameter (Mann-Whitney test, $p < 0.0001$). Interestingly, this trend was reversed when comparing vessels between 100-150μm in diameter but this may be due to imbalance in sample sizes (Control n = 33, SPMS n = 13 segments).

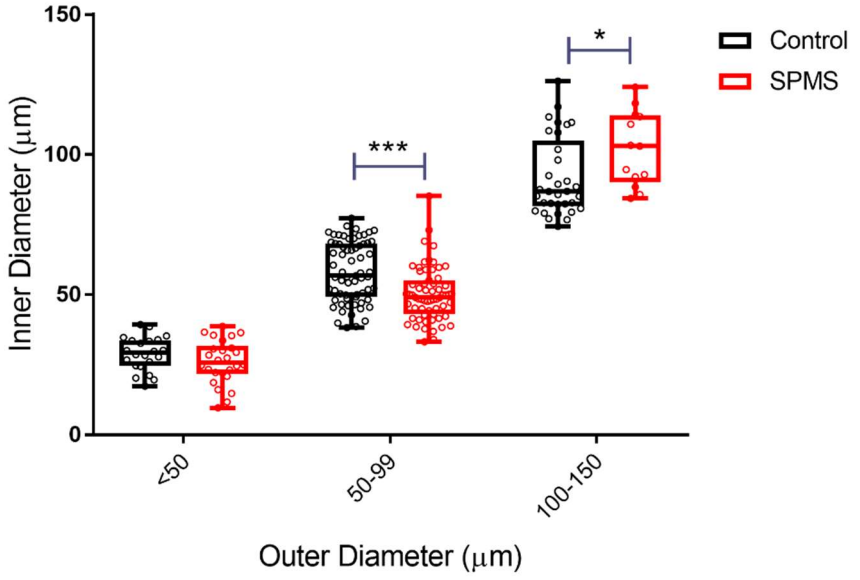

Figure 5.7: Box and whisker plots with overlaid scatter plots of outer diameter to inner diameter in arterioles of control participants and SPMS patients. There was a significant difference between SPMS patients and controls in inner diameter in vessels 50-99μm diameter ($p < 0.0001$) and in vessels 100-150μm diameter ($p = 0.01$) as measured with Mann-Whitney tests. There was no significant difference in inner diameter in vessels less than 50μm outer diameter ($p = 0.27$). *P<0.05; ***P<0.0005.

Outer Diameter (μm)	Number of Segments		Median Inner Diameter (μm) (IQ Range)		Mann-Whitney test (p)
	Control (n = 12)	SPMS (n = 10)	Control	SPMS	
<50	22	26	29.23 (9.08)	25.86 (9.88)	0.27
50-99	67	63	56.77 (18.92)	49.02 (12.1)	<0.0001
100-150	33	13	86.86 (23.39)	103 (23.66)	0.01

Table 5.4: Summary of inner diameter results grouped by vessel sizes.

In order to further examine the relationship between vessel thickness and wall thickness, WCSA was compared to vessel diameter on a log-log scale (Figure 5.8). This metric represents the full area covered by the vessel wall, and the relationship between WCSA and outer diameter has been used previously as a method to elucidate the type of vessel remodelling occurring in retinal vascular disease (Hillard et al, 2016). Comparing the relationship between WCSA to outer diameter in SPMS and control vessel segments (Figure 5.8) revealed identical slopes ($r = 0.92$, $r = 0.95$, respectively) but a significant difference in

elevation between slopes (p = 0.03), indicating for a given outer diameter a vessel segment from an SPMS patient would have a higher WCSA than a control subject, demonstrating thicker walls.

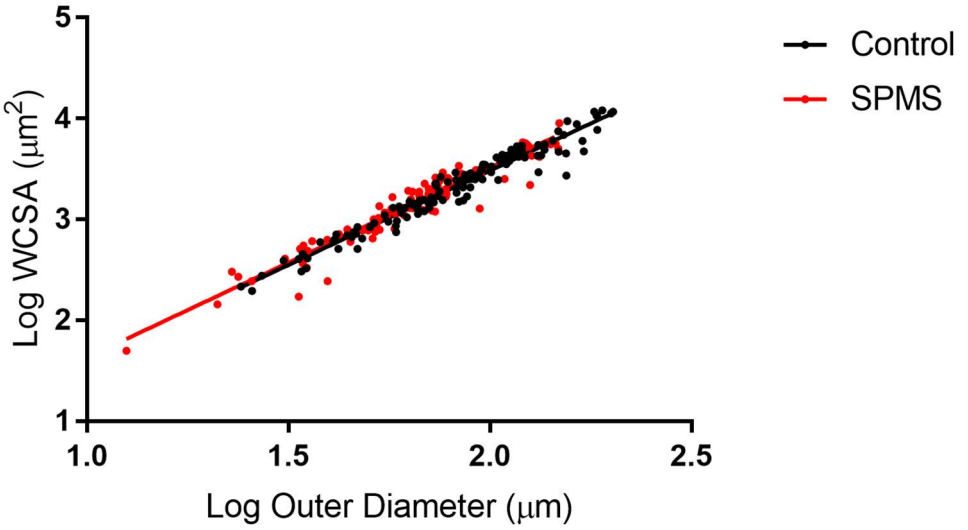

Figure 5.8: Relationship between vessel diameter and wall cross-sectional area (WCSA) in arterioles of SPMS patients and age-matched controls. Linear regression coefficients (r) were 0.92 for SPMS patients and 0.95 for controls. There was no significant difference between slopes (p = 0.80), but there was a significant difference in elevations between slopes (p = 0.03)

To establish if this elevation between slopes was more prominent in certain vessel sizes, as with the relationship between ID and OD, WCSA was compared according to vessel size. There was no significant difference between any of the groups of vessel sizes (Mann-Whitney test, Figure 5.9), indicating although WCSA was subtly increased in SPMS patients there is a large amount of overlap between the groups.

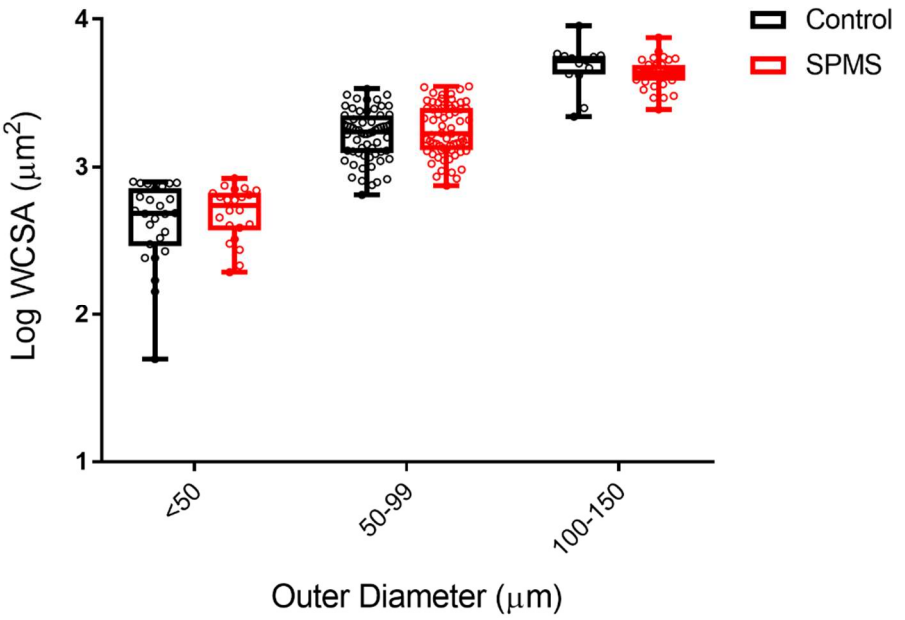

Figure 5.9: Box and whisker plots with overlaid scatter plots of outer diameter to log WCSA in arterioles of control participants and SPMS patients. There was no significant difference in WCSA of arterioles of any diameter grouping between SPMS patients and control participants (Mann-Whitney tests, p = 0.67, p = 0.26, p = 0.09 for vessels of outer diameter <50µm, 50-99µm and 100-150µm respectively)

It could be argued that the difference in vessel diameters seen in our SPMS cohort may be due to the location of imaging, as this was dependent on the AOSLO user's selection of vessel segments. However, when we plot locations for all vessel segments analysed for both SPMS and control patients (Figure 5.10), there is clear overlap.

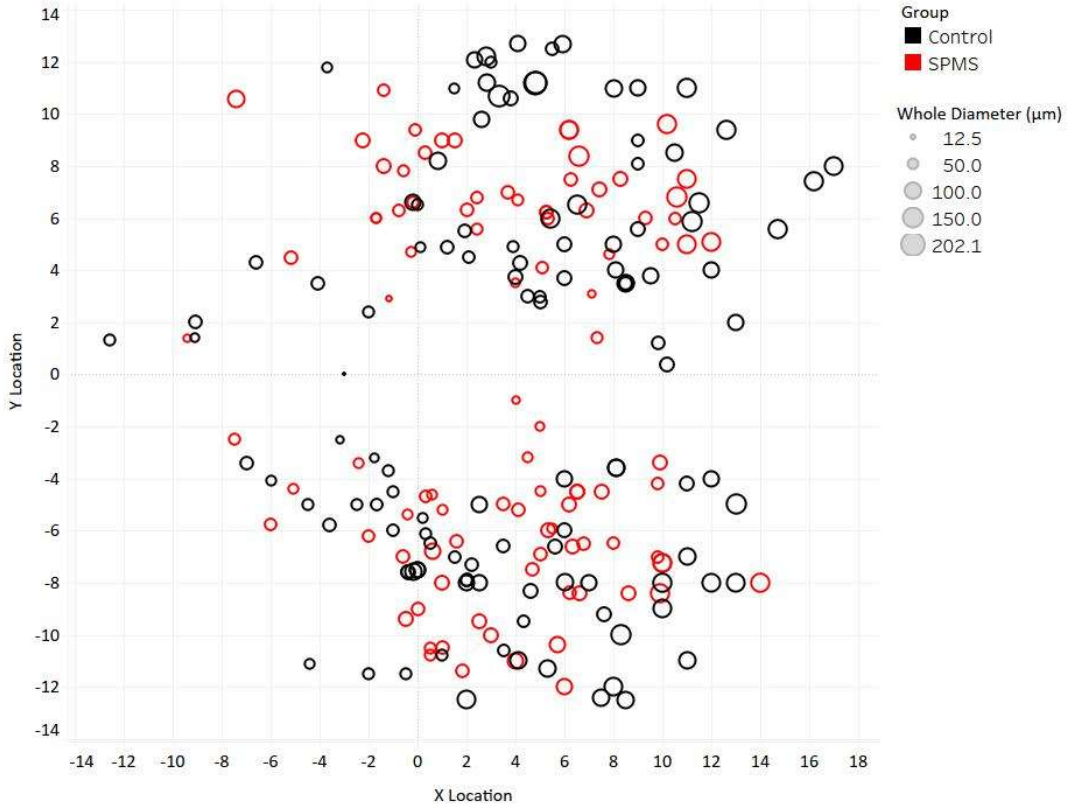

Figure 5.10: Scatter plot of vessel locations used in vessel diameter measurements. Each imaging location is either from a right eye, or has been converted to mirror its original location. The colour of dots relates to the patient group (SPMS or control) and the size of dots relates to the diameter of the vessel measured at that location. Vessel segments (n = 15) from three patients have been excluded as the fixation target was not aligned correctly during their imaging session. This plot demonstrates a distinct overlap between the locations of vessel segments measured in SPMS and control patients.

5.3.3 Velocity and Flow

5.3.3.1 Subjects

One SPMS patient and one control participant were excluded from velocity and flow measurements due to inability to measure complete cardiac cycles caused by missing frames or poor image quality, therefore nine SPMS patients and eleven sex- and age-matched controls were used in this section. One eye from each patient was used in the analysis.

5.3.3.2 Velocity

As anticipated, we found a significant correlation between mean velocity and diameter in arterioles, where velocity increased with increasing diameter (Figure 5.11). To determine if there was a difference between control and SPMS subjects, linear regression coefficients (r) were calculated giving values of 0.48 for SPMS patients and 0.12 for controls. When compared, the groups demonstrated no significant difference between slopes (p = 0.95), but there was a significant difference in elevations between slopes (p = 0.0005), which indicates for a vessel of a given lumen diameter, velocity is significantly slower in SPMS patients.

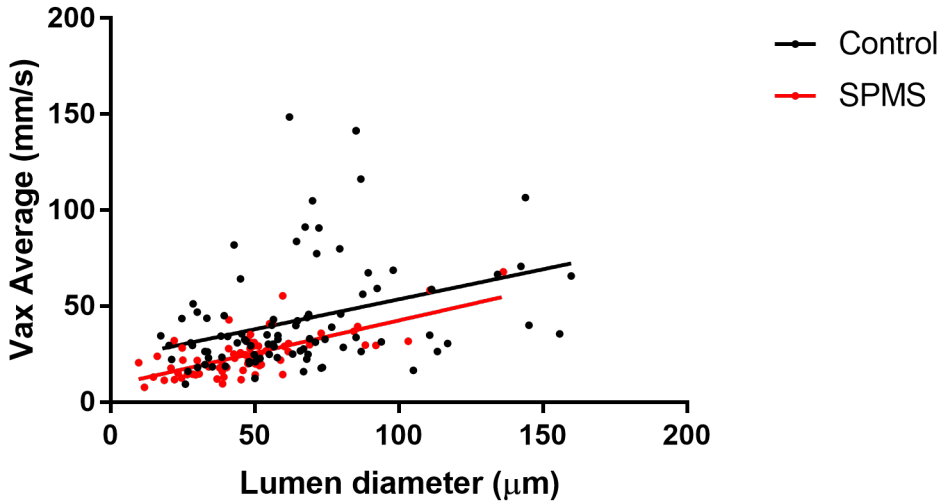

Figure 5.11: Relationship between Vax Average and Lumen Diameter in the arterioles of SPMS patients and controls. Linear regression coefficients (r) were 0.48 for SPMS patients and 0.12 for controls. There was no significant difference between slopes (p = 0.84). There was a significant difference in elevations between slopes (p = 0.0005).

This difference in elevation was then further explored to determine if this effect was confined to certain vessel groups. When vessels were grouped to different lumen diameters, velocity was significantly reduced in vessels <30μm (p = 0.02) and 30-59μm (p = 0.002) in SPMS patients, as measured with Mann-Whitney tests (Figure 5.12, Table 5.5). Whilst there was a trend towards a reduced velocity in vessels of 60-90μm from SPMS,

there was no significant difference between control and SPMS vessels. The sample size of the latter data set, however, had fewer measured blood vessels from SPMS patients (Table 5.5).

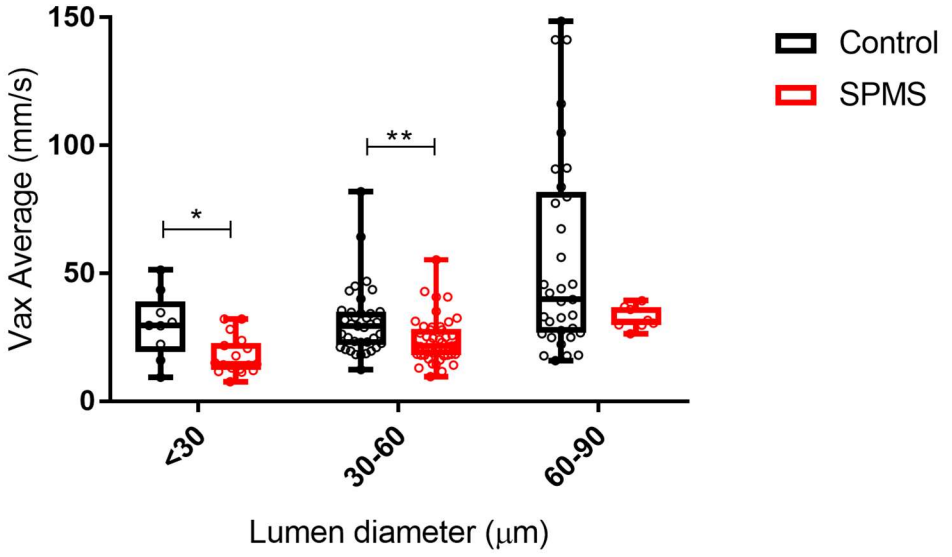

Figure 5.12: Box and whisker plots with overlaid scatter plots of lumen diameter versus Vax Average in three vessel size groups. There was a significant difference between SPMS patients and controls in Vax Average in vessels <30μm (p = 0.02) and 30-59μm (p = 0.002) as measured with Mann-Whitney tests. There was no significant difference in Vax average in vessels with a lumen diameter of 60-90μm. *P<0.05; **P<0.005.

Lumen Diameter (μm)	Number of Segments		Median Vax Average (IQ Range)		Mann-Whitney test (p)
	Control (n = 11)	SPMS (n = 9)	Control	SPMS	
<30	9	17	29.65 (19.88)	14.59 (10.57)	0.02
30-59	37	46	29.39 (13.04)	21.67 (10.18)	0.0002
60-90	33	8	39.85 (55.26)	31.15 (6.86)	0.27

Table 5.5: Summary of velocity data grouped by vessel sizes

5.3.3.3 Measurements of Resistive Index

We wanted to investigate if these changes were related to a change in resistive index of arterioles, however there was no significant correlation between resistive index and whole vessel diameter in either control or SPMS patients (r = 0.02, r = 0.07 for control and SPMS patients respectively) (Figure 5.13). When compared, there was also no significant difference between slopes (p = 0.67) or difference in elevation between slopes (p = 0.66) in MS and control patients indicating that SPMS does not impact on the resistance of arterioles at the vessel sizes measured.

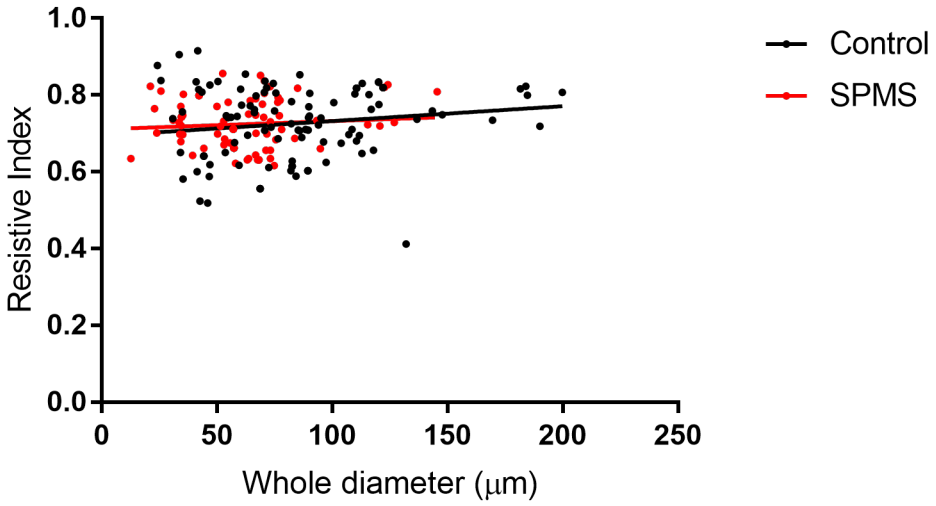

Figure 5.13: Relationship between whole diameter and resistive index in SPMS and control patients. Linear regression coefficients (r) were 0.007 for SPMS patients and 0.02 for controls. There was no significant difference between slopes (p = 0.67) or elevation between slopes (p = 0.66) in MS and control patients.

5.3.3.4 Flow

We also examined what impact changes in vessel structure had on vessel flow in SPMS patients. Following calculation of blood flow, we observed that blood flow increased with lumen diameter for both controls and SPMS patients, as shown on a log-log scale (Figure 5.14) ($r = 0.82$, $r = 0.92$ for control and SPMS patients, respectively). When compared, whilst there was no significant difference between slopes ($p = 0.93$), there was a significant difference in elevations between slopes ($p = 0.0001$), which indicated for a given lumen diameter there was significantly slower flow in arterioles of SPMS patients.

Murray's Law, which can be used to describe the optimal state of flow in blood vessels, states that the volumetric flow rate is proportional to the cube of the radius optimised for the minimum amount of work required to drive and maintain fluid (Nichols et al, 2011). The exponent for blood flow as a function of lumen diameter was approximate to a cubic relationship for both SPMS (Exponent: 3.7) and control groups (Exponent 3.85), indicating Murray's Law applies here (Figure 5.14).

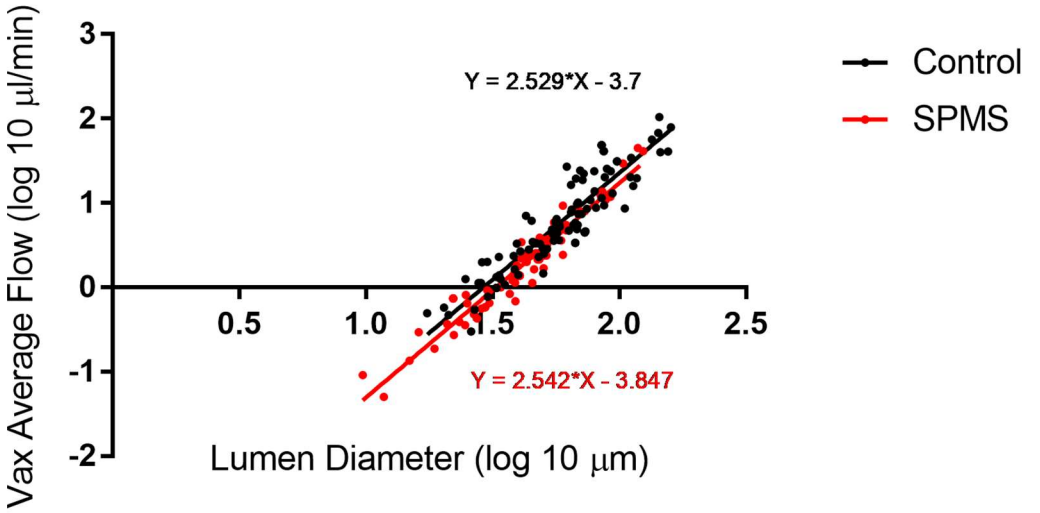

Figure 5.14: Log-log scale of Vax Average Blood flow vs Lumen Diameter comparing SPMS patients to controls. Linear regression coefficients (r) were 0.92 for SPMS patients and 0.82 for controls. There was no significant difference between slopes (p = 0.93). There was a significant difference in elevations between slopes (p = 0.0001).

We also investigated if this difference was more prominent in certain vessel sizes. When examining different groups of lumen diameters, flow was significantly decreased in SPMS patients in vessels with a lumen diameter of approximately 50 – 80µm (Figure 5.15, Table 5.6). There was however no significant difference in flow in vessels with a lumen diameter approximately 30-50µm and 80-126µm. This suggests that flow changes may be affecting vessels differently depending on their size. However, at the largest vessel size (approx. 79-126µm) this result could have been impacted by the wide variation of flow seen in SPMS vessels.

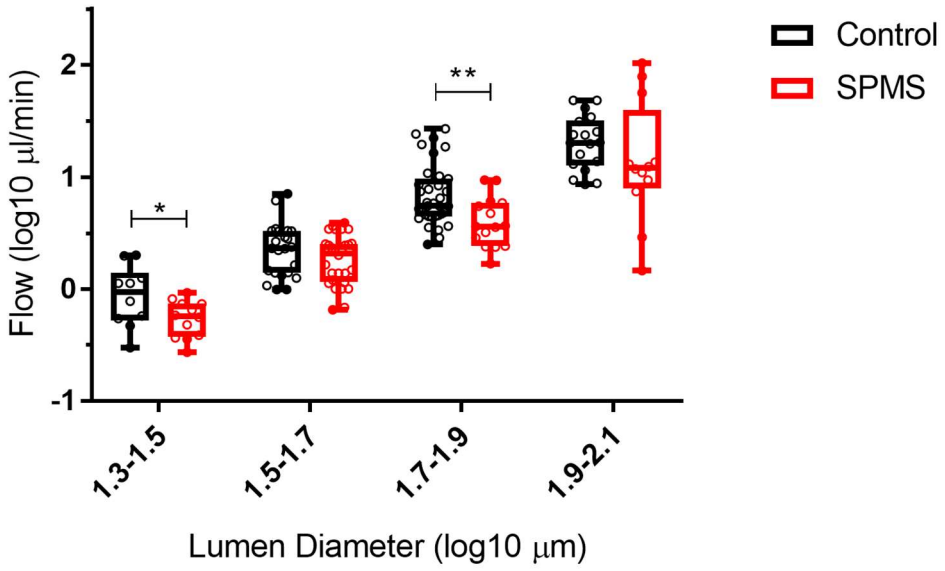

Figure 5.15: Box and whisker plots with overlaid scatter plots of lumen diameter (log10 µm) versus Vax Average flow (log10 ul/min) in three vessel size groups. There was a significant difference between SPMS patients and controls in vessels 1-3-<1.5 and 1.7-<1.9 (log 10 µm) as measured with t-test. There was no significant difference in flow in vessels with a lumen diameter 1.5-<1.7 and 1.9-2.1 (log 10 µm). *P<0.05; **P<0.005.

Lumen Diameter (log 10 µm)	Lumen Diameter (µm)	Number of Segments		Mean Flow (log10 µm) (Standard Deviation)		T-test (p)
		Control (n = 11)	SPMS (n = 10)	Control	SPMS	
1.3-<1.5	20.0-<31.6	10	12	-0.07 (0.27)	-0.27 (0.17)	0.04
1.5-<1.7	31.6-50.0	23	28	0.35 (0.24)	0.26 (0.23)	0.19
1.7-<1.9	50.1-79.3	35	15	0.83 (0.27)	0.59 (0.22)	0.004
1.9-2.1	79.4-125.9	18	12	1.3 (0.24)	1.13 (0.54)	0.25

Table 5.6: Summary of flow data grouped by vessel sizes

5.3.4 Retinal Oximetry

5.3.4.1 Samples

One eye of each control participant was used in this analysis. The right eye of each control participant was used unless it was unavailable. The eyes of SPMS patients were considered independent if one or both eyes had a history of optic neuritis, therefore in some cases both eyes of an SPMS patient were included in the analysis. One SPMS eye was not

captured due to poor fixation and four control eyes were not captured as only one was dilated for the experiment at request of the subject. Following retinal oximetry, one control eye and two SPMS eyes were excluded due to poor image quality (Table 5.7). Vessel diameters, AV difference, arterial and venular saturation were all normally distributed as measured by Shapiro-Wilk test (p = 0.07, p = 0.08, p = 0.20, p = 0.09 respectively).

	N eyes	***N patients***
Control	11	11
SPMS	14	10
ON -	8	8
ON +	6	5

Table 5.7: Summary of eyes used in retinal oximetry analysis.

5.3.4.2 Saturation Measurements

There was no significant difference in arterial or venular saturation between control and SPMS groups (unpaired t-test, p = 0.96, p = 0.76), and control and patients grouped by ON status (One-way ANOVA, p = 0.50, p = 0.91 respectively). There was no significant difference in AV difference between control and SPMS patients (unpaired t-test, p = 0.78) or control and ON+ or ON- eyes (One-way ANOVA, p = 0.90 respectively). These results suggest that there is no difference between SPMS groups, or SPMS and the control group, in the amount of oxygen being delivered to tissues (arterial saturation), the amount of oxygen returning from tissues (venular saturation) or the relative amount of oxygen being absorbed from tissues (AV difference).

5.3.4.3 Average Diameter

There was a significant difference in average vessel diameter between control and SPMS patients (unpaired t-test, p = 0.02) (Table 5.8) but when the SPMS group was divided according to history of optic neuritis, there was no significant different in diameter between control and ON+ or ON- eyes (one-way ANOVA, p = 0.07) (Table 5.9). This indicated the vessels included in retinal oximetry analysis, between 1.5 and 3 disc diameters around the optic nerve head, are thinner in SPMS patients than controls and this difference does not appear to be related to history of optic neuritis, however the small sample sizes included in this analysis may not provide sufficient power to detect a change between these groups (Figure 5.16).

	Parameter	Control (n = 11)	SPMS (n = 14)	P value (Unpaired t-test)
Mean (SD)	**Arterial Saturation**	89.07 (3.824)	88.95 (7.214)	0.9618
	Venular Saturation	53.55 (7.135)	52.26 (12.61)	0.7642
	AV Difference	35.52 (6.483)	36.7 (12.42)	0.7784
	Vessel Diameter	136.6 (14.54)	125.9 (6.341)	0.0210

Table 5.8: Unpaired t-test results comparing control patients to SPMS patients

	Parameter	Control (n = 11)	ON – (n = 8)	ON + (n = 6)	P value (One-way ANOVA)
Mean (SD)	**Arterial Saturation**	89.07 (3.824)	90.59 (6.683)	86.77 (7.927)	0.5022
	Venular Saturation	53.55 (7.135)	53.02 (12.41)	51.24 (13.99)	0.9138
	AV Difference	35.52 (6.483)	37.57 (13.98)	35.53 (11.15)	0.9016
	Vessel Diameter	136.6 (14.54)	124.9 (5.898)	127.3 (7.2)	0.0682

Table 5.9: One-way ANOVA results comparing oximetry metrics of control eyes, ON positive eyes and ON negative eyes.

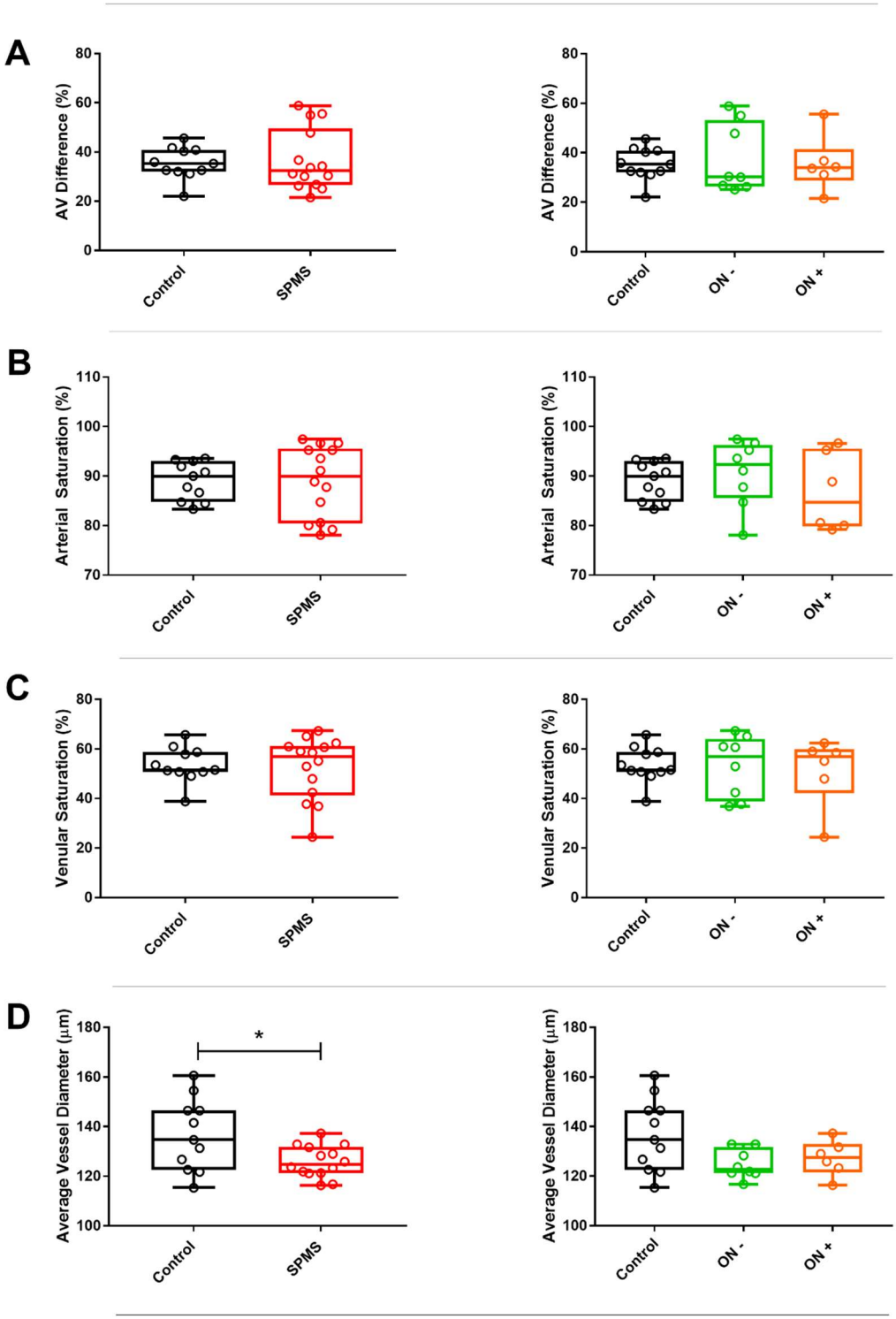

Figure 5.16: Summary of retinal oximetry results comparing both control and SPMS groups, and comparing the control group to eyes with (ON+) and without (ON-) a history of optic neuritis across AV difference (A), arterial saturation (B), venular saturation (C) and mean vessel diameter (D). There was no significant difference in groups across oximetry measurements (A-C) but there was a significant difference in average vessel diameter between SPMS patients and controls (D), which was not observed when the group was split by history of ON. *P<0.05.

5.4 Summary

This is the first reported summary of vascular alterations in SPMS imaged with AOSLO. We have shown both structural alterations in retinal vessels of SPMS patients, as well as functional alterations of speed and flow of cells through vessels.

5.4.1 Vessel Diameter

Using AOSLO imaging, we found that the relationship between wall and lumen diameters was significantly altered in SPMS patients compared to age matched controls. In SPMS patients, vessels with similarly sized walls had significantly narrower lumens. This result is supported by findings from the Oxymap, where a significant decrease in average peripapillary vessel diameter was found.

Although many studies have explored vessel density in multiple sclerosis (Feucht et al, 2019; Lanzillo et al, 2017; Ulusoy et al, 2020; Wang et al, 2014), there are few examining vessel diameter. One study measured vessel diameter in a heterogenous group of MS patients using the shadows formed by blood vessels on optic nerve OCT ring scans (Bhaduri et al, 2016), identifying significant vessel narrowing in the region. The results of this study corroborate our findings as this location, the peripapillary region, mirrors the location used to calculate vessel diameter by the Oxymap. Vasoconstriction elsewhere in the cerebral vasculature has been widely reported in MS. Chronic cerebrospinal venous insufficiency (CCSVI), a condition causing constriction of the cerebrospinal veins has been suggested, somewhat controversially (Bagert et al, 2011), as a significant factor in the development of multiple sclerosis (Zamboni & Galeotti, 2010). Vessel narrowing within MS lesions has been detected using MRI (Gaitan et al, 2013) suggesting a direct impact of disease plaques on vessel diameter. Vasoconstriction in SPMS specifically could be caused by a multitude of factors, including a reduction in metabolic demand, vessel remodelling and vascular mediators released during the disease process.

Vasoconstriction may be partially attributed to a reduction in metabolic demand. Vessel diameter in the retina is tightly controlled and responsive to changes in local tissue needs (Falsini et al, 2002). Consistent diminution in metabolic demand, as a result in inner retinal atrophy, would result in vasoconstriction. There is still some debate over the direction of causation of vascular changes in multiple sclerosis – whether they are purely the result of a drop in metabolic demand or whether vascular changes are a primary cause of neuronal loss. An extended longitudinal study combining structural measurements of both cellular layers and blood vessels would be required to determine if vessel changes precede degeneration or vice versa.

Vessel narrowing measured with AOSLO appears especially profound in larger vessels, supported by peripapillary narrowing measured using the Oxymap. This result could indicate that vessel diameter is affected in MS primarily in the optic nerve region, where neurodegeneration is most prominent, and its affects downstream are weaker. Measurement variability, however, could play a large part in detecting differences in smaller vessels, as any measurement error would have a more significant impact on smaller vessels where vessel walls are less clearly demarcated.

Vessel narrowing could also be attributed to local production of vascular mediators, such as endothelin-1 and nitric oxide. Decreased cerebral perfusion in MS has also been partially attributed to the disease's impact on endothelium-derived relaxing factors, such as nitric oxide. Nitric oxide (NO) known to be present at high concentrations in MS as a result of repetitive vascular inflammatory cascades, especially in the relapsing-remitting phase of the disease (Acar et al, 2003). Chronic over-production of NO could desensitise endothelial and smooth muscle function, impairing the blood vessel's ability to dilate. This chronic inhibition of dilation would also reduce capacity for neurovascular coupling and functional dilation, causing hypoxia driven by neuronal demand. Endothelin-1 (ET-1), a potent

vasoconstrictor, is thought to be released by reactive astrocytes and is significantly elevated in the plasma of MS patients (Haufschild et al, 2001). ET-1 appears to mediate vasoconstriction in the CNS, as treatment of MS patients with an ET-1 agonist (bosentan) results in a reversal of low cerebral blood flow back to normal levels (D'Haeseleer et al, 2013). Increased superoxide production, as seen in MS, may also increase vasoconstrictor tone by stimulation of endothelin-1 in endothelial cells (Kahler et al, 2000). The interactions between ET-1 and NO in SPMS are not well described, but it can be assumed that consistently high concentrations of these mediators within circulation would have a lasting impact on vessel tone, potentially resulting in narrowed vessels unable to functionally dilate. This effect would be compounded by damage to the blood brain barrier and neurovascular unit, which would lead uncoupling of demand to response and further limit the likelihood of sufficient perfusion of the tissues which require it.

5.4.2 Vessel remodelling

In our cohort of SPMS patients, lumen diameter was significantly reduced and wall to lumen ratio (WLR) was increased, yet wall cross sectional area (WCSA) was maintained. The changes seen in vessel structure in SPMS could be explained by a remodelling of the microvasculature in response to an increase in intraluminal pressure, resulting from changes in blood viscosity and increased downstream resistance.

There are two main ways vessels may be remodelled; hypertrophic and eutrophic remodelling. These types of remodelling can be distinguished by their effects on the retinal lumen. In hypertrophic remodelling the vessel wall thickens and the outer diameter is increased, maintaining the original width of the vessel lumen (Rizzoni et al, 1996). In contrast, eutrophic remodelling causes inward constriction of the vessel, maintaining the original outer diameter of the vessel but narrowing the vessel lumen (Baumbach & Heistad, 1989). WLR is a commonly used metric to define intraluminal vascular remodelling (Ritt &

Schmieder, 2009), and has been shown in subcutaneous blood vessels to serve as a reliable prognostic marker for hypertension (Park & Schiffrin, 2001). Another metric, WCSA, can also be used to distinguish between eutrophic and hypertrophic remodelling, as this measurement is stable in eutrophic remodelling but will increase in hypertrophic states (Rosei & Rizzoni, 2010).

In this study, we used a number of vessel metrics to examine vessel components in SPMS. We investigated the relationship between ID and OD, which allows us to determine if there is a fundamental relationship between wall thickness and lumen diameter, detect if remodelling is taking place, and if so by what mechanism (Mulvany, 2012). We found a tight linear relationship between ID and OD for both SPMS patient and controls, however the results for control patients were significantly elevated above SPMS patients demonstrating significant lumen narrowing for a given vessel size. This difference has been demonstrated previously in eutrophic remodelling of blood vessels in hypertensive patients using AOSLO (Hillard et al, 2016). Using both our WLR and WCSA results it is possible to distinguish between eutrophic and hypertrophic remodelling (Heagerty et al, 1993). As eutrophic remodelling is characterised by a constriction of vessel lumen due to vasoconstriction and rearrangement of smooth muscle cells, WCSA remains unchanged and WLR is increased. Conversely, hypertrophic remodelling results in an increase in both WCSA and WLR. In our SPMS patients there was a significant elevation in WCSA and a significant elevation in WLR, so it is possible that both aspects are occurring. However, when grouped by vessel size the increase in WCSA in SPMS vessels was no longer significant, suggesting that the effect on the content of the vessel wall is minimal. Results from the Oxymap demonstrated a significant reduction in lumen diameter at the optic nerve head, supporting this idea of vasoconstriction at this vessel size.

Eutrophic and hypertrophic remodelling are characterised both by their distinct effects on vessels but also by their mechanisms of action. The classic reduction in lumen diameter demonstrated in eutrophic remodelling is thought to be mediated by a functional response of the vessel wall to increased luminal pressure, known as myogenic tone (Wallis et al, 1996). This prolonged constriction of the vessel wall is only thought to occur in small resistance arteries in order to protect downstream capillaries from harmful elevations in pressure. In contrast to hypertrophic remodelling, caused by hypertrophy and hyperplasia of smooth muscle cells in the arterial wall, the content of the vessel wall is unchanged in eutrophic remodelling, resulting in preservation of wall cross sectional area. We have to of course consider that the components of retinal vessel walls vary across vessel sizes and cannot all be compared directly. There are some suggestions in our results that arteries of different sizes may respond differently to SPMS processes. Reports from histological data demonstrate that retinal vessels along the main arterial branches maintain their muscular layers up until around 20µm in diameter, at which point they can be considered true arterioles, and single flow capillaries occur within the range of 5-8µm (Hogan & Feeney, 1963). When comparing wall metrics between groups, wall thicknesses were increased in vessels between 50-100µm diameter but there was no detectable difference in vessels below 50µm in diameter, which may reflect the increasingly small amount of smooth muscle in the walls of these vessels which makes them unlikely to respond to changes in pressure in the same way as larger arteries.

There is much published on the effects of hypertension on vessel remodelling in the retina, therefore we can use this as an initial comparator to potential vascular remodelling occurring in SPMS. Hypertension and pre-hypertension are common in MS (Marrie et al, 2016), and have been associated with brain integrity and disability outcomes in MS (Dagan et al, 2016). Eutrophic remodelling has been demonstrated in the retina in patients with hypertension (Hillard et al, 2016; Koch et al, 2014). Narrowing of the lumen may also be

further exacerbated by chronic vasoconstriction, reducing the overall vessel diameter, which has already been suggested as a factor in cerebral hypoperfusion in multiple sclerosis (D'Haeseleer et al, 2013). It has been suggested that a combination of the two types of remodelling occurs in the hypertensive retina (Hillard et al, 2016), as seen in systemic circulation in response to hypertension (Renna et al, 2013). WLR, as measured with SLDF, was previously shown to be associated with history of a cerebrovascular event (Harazny et al, 2007) and hypertrophic changes in peripapillary vessels has been associated with cerebrovascular damage in patients with uncontrolled hypertension (Baleanu et al, 2009), demonstrating hypertrophic remodelling of vessels can occur at this vessel size in this extreme circumstance, but this may not reflect the response of smaller vessels to hypertension. It is also possible that rarefaction of retinal capillaries in MS, identified by other groups in MS although not detected by us (see Chapter 3), may cause increased downstream resistance to blood flow therefore resulting in retinal arterial hypertension and subsequent vessel remodelling (Mayet & Hughes, 2003). As discussed previously, oxidative stress has been shown to correlated with disease duration in MS (Groen et al, 2016) and is known to induce vascular remodelling (Fortuno et al, 2005), which may explain the changes seen in SPMS. Retinal vascular changes reported in this chapter reflect that seen in previous studies of hypertension, and investigating the relationship between SPMS and hypertension may provide a useful starting point as the mechanism for the retinal vascular remodelling seen in SPMS.

Increased vessel rigidity (Kochkorov et al, 2009) has also been found using the Retinal Vessel Analyser by calculating the pulse delay between retinal and choroidal circulation. The most profound vessel rigidity was detected in MS in vessels distal to the optic nerve, suggesting a greater impact on smaller blood vessels, however we did not identify that in our cohort. This rigidity could be the result of parietal thickening in MS, as can occur due to hypertrophic remodelling in hypertension (Laurent, 1995), however arterial hypertrophy

was not definitively identified in our SPMS cohort. Myogenic tone, as a result of eutrophic remodelling, would also have a stiffening effect on arteries. Additionally, an increase in distending pressure inside a blood vessel, as found in hypertension, can also cause arterial stiffness as blood vessels are non-linearly elastic and they become stiffer when greater pressure is put on them (Mayet & Hughes, 2003). Resistive index can be used as a measurement of vascular compliance (Bude & Rubin, 1999) however we did not find any significant difference in resistive index between SPMS patients and controls, which suggests retinal arteries, although perhaps undergoing remodelling, are not altered in their compliance and ability to transmit pulsatile forces.

Vasoconstriction in SPMS could have an important influence on other diagnostic technologies used in the disease. RNFL thickness is also influenced by retinal vessel diameter, therefore the recognised thinning of the RNFL in MS as a result of cell loss could be compounded by a reduction in vessel diameter (Pereira et al, 2014), and this may have to be considered in OCT studies of SPMS. Further studies are needed to better understand the importance of vessel remodelling in SPMS and evaluate the relationship between disease and microvascular function.

5.4.3 Factors affecting flow

We found a significant reduction in both blood cell velocity and blood flow in retinal vessels of MS patients. As with structural changes, we have to consider that not all vessel sizes will be equally impacted functionally by SPMS. Vessel diameter has a direct impact on velocity and flow, and we have to consider that velocity within a vessel segment is influenced by upstream pressure and downstream resistance to flow. We found that although structural changes were primarily detected in medium sized vessels in SPMS, functional changes in velocity and flow were detected in both small (<30µm) and medium sized (30-80µm)

arterioles and arteries, reflecting the directional nature of flow and the significant impact upstream remodelling can have on downstream branches.

Although there is a growing volume of evidence on vascular density changes in the MS retina, there is a paucity of evidence on velocity and flow changes in the retina. Reduced vessel velocity and flow in MS patients has been demonstrated using the RFI (Jiang et al, 2016), but focussed on small perifoveal vessels (Mean Diameter: 18μm). There are previous reports of retinal blood flow reduction as measured by colour Doppler imaging in MS (Modrzejewska et al, 2007; Pache et al, 2003), however these are limited to retrobulbar vessels which do not necessarily conform to the same rules as retinal vessels. Our results are also supported by evidence of reduced cerebral blood flow (Adhya et al, 2006; D'Haeseleer et al, 2013; Law et al, 2004) and increased cerebral circulation times (Monti et al, 2015) in MS.

Slowing of blood velocity in MS could be the consequence of reduction of metabolic need, vasoconstriction or increased blood viscosity. Atrophy of the RNFL and GCL are ubiquitous to all types of multiple sclerosis, and as mentioned, are likely to have a direct impact on vascular activity in the retina, such as vessel dilation and flow, as the relationship between supply and metabolic demand in the retina is tightly controlled. Changes in vessel diameter have a direct effect on both cell velocity and overall flow, as cells in smaller vessels move more slowly and are subject to different forces, such as changes in viscosity and resistance, therefore vasoconstriction could play an important role in the velocity and flow changes which we have encountered within MS. The viscosity of blood may also have a significant impact on blood flow in SPMS patients. Blood viscosity increases with increased red cell aggregation, and there is evidence for increased aggregation in SPMS patients (Groen et al, 2018; Groen et al, 2016; Simpson et al, 1987). Excessive aggregation increases resistance at the capillary level, thereby increasing pressure on arteries and arterioles. The combination

of these factors; metabolic demand, vasoconstriction and aggregation, could significantly impair the rate and volume of blood flow in the retina in SPMS.

The relationship between vessel diameter and flow is predicted as a cubic relationship, as described by Murray's law of branching vasculature (Murray, 1926). We found, in close agreement, that mean flow varied with vessel diameter in a cubic relationship in control participants (for power fit, exponent = 3.7, Figure 5.15), which is higher than that seen in the control group of a previous XT study (Palochak et al, 2019), however that particular study includes subjects of a lower age range. The fitting component of the SPMS group was higher than controls, at 3.85, which is interesting as deviations from Murray's law can result from changes in blood viscosity and vessel diameter in pathologic situations. In contrast to Palochak *et al*, we have focussed on the relationship between lumen diameter and flow, as opposed to the relationship between outer diameter and flow as alterations in vessel wall thickness would have impacted our results.

5.4.4 Retinal Oximetry

We did not find any difference in retinal oximetry measures between our SPMS patients and controls, which contradicts most of the findings in MS. Retinal oxygen saturation in MS has been assessed previously using the Oxymap (Einarsdottir et al, 2018), revealing increased venular saturation in MS patients which was more profound in ON+ eyes, suggesting a reduction in oxygen uptake. However, this study did not distinguish between RRMS and SPMS patients, and EDSS scores were not included in results so we cannot compare that group directly to our cohort. Reduced cerebral oxygen saturation has also been shown previously in the brain using NIRS, although hypoxic regions were not found in every patient with the condition (Yang & Dunn, 2015). Inflammation can also significantly impact retinal oxygen saturation as demonstrated in a study of giant cell arteritis, characterised by a mass inflammatory response (Weyand et al, 2004), which showed

similar increases in venular oxygen saturation as in MS (Turksever et al, 2014). These changes in saturation could therefore be more significant in the earlier stages of MS, due to heightened inflammation, and could return to normal levels in the later progressive stages of the disease. Despite oxygen saturation levels being comparable to control subjects in our study, this does not necessarily mean the retina is receiving sufficient oxygen in SPMS. As retinal vessel diameter and retinal blood flow are significantly decreased, it may be that an insufficient volume of oxygenated blood is meeting retinal tissues due to the structural changes within these vessels.

There are however limitations to the Oxymap which could have influenced our results, such as its propensity to image artefact effects and need for strict standardisation of images. The Oxymap can only be used for vessels >56µm in diameter due to measurement variability in narrower vessels, therefore we could not use this technique to detect alterations in oximetry at this level. Accuracy of saturation measurement is also image quality dependent, making results susceptible to artefacts caused by optical scattering, such as cataracts or vitreous infiltrates. We used age-matched participants to control for this issue. The angle of gaze can have a significant impact in saturation results therefore standardisation of image collection is essential in maintaining repeatability (Palsson et al, 2012). Our image collection was standardised, and by analysing oximetry results in a defined region (1.5-3 disc diameters from optic nerve) we further ensured standardisation of results between patients. When evaluating vessel diameters using the Oxymap, we did not account for retinal magnification. Myopia can also have an effect on saturation measurement (Zheng et al, 2015) and we did not account for axial length in Oxymap results. We did, however, exclude participants with pathologic myopia (> -7D), therefore any small refractive error would likely have a negligible effect on saturation values. The sample size used in our study was also small, precluding any definitive conclusion on retinal oxygenation in SPMS.

5.4.5 Limitations of study

One aspect which we have not explored in detail is the impact of previous treatments for MS on retinal vessels. Fingolimod, an immunomodulating drug regularly used as a second-line treatment for active RRMS (NICE, 2020) can have significant vascular side effects in the retina including endotheliopathy and macular oedema (Nolan et al, 2013). Fortunately, if these issues appear the effects tend to fully resolve following cessation of fingolimod treatment (Chui et al, 2013; Turaka & Bryan, 2012). It is possible, however, that the high resolution at which we are imaging we may detect sub-clinical vascular issues which could be related to previous fingolimod treatment. Two patients in our cohort had a history of fingolimod treatment and did not report any ocular side effects, therefore we think this had a limited effect on our results. Previous fingolimod treatment should however be considered when stratifying patients in larger cohorts in future.

Another limitation of our study is in the sampling of vessels across our participants. We did not collect as many images of large vessels (>100μm) from SPMS patients than control participants. This may be due to two factors; fixational ability of SPMS patients and generalised vasoconstriction. Vessel size within the retina is mainly determined by proximity to the major arteries and veins entering the retina through the optic nerve head. In order to image these vessel branches with AOSLO, a patient must fixate on a spot far from the primary position of gaze and maintain that position throughout imaging. From our experience this can be challenging for SPMS patients, and generally leads to poor quality imaging which ultimately is excluded from analysis. This poor fixational ability could be related to a range of eye movement abnormalities identified in MS (Serra et al, 2003). Additionally, the presence of generalised vasoconstriction, suggested by the results of this study, would result in a paucity of large vessels in a location within the range of a patient's fixational capabilities and would also result in poorer sampling of these vessels.

One limitation of our imaging protocol was that certain clinical markers which could influence vascular measurements were not assessed before or during imaging. Systemic blood pressure changes are known to have significant effects on retinal blood flow and flow dynamics (Fuchsjager-Mayrl et al, 2001). We attempted to account for this by ensuring patients were seated for at least 5 minutes prior to beginning imaging. SPMS patients also had their blood pressure measured the day prior to our imaging as part of the MSOpt trial, and all were within normal range at that time. This reassures us that in the least our patients did not have pathological blood pressure changes which were not accounted for in our trial. As arterial hypertension and aging also affect the structure of arteries this should be considered in our subjects. There are reports of blood pressure alterations in MS patients (Dagan et al, 2016), possibly as a result of poor autoregulation. None of our patients reported clinically relevant high blood pressure, and the patient and control groups were matched for age, therefore this is unlikely to affect our results. Finally, we did not measure or account for glucose level in either groups, which could have a significant impact on retinal vessel calibre (Grunwald et al, 1987). SPMS patients were however screened for diabetes before recruitment, and none of the control patients reported a history of diabetes, so the relative impact glucose levels would have had was likely to be small.

5.4.6 Conclusion of Chapter

Microvascular changes in SPMS are increasingly being recognised as significant factors in the progression of the disease, however detection and monitoring of microvascular changes in the CNS presents challenges. This is the first report of vascular alterations in the retina in SPMS, identifying changes to both the structure and function of retinal vessels in this disease (Table 5.10). The retinal vasculature may serve as a new biomarker in SPMS; helping us monitor the effects of new treatments in clinical trials and identify new vascular targets for neuroprotection, which have so far been limited.

Parameter	Effect on SPMS	Figure Number
WLR	↑↑↑ Medium Vessels	5.5
ID:OD	↓↓↓ Medium Vessels, ↑ Large Vessels	5.6
WCSA	No Difference All Vessels	5.8
Blood Velocity	↓ Small Vessels, ↓↓ Medium Vessels	5.12
Blood Flow	↓ Smallest Vessels, ↓↓ Medium Vessels	5.15
Arterial Saturation	No Difference	5.16
Venular Saturation	No Difference	
AV Difference	No Difference	

Table 5.10: Summary of Chapter 5 results. The number of arrows indicates the significance level of difference between the SPMS group compared to age- and gender-matched control subjects. The "size" of vessels described refers to the vessel size described in each individual figure, and is a general description not directly comparable between all figures. WLR: Wall to Lumen Ratio, ID:OD : Ratio of Inner Diameter to Outer Diameter, WCSA: Wall Cross Sectional Area, AV Difference: Arteriovenous Difference.

General Summary of the Results, Conclusions, Limitations of the Thesis and Proposal for Future Works

To date, less attention has been paid to the potential effect of blood vessel dysfunction in MS pathophysiology compared with neuronal damage. Furthermore, despite effective treatment for the early relapsing remitting phases, effective treatments for the secondary progressive phase of the disease are limited. This indicates that other mechanisms may be responsible for the later phases of disease and alternative targets for treatments, such as the vasculature, need to be explored. There is a growing body of knowledge surrounding the CNS vasculature in multiple sclerosis and its potential impact on the disease, although there are temporal and spatial resolution limitations to *in vivo* imaging of the CNS vasculature which hinder its utility. This issue could be addressed by imaging the microvasculature of the retina instead, an anatomical and physiological analogue of the CNS, which can be visualised non-invasively at high resolution using a number of different techniques.

Research into the effects of SPMS on the retinal vasculature in SPMS is generally limited with most articles in MS concentrating on either earlier phases of MS or pooling all phases together (Table 6.1). SPMS should not be considered simply an extension of CIS or RRMS for a number of reasons. SPMS differs from RRMS in its inflammatory profile and cumulative increase in disability. Patients with SPMS also tend to present with significant neurodegeneration from the earlier phases of the disease and their vascular landscape is likely already impacted by previous treatments for RRMS. Additionally, not all RRMS patients will go on to progressive disease, and there are complex factors which make certain patients more likely to develop SPMS (Vasconcelos et al, 2016). For all these reasons SPMS patients cannot be considered a “worse” case of RRMS as the factors which

influence microvascular structure and function are already established, therefore studies specific to the retinal vasculature in SPMS are required.

Technique	Authors	MS Subtype Included			
		CIS	RRMS	SPMS	Did not distinguish
OCT	Bhaduri et al, 2016				
RVA	Kochkorov et al, 2009				
RFI	Jiang et al, 2016				
	Liu et al, 2019				
OCTA	Wang et al, 2014				
	Lanzillo et al, 2017				
	Spain et al, 2018				*
	Yilmaz et al, 2019				
	Murphy et al, 2019				
	Feucht et al, 2019				
	Ulusoy et al, 2020				

Table 6.1: Summary of reports of optical retinal vascular imaging in MS. OCT: optical coherence tomography, RVA: retinal vessel analyser, RFI: retinal function imager, OCTA: optical coherence tomography angiography, MS: multiple sclerosis, CIS: clinically isolated syndrome, RRMS: relapsing remitting multiple sclerosis, SPMS: secondary progressive multiple sclerosis. *SPMS patients were specifically included in this study, but in analysis were pooled with all other subtypes.

This thesis was formed around identifying microvascular abnormalities in SPMS and developing imaging biomarkers in the retinal microvasculature to use in studies of neuroprotective agents in the disease. We studied cohorts of healthy control volunteers and MS patients to investigate changes in the microvasculature and establish new techniques for microvascular imaging. This thesis is divided into three parts, first a pilot study on the retinal microvasculature across RRMS and SPMS to investigate how the microvasculature changes across the disease to establish most the appropriate biomarkers. Second, development and validation of new semi-automated techniques to measure retinal blood flow, which was crucial for the final section, where we investigated blood flow and

blood vessel structure at all levels of the vascular tree in SPMS patients and age-matched controls.

6.1 Observations from Pilot Data

In this part of the thesis, we aimed to evaluate both structure and function of the microvasculature across different stages of MS and compare the results to that of healthy controls using a number of different ophthalmic imaging tools. This allowed us to determine the most appropriate protocols for vascular investigation in these patients. Investigation of inner retinal structure was performed using OCT in order to establish general structural differences in the study cohorts, and was found to be representative of previous MS research, demonstrating that as the disease progresses so does the level of inner retinal atrophy. Assessment of OCTA images from RRMS and SPMS patients revealed no significant difference in vessel density or fractal dimension in a small sample of patients, suggesting overall gross vascular architecture was unaffected by the disease. As the purported microvascular impact of MS is likely small and sub-clinical, grading of AOSLO images of the microvasculature was performed to establish if there were any alterations of the inner retinal vasculature at high-resolution. In order to investigate function at the capillary level, erythrocyte aggregate velocity was also measured as a surrogate of general blood velocity in the retina and was found to be reduced. Moreover, a sub-analysis was also performed on the presence of microcysts within the retina and it was found that one type of microcyst (Type 3) was found only in SPMS patients suggesting this could be used as a biomarker of pathology in these patients.

Surprisingly, we also found some inner retinal anatomical and microvascular anomalies in healthy control patients, especially in the case of microcysts, where Type 1 and 2 were found in similar frequencies in control and MS patients. Our understanding is still limited in what is “normal” for the inner retina, especially at the resolution possible using AOSLO, and

further investigations of large cohorts of control patients of all ages is required in order to establish normal ranges for these anomalies and understand their aetiology.

6.2 Development of Analysis Tools for Velocity Measurement

In Chapter 4, we developed and validated a novel method of analysis for XT Imaging to be used for detailed assessment of the retinal microvasculature in SPMS. The rationale for this study was that XT imaging has great potential as a form of non-invasive imaging of retinal blood flow, but this is limited by the lack of automated analysis available. Our results showed that using a previously published tool (Directionality) with some pre-processing of images led to an excellent agreement between videos of high quality, and that measuring three cycles is sufficient to achieve a representative average velocity. We were able to use these findings in the final section of this thesis to investigate blood velocity and flow in control patients and an SPMS cohort.

Previous investigations of vascular function using XT imaging, including our own, have used a reductionist approach in measuring retinal blood velocity, isolating the peaks and troughs of cardiac cycles and disregarding the potential wealth of information available in the remainder of the cardiac cycle (Palochak et al, 2019; Zhong et al, 2012; Zhong et al, 2011). This was due to a number of reasons including lack of efficient measurement tools. The semi-automated process developed in this thesis could be used to further examine changes occurring across the cardiac cycle by utilising other markers developed from Doppler imaging (Maruyoshi et al, 2010) to learn more about vascular function not limited to the measurement of average velocity across a cycle.

There are additional analyses which can be extracted from the Fourier Transform of XT images which are not explored in this thesis, but would be beneficial to future researchers on this topic. Firstly, the dispersion and length of the power spectrum reflects the frequency of directional components within an image. The frequency of directional

components would likely reflect the number of cells measured at one time, therefore allowing for a direct calculation of flow as cells by unit time, unhindered by the assumptions of flow required by Poiseuille calculation (Nichols et al, 2011) to produce a value of volume by unit time. Comparing the results from power spectrum analysis and traditional Poiseuille calculation would allow us to understand the potential limitations of using this technique within small vessels of the retina.

6.3 Structure and Function of the Retinal Vasculature in SPMS

In Chapter 5, we were able to identify changes in the structure and function of retinal blood vessels at all levels of the vascular tree in SPMS. Vessel structure, blood velocity and blood flow were measured in arterioles from 12µm to 202µm in diameter in both SPMS patients and age-matched controls using AOSLO, and retinal oxygen saturation in the peripapillary vessels was measured using the Oxymap. Evidence of vascular remodelling and significant reductions in both blood velocity and flow in the arterial network were seen in SPMS patients using AOSLO. There was no significant difference in retinal oxygen saturation in SPMS patients and controls, but the results from this analysis did highlight generalised vasoconstriction at the peripapillary level in SPMS patients.

By interpreting the data of the present study together with Chapter 3, where we looked more superficially at vasculature using OCTA, we can begin to understand that whilst SPMS does not appear to cause significant changes to the general vascular architecture, there are subtle, but nonetheless potentially important changes occurring to blood vessels both in their structure and function. The reduction in arterial blood velocity in SPMS patients may explain the slowing of ECAs seen in Chapter 3, as although we did not investigate capillary velocity in this chapter, upstream changes of arterial velocity in arterioles would significantly impact downstream velocity and flow. Changes in velocity and flow may also be attributed to generalised vasoconstriction, as results from both WLR analysis and retinal

oximetry suggest vessel diameter has decreased across the vascular tree. This was not measured using AOSLO in Chapter 3 as the protocol used meant we could not distinguish arteries from veins. As reduction in vessel diameter was detected in the peripapillary region using the Oxymap, and structural alterations suggestive of narrowing were found across all levels of the arteriolar network using AOSLO, this suggests that vasoconstriction is occurring widely across the retina. Using a larger sample size, it would be interesting to examine the relationship between inner retinal structure and vessel size using OCT and AOSLO to determine if neurodegeneration has a direct impact on vessel thickness. As in Chapter 3, it would also be interesting to use the imaging markers from Chapter 5 in RRMS patients to examine the temporality of these changes and uncover if vasoconstriction is a late stage phenomenon in MS mainly related to degeneration and metabolic demand, or if it is present early in the disease.

We did not find a difference in resistive index between SPMS patients and control subjects, which corroborates our findings on small vessel compliance in Chapter 3, although we have to consider that larger arteries (>50um) and small arterioles (<20um) may not be reflective of each other due to structural differences in vessels as they branch further down the vascular tree (Hogan & Feeney, 1963). If there are changes in the stiffness of vessels in SPMS, this could also be investigated further with detailed investigation of the velocity curves themselves, which the protocol developed in Chapter 4 allows us to extract.

Retinal oxygen saturation was not found to be significantly different in SPMS patients than controls, however with our relatively small sample size we may not have had the statistical power to detect this difference. It would be interesting to repeat this investigation with a larger cohort of subjects to see if there is a significant difference in saturation and also if saturation for both SPMS patients and controls could be correlated with structural measurements of the retina. Investigating the relationship between AV difference and the

presence of Type 3 retinal microcysts, as seen in Chapter 3, would also be interesting as one hypothesis for the development of microcysts is retrograde degeneration (Lujan & Horton, 2013), which if present should lead to a decrease in AV difference as less oxygen is extracted by atrophied tissues.

It was not possible to perform OCT or OCTA on control subjects in Chapter 5 due to lack of access to equipment. Comparison of structural information gained from both techniques in both SPMS patients and control subjects to results from AOSLO and Oxymap would allow us to further examine if neurodegeneration leads to vasoconstriction, and correlate data on neurodegeneration to metabolic response. Combining all these techniques may offer ways to explore temporal patterns in vascular changes and atrophy of retinal layers, aiding important insights into the pathological processes which drive progression in SPMS.

Due to the effective treatments available for RRMS, secondary progressive patients often present with milder symptoms and have a greater quality of life in their disease than ever before. As these patients age, however, the consequences of aging on their retina must be considered when designing clinical trials for MS. We had carefully matched control patients for age and sex to the SPMS cohort, however as SPMS is a variable disease in its presentation and progression (Thompson et al, 2018) a larger sample size would be required to validate the findings shown in this thesis.

6.4 Limitations

There are some limitations across this thesis which warrant discussion, namely the availability of medical history, insight into the impact of optic neuritis and imaging resolution. Our approach was to use information gathered from analysis of images only, however information on visual acuity, length of disease and history of treatment could also be combined with imaging data to provide a more complete view on the impact of microvascular change in SPMS.

In most cases we selected the patient's eye without history of ON if that was available, as AOSLO is reliant on good fixation. This limits the scope of our findings as it is likely that investigating eyes with a history of optic neuritis would allow us to detect more drastic differences in the retinal vasculature and surrounding structure and would allow us to understand the impact ON has on the microvasculature. Careful consideration of the effects of optic neuritis ought to be included in future studies, and patients should be stratified according to their previous history of ON, however this will increase the required sample size.

One limitation of this thesis is in its lack of differentiation of individual vascular layers using AOSLO. There are two reasons for this, first due to the *en-face* nature of AOSLO it was difficult to determine the exact layer being imaged and as the capillary regions being imaged were relatively central (within 10 degrees of fixation) stratification between layers was less clearly defined meaning the intermediate and superficial layers were likely imaged simultaneously. Secondly, in Chapter 5 we focussed our attention to arteries and their branches which are embedded within the RNFL and therefore we did not image the intermediate or deep layers. This may have limited the scope of our research, as some OCTA studies of MS have reported pronounced effects on the deeper capillary layers (Feucht et al, 2019; Yilmaz et al, 2019), which we would have missed. Further insight may have been gained by superimposing AOSLO images onto OCTA images in order to utilise the segmentation capability of OCTA to differentiate vascular layers. Combining measurements from both the separate capillary beds and the vessels supplying and draining them would allow for a more nuanced assessment of microvascular disease, both in SPMS and other microvascular disorders of the retina.

6.5 Future Directions

With the identification of retinal imaging markers previously unreported in multiple sclerosis and development of new semi-automated analyses, there are a number of directions future research can pursue from the results of this thesis.

The presence of large microcysts in our MS patients in Chapter 3 was substantially higher (3/16 patients, 18.75%) than reported previously using OCT (15/303 patients, 5% reported by Gelfand *et al* (2012)). This is perhaps unsurprising due to the high resolution which can be achieved with AOSLO, and the size of cysts imaged as even using a highly dense OCT scan these cysts may go undetected. It is also unclear as to the activity of these cysts over time. It may be that cysts resolve, or they remain stagnant leaving a permanent scar on the inner retinal landscape. This should be investigated in future in longitudinal studies both in patients with disease and healthy cohorts to understand in what time scale, if any, these cysts resolve and what changes should be considered pathological.

We did not explore single cell flow in this thesis, despite the fact pronounced changes in blood flow were found at the capillary level of MS patients using the RFI (Jiang et al, 2020). Single-cell flow in SPMS could be measured by researchers using the AOSLO offset-imaging technique, developed by de Castro *et al* (2016). Cell velocity in capillaries, as measured using offset imaging, could help to identify the sequence of events that leads to the structural alterations seen in Chapter 3 and vascular remodelling changes identified in Chapter 5. If blood velocity in capillaries is significantly reduced in MS patients it is likely that it is a consequence of the upstream reduction in arterial blood velocity and flow observed in Chapter 5. If capillary velocity is not significantly reduced, it is possible that vascular pruning, identified in other studies of OCTA in MS (Feucht et al, 2019; Ulusoy et al, 2020; Wang et al, 2014; Yilmaz et al, 2019), serves to maintain capillary resistance and therefore velocity through capillaries, which could be investigated by correlating cell velocity to vessel density and calculating average tissue flow.

Retinal atrophy related to MS may also cause poor vascular regulation in the retina, meaning when tissue needs are increased for example in response to stimulus, functional dilation is not initiated and retinal tissue enters a hypoxic state. Responsiveness of vessels to local needs is an essential function of the microvasculature, and the loss of this function has been noted in several ophthalmic diseases such as diabetic retinopathy (Karami et al, 2012) and glaucoma (Fuchsjager-Mayrl et al, 2004). Damage to autoregulatory functions could explain some of the issues seen in MS patients, and could be investigated using AOSLO. Functional response of blood vessels to local stimulation has been successfully measured using XT imaging (Zhong et al, 2012), although this technique has not yet been used in the presence of disease. One limitation to using XT imaging for functional studies of retinal response is the demanding nature of manual analysis, as a number of cycles would have to be measured to establish a baseline then additional cycles would have to be measured to assess the response of blood vessels. Using the protocols developed in Chapter 4, researchers can now accurately measure cycles in a semi-automated manner making this process more efficient and ensuring functional studies using XT imaging are more appealing to researchers.

One aspect of blood flow which was not explored in this thesis is the flow velocity profile. Blood velocity changes across the profile of a blood vessel, with blood cells moving fastest at the centre and slowest at the vessel walls. With XT AOSLO analysis in Chapter 5, we measure the central lumen velocity to ensure that we achieve a consistent result across vessels, however as we can image the entire vessel profile with XT imaging there is a wealth of information contained within each image which may provide insights into SPMS pathogenesis. Our understanding of inflammation within retinal blood vessels in SPMS is limited, and analysis of XT velocity profiles across a blood vessel could be used to investigate this, as increased lagging of cells at the vessel wall is indicative of inflammation and could be measured using flow profile analysis. Furthermore, red cell aggregation which

could be an important element of MS pathogenesis also has a direct effect on the shape of the flow profile (Bishop et al, 2001), and so AOSLO could be used as an *in vivo*, non-invasive tool to investigate this.

It is unclear if the vascular changes detected in SPMS are a cause or result of neurodegeneration. Regardless, the presence of vasoconstriction as identified in this thesis will likely result in further vascular change, as a vicious cycle could ensue where long-standing vasoconstriction as a result reduced metabolic demand cannot sustain functional dilation, causing hypoxia, cell death and a further drop in metabolic demand. Treatment options for SPMS are limited, and previously have focused on addressing the low-level inflammation still present in the disease. The vascular changes identified in this thesis supports the promotion of vasoconstriction as a potential therapeutic target in SPMS. This option has been previously explored in MS using bosentan and nimodipine. Bosentan, an ET-1 agonist, was successfully used to return reduced cerebral blood flow to normal levels in MS patients (D'Haeseleer et al, 2013). Nimodipine, a CNS-selective vasodilating agent, has been shown to reduce dysfunction and demyelination in EAE, and although this study focused mainly on treating the impact of relapses in the early stages of MS, it highlights a valid therapeutic target for both RRMS and SPMS (Desai et al, 2020). Interestingly, simvastatin, a lipophilic statin which is purported to have vasodilatory effects (Sasaki et al, 2013), has been demonstrated to significantly reduce the rate of brain atrophy in SPMS independent of any effect on inflammation (Chataway et al, 2014). Vasodilation, or at least a reversal of vasoconstriction, would halt the vicious cycle of atrophy and vessel narrowing which could be attributing to progression in SPMS. It is unlikely that improving blood flow in this way would recover the cells lost to SPMS, but it could at least protect the remaining cells from further hypoxia and potentially make them more resilient to ongoing oxidative damage and inflammation.

Vascular alterations in the retina have also been noted in other brain diseases with a purported microvascular effect, such as Alzheimer's disease (AD), and the imaging markers developed in this thesis may be beneficial to study of these diseases. For example, previous reports in AD have been based on either macrovascular findings on colour fundus imaging (Lesage et al, 2009; Patton et al, 2007) or on microvascular findings from post-mortem retina (Koronyo et al, 2017). Imaging markers similar to those reported in this thesis have been noted in mouse models of AD such as "stalled flow", akin to erythrocyte aggregation (Hernandez et al, 2019). Utilising the power of AOSLO in studies of Alzheimer's disease would allow researchers to investigate these microvascular changes *in-vivo* and detect subtle changes in the vasculature.

6.6 Conclusion

This thesis adds valuable information to the literature surrounding the retinal microvasculature in MS, particularly as we have concentrated on the underserved subtype of SPMS. We have identified imaging biomarkers that could allow us to further explore and identify other vascular abnormalities of retinal vessels in MS. Development of these biomarkers mean we can now use the retinal vessels as an imaging endpoint in studies of neuroprotective drugs in MS, especially those with a vascular effect. Our research has also thrown light to novel areas of investigation in the retinal vasculature which were not pursued in this thesis.

6.7 Statement

This thesis was part of a larger study, MSOpt, a randomised controlled trial of simvastatin treatment in SPMS and exploration of its mechanism. Due to issues beyond our control, the MSOpt trial was extended beyond the duration of the PhD. There were significant issues with the primary outcome measure of the trial, as a new MRI was commissioned at the beginning of the trial which led to delays and the MRI suffered water damage due to a flood which further delayed recruitment. This PhD constitutes preliminary data on the development of techniques used in the ophthalmic imaging portion of this trial, and comparison of results from control patients to a group of SPMS patients prior to treatment. It also explored the use of this technology in RRMS patients and a control cohort. The MSOpt trial remains ongoing as of October 2020 and is being extended further due to the difficult landscape of patient recruitment during the COVID-19 pandemic.

References

Abràmoff, M. D., Garvin, M. K. & Sonka, M. (2010) Retinal Imaging and Image Analysis. *IEEE transactions on medical imaging*, 3, 169-208.

Acar, G., Idiman, F., Idiman, E., Kirkali, G., Cakmakci, H. & Ozakbas, S. (2003) Nitric oxide as an activity marker in multiple sclerosis. *Journal of Neurology*, 250(5), 588-592.

Adams, C. W. M. (1988) Perivascular iron deposition and other vascular damage in multiple sclerosis. *Journal of Neurology Neurosurgery and Psychiatry*, 51(2), 260-265.

Adhya, S., Johnson, G., Herbert, J., Jaggi, H., Babb, J. S., Grossman, R. I. & Inglese, M. (2006) Pattern of hemodynamic impairment in multiple sclerosis: Dynamic susceptibility contrast perfusion MR imaging at 3.0 T. *Neuroimage*, 33(4), 1029-1035.

Ahlgren, C., Oden, A. & Lycke, J. (2011) High nationwide prevalence of multiple sclerosis in Sweden. *Multiple Sclerosis Journal*, 17(8), 901-908.

Ahlgren, C., Oden, A. & Lycke, J. (2012) A nationwide survey of the prevalence of multiple sclerosis in immigrant populations of Sweden. *Multiple Sclerosis Journal*, 18(8), 1099-1107.

Al-Radaideh, A. M., Wharton, S. J., Lim, S. Y., Tench, C. R., Morgan, P. S., Bowtell, R. W., Constantinescu, C. S. & Gowland, P. A. (2013) Increased iron accumulation occurs in the earliest stages of demyelinating disease: an ultra-high field susceptibility mapping study in Clinically Isolated Syndrome. *Multiple Sclerosis Journal*, 19(7), 896-903.

Aranow, C. (2011) Vitamin D and the Immune System. *Journal of Investigative Medicine*, 59(6), 881-886.

Arichika, S., Uji, A., Hangai, M., Ooto, S. & Yoshimura, N. (2013) Noninvasive and Direct Monitoring of Erythrocyte Aggregates in Human Retinal Microvasculature Using Adaptive Optics Scanning Laser Ophthalmoscopy. *Investigative Ophthalmology & Visual Science*, 54(6), 4394-4402.

Arichika, S., Uji, A., Murakami, T., Unoki, N., Yoshitake, S., Dodo, Y., Ooto, S., Miyamoto, K. & Yoshimura, N. (2014a) Retinal Hemorheologic Characterization of Early-Stage Diabetic Retinopathy Using Adaptive Optics Scanning Laser Ophthalmoscopy. *Investigative Ophthalmology & Visual Science*, 55(12), 8513-8522.

Arichika, S., Uji, A., Ooto, S., Miyamoto, K. & Yoshimura, N. (2014b) Adaptive Optics-Assisted Identification of Preferential Erythrocyte Aggregate Pathways in the Human Retinal Microvasculature. *Plos One*, 9(2), 7.

Arnold, A. C. (2005) Evolving management of optic neuritis and multiple sclerosis. *American Journal of Ophthalmology*, 139(6), 1101-1108.

Ascherio, A. & Munger, K. L. (2007) Environmental risk factors for multiple sclerosis. Part I: The role of infection. *Annals of Neurology*, 61(4), 288-299.

Avila, C. P., Bartsch, D. U., Bitner, D. G., Cheng, L. Y., Mueller, A. J., Karavellas, M. P. & Freeman, W. R. (1998) Retinal blood flow measurements in branch retinal vein occlusion

using scanning laser Doppler flowmetry. *American Journal of Ophthalmology*, 126(5), 683-690.

Bagert, B. A., Marder, E. & Stüve, O. (2011) Chronic Cerebrospinal Venous Insufficiency and Multiple Sclerosis. *Archives of Neurology*, 68(11), 1379-1384.

Baleanu, D., Ritt, M., Harazny, J., Heckmann, J., Schmieder, R. E. & Michelson, G. (2009) Wall-to-Lumen Ratio of Retinal Arterioles and Arteriole-to-Venule Ratio of Retinal Vessels in Patients with Cerebrovascular Damage. *Investigative Ophthalmology & Visual Science*, 50(9), 4351-4359.

Balfour, H. H., Sifakis, F., Sliman, J. A., Knight, J. A., Schmeling, D. O. & Thomas, W. (2013) Age-Specific Prevalence of Epstein-Barr Virus Infection Among Individuals Aged 6-19 Years in the United States and Factors Affecting Its Acquisition. *Journal of Infectious Diseases*, 208(8), 1286-1293.

Baranzini, S. E. & Oksenberg, J. R. (2017) The Genetics of Multiple Sclerosis: From 0 to 200 in 50 Years. *Trends in Genetics*, 33(12), 960-970.

Baskurt, O. K. & Meiselman, H. J. (2013) Erythrocyte aggregation: Basic aspects and clinical importance. *Clinical Hemorheology and Microcirculation*, 53(1-2), 23-37.

Baumbach, G. L. & Heistad, D. D. (1989) Remodeling of cerebral arterioles in chronic hypertension. *Hypertension*, 13(6), 968-972.

Bedggood, P. & Metha, A. (2012) Direct visualization and characterization of erythrocyte flow in human retinal capillaries. *Biomedical Optics Express*, 3(12), 14.

Behbehani, R., Abu Al-Hassan, A., Al-Salahat, A., Sriraman, D., Oakley, J. D. & Alroughani, R. (2017) Optical coherence tomography segmentation analysis in relapsing remitting versus progressive multiple sclerosis. *Plos One*, 12(2).

Bermel, R. A., Puli, S. R., Rudick, R. A., Weinstock-Guttman, B., Fisher, E., Munschauer, F. E. & Bakshi, R. (2005) Prediction of longitudinal brain atrophy in multiple sclerosis by gray matter magnetic resonance imaging T2 hypointensity. *Archives of Neurology*, 62(9), 1371-1376.

Bhaduri, B., Nolan, R. M., Shelton, R. L., Pilutti, L. A., Motl, R. W., Moss, H. E., Pula, J. H. & Boppart, S. A. (2016) Detection of retinal blood vessel changes in multiple sclerosis with optical coherence tomography. *Biomedical Optics Express*, 7(6), 2321-2330.

Bhanushali, D., Anegondi, N., Gadde, S. G. K., Srinivasan, P., Chidambara, L., Yadav, N. K. & Roy, A. S. (2016) Linking Retinal Microvasculature Features With Severity of Diabetic Retinopathy Using Optical Coherence Tomography Angiography. *Investigative Ophthalmology & Visual Science*, 57(9), OCT519-OCT525.

Bishop, J. J., Nance, P. R., Popel, A. S., Intaglietta, M. & Johnson, P. C. (2001) Effect of erythrocyte aggregation on velocity profiles in venules. *American Journal of Physiology-Heart and Circulatory Physiology*, 280(1), H222-H236.

Blumenthal, E. Z., Parikh, R. S., Pe'er, J., Naik, M., Kaliner, E., Cohen, M. J., Prabakaran, S., Kogan, M. & Thomas, R. (2009) Retinal nerve fibre layer imaging compared with histological measurements in a human eye. *Eye*, 23(1), 171-175.

Bornstein, M. B., Miller, A., Slagle, S., Weitzman, M., Drexler, E., Keilson, M., Spada, V., Weiss, W., Appel, S., Rolak, L., Harati, Y., Brown, S., Arnon, R., Jacobsohn, I., Teitelbaum, D. & Sela, M. (1991) A placebo-controlled, double-blind, randomized, two-center, pilot trial of Cop 1 in chronic progressive multiple sclerosis. *Neurology*, 41(4), 533-539.

Brar, M., Yuson, R., Kozak, I., Mojana, F., Cheng, L. Y., Bartsch, D. U., Oster, S. F. & Freeman, W. R. (2010) Correlation between morphologic features on spectral-domain optical coherence tomography and angiographic leakage patterns in macular edema. *Retina*, 30(3), 383-389.

Brass, S. D., Benedict, R. H. B., Weinstock-Guttman, B., Munschauer, F. & Bakshi, R. (2006) Cognitive impairment is associated with subcortical magnetic resonance imaging grey matter T2 hypointensity in multiple sclerosis. *Multiple Sclerosis Journal*, 12(4), 437-444.

Brex, P. A., Ciccarelli, O., O'Riordan, J. I., Sailer, M., Thompson, A. J. & Miller, D. H. (2002) A longitudinal study of abnormalities on MRI and disability from multiple sclerosis. *New England Journal of Medicine*, 346(3), 158-164.

Brunetti, A., Ricchieri, G. L., Patrassi, G. M., Girolami, A. & Tavolato, B. (1981) Rheological and fibrinolytic findings in multiple sclerosis. *Journal of Neurology Neurosurgery and Psychiatry*, 44(4), 340-343.

Bude, R. O. & Rubin, J. M. (1999) Relationship between the resistive index and vascular compliance and resistance. *Radiology*, 211(2), 411-417.

Burns, S. A., Elsner, A. E., Chui, T. Y., Vannasdale, D. A., Jr., Clark, C. A., Gast, T. J., Malinovsky, V. E. & Phan, A. D. (2014) In vivo adaptive optics microvascular imaging in diabetic patients without clinically severe diabetic retinopathy. *Biomed Opt Express*, 5(3), 961-74.

Button, J., Al-Louzi, O., Lang, A., Bhargava, P., Newsome, S. D., Frohman, T., Balcer, L. J., Frohman, E. M., Prince, J., Calabresi, P. A. & Saidha, S. (2017) Disease-modifying therapies modulate retinal atrophy in multiple sclerosis A retrospective study. *Neurology*, 88(6), 525-532.

Byrne, S. N. & Halliday, G. M. (2005) B cells activated in lymph nodes in response to ultraviolet irradiation or by interleukin-10 inhibit dendritic cell induction of immunity. *Journal of Investigative Dermatology*, 124(3), 570-578.

Campbell, J. P., Zhang, M., Hwang, T. S., Bailey, S. T., Wilson, D. J., Jia, Y. & Huang, D. (2017) Detailed Vascular Anatomy of the Human Retina by Projection-Resolved Optical Coherence Tomography Angiography. *Scientific Reports*, 7.

Charcot, J. M. (1868) Histologie de la sclérose en plaques. *Gazette des Hôpitaux Civils et Militaires*.

Chataway, J., Schuerer, N., Alsanousi, A., Chan, D., MacManus, D., Hunter, K., Anderson, V., Bangham, C. R. M., Clegg, S., Nielsen, C., Fox, N. C., Wilkie, D., Nicholas, J. M., Calder, V. L., Greenwood, J., Frost, C. & Nicholas, R. (2014) Effect of high-dose simvastatin on brain atrophy and disability in secondary progressive multiple sclerosis (MS-STAT): a randomised, placebo-controlled, phase 2 trial. *Lancet*, 383(9936), 2213-2221.

Christensen, S., Farkas, D. K., Pedersen, L., Miret, M., Christiansen, C. F. & Sorensen, H. T. (2012) Multiple Sclerosis and Risk of Venous Thromboembolism: A Population-Based Cohort Study. *Neuroepidemiology*, 38(2), 76-83.

Christian, K., Barash, H., Izhaky, D., Burgansky-Eliash, Z., Nelson, D. A., Barak, A., Lowenstein, A. & Grinvald, A. (2010) High Reproducibility of Retinal Blood Flow Velocity Measurements Using the Retinal Function Imager. *Investigative Ophthalmology & Visual Science*, 51(13).

Chui, J., Herkes, G. K. & Chang, A. (2013) Management of Fingolimod-Associated Macular Edema. *Jama Ophthalmology*, 131(5), 694-696.

Chui, T. Y. P., Pinhas, A., Gan, A., Razeen, M., Shah, N., Cheang, E., Liu, C. L., Dubra, A. & Rosen, R. B. (2016) Longitudinal imaging of microvascular remodelling in proliferative diabetic retinopathy using adaptive optics scanning light ophthalmoscopy. *Ophthalmic and Physiological Optics*, 36(3), 290-302.

Chui, T. Y. P., VanNasdale, D. A. & Burns, S. A. (2012) The use of forward scatter to improve retinal vascular imaging with an adaptive optics scanning laser ophthalmoscope. *Biomedical Optics Express*, 3(10), 2537-2549.

Cogan, D. G. & Kuwabara, T. (1984) Comparison of retinal and cerebral vasculature in trypsin digest preparations. *British Journal of Ophthalmology*, 68(1), 10-12.

Compston, A. & Coles, A. (2002) Multiple sclerosis (vol 359, pg 1221, 2002). *Lancet*, 360(9333), 648-648.

Cooper, R. F., Langlo, C. S., Dubra, A. & Carroll, J. (2013) Automatic detection of modal spacing (Yellott's ring) in adaptive optics scanning light ophthalmoscope images. *Ophthalmic and Physiological Optics*, 33(4), 540-549.

Costello, F. & Burton, J. M. (2018) Retinal imaging with optical coherence tomography: a biomarker in multiple sclerosis? *Eye and Brain*, 10, 47-63.

Craelius, W., Migdal, M. W., Luessenhop, C. P., Sugar, A. & Mihalakis, I. (1982) Iron deposits surrounding multiple sclerosis plaques. *Archives of Pathology & Laboratory Medicine*, 106(8), 397-399.

Cummins, E. P., Berra, E., Comerford, K. M., Ginouves, A., Fitzgerald, K. T., Seeballuck, F., Godson, C., Nielsen, J. E., Moynagh, P., Pouyssegur, J. & Taylor, C. T. (2006) Prolyl hydroxylase-1 negatively regulates I kappa B kinase-beta, giving insight into hypoxia-induced NF kappa B activity. *Proceedings of the National Academy of Sciences of the United States of America*, 103(48), 18154-18159.

D'Haeseleer, M., Beelen, R., Fierens, Y., Cambron, M., Vanbinst, A. M., Verborgh, C., Demey, J. & De Keyser, J. (2013) Cerebral hypoperfusion in multiple sclerosis is reversible and mediated by endothelin-1. *Proceedings of the National Academy of Sciences of the United States of America*, 110(14), 5654-5658.

Dacey, D. M. (1993) The mosaic of midget ganglion cells in the human retina. *Journal of Neuroscience*, 13(12), 5334-5355.

Dagan, A., Gringouz, I., Kliers, I. & Segal, G. (2016) Disability Progression in Multiple Sclerosis Is Affected by the Emergence of Comorbid Arterial Hypertension. *Journal of Clinical Neurology*, 12(3), 345-350.

Dawson, J. W. (1916) The Histology of Disseminated Sclerosis. *Edinburgh Medical Journal*, 17(4), 229-241.

de Castro, A., Huang, G., Sawides, L., Luo, T. & Burns, S. A. (2016) Rapid high resolution imaging with a dual-channel scanning technique. *Optics Letters*, 41(8), 1881-1884.

Desai, R. A., Davies, A. L., Del Rossi, N., Tachrount, M., Dyson, A., Gustavson, B., Kaynezhad, P., Mackenzie, L., van der Putten, M. A., McElroy, D., Schiza, D., Linington, C., Singer, M., Harvey, A. R., Tachtsidis, I., Golay, X. & Smith, K. J. (2020) Nimodipine Reduces Dysfunction and Demyelination in Models of Multiple Sclerosis. *Annals of Neurology*, 88(1), 123-136.

Desai, R. A., Davies, A. L., Tachrount, M., Kasti, M., Laulund, F., Golay, X. & Smith, K. J. (2016) Cause and prevention of demyelination in a model multiple sclerosis lesion. *Annals of Neurology*, 79(4), 591-604.

Detre, J. A. & Wang, J. J. (2002) Technical aspects and utility of fMRI using BOLD and ASL. *Clinical Neurophysiology*, 113(5), 621-634.

Dimitrova, G. & Kato, S. (2010) Color Doppler Imaging of Retinal Diseases. *Survey of Ophthalmology*, 55(3), 193-214.

Dubis, A. (2012) *Characterising Foveal Morphology in the Normal and Diseased Retina*. Doctor of Philosophy. Medical College of Wisconsin.

Dubow, M., Pinhas, A., Shah, N., Cooper, R. F., Gan, A., Gentile, R. C., Hendrix, V., Sulai, Y. N., Carroll, J., Chui, T. Y. P., Walsh, J. B., Weitz, R., Dubra, A. & Rosen, R. B. (2014) Classification of Human Retinal Microaneurysms Using Adaptive Optics Scanning Light Ophthalmoscope Fluorescein Angiography. *Investigative Ophthalmology & Visual Science*, 55(3), 1299-1309.

Dubra, A. & Sulai, Y. (2011) Reflective afocal broadband adaptive optics scanning ophthalmoscope. *Biomedical Optics Express*, 2(6), 1757-1768.

Dutta, R., McDonough, J., Yin, X. G., Peterson, J., Chang, A., Torres, T., Gudz, T., Macklin, E. B., Lewis, D. A., Fox, R. J., Rudick, R., Mirnics, K. & Trapp, B. D. (2006) Mitochondrial dysfunction as a cause of axonal degeneration in multiple sclerosis patients. *Annals of Neurology*, 59(3), 478-489.

Dutta, R. & Trapp, B. D. (2011) Mechanisms of neuronal dysfunction and degeneration in multiple sclerosis. *Progress in Neurobiology*, 93(1), 1-12.

Einarsdottir, A. B., Olafsdottir, O. B., Hjaltason, H. & Hardarson, S. H. (2018) Retinal oximetry is affected in multiple sclerosis. *Acta Ophthalmologica*, 96(5), 528-530.

Eliasdottir, T. S., Bragason, D., Hardarson, S. H., Vacchiano, C., Gislason, T., Kristjansdottir, J. V., Kristjansdottir, G. & Stefansson, E. (2017) Retinal oximetry measures systemic hypoxia in central nervous system vessels in chronic obstructive pulmonary disease. *Plos One*, 12(3).

Elovaara, I., Ukkonen, M., Leppakynnas, M., Lehtimaki, T., Luomala, M., Peltola, J. & Dastidar, P. (2000) Adhesion molecules in multiple sclerosis - Relation to subtypes of disease methylprednisolone therapy. *Archives of Neurology*, 57(4), 546-551.

Elsayed, M., Mura, M., Al Dhibi, H., Schellini, S., Malik, R., Kozak, I. & Schatz, P. (2019) Sickle cell retinopathy. A focused review. *Graefes Archive for Clinical and Experimental Ophthalmology*, 257(7), 1353-1364.

Fairless, R., Williams, S. K., Hoffmann, D. B., Stojic, A., Hochmeister, S., Schmitz, F., Storch, M. K. & Diem, R. (2012) Preclinical Retinal Neurodegeneration in a Model of Multiple Sclerosis. *Journal of Neuroscience*, 32(16), 5585-5597.

Falsini, B., Riva, C. E. & Logean, E. (2002) Flicker-evoked changes in human optic nerve blood flow: Relationship with retinal neural activity. *Investigative Ophthalmology & Visual Science*, 43(7), 2309-2316.

Feucht, N., Maier, M., Lepennetier, G., Pettenkofer, M., Wetzlmair, C., Daltrozzo, T., Scherm, P., Zimmer, C., Hoshi, M. M., Hemmer, B., Korn, T. & Knier, B. (2019) Optical coherence tomography angiography indicates associations of the retinal vascular network and disease activity in multiple sclerosis. *Multiple Sclerosis Journal*, 25(2), 224-234.

Filippi, M., Rocca, M. A., Martino, G., Horsfield, M. A. & Comi, G. (1998) Magnetization transfer changes in the normal appearing white matter precede the appearance of enhancing lesions in patients with multiple sclerosis. *Annals of Neurology*, 43(6), 809-814.

Fisher, J. B., Jacobs, D. A., Markowitz, C. E., Galetta, S. L., Volpe, N. J., Nano-Schiavi, M. L., Baier, M. L., Frohman, E. M., Winslow, H., Frohman, T. C., Calabresi, P. A., Maguire, M. G., Cutter, G. R. & Balcer, L. J. (2006) Relation of visual function to retinal nerve fiber layer thickness in multiple sclerosis. *Ophthalmology*, 113(2), 324-332.

Fortuno, A., San Jose, G., Moreno, M. U., Diez, J. & Zalba, G. (2005) Oxidative stress and vascular remodelling. *Experimental Physiology*, 90(4), 457-462.

Frank, R. N., Turczyn, T. J. & Das, A. (1990) Pericyte coverage of retinal and cerebral capillaries. *Investigative Ophthalmology & Visual Science*, 31(6), 999-1007.

Freedman, M. S., Bar-Or, A., Oger, J., Traboulsee, A., Patry, D., Young, C., Olsson, T., Li, D., Hartung, H. P., Krantz, M., Ferenczi, L., Verco, T. & Investigators, M.-. (2011) A phase III study evaluating the efficacy and safety of MBP8298 in secondary progressive MS. *Neurology*, 77(16), 1551-1560.

Frischer, J. M., Bramow, S., Dal-Bianco, A., Lucchinetti, C. F., Rauschka, H., Schmidbauer, M., Laursen, H., Sorensen, P. S. & Lassmann, H. (2009) The relation between inflammation and neurodegeneration in multiple sclerosis brains. *Brain*, 132, 1175-1189.

Fuchsjager-Mayrl, G., Polak, K., Luksch, A., Polska, E., Dorner, G. T., Rainer, G., Eichler, H. G. & Schmetterer, L. (2001) Retinal blood flow and systemic blood pressure in health young subjects. *Graefes Archive for Clinical and Experimental Ophthalmology*, 239(9), 673-677.

Fuchsjager-Mayrl, G., Wally, B., Georgopoulos, M., Rainer, G., Kircher, K., Buehl, W., Amoako-Mensah, T., Eichler, H. G., Vass, C. & Schmetterer, L. (2004) Ocular blood flow and systemic blood pressure in patients with primary open-angle glaucoma and ocular hypertension. *Investigative Ophthalmology & Visual Science*, 45(3), 834-839.

Gaitan, M. I., de Alwis, M. P., Sati, P., Nair, G. & Reich, D. S. (2013) Multiple sclerosis shrinks intralesional, and enlarges extralesional, brain parenchymal veins. *Neurology*, 80(2), 145-151.

Gale, C. R. & Martyn, C. N. (1995) Migrant studies in multiple sclerosis. *Progress in Neurobiology*, 47(4-5), 425-448.

Garvin, M. K., Abramoff, M. D., Wu, X. D., Russell, S. R., Burns, T. L. & Sonka, M. (2009) Automated 3-D Intraretinal Layer Segmentation of Macular Spectral-Domain Optical Coherence Tomography Images. *Ieee Transactions on Medical Imaging*, 28(9), 1436-1447.

Geirsdottir, A., Palsson, O., Hardarson, S. H., Olafsdottir, O. B., Kristjansdottir, J. V. & Stefansson, E. (2012) Retinal Vessel Oxygen Saturation in Healthy Individuals. *Investigative Ophthalmology & Visual Science*, 53(9), 5433-5442.

Gelfand, J. M., Nolan, R., Schwartz, D. M., Graves, J. & Green, A. J. (2012) Microcystic macular oedema in multiple sclerosis is associated with disease severity. *Brain*, 135, 1786-1793.

Gill, J. S., Moosajee, M. & Dubis, A. M. (2019) Cellular imaging of inherited retinal diseases using adaptive optics. *Eye*, 33(11), 1683-1698.

Gills, J. P., Jr. & Wadsworth, J. A. (1966) Degeneration of the inner nuclear layer of the retina following lesions of the optic nerve. *Transactions of the American Ophthalmological Society*, 64, 66-88.

Gordon-Lipkin, E., Chodkowski, B., Reich, D. S., Smith, S. A., Pulicken, M., Balcer, L. J., Frohman, E. M., Cutter, G. & Calabresi, P. A. (2007) Retinal nerve fiber layer is associated with brain atrophy in multiple sclerosis. *Neurology*, 69(16), 1603-1609.

Green, A. J., McQuaid, S., Hauser, S. L., Allen, I. V. & Lyness, R. (2010) Ocular pathology in multiple sclerosis: retinal atrophy and inflammation irrespective of disease duration. *Brain*, 133(Pt 6), 1591-601.

Grinvald, A., Izhaky, D. & Nelson, D. R. (2007) Retinal Blood Flow Measurements With the Retinal Function Imager. *Investigative Ophthalmology & Visual Science*, 48(13), 3842-3842.

Groen, K., Maltby, V. E., Lea, R. A., Sanders, K. A., Fink, J. L., Scott, R. J., Tajouri, L. & Lechner-Scott, J. (2018) Erythrocyte microRNA sequencing reveals differential expression in relapsing-remitting multiple sclerosis. *Bmc Medical Genomics*, 11.

Groen, K., Maltby, V. E., Sanders, K. A., Scott, R. J., Tajouri, L. & Lechner-Scott, J. (2016) Erythrocytes in multiple sclerosis–forgotten contributors to the pathophysiology? *Multiple Sclerosis Journal–Experimental, Translational and Clinical*, 2, 2055217316649981.

Grunwald, J. E., Riva, C. E., Martin, D. B., Quint, A. R. & Epstein, P. A. (1987) Effect of an insulin-induced decrease in blood glucose on the human diabetic retinal

circulation. *Ophthalmology*, 94(12), 1614-1620.

Gu, B. Y., Wang, X. L., Twa, M. D., Tam, J., Girkin, C. A. & Zhang, Y. H. (2018) Noninvasive in vivo characterization of erythrocyte motion in human retinal capillaries using high-speed adaptive optics near-confocal imaging. *Biomedical Optics Express*, 9(8).

Guevara-Torres, A., Joseph, A. & Schallek, J. B. (2016) Label free measurement of retinal blood cell flux, velocity, hematocrit and capillary width in the living mouse eye. *Biomed Opt Express*, 7(10), 4228-4249.

Guo, Y., Yao, G., Lei, B. & Tan, J. L. (2008) Monte Carlo model for studying the effects of melanin concentrations on retina light absorption. *Journal of the Optical Society of America a-Optics Image Science and Vision*, 25(2), 304-311.

Haider, L., Zrzavy, T., Hametner, S., Hoftberger, R., Bagnato, F., Grabner, G., Trattnig, S., Pfeifenbring, S., Brueck, W. & Lassmann, H. (2016) The topograpy of demyelination and neurodegeneration in the multiple sclerosis brain. *Brain*, 139, 807-815.

Hallgren, B. & Sourander, P. (1958) THE EFFECT OF AGE ON THE NON-HAEMIN IRON IN THE HUMAN BRAIN. *Journal of Neurochemistry*, 3(1), 41-51.

Hametner, S., Wimmer, I., Haider, L., Pfeifenbring, S., Bruck, W. & Lassmann, H. (2013) Iron and Neurodegeneration in the Multiple Sclerosis Brain. *Annals of Neurology*, 74(6), 848-861.

Hammond, S. R., English, D. R. & McLeod, J. G. (2000) The age-range of risk of developing multiple sclerosis - Evidence from a migrant population in Australia. *Brain*, 123, 968-974.

Harazny, J. M., Ritt, M., Baleanu, D., Ott, C., Heckmann, J., Schlaich, M. P., Michelson, G. & Schmieder, R. E. (2007) Increased wall: Lumen ratio of retinal arterioles in male patients with a history of a cerebrovascular event. *Hypertension*, 50(4), 623-629.

Harris, A., Kagemann, L. & Cioffi, G. A. (1998) Assessment of human ocular hemodynamics. *Survey of Ophthalmology*, 42(6), 509-533.

Hartung, H. P., Gonsette, R., Konig, N., Kwiecinski, H., Guseo, A., Morrissey, S. P., Krapf, H., Zwingers, T. & Mims (2002) Mitoxantrone in progressive multiple sclerosis: a placebo-controlled, double-blind, randomised, multicentre trial. *Lancet*, 360(9350), 2018-2025.

Haufschild, T., Shaw, S. G., Kesselring, J. & Flammer, J. (2001) Increased endothelin-1 plasma levels in patients with multiple sclerosis. *Journal of Neuro-Ophthalmology*, 21(1), 37-38.

Hawkins, B. T. & Davis, T. P. (2005) The blood-brain barrier/neurovascular unit in health and disease. *Pharmacological Reviews*, 57(2), 173-185.

Hayreh, S. S. (1962) The ophthalmic artery: III. Branches. *The British journal of ophthalmology*, 46(4), 212.

Heagerty, A. M., Aalkjaer, C., Bund, S. J., Korsgaard, N. & Mulvany, M. J. (1993) Small artery structure in hypertension. Dual processes of remodeling and growth. *Hypertension*, 21(4), 391-397.

Hebel, R. & Hollander, H. (1983) Size and distribution of ganglion cells in the human retina. *Anatomy and Embryology*, 168(1), 125-136.

Herman, I. M. & Damore, P. A. (1985) Microvascular pericytes contain muscle and nonmuscle actins. *Journal of Cell Biology*, 101(1), 43-52.

Hermann, B., Fernandez, E. J., Unterhuber, A., Sattmann, H., Fercher, A. F., Drexler, W., Prieto, P. M. & Artal, P. (2004) Adaptive-optics ultrahigh-resolution optical coherence tomography. *Optics Letters*, 29(18), 2142-2144.

Hernandez, J. C. C., Bracko, O., Kersbergen, C. J., Muse, V., Haft-Javaherian, M., Berg, M., Park, L., Vinarcsik, L. K., Ivasyk, I., Rivera, D. A., Kang, Y. M., Cortes-Canteli, M., Peyrounette, M., Doyeux, V., Smith, A., Zhou, J., Otte, G., Beverly, J. D., Davenport, E., Davit, Y., Lin, C. P., Strickland, S., Iadecola, C., Lorthois, S., Nishimura, N. & Schaffer, C. B. (2019) Neutrophil adhesion in brain capillaries reduces cortical blood flow and impairs memory function in Alzheimer's disease mouse models. *Nature Neuroscience*, 22(3), 413-+.

Herndon, R. M. (2002) Medical hypothesis - Why secondary progressive multiple sclerosis is a relentlessly progressive illness. *Archives of Neurology*, 59(2), 301-304.

Higashiyama, T., Nishida, Y. & Ohji, M. (2017) Optical coherence tomography angiography in eyes with good visual acuity recovery after treatment for optic neuritis. *PloS ONE*, 12(2).

Hillard, J. G., Gast, T. J., Chui, T. Y. P., Sapir, D. & Burns, S. A. (2016) Retinal Arterioles in Hypo-, Normo-, and Hypertensive Subjects Measured Using Adaptive Optics. *Translational Vision Science & Technology*, 5(4).

Hobom, M., Storch, M. K., Weisser, R., Maier, K., Radhakrishnan, A., Kramer, B., Bahr, M. & Diem, R. (2004) Mechanisms and time course of neuronal degeneration in experimental autoimmune encephalomyelitis. *Brain Pathology*, 14(2), 148-157.

Hogan, M. J. & Feeney, L. (1963) The ultrastructure of the retinal vessels: II. The small vessels. *Journal of ultrastructure research*, 9(1-2), 29-46.

Holland, N., Burks, J. & Schneider, D. (2010) *Primary Progressive Multiple Sclerosis: What You Need to Know.*The National Multiple Sclerosis Society.

Hon, G. M., Hassan, M. S., van Rensburg, S. J., Erasmus, R. T., Abel, S. & Matsha, T. E. (2011) The Haematological Profile of Patients with Multiple Sclerosis. *Journal of Neurochemistry*, 118, 147-147.

Hong, Y., Tang, H. R., Ma, M., Chen, N., Xie, X. & He, L. (2019) Multiple sclerosis and stroke: a systematic review and meta-analysis. *BMC Neurology*, 19.

Horstmann, L., Schmid, H., Heinen, A. P., Kurschus, F. C., Dick, H. B. & Joachim, S. C. (2013) Inflammatory demyelination induces glia alterations and ganglion cell loss in the retina of an experimental autoimmune encephalomyelitis model. *Journal of Neuroinflammation*, 10.

Hu, D. N., Simon, J. D. & Sarna, T. (2008) Role of ocular melanin in ophthalmic physiology and pathology. *Photochemistry and Photobiology*, 84(3), 639-644.

Iftikhar, M., Zafar, S., Gonzalez, N., Murphy, O., Kwakyi, M. S. O., Feldman, B. S. S., Calabresi, P. A., Saidha, S. & Channa, R. (2019) Image Artifacts in Optical Coherence Tomography Angiography Among Patients With Multiple Sclerosis. *Current Eye Research*, 44(5), 558-563.

Jiang, H., Delgado, S., Tan, J., Liu, C., Rammohan, K. W., DeBuc, D. C., Lam, B. L., Feuer, W. J. & Wang, J. H. (2016) Impaired retinal microcirculation in multiple sclerosis. *Multiple Sclerosis Journal*, 22(14), 1812-1820.

Jiang, H., Gameiro, G. R., Liu, Y., Lin, Y., Hernandez, J., Deng, Y. Q., Gregori, G., Delgado, S. & Wang, J. H. (2020) Visual Function and Disability Are Associated with Increased Retinal Volumetric Vessel Density in Patients with Multiple Sclerosis. *American Journal of Ophthalmology*, 213, 34-45.

Joseph, A., Guevara-Torres, A. & Schallek, J. (2019) Imaging single-cell blood flow in the smallest to largest vessels in the living retina. *Elife*, 8.

Kahler, J., Mendel, S., Weckmuller, J., Orzechowski, H. D., Mittmann, C., Koster, R., Paul, M., Meinertz, T. & Munzel, T. (2000) Oxidative stress increases synthesis of big endothelin-1 by activation of the endothelin-1 promoter. *Journal of Molecular and Cellular Cardiology*, 32(8), 1429-1437.

Kapoor, R., Furby, J., Hayton, T., Smith, K. J., Altmann, D. R., Brenner, R., Chataway, J., Hughes, R. A. C. & Miller, D. H. (2010) Lamotrigine for neuroprotection in secondary progressive multiple sclerosis: a randomised, double-blind, placebo-controlled, parallel-group trial. *Lancet Neurology*, 9(7), 681-688.

Karami, M., Janghorbani, M., Dehghani, A., Khaksar, K. & Kaviani, A. (2012) Orbital Doppler evaluation of blood flow velocities in patients with diabetic retinopathy. *The review of diabetic studies : RDS*, 9(2-3), 104-11.

Karst, S. G., Lammer, J., Radwan, S. H., Kwak, H., Silva, P. S., Burns, S. A., Aiello, L. P. & Sun, J. K. (2018) Characterization of In Vivo Retinal Lesions of Diabetic Retinopathy Using Adaptive Optics Scanning Laser Ophthalmoscopy. *International Journal of Endocrinology*.

Kaya, D., Kaya, M., Ozakbas, S. & Idiman, E. (2014) Uveitis associated with multiple sclerosis: complications and visual prognosis. *International Journal of Ophthalmology*, 7(6), 1010-1013.

Koch, E., Rosenbaum, D., Brolly, A., Sahel, J. A., Chaumet-Riffaud, P., Girerd, X., Rossant, F. & Paques, M. (2014) Morphometric analysis of small arteries in the human retina using adaptive optics imaging: relationship with blood pressure and focal vascular changes. *Journal of Hypertension*, 32(4), 890-898.

Kochkorov, A., Gugleta, K., Kavroulaki, D., Katamay, R., Weier, K., Mehling, M., Kappos, L., Flammer, J. & Orgul, S. (2009) Rigidity of Retinal Vessels in Patients with Multiple Sclerosis. *Klinische Monatsblatter Fur Augenheilkunde*, 226(4), 276-279.

Kolb, H., Fernandez, E. & Nelson, R. (2005) The organization of the retina and visual system. *Webvision-The Organization of the Retina and Visual System*.

Koronyo, Y., Biggs, D., Barron, E., Boyer, D. S., Pearlman, J. A., Au, W. J., Kile, S. J., Blanco, A., Fuchs, D. T., Ashfaq, A., Frautschy, S., Cole, G. M., Miller, C. A., Hinton, D. R., Verdooner, S. R., Black, K. L. & Koronyo-Hamaoui, M. (2017) Retinal amyloid pathology and proof-of-concept imaging trial in Alzheimer's disease. *Jci Insight*, 2(16).

Koudriavtseva, T., Renna, R., Plantone, D., Mandoj, C., Piattella, M. C. & Giannarelli, D. (2015) Association between Anemia and Multiple Sclerosis. *European Neurology*, 73(3-4), 233-237.

Kutzelnigg, A., Lucchinetti, C. F., Stadelmann, C., Bruck, W., Rauschka, H., Bergmann, M., Schmidbauer, M., Parisi, J. E. & Lassmann, H. (2005) Cortical demyelination and diffuse white matter injury in multiple sclerosis. *Brain*, 128, 2705-2712.

Lang, H. L. E., Jacobsen, H., Ikemizu, S., Andersson, C., Harlos, K., Madsen, L., Hjorth, P., Sondergaard, L., Svejgaard, A., Wucherpfennig, K., Stuart, D. I., Bell, J. I., Jones, E. Y. & Fugger, L. (2002) A functional and structural basis for TCR cross-reactivity in multiple sclerosis. *Nature Immunology*, 3(10), 940-943.

Lanzillo, R., Cennamo, G., Criscuolo, C., Carotenuto, A., Velotti, N., Sparnelli, F., Cianflone, A., Moccia, M. & Brescia Morra, V. (2017) Optical coherence tomography angiography retinal vascular network assessment in multiple sclerosis. *Multiple sclerosis (Houndmills, Basingstoke, England)*, 1352458517729463-1352458517729463.

Lanzillo, R., Cennamo, G., Moccia, M., Criscuolo, C., Carotenuto, A., Frattaruolo, N., Sparnelli, F., Melenzane, A., Lamberti, A., Servillo, G., Tranfa, F., De Crecchio, G. & Morra, V. B. (2019) Retinal vascular density in multiple sclerosis: a 1-year follow-up. *European Journal of Neurology*, 26(1), 198-201.

Lassen, N. A. (1959) Cerebral Blood Flow and Oxygen Consumption in Man. *Physiological Reviews*, 39(2), 183-238.

Laurent, S. (1995) Arterial Wall Hypertrophy And Stiffness In Essential Hypertensive Patients. *Hypertension*, 26(2), 355-362.

Law, M., Saindane, A. M., Ge, Y. L., Babb, J. S., Johnson, G., Mannon, L. J., Herbert, J. & Grossman, R. I. (2004) Microvascular abnormality in relapsing-remitting multiple sclerosis: Perfusion MR imaging findings in normal-appearing white matter. *Radiology*, 231(3), 645-652.

Lazzarino, G., Amorini, A. M., Petzold, A., Gasperini, C., Ruggieri, S., Quartuccio, M. E., Di Stasio, E. & Tavazzi, B. (2017) Serum Compounds of Energy Metabolism Impairment Are Related to Disability, Disease Course and Neuroimaging in Multiple Sclerosis. *Molecular Neurobiology*, 54(9), 7520-7533.

Lesage, S. R., Mosley, T. H., Wong, T. Y., Szklo, M., Knopman, D., Catellier, D. J., Cole, S. R., Klein, R., Coresh, J., Coker, L. H. & Sharrett, A. R. (2009) Retinal microvascular abnormalities and cognitive decline The ARIC 14-year follow-up study. *Neurology*, 73(11), 862-868.

Lewin, A., Hamilton, S., Witkover, A., Langford, P., Nicholas, R., Chataway, J. & Bangham, C. R. M. (2016) Free serum haemoglobin is associated with brain atrophy in secondary progressive multiple sclerosis. *Wellcome open research*, 1, 10-10.

Liang, J. Z., Williams, D. R. & Miller, D. T. (1997) High resolution imaging of the living human retina with adaptive optics. *Investigative Ophthalmology & Visual Science*, 38(4), 55-55.

Lightman, S., McDonald, W. I., Bird, A. C., Francis, D. A., Hoskins, A., Batchelor, J. R. & Halliday, A. M. (1987) RETINAL VENOUS SHEATHING IN OPTIC NEURITIS - ITS SIGNIFICANCE FOR THE PATHOGENESIS OF MULTIPLE-SCLEROSIS. *Brain*, 110, 405-414.

Liu, Y., Delgado, S., Jiang, H., Lin, Y., Hernandez, J., Deng, Y., Gameiro, G. R. & Wang, J. (2019) Retinal Tissue Perfusion in Patients with Multiple Sclerosis. *Current eye research*, 1-7.

Ljubisavljevic, S., Stojanovic, I., Cvetkovic, T., Vojinovic, S., Stojanov, D., Stojanovic, D., Stefanovic, N. & Pavlovic, D. (2014) Erythrocytes' antioxidative capacity as a potential marker of oxidative stress intensity in neuroinflammation. *Journal of the Neurological Sciences*, 337(1-2), 8-13.

Lu, F. M., Selak, M., O'Connor, J., Croul, S., Lorenzana, C., Butunoi, C. & Kalman, B. (2000) Oxidative damage to mitochondrial DNA and activity of mitochondrial enzymes in chronic active lesions of multiple sclerosis. *Journal of the Neurological Sciences*, 177(2), 95-103.

Lublin, F. D., Reingold, S. C., Cohen, J. A., Cutter, G. R., Sorensen, P. S., Thompson, A. J., Wolinsky, J. S., Balcer, L. J., Banwell, B., Barkhof, F., Bebo, B., Calabresi, P. A., Clanet, M., Comi, G., Fox, R. J., Freedman, M. S., Goodman, A. D., Inglese, M., Kappos, L., Kieseier, B. C., Lincoln, J. A., Lubetzki, C., Miller, A. E., Montalban, X., O'Connor, P. W., Petkau, J., Pozzilli, C., Rudick, R. A., Sormani, M. P., Stuve, O., Waubant, E. & Polman, C. H. (2014) Defining the clinical course of multiple sclerosis The 2013 revisions. *Neurology*, 83(3), 278-286.

Lujan, B. J. & Horton, J. C. (2013) Microcysts in the inner nuclear layer from optic atrophy are caused by retrograde trans-synaptic degeneration combined with vitreous traction on the retinal surface. *Brain*, 136.

Luo, X., Shen, Y. M., Jiang, M. N., Lou, X. F. & Shen, Y. (2015) Ocular Blood Flow Autoregulation Mechanisms and Methods. *Journal of Ophthalmology*.

Magliozzi, R., Howell, O., Vora, A., Serafini, B., Nicholas, R., Puopolo, M., Reynolds, R. & Aloisi, F. (2007) Meningeal B-cell follicles in secondary progressive multiple sclerosis associate with early onset of disease and severe cortical pathology. *Brain*, 130, 1089-1104.

Malpass, K. (2012) Multiple sclerosis: 'Outside-in' demyelination in MS. *Nature reviews. Neurology*, 8(2), 61-61.

Mancardi, G. L., Perdelli, F., Rivano, C., Leonardi, A. & Bugiani, O. (1980) Thickening of the basement membrane of cortical capillaries in Alzheimer's disease. *Acta Neuropathologica*, 49(1), 79-83.

Marrie, R. A., Fisk, J., Tremlett, H., Wolfson, C., Warren, S., Blanchard, J., Patten, S. B., Epidemiology, C. T. & Impac (2016) Differing trends in the incidence of vascular comorbidity in MS and the general population. *Neurology-Clinical Practice*, 6(2), 120-128.

Marrie, R. A., Rudick, R., Horwitz, R., Cutter, G., Tyry, T., Campagnolo, D. & Vollmer, T. (2010) Vascular comorbidity is associated with more rapid disability progression in multiple sclerosis. *Neurology*, 74(13), 1041-1047.

Marshall, O., Chawla, S., Lu, H. Z., Pape, L. & Ge, Y. L. (2016) Cerebral blood flow modulation insufficiency in brain networks in multiple sclerosis: A hypercapnia MRI study. *Journal of Cerebral Blood Flow and Metabolism*, 36(12), 2087-2095.

Martin, A. R., Bailie, J. R., Robson, T., McKeown, S. R., Al-Assar, O., McFarland, A. & Hirst, D. G. (2000) Retinal pericytes control expression of nitric oxide synthase and endothelin-1 in microvascular endothelial cells. *Microvascular Research*, 59(1), 131-139.

Martin, J. A., Poonja, S. & Roorda, A. (2005) Non-invasive assessment of parafoveal capillary leukocyte pulsatility. *Investigative Ophthalmology & Visual Science*, 46.

Martin, J. A. & Roorda, A. (2009) Pulsatility of parafoveal capillary leukocytes. *Experimental Eye Research*, 88(3), 356-360.

Martinez-Lapiscina, E. H., Arnow, S., Wilson, J. A., Saidha, S., Preiningerova, J. L., Oberwahrenbrock, T., Brandt, A. U., Pablo, L. E., Guerrieri, S., Gonzalez, I., Outteryck, O., Mueller, A. K., Albrecht, P., Chan, W., Lukas, S., Balk, L. J., Fraser, C., Frederiksen, J. L., Resto, J., Frohman, T., Cordano, C., Zubizarreta, I., Andorra, M., Sanchez-Dalmau, B., Saiz, A., Bermel, R., Klistorner, A., Petzold, A., Schippling, S., Costello, F., Aktas, O., Vermersch, P., Oreja-Guevara, C., Comi, G., Leocani, L., Garcia-Martin, E., Paul, F., Havrdova, E., Frohman, E., Balcer, L. J., Green, A. J., Calabresi, P. A., Villoslada, P. & Consortium, I. (2016) Retinal thickness measured with optical coherence tomography and risk of disability worsening in multiple sclerosis: a cohort study. *Lancet Neurology*, 15(6), 574-584.

Maruyoshi, H., Kojima, S., Nagayoshi, Y., Horibata, Y., Kaikita, K., Sugiyama, S. & Ogawa, H. (2010) Waveform of Ophthalmic Artery Doppler Flow Predicts the Severity of Systemic Atherosclerosis. *Circulation Journal*, 74(6), 1251-1256.

Mayet, J. & Hughes, A. (2003) Cardiac and vascular pathophysiology in hypertension. *Heart*, 89(9), 1104-1109.

McConnell, H. L., Kersch, C. N., Woltjer, R. L. & Neuwelt, E. A. (2017) The Translational Significance of the Neurovascular Unit*. *Journal of Biological Chemistry*, 292(3), 762-770.

McLeod, D. S., Goldberg, M. F. & Lutty, G. A. (1993) Dual-perspective analysis of vascular formations in sickle cell retinopathy. *Archives of Ophthalmology*, 111(9), 1234-1245.

Meadway, A., McKeown, A., Samuels, B. C. & Sincich, L. (2020) Lifecycle and lensing of a macular microcyst. *Ophthalmic research*.

Metea, M. R. & Newman, E. A. (2007) Signalling within the neurovascular unit in the mammalian retina. *Experimental Physiology*, 92(4), 635-640.

Michelson, G., Waerntges, S., Baleanu, D., Welzenbach, J., Ohno-Jinno, A., Pogorelov, P. & Harazny, J. (2007) Morphometric age-related evaluation of small retinal vessels by scanning laser Doppler flowmetry: determination of a vessel wall index. *Retina*, 27(4), 490-498.

Miller, D. T., Williams, D. R., Morris, G. M. & Liang, J. Z. (1996) Images of cone photoreceptors in the living human eye. *Vision Research*, 36(8), 1067-1079.

Mo, S., Krawitz, B., Efstathiadis, E., Geyman, L., Weitz, R., Chui, T. Y. P., Carroll, J., Dubra, A. & Rosen, R. B. (2016) Imaging Foveal Microvasculature: Optical Coherence Tomography Angiography Versus Adaptive Optics Scanning Light Ophthalmoscope Fluorescein Angiography. *Investigative Ophthalmology & Visual Science*, 57(9), OCT130-OCT140.

Modrzejewska, M., Karczewicz, D. & Wilk, G. (2007) Assessment of blood flow velocity in eyeball arteries in multiple sclerosis patients with past retrobulbar optic neuritis in color Doppler ultrasonography. *Klinika oczna*, 109(4-6), 183-6.

Mohan, A., Dabir, S., Kurian, M., Shetty, R., Chidambara, L. & Kumar, R. S. (2016) Perivascular and Quadrant Nerve Fiber Layer Thickness and Its Relationship with Oxygen Saturation. *Current Eye Research*, 41(9), 1223-1228.

Montalban, X., Hauser, S. L., Kappos, L., Arnold, D. L., Bar-Or, A., Comi, G., de Seze, J., Giovannoni, G., Hartung, H. P., Hemmer, B., Lublin, F., Rammohan, K. W., Selmaj, K., Traboulsee, A., Sauter, A., Masterman, D., Fontoura, P., Belachew, S., Garren, H., Mairon, N., Chin, P., Wolinsky, J. S. & Investigators, O. C. (2017) Ocrelizumab versus Placebo in Primary Progressive Multiple Sclerosis. *New England Journal of Medicine*, 376(3), 209-220.

Monti, L., Donati, D., Menci, E., Cioni, S., Bellini, M., Grazzini, I., Leonini, S., Galluzzi, P., Severi, S., Burroni, L., Casasco, A., Morbidelli, L., Santarnecchi, E. & Piu, P. (2015) Cerebral Circulation Time is Prolonged and Not Correlated with EDSS in Multiple Sclerosis Patients: A Study Using Digital Subtracted Angiography. *Plos One*, 10(2).

Morgan, J. I. W., Han, G., Klinman, E., Maguire, W. M., Chung, D. C., Maguire, A. M. & Bennett, J. (2014) High-Resolution Adaptive Optics Retinal Imaging of Cellular Structure in Choroideremia. *Investigative Ophthalmology & Visual Science*, 55(10), 6381-6397.

Mulvany, M. J. (2012) Small Artery Remodelling in Hypertension. *Basic & Clinical Pharmacology & Toxicology*, 110(1), 49-55.

Munger, K. L., Levin, L. I., Hollis, B. W., Howard, N. S. & Ascherio, A. (2006) Serum 25-hydroxyvitamin D levels and risk of multiple sclerosis. *Jama-Journal of the American Medical Association*, 296(23), 2832-2838.

Muoio, V., Persson, P. B. & Sendeski, M. M. (2014) The neurovascular unit - concept review. *Acta Physiologica*, 210(4), 790-798.

Murphy, O. C., Kwakyi, O., Iftikhar, M., Zafar, S., Lambe, J., Pellegrini, N., Sotirchos, E. S., Gonzalez-Caldito, N., Ogbuokiri, E., Filippatou, A., Risher, H., Cowley, N., Feldman, S., Fioravante, N., Frohman, E. M., Frohman, T. C., Balcer, L. J., Prince, J. L., Channa, R., Calabresi, P. A. & Saidha, S. (2019) Alterations in the retinal vasculature occur in multiple sclerosis and exhibit novel correlations with disability and visual function measures. *Multiple sclerosis (Houndmills, Basingstoke, England)*, 1352458519845116-1352458519845116.

Murray, C. D. (1926) The Physiological Principle of Minimum Work: I. The Vascular System and The Cost of Blood Volume. *Proceedings of the National Academy of Sciences of the United States of America*, 12, 207-214.

Mwanza, J. C., Oakley, J. D., Budenz, D. L., Chang, R. T., Knight, O. J. & Feuer, W. J. (2011) Macular Ganglion Cell-Inner Plexiform Layer: Automated Detection and Thickness Reproducibility with Spectral Domain-Optical Coherence Tomography in Glaucoma. *Investigative Ophthalmology & Visual Science*, 52(11), 8323-8329.

Nakano, Y., Shimazaki, T., Kobayashi, N., Miyoshi, Y., Ono, A., Kobayashi, M., Shiragami, C., Hirooka, K. & Tsujikawa, A. (2016) Retinal Oximetry in a Healthy Japanese Population. *Plos One*, 11(7).

NICE (2020) *Disease-modifying therapies for multiple sclerosis.*

Nichols, W. W., Orourke, M. F. & Vlachopoulos, C. (2011) McDonald's Blood Flow in Arteries: Theoretical, Experimental and Clinical Principles, 6th Edition. *Mcdonald's Blood Flow in Arteries: Theoretical, Experimental and Clinical Principles, 6th Edition*, 1-741.

Nitta, E., Hirooka, K., Shimazaki, T., Sato, S., Ukegawa, K., Nakano, Y. & Tsujikawa, A. (2017) Retinal oxygen saturation before and after glaucoma surgery. *Acta Ophthalmologica*, 95(5), E350-E353.

Nolan, R., Gelfand, J. M. & Green, A. J. (2013) Fingolimod treatment in multiple sclerosis leads to increased macular volume. *Neurology*, 80(2), 139-144.

Noseworthy, J. H. (1991) The Canadian cooperative trial of cyclophosphamide and plasma-exchange in progressive multiple sclerosis. *Lancet*, 337(8739), 441-446.

Ortiz-Perez, S., Martinez-Lapiscina, E. H., Gabilondo, I., Fraga-Pumar, E., Martinez-Heras, E., Saiz, A., Sanchez-Dalmau, B. & Villoslada, P. (2013) Retinal periphlebitis is associated with multiple sclerosis severity. *Neurology*, 81(10), 877-881.

Pache, M., Kaiser, H. J., Akhalbedashvili, N., Lienert, C., Dubler, B., Kappos, L. & Flammer, J. (2003) Extraocular blood flow and endothelin-1 plasma levels in patients with multiple sclerosis. *European Neurology*, 49(3), 164-168.

Paling, D., Petersen, E. T., Tozer, D. J., Altmann, D. R., Wheeler-Kingshott, C. A., Kapoor, R., Miller, D. H. & Golay, X. (2014) Cerebral arterial bolus arrival time is prolonged in multiple sclerosis and associated with disability. *Journal of Cerebral Blood Flow and Metabolism*, 34(1), 34-42.

Palochak, C. M. A., Lee, H. E., Song, J., Geng, A., Linsenmeier, R. A., Burns, S. A. & Fawzi, A. A. (2019) Retinal Blood Velocity and Flow in Early Diabetes and Diabetic Retinopathy Using Adaptive Optics Scanning Laser Ophthalmoscopy. *Journal of clinical medicine*, 8(8).

Palsson, O., Geirsdottir, A., Hardarson, S. H., Olafsdottir, O. B., Kristjansdottir, J. V. & Stefansson, E. (2012) Retinal Oximetry Images Must Be Standardized: A Methodological Analysis. *Investigative Ophthalmology & Visual Science*, 53(4), 1729-1733.

Park, J. B. & Schiffrin, E. L. (2001) Small artery remodeling is the most prevalent (earliest?) form of target organ damage in mild essential hypertension. *Journal of Hypertension*, 19(5), 921-930.

Patton, N., Pattie, A., MacGillivray, T., Aslam, T., Dhillon, B., Gow, A., Starr, J. M., Whalley, L. J. & Deary, I. J. (2007) The association between retinal vascular network geometry and cognitive ability in an elderly population. *Investigative Ophthalmology & Visual Science*, 48(5), 1995-2000.

Paul, J. P., O'Connell, R. A., Hosking, S. L., Anderson, A. J. & Bui, B. V. (2013) Retinal Oxygen Saturation: Novel Analysis Method for the Oxymap. *Optometry and Vision Science*, 90(10), 1104-1110.

Pearce, J. M. S. (2005) Historical descriptions of multiple sclerosis - The stories of Augustus D'Este and The Journal of a Disappointed Man. *European Neurology*, 54(1), 49-53.

Penman, A., Talbot, J. F., Chuang, E. L., Bird, A. C. & Serjeant, G. R. (1994) Peripheral retinal vasculature in normal Jamaican children. *British Journal of Ophthalmology*, 78(8), 615-617.

Pereira, I., Weber, S., Holzer, S., Resch, H., Kiss, B., Fischer, G. & Vass, C. (2014) Correlation between retinal vessel density profile and circumpapillary RNFL thickness measured with

Fourier-domain optical coherence tomography. *British Journal of Ophthalmology*, 98(4), 538-543.

Petcharunpaisan, S., Ramalho, J. & Castillo, M. (2010) Arterial spin labeling in neuroimaging. *World Journal of Radiology*, 2(10), 384-98.

Petzold, A., de Boer, J. F., Schippling, S., Vermersch, P., Kardon, R., Green, A., Calabresi, P. A. & Polman, C. (2010) Optical coherence tomography in multiple sclerosis: a systematic review and meta-analysis. *Lancet Neurology*, 9(9), 921-932.

Plumb, J., McQuaid, S., Mirakhur, M. & Kirk, J. (2002) Abnormal endothelial tight junctions in active lesions and normal-appearing white matter in multiple sclerosis. *Brain Pathology*, 12(2), 154-169.

Polidoro, G., Diilio, C., Arduini, A., Larovere, G. & Federici, G. (1984) Superoxide dismutase, reduced glutathione and TBA-reactive products in erythrocytes of

patients with multiple sclerosis. *International Journal of Biochemistry*, 16(5), 505-9.

Pollock, S., Harrison, M. J. G. & Oconnell, G. (1982) Erythrocyte deformability in multiple sclerosis. *Journal of Neurology Neurosurgery and Psychiatry*, 45(8), 762-762.

Prat, A., Biernacki, K., Lavoie, J. F., Poirier, J., Duquette, P. & Antel, J. P. (2002) Migration of multiple sclerosis lymphocytes through brain endothelium. *Archives of Neurology*, 59(3), 391-397.

Prineas, J. W., Kwon, E. E., Cho, E. S., Sharer, L. R., Barnett, M. H., Oleszak, E. L., Hoffman, B. & Morgan, B. P. (2001) Immunopathology of secondary-progressive multiple sclerosis. *Annals of Neurology*, 50(5), 646-657.

Prineas, J. W. & Wright, R. G. (1978) Macrophages, lymphocytes, and plasma-cells in the perivascular compartment in chronic multiple sclerosis. *Laboratory Investigation*, 38(4), 409-421.

Rashid, W., Parkes, L. M., Ingle, G. T., Chard, D. T., Toosy, A. T., Altmann, D. R., Symms, M. R., Tofts, P. S., Thompson, A. J. & Miller, D. H. (2004) Abnormalities of cerebral perfusion in multiple sclerosis. *Journal of Neurology Neurosurgery and Psychiatry*, 75(9), 1288-1293.

Renna, N. F., de Las Heras, N. & Miatello, R. M. (2013) Pathophysiology of vascular remodeling in hypertension. *International journal of hypertension*, 2013, 808353-808353.

Richardson, R., Tracey-White, D., Webster, A. & Moosajee, M. (2017) The zebrafish eye-a paradigm for investigating human ocular genetics. *Eye*, 31(1), 68-86.

Ritt, M. & Schmieder, R. E. (2009) Wall-to-Lumen Ratio of Retinal Arterioles as a Tool to Assess Vascular Changes. *Hypertension*, 54(2), 384-387.

Rizzoni, D., Porteri, E., Castellano, M., Bettoni, G., Muiesan, M. L., Muiesan, P., Giulini, S. M. & AgabitiRosei, E. (1996) Vascular hypertrophy and remodeling in secondary hypertension. *Hypertension*, 28(5), 785-790.

Robertson, N. P., Fraser, M., Deans, J., Clayton, D., Walker, N. & Compston, D. A. S. (1996) Age-adjusted recurrence risks for relatives of patients with multiple sclerosis. *Brain*, 119, 449-455.

Rocca, M. A., Battaglini, M., Benedict, R. H. B., De Stefano, N., Geurts, J. J. G., Henry, R. G., Horsfield, M. A., Jenkinson, M., Pagani, E. & Filippi, M. (2017) Brain MRI atrophy quantification in MS From methods to clinical application. *Neurology*, 88(4), 403-413.

Roorda, A., Romero-Borja, F., Donnelly, W. J., Queener, H., Hebert, T. J. & Campbell, M. C. W. (2002) Adaptive optics scanning laser ophthalmoscopy. *Optics Express*, 10(9), 405-412.

Rosei, E. A. & Rizzoni, D. (2010) Small artery remodelling in diabetes. *Journal of Cellular and Molecular Medicine*, 14(5), 1030-1036.

Roshanisefat, H., Bahmanyar, S., Hillert, J., Olsson, T. & Montgomery, S. (2014) Multiple sclerosis clinical course and cardiovascular disease risk - Swedish cohort study. *European Journal of Neurology*, 21(11), 1353-+.

Rovaris, M., Confavreux, C., Furion, R., Kappos, L., Comi, G. & Filippi, M. (2006) Secondary progressive multiple sclerosis: current knowledge and future challenges. *Lancet Neurology*, 5(4), 343-354.

Rucker, H. K., Wynder, H. J. & Thomas, W. E. (2000) Cellular mechanisms of CNS pericytes. *Brain Research Bulletin*, 51(5), 363-369.

Sadeghian, M., Mastrolia, V., Haddad, A. R., Mosley, A., Mullali, G., Schiza, D., Sajic, M., Hargreaves, I., Heales, S., Duchen, M. R. & Smith, K. J. (2016) Mitochondrial dysfunction is an important cause of neurological deficits in an inflammatory model of multiple sclerosis. *Scientific Reports*, 6.

Sadovnick, A. D. & Baird, P. A. (1988) The familial nature of multiple sclerosis - age-corrected empiric recurrence risks for children and siblings of patients. *Neurology*, 38(6), 990-991.

Saidha, S., Al-Louzi, O., Ratchford, J. N., Bhargava, P., Oh, J., Newsome, S. D., Prince, J. L., Pham, D., Roy, S., van Zijl, P., Balcer, L. J., Frohman, E. M., Reich, D. S., Crainiceanu, C. & Calabresi, P. A. (2015) Optical coherence tomography reflects brain atrophy in multiple sclerosis: A four-year study. *Annals of Neurology*, 78(5), 801-813.

Saidha, S., Sotirchos, E. S., Ibrahim, M. A., Crainiceanu, C. M., Gelfand, J. M., Sepah, Y. J., Ratchford, J. N., Oh, J., Seigo, M. A., Newsome, S. D., Balcer, L. J., Frohman, E. M., Green, A. J., Nguyen, Q. D. & Calabresi, P. A. (2012) Microcystic macular oedema, thickness of the inner nuclear layer of the retina, and disease characteristics in multiple sclerosis: a retrospective study. *Lancet Neurology*, 11(11), 963-972.

Sasaki, M., Gan, W. L., Kawasaki, R., Hodgson, L., Lee, K. Y., Wong, T. Y., Lamoureux, E., Robman, L. & Guymer, R. (2013) Effect of simvastatin on retinal vascular caliber: the Age-Related Maculopathy Statin Study. *Acta Ophthalmologica*, 91(5), E418-E419.

Schippling, S., Balk, L. J., Costello, F., Albrecht, P., Balcer, L., Calabresi, P. A., Frederiksen, J., Frohman, E., Green, A. J., Klistorner, A., Outteryck, O., Paul, F., Plant, G. T., Traber, G., Vermersch, P., Villoslada, P., Wolf, S. & Petzold, A. (2015) Quality control for retinal OCT in

multiple sclerosis: validation of the OSCAR-IB criteria. *Multiple Sclerosis Journal*, 21(2), 163-170.

Schneider, C. A., Rasband, W. S. & Eliceiri, K. W. (2012) NIH Image to ImageJ: 25 years of image analysis. *Nature Methods*, 9(7), 671-675.

Schroeter, M., Dennin, M. A., Walberer, M., Backes, H., Neumaier, B., Fink, G. R. & Graf, R. (2009) Neuroinflammation extends brain tissue at risk to vital peri-infarct tissue: a double tracer C-11 PK11195-and F-18 FDG-PET study. *Journal of Cerebral Blood Flow and Metabolism*, 29(6), 1216-1225.

Schwarz, T. (2008) 25 years of UV-induced immunosuppression mediated by T cells - From disregarded T suppressor cells to highly respected regulatory T cells. *Photochemistry and Photobiology*, 84(1), 10-18.

Scoles, D., Higgins, B. P., Cooper, R. F., Dubis, A. M., Summerfelt, P., Weinberg, D. V., Kim, J. E., Stepien, K. E., Carroll, J. & Dubra, A. (2014) Microscopic Inner Retinal Hyper-Reflective Phenotypes in Retinal and Neurologic Disease. *Investigative Ophthalmology & Visual Science*, 55(7), 4015-4029.

Scoles, D., Sulai, Y. N. & Dubra, A. (2013) In vivo dark-field imaging of the retinal pigment epithelium cell mosaic. *Biomedical Optics Express*, 4(9), 1710-1723.

Serafini, B., Rosicarelli, B., Magliozzi, R., Stigliano, E. & Aloisi, F. (2004) Detection of ectopic B-cell follicles with germinal centers in the meninges of patients with secondary progressive multiple sclerosis. *Brain Pathology*, 14(2), 164-174.

Serra, A., Derwenskus, J., Downey, D. L. & Leigh, R. J. (2003) Role of eye movement examination and subjective visual vertical in clinical evaluation of multiple sclerosis. *Journal of Neurology*, 250(5), 569-575.

Simpson, L. O., Shand, B. I., Olds, R. J., Larking, P. W. & Arnott, M. J. (1987) Red Cell and Hemorheological Changes in Multiple Sclerosis. *Pathology*, 19(1), 51-55.

Singleton, C. D., Robertson, D., Byrne, D. W. & Joos, K. M. (2003) Effect of posture on blood and intraocular pressures in multiple system atrophy, pure autonomic failure, and baroreflex failure. *Circulation*, 108(19), 2349-2354.

Smith, A. L. & Cohen, J. A. (2016) Fingolimod failure in progressive MS INFORMS future trials. *Nature Reviews Neurology*, 12(5).

Soldan, S. S., Retuerto, A. I. A., Sicotte, N. L. & Voskuhl, R. R. (2004) Dysregulation of IL-10 and IL-12p40 in secondary progressive multiple sclerosis. *Journal of Neuroimmunology*, 146(1-2), 209-215.

Sorensen, T. L. & Sellebjerg, F. (2001) Distinct chemokine receptor and cytokine expression profile in secondary progressive MS. *Neurology*, 57(8), 1371-1376.

Sosa, S. M. & Smith, K. J. (2017) Understanding a role for hypoxia in lesion formation and location in the deep and periventricular white matter in small vessel disease and multiple sclerosis. *Clinical Science*, 131(20), 2503-2524.

Sotirchos, E. S., Caldito, N. G., Filippatou, A., Fitzgerald, K. C., Murphy, O. C., Lambe, J., Nguyen, J., Button, J., Ogbuokiri, E., Crainiceanu, C. M., Prince, J. L., Calabresi, P. A., Saidha, S. & Int Multiple Sclerosis Visual, S. (2020) Progressive Multiple Sclerosis Is Associated with Faster and Specific Retinal Layer Atrophy. *Annals of Neurology*, 87(6), 885-896.

Spaide, R. F., Fujimoto, J. G. & Waheed, N. K. (2015) Image Artifacts in Optical Coherence Tomography Angiography. *Retina-the Journal of Retinal and Vitreous Diseases*, 35(11), 2163-2180.

Spain, R. I., Liu, L., Zhang, X. B., Jia, Y. L., Tan, O., Bourdette, D. & Huang, D. (2018) Optical coherence tomography angiography enhances the detection of optic nerve damage in multiple sclerosis. *British Journal of Ophthalmology*, 102(4), 520-524.

Spencer, J. I., Bell, J. S. & DeLuca, G. C. (2018) Vascular pathology in multiple sclerosis: reframing pathogenesis around the blood-brain barrier. *Journal of Neurology Neurosurgery and Psychiatry*, 89(1), 42-52.

Stadelmann, C., Ludwin, S., Tabira, T., Guseo, A., Lucchinetti, C. F., Leel-Ossy, L., Ordinario, A. T., Bruck, W. & Lassmann, H. (2005) Tissue preconditioning may explain concentric lesions in Balo's type of multiple sclerosis. *Brain*, 128, 979-987.

Stamatovic, S. M., Keep, R. F. & Andjelkovic, A. V. (2008) Brain endothelial cell-cell junctions: How to "Open" the blood brain barrier. *Current Neuropharmacology*, 6(3), 179-192.

Stevenson, W., Ponce, C. M. P., Agarwal, D. R., Gelman, R. & Christoforidis, J. B. (2016) Epiretinal membrane: optical coherence tomography-based diagnosis and classification. *Clinical Ophthalmology*, 10, 527-534.

Stys, P. K., Zamponi, G. W., van Minnen, J. & Geurts, J. J. G. (2012) Will the real multiple sclerosis please stand up? *Nature Reviews Neuroscience*, 13(7), 507-514.

Sugiyama, T., Araie, M., Riva, C. E., Schmetterer, L., Orgul, S. & Ocular Blood Flow Res, A. (2010) Use of laser speckle flowgraphy in ocular blood flow research. *Acta Ophthalmologica*, 88(7), 723-729.

Syc, S. B., Warner, C. V., Hiremath, G. S., Farrell, S. K., Ratchford, J. N., Conger, A., Frohman, T., Cutter, G., Balcer, L. J., Frohman, E. M. & Calabresi, P. A. (2010) Reproducibility of high-resolution optical coherence tomography in multiple sclerosis. *Multiple Sclerosis Journal*, 16(7), 829-839.

Tam, J. & Roorda, A. (2011) Speed quantification and tracking of moving objects in adaptive optics scanning laser ophthalmoscopy. *Journal of Biomedical Optics*, 16(3).

Tam, J., Tiruveedhula, P. & Roorda, A. (2011) Characterization of single-file flow through human retinal parafoveal capillaries using an adaptive optics scanning laser ophthalmoscope. *Biomedical Optics Express*, 2(4), 781-793.

Tettey, P., Siejka, D., Simpson, S., Taylor, B., Blizzard, L., Ponsonby, A. L., Dwyer, T. & van der Mei, I. (2016) Frequency of Comorbidities and Their Association with Clinical Disability and Relapse in Multiple Sclerosis. *Neuroepidemiology*, 46(2), 106-113.

Tettey, P., Simpson, S., Taylor, B. V. & van der Mei, I. A. F. (2014) Vascular comorbidities in the onset and progression of multiple sclerosis. *Journal of the Neurological Sciences*, 347(1-2), 23-33.

Thomas, W. E. (1999) Brain macrophages: on the role of pericytes and perivascular cells. *Brain Research Reviews*, 31(1), 42-57.

Thompson, A. J., Banwell, B. L., Barkhof, F., Carroll, W. M., Coetzee, T., Comi, G., Correale, J., Fazekas, F., Filippi, M., Freedman, M. S., Fujihara, K., Galetta, S. L., Hartung, H. P., Kappos, L., Lublin, F. D., Marrie, R. A., Miller, A. E., Miller, D. H., Montalban, X., Mowry, E. M., Sorensen, P. S., Tintore, M., Traboulsee, A. L., Trojano, M., Uitdehaag, B. M. J., Vukusic, S., Waubant, E., Weinshenker, B. G., Reingold, S. C. & Cohen, J. A. (2017) Diagnosis of multiple sclerosis: 2017 revisions of the McDonald criteria. *The Lancet. Neurology*.

Thompson, A. J., Baranzini, S. E., Geurts, J., Hemmer, B. & Ciccarelli, O. (2018) Multiple sclerosis. *Lancet*, 391(10130), 1622-1636.

Toussaint, D., Perier, O., Verstappen, A. & Bervoets, S. (1983) Clinicopathological study of the visual pathways, eyes, and cerebral hemispheres in 32 cases

of disseminated sclerosis. *Journal of Clinical Neuro-Ophthalmology*, 3(3), 211-220.

Trapp, B. D. & Nave, K. A. (2008) Multiple sclerosis: An immune or neurodegenerative disorder? *Annual Review of Neuroscience*, 31, 247-269.

Trapp, B. D. & Stys, P. K. (2009) Virtual hypoxia and chronic necrosis of demyelinated axons in multiple sclerosis. *Lancet Neurology*, 8(3), 280-291.

Trost, A., Lange, S., Schroedl, F., Bruckner, D., Motloch, K. A., Bogner, B., Kaser-Eichberger, A., Strohmaier, C., Runge, C., Aigner, L., Rivera, F. J. & Reitsamer, H. A. (2016) Brain and Retinal Pericytes: Origin, Function and Role. *Frontiers in Cellular Neuroscience*, 10.

Tseng, C. H., Huang, W. S., Lin, C. L. & Chang, Y. J. (2015) Increased risk of ischaemic stroke among patients with multiple sclerosis. *European Journal of Neurology*, 22(3), 500-506.

Turaka, K. & Bryan, J. S. (2012) Does fingolimod in multiple sclerosis patients cause macular edema? *Journal of Neurology*, 259(2), 386-388.

Turksever, C., Daikeler, T., Konieczka, K. & Todorova, M. G. (2014) Retinal Vessel Oxygen Saturation in Giant Cell Arteritis Patients without Ocular Symptoms. *Klinische Monatsblatter Fur Augenheilkunde*, 231(4), 442-446.

Ulusoy, M. O., Horasanli, B. & Isik-Ulusoy, S. (2020) Optical coherence tomography angiography findings of multiple sclerosis with or without optic neuritis. *Neurological Research*.

Varga, A. W., Johnson, G., Babb, J. S., Herbert, J., Grossman, R. I. & Inglese, M. (2009) White matter hemodynamic abnormalities precede sub-cortical gray matter changes in multiple sclerosis. *Journal of the Neurological Sciences*, 282(1-2), 28-33.

Vasconcelos, C. C. F., Aurencao, J. C. K., Thuler, L. C. S., Camargo, S., Alvarenga, M. P. & Alvarenga, R. M. P. (2016) Prognostic factors associated with long-term disability and

secondary progression in patients with Multiple Sclerosis. *Multiple Sclerosis and Related Disorders*, 8, 27-34.

Villamarin, A., Roy, S. & Stergiopulos, N. (2012) Eye Vessel Compliance as a Function of Intraocular and Arterial Pressure and Eye Compliance. *Investigative Ophthalmology & Visual Science*, 53(6), 2831-2836.

Wallis, S. J., Firth, J. & Dunn, W. R. (1996) Pressure-induced myogenic responses in human isolated cerebral resistance arteries. *Stroke*, 27(12), 2287-2290.

Wang, C.-Y., Liu, P.-Y. & Liao, J. K. (2008) Pleiotropic effects of statin therapy: molecular mechanisms and clinical results. *Trends in Molecular Medicine*, 14(1), 37-44.

Wang, R., Liang, Z. Z. & Liu, X. (2019) Diagnostic accuracy of optical coherence tomography angiography for choroidal neovascularization: a systematic review and meta-analysis. *Bmc Ophthalmology*, 19.

Wang, X. G., Jia, Y. L., Spain, R., Potsaid, B., Liu, J. J., Baumann, B., Hornegger, J., Fujimoto, J. G., Wu, Q. & Huang, D. (2014) Optical coherence tomography angiography of optic nerve head and parafovea in multiple sclerosis. *British Journal of Ophthalmology*, 98(10), 1368-1373.

Waubant, E., Lucas, R., Mowry, E., Grayest, J., Olsson, T., Alfredsson, L. & Langer-Gould, A. (2019) Environmental and genetic risk factors for MS: an integrated review. *Annals of Clinical and Translational Neurology*, 6(9), 1905-1922.

Weinhaus, R. S., Burke, J. M., Delori, F. C. & Snodderly, D. M. (1995) Comparison of fluorescein angiography with microvascular

anatomy of macaque retinas. *Experimental Eye Research*, 61(1), 1-16.

Wells-Gray, E. M., Choi, S. S., Slabaugh, M., Weber, P. & Doble, N. (2018) Inner Retinal Changes in Primary Open Angle Glaucoma Revealed through Adaptive Optics Optical Coherence Tomography. *Journal of glaucoma*.

Weyand, C. M., Ma-Krupa, W. & Goronzy, J. J. (2004) Immunopathways in giant cell arteritis and polymyalgia rheumatica. *Autoimmunity Reviews*, 3(1), 46-53.

Witte, M. E., Bo, L., Rodenburg, R. J., Belien, J. A., Musters, R., Hazes, T., Wintjes, L. T., Smeitink, J. A., Geurts, J. J. G., De Vries, H. E., van der Valk, P. & van Horssen, J. (2009) Enhanced number and activity of mitochondria in multiple sclerosis lesions. *Journal of Pathology*, 219(2), 193-204.

Yang, R. Z. & Dunn, J. F. (2015) Reduced cortical microvascular oxygenation in multiple sclerosis: a blinded, case-controlled study using a novel quantitative near-infrared spectroscopy method. *Scientific Reports*, 5.

Yang, Y., Kim, S. & Kim, J. (1997) Visualization of retinal and choroidal blood flow with fluorescein leukocyte angiography in rabbits. *Graefes Archive for Clinical and Experimental Ophthalmology*, 235(1), 27-31.

Yilmaz, H., Ersoy, A. & Icel, E. (2019) Assessments of vessel density and foveal avascular zone metrics in multiple sclerosis: an optical coherence tomography angiography study. *Eye (London, England)*.

Zahid, S., Dolz-Marco, R., Freund, K. B., Balaratnasingam, C., Dansingani, K., Gilani, F., Mehta, N., Young, E., Klifto, M. R., Chae, B., Yannuzzi, L. A. & Young, J. A. (2016) Fractal Dimensional Analysis of Optical Coherence Tomography Angiography in Eyes With Diabetic Retinopathy. *Investigative Ophthalmology & Visual Science*, 57(11), 4940-4947.

Zajicek, J., Ball, S., Wright, D., Vickery, J., Nunn, A., Miller, D., Cano, M. G., McManus, D., Mallik, S., Hobart, J. & Grp, C. I. (2013) Effect of dronabinol on progression in progressive multiple sclerosis (CUPID): a randomised, placebo-controlled trial. *Lancet Neurology*, 12(9), 857-865.

Zaleska-Zmijewska, A., Piatkiewicz, P., Smigielska, B., Sokolowska-Oracz, A., Wawrzyniak, Z. M., Romaniuk, D., Szaflik, J. & Szaflik, J. P. (2017) Retinal Photoreceptors and Microvascular Changes in Prediabetes Measured with Adaptive Optics (rtx1 (TM)): A Case-Control Study. *Journal of Diabetes Research*.

Zamboni, P. & Galeotti, R. (2010) The chronic cerebrospinal venous insufficiency syndrome. *Phlebology*, 25(6), 269-279.

Zamzam, D. A., Gaafar, A. A., Ismail, A. T., Elbassiouny, A., Tork, M. A. & Hamdy, H. (2015) Retinal nerve fiber layer thickness in multiple sclerosis subtypes. *The Egyptian Journal of Neurology, Psychiatry and Neurosurgery*, 52(3), 216.

Zar, J. H. (2010) *Biostatistical Analysis.*Prentice Hall.

Zhang, Y., Zabad, R. K., Wei, X., Metz, L. M., Hill, M. D. & Mitchell, J. R. (2007) Deep grey matter "black T2" on 3 tesla magnetic resonance imaging correlates with disability in multiple sclerosis. *Multiple Sclerosis Journal*, 13(7), 880-883.

Zheng, Q. S., Zong, Y., Li, L., Huang, X., Lin, L. L., Yang, W., Yuan, Y. G., Li, Y. J., He, H. N. & Gao, Q. Y. (2015) Retinal vessel oxygen saturation and vessel diameter in high myopia. *Ophthalmic and Physiological Optics*, 35(5), 562-569.

Zhong, Z. Y., Huang, G., Chui, T. Y. P., Petrig, B. L. & Burns, S. A. (2012) Local flicker stimulation evokes local retinal blood velocity changes. *Journal of Vision*, 12(6).

Zhong, Z. Y., Petrig, B. L., Qi, X. F. & Burns, S. A. (2008) In vivo measurement of erythrocyte velocity and retinal blood flow using adaptive optics scanning laser ophthalmoscopy. *Optics Express*, 16(17), 12746-12756.

Zhong, Z. Y., Song, H. X., Chui, T. Y. P., Petrig, B. L. & Burns, S. A. (2011) Noninvasive Measurements and Analysis of Blood Velocity Profiles in Human Retinal Vessels. *Investigative Ophthalmology & Visual Science*, 52(7), 4151-4157.

Appendix

MSOpt Study Recruitment Criteria (Protocol v1.5)

MSOpt Trial Participant Inclusion Criteria

The following inclusion criteria must be met (answer yes) when assessing patient's eligibility onto the trial.

1. Patients must have a confirmed diagnosis of multiple sclerosis according to revised McDonald criteria and have entered the secondary progressive stage. (Polman et al., 2011, Lublin, 2014)
   Steady progression rather than relapse must be the major cause of increasing disability in the preceding 2 years. Progression can be evident from either an increase of at least one point on the EDSS or clinical documentation of increasing disability.
2. EDSS 4.0 – 6.5 (inclusive).
3. Male and Females aged 18 to 65
4. Females of childbearing potential and males with partners who are of childbearing age must be willing to use an effective method of contraception (Double barrier method of birth control or True abstinence) from the time consent is signed until 6 weeks after treatment discontinuation and inform the trial team if pregnancy occurs. For the purpose of clarity, True abstinence is when this is in line with the preferred and usual lifestyle of the subject. Periodic abstinence (e.g., calendar, ovulation, symptothermal, post-ovulation methods), declaration of abstinence, withdrawal, spermicides only or lactational amenorrhoea method for the duration of a trial, are not acceptable methods of contraception.
5. Females of childbearing potential have a negative pregnancy test within 7 days prior to being registered/randomised. Participants are considered not of child bearing potential if they are surgically sterile (i.e. they have undergone a hysterectomy, bilateral tubal ligation, or bilateral oophorectomy) or they are postmenopausal.
6. Willing and able to comply with the trial protocol (e.g. can tolerate MRI and fulfils the requirements for MRI, e.g. not fitted with pacemakers or permanent hearing aids) ability to understand and complete questionnaires.
7. Willing and able to provide written informed consent.
8. Willing to ingest gelatine (placebo will contain this). Participants must therefore be informed sensitive to personal beliefs e.g. faith, diet.

MSOpt Trial Participant Exclusion Criteria

Patients presenting with any of the following exclusion criteria (i.e. answers yes) at screening will not be eligible to proceed with the trial:

1. Unable to give informed consent.
2. Primary progressive MS.
3. Those that have experienced a relapse or have been treated with steroids (both intravenous and oral) for multiple sclerosis relapse within 3 months of the screening visit. These patients may undergo a further screening visit once the 3-month window has expired and may be included if no steroid treatment has been administered in the intervening period. Patients on steroids for another medical condition may enter as long as the steroid prescription is not for multiple sclerosis (relapse/ progression).

4. Patient is already taking or is anticipated to be taking a statin or lomitapide for cholesterol control.
5. Any medications that unfavourably interact with statins as per Spc recommendations e.g.: fibrates, nicotinic acid, cyclosporin, azole anti-fungal preparations, macrolideantibiotics, protease inhibitors, nefazodone, verapamil, amiodarone, large amounts of grapefruit juice or alcohol abuse within 6 months.
6. The use of immunosuppressants (e.g. azathioprine, methotrexate, cyclosporin) or disease modifying treatments (avonex, rebif, betaferon, glatiramer, dimethyl fumerate, fingolimod) within the previous 6 months.
7. The use of mitoxantrone if treated within the last 12 months.
8. Patient has received treatment with alemtuzumab.
9. Use of other experimental disease modifying treatment (including research in an investigational medicinal product) within 6 months of baseline visit.
10. Active Hepatic disease or known severe renal failure (creatinine clearance <30ml/min).
11. Screening levels of alanine aminotransferase (ALT), aspartate aminotransferase (AST) or creatine kinase (CK) are three times the upper limit of normal patients.
12. If the patient reports any ophthalmic conditions such as glaucoma, ocular trauma or degenerative eye disease.
13. Patient unable to tolerate or unsuitable to have baseline MRI scan (e.g. metal implants, heart pacemaker) or MRI scan not of adequate quality for analysis (e.g. too much movement artefact).
14. Females who are pregnant, planning pregnancy or breastfeeding.
15. Allergies to IMP active substance or to any excipients of IMP and placebo or other conditions that contraindicate use of galactose (e.g. Hereditary galactose intolerance, Lactase deficiency, glucose-galactose malabsorption)